

AD-A247 133



Naval Oceanographic and Atmospheric Research Laboratory

NOARL Report 28 October 1991

2070151

(2) ✓

SBIN/NORDA

# Theory and Application of Scattering from an Object in an Ocean Waveguide

DTIC  
ELECTE  
FEB 21 1992  
S D D

Guy V. Norton  
Numerical Modeling Division  
Ocean Acoustics & Technology Directorate

92 2 14 074

92-03943

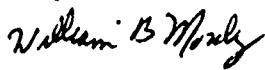


Approved for public release; distribution is unlimited. Naval Oceanographic and Atmospheric Research Laboratory, Stennis Space Center, Mississippi 39529-5004.

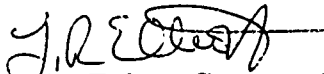
## Foreword

Determining the scattered field from objects in a waveguide has been difficult and is of great importance to the U.S. Navy. Since future detection methods will exploit for both long- and short-range bistatic detections of submerged objects, determining whether various system/detection scenarios are feasible will depend on both experiments and numerical model studies. Numerical studies are particularly appealing, since they are considerably less expensive than experiments and, in terms of a time frame, many numerical studies can be done for any given experiment. Moreover, numerical studies can also be used to suggest experiments.

This report proposes a numerical scheme that will adequately describe scattering from realistic objects (submarines) in an ocean waveguide. The type of object used in this report was a spheroid, and the object was assumed to have Dirichlet boundary conditions.



W. B. Moseley  
Technical Director



L. R. Elliott, Commander, USN  
Commanding Officer

## Executive Summary

---

A method was developed to describe acoustical scattering from an object in a waveguide by using normal mode theory to describe the incident field. Each mode is decomposed at the object into a pair of upgoing and downgoing plane waves. A transition matrix was used (developed via the extended boundary condition method of Waterman) to determine the resulting near-field scattered field. The far-field scattered field was determined by invoking Huygens' principle. This far-field solution satisfies all boundary conditions and preserves continuity of the solution throughout all space.

The examples show that the object is correctly coupled to the waveguide. This was done by showing that the object's scattered field acts as a secondary source and that this scattered field obeyed the same boundary conditions as the point source field.

This method of determining the scattered field from a three-dimensional object allows one to determine not only the correct target strength (intensity), but also to properly determine the phase. In addition this method allows the investigation of the interaction between the incident field and the waveguide, the incident field with the object, and the object's scattered field with the waveguide. In this manner a better understanding of the ongoing physical processes can be obtained.

Accession For	
NTIS CRA&I	<input checked="checked" type="checkbox"/>
DTIC TAB	<input type="checkbox"/>
Unannounced	<input type="checkbox"/>
Justification .....	
By .....	
Distribution / .....	
Availability Codes	
Dist	Avail and/or Special
A-1	



# Acknowledgments

---

I would like to express my appreciation to NOARL (Naval Oceanographic and Atmospheric Research Laboratory) management for their continued support through these endeavors. This support was provided through Program Element 0601153N, Mrs. Halcyon E. Morris, program manager, and by the Office of Naval Research 6.1 project office.

One person provided the major technical support for this project through fruitful and colorful discussions. I express appreciation to Dr. M. F. Werby. This work served as my Ph.D. dissertation in the Physics Department at Tulane University. As a consequence, additional valuable advice was provided by the various members of my graduate committee, including Dr. R. Purrington, Dr. J. Kyame and Dr. W. Reed. For additional relevant comments I would like to recognize Mr. Richard S. Keiffer, Dr. Jorge C. Novarini, Dr. Stanley A. Chin-Bing, and Dr. Michael D. Collins.

The mention of commercial products or the use of company names does not in any way imply endorsement by the U.S. Navy or NOARL.

# Contents

---

Synopsis	1
Summary	1
Recommendations	1
Appendix: Theory and Application of Scattering from an Object in an Ocean Waveguide	3

# Theory and Application of Scattering from an Object in an Ocean Waveguide

---

## Synopsis

The treatment of scattering from submerged objects in an unbounded environment is of considerable interest to both the academic and technological communities. Several approaches have yielded results for different classes of problems and have proven manageable for the free environment case. The solution of scattering from objects in a waveguide has been a difficult and almost intractable problem to do in an exact framework, due to the coupling of effects from the object's scattered field with that of the boundaries. It is, however, a problem that is of great importance to the U.S. Navy community, since future detection methods are going to exploit both long- and short-range bistatic detections of threat submarines. The ability to determine whether various system/detection scenarios are feasible will depend on both experiments and numerical model studies. Numerical studies are particularly appealing, since they are considerably less expensive than experiments and in terms of time, many numerical studies can be performed for any given experiment. Moreover, numerical studies can be used to suggest experiments. The objective of this work is to develop a model suitable for such studies in an approximate but accurate framework.

## Summary

The study described in the appendix presents a coherent, self-consistent method to describe acoustical scattering and propagation from an object in a waveguide. The method is based on Huygens' principle. The object was a spheroid with Dirichlet boundary conditions. The study began by developing the extended boundary condition (EBC) method<sup>1-3</sup> to describe acoustical scattering from three-dimensional objects in free space. This method was used to describe scattering from objects with both

Neuman and Dirichlet boundary conditions and has been extended for elastic objects. Next, the theory of acoustic propagation in a fluid was developed from first principles and both normal mode and ray theory were developed to describe propagation in the simplest type of acoustic waveguide.

The mathematical expression that describes the object's far-field scattered field is developed here through the use of Huygens' principle. The near-field scattered field, developed by allowing a transition matrix (developed by the EBC method) to map the incident field onto the scattered field, was coupled to the Green's function, which satisfies the waveguide. This application of Huygens' principle leads to a manageable direct solution of the problem. This method also satisfies all appropriate boundary conditions and yields a continuous solution throughout space. This expression is then applied to a Pekeris waveguide and finally to a more general range-independent waveguide.

The examples presented in the last two chapters of the appendix were designed to demonstrate that the object's scattered field is correctly coupled to the waveguide. This was accomplished by showing that the object acted as a secondary source in the waveguide. Its field obeyed (satisfied) the same boundary conditions for the waveguide as the point source field.

## Recommendations

The results obtained are for a waveguide that is range independent; that is, the sound speed profile in the water column and the sediment vary only in depth and not in range, and the bathymetry does not change with respect to range. In addition, the object is expected to be in the far field of the source. The model could simulate range dependency by either

applying the adiabatic approximation or by coupling the discrete (propagating) modes. Additionally, if the continuous spectrum of the incident field is included and not just the discrete spectrum, then the object could be located near the source where the continuous spectrum could play an important role. The addition of range dependency would be the most valuable addition to the model.

The incident field was allowed to interact only once with the object; that is, the primary interaction of the incident field with the scatterer was retained, and the subsequent interactions of the scattered field between the boundaries of the waveguide and the scatterer were ignored. This is not a limitation, since

the resulting field would consist of high-angle energy and would dissipate quickly in an ocean environment.

## References

1. Waterman, P. C. (1965). Matrix Formulation of Electromagnetic Scattering. *Proc. IEEE* 53:805-812.
2. Waterman, P. C. (1969). New Foundation of Acoustic Scattering. *J. Acoust. Soc. Am.* 45:1417-1429.
3. Waterman, P. C. (1977). Matrix Theory of Elastic Wave Scattering II. A New Conservative Law. *J. Acoust. Soc. Am.* 63:1320-1325.

# Appendix

---

## Theory and Application of Scattering from an Object in an Ocean Waveguide

Guy V. Norton

---

Chapter 1. Introduction	1
Chapter 2. Free Space Scattering	3
Chapter 3. Acoustic Propagation in a Waveguide	23
Chapter 4. Methods Describing Scattering from Objects in a Waveguide	71
Chapter 5. Application of Huygens' Method to an Isovelocity Waveguide	78
Chapter 6. Application of Huygens' Principle to a Multilayered Waveguide	150
Conclusions	177
Appendix A: Comparison Between the E. B. C. Method and an Analytical Solution for the Scattered Field Produced by a Plane Wave Incident Upon a Sphere	178
Appendix B: Derivation of Eq. (3-122)	182
Appendix C: Validation of Propagation Models	188
Appendix D: Modal Attenuation Coefficients Used in the Normal Mode Programs	211
Appendix E: Comparison of the Scattered Field Obtained Using the Present Method and a Projection Method	214



## CHAPTER 1

### INTRODUCTION

#### Goals of Research

This research project will answer the following question. What is the acoustic pressure at a field point in an underwater acoustic waveguide when a three dimensional object is present? This research project concerns classical wave propagation, diffraction and scattering effects. An inherent assumption is that the object's dimension's (length and width) are small compared to the waveguides dimensions. We therefore are assuming that the object will make a small perturbation to the acoustic field produced by a monochromatic point source. We assume then that the wave equation will properly describe the acoustic wave propagating in the waveguide. We assume also that the field can be expressed as a near field scattered field and a far field scattered field. The near field scattered field will only be valid near the object, before it interacts with the waveguide and the far field scattered field will be appropriate in the far field of the object, that is when the scattered field has interacted with the waveguide boundaries. With these assumptions, this project can be subdivided into four distinct sub areas. First the incident field must be determined, that is the acoustic field in the absence of the object or scatterer. Second, the incident field which insonifies the object is mathematically acted on by a transition matrix which transforms the incident field into the near field scattered field. Next, the near field scattered field is coupled to the waveguide via invoking Huygens' principle (see chapter 4). Finally, we obtain the total field by coherently adding the incident and scattered field.

Because of the way the problem divides mathematically, we have divided this discussion into two parts. The first is concerned mainly with theory and results pertaining to free space scattering (chapter 2) and acoustic propagation in a waveguide (chapter 3). This is done in order to first define the physics that defines scattering from an object (via a matrix mapping) and the propagation of this and the incident field in a waveguide. In part 2 (chapters 3-6) of this dissertation we present the various methods that were used prior to the present work. We then present formally this new method based on Huygens' principle (chapter 4) and in Chapters 5-6 apply the method to two acoustic waveguides. The first is a waveguide composed of an isovelocity water-layer over an isovelocity fluid half-space and the second is a multilayered waveguide consisting of multiple isovelocity sound and density layers over an isovelocity half space.

Appendix A validates the Extended Boundary Condition (see chapter 2) code by showing a comparison of the scattered field generated by this method with the analytical solution for the case when a plane wave is incident upon a sphere. Appendix B shows a derivation of a result needed in the development of the acoustic field in a waveguide. Appendix C is a validation of the propagation models used in this dissertation. Appendix D is a brief description of the attenuation term used in the two waveguides. Appendix E shows the comparison of the scattered field using the proposed method based on Huygens' principle along with a different method described in Chapter 4. These results were presented by the author at the Second Joint Meeting of the Acoustical Society of America and the Acoustical Society of Japan 14-18, Nov. 1988 in Honolulu.

## CHAPTER 2

### FREE SPACE SCATTERING

In this chapter we give a brief overview of the usual methods used to describe acoustical scattering prior to the introduction of the Extended Boundary Condition (EBC) method. We then develop the EBC method, which is used in this dissertation to describe the near scattered field. We complete this chapter by showing some representable free space scattering results from this method for both far and near field. The references listed represent a fraction of the work being done by the scattering community using this method and is not meant to be all inclusive.

#### Early Free Space Scattering Techniques

Historically there are three predominate methods employed to solve scattering and/or diffraction problems. They are separation of variables, variational techniques, and the direct numerical solution of integral equations.

The separation of variables technique has been used for objects bounded by quadric (separable) surfaces. The technique can be used as long as the scalar wave equation governing the problem can be solved by separation of variables. This method solves the wave equation, (a linear partial differential equation) by *separating* the original equation into a set of ordinary differential equations, each involving only one variable. The general solution is a product of the solutions to the ordinary differential equations. For

example, consider a spheroidal object. One can use the spheroidal coordinate system to represent the incident and scattered wavefunctions by a series of spheroidal wavefunctions. This requires that the wave equation be separated in the spheroidal coordinate system. This approach has been carried out by Burke, who has solved the scattering problem for a plane wave incident upon an impenetrable spheroid having Dirichlet boundary conditions (1) (which fixes the value of the wavefunction on the surface) as well as for a rigid spheroid having Neuman boundary conditions (2) (which fixes the value of the normal derivative of the wavefunction on the surface). He has also solved the problem of a plane wave incident upon a penetrable spheroid. (3) Yeh has solved the problem for a plane wave incident upon a penetrable liquid prolate spheroid. (4) The liquid prolate spheroid is the limiting case of an elastic spheroid with zero shear modulus. The main reason this approximation was adopted was because the vector wave equations are not separable in spheroidal coordinates. The secondary reason being that due to the complexity of spheroidal coordinates, laborious computations had to be carried out in order to obtain numerical values. There are other coordinate systems, one could use to solve various scattering problems, spherical, cylindrical, etc., depending on the type of object or objects one is concerned with. Considering only confocal quadric surfaces and more specifically ellipsoids, there are nine coordinate systems which can be obtained from ellipsoidal coordinates. (5) To solve the scattering problem, a large part of the computational effort goes into the evaluation of the wavefunctions themselves except for the sphere and the circular cylinder, for which efficient recursion relations are available. (5)

Levine and Schwinger (6) described the variational method for the diffraction of a scalar plane wave by an aperture in an infinite plane screen. In describing diffraction from general bodies the main effort goes into

evaluating matrix elements, which consist of repeated surface integrals requiring fourfold numerical quadrature or volume integrals requiring sixfold numerical quadrature. In each case the integrals have singular kernels.

The integral equation method has the advantage of generality, for usually the integral is invariant under coordinate transformation. Once the Greens function is found for the appropriate geometry, the solution of the scalar wave equation may be found. The problem with this method is that for many cases the integral cannot be integrated in closed form and numerical values are then extremely difficult to obtain. However, with the advent of the digital computer, this method has been used by various individuals. (7-12) More recently the integral equations have been classified into two types, depending upon the observation points. (13) Surface integral equations have the observation points lying on the surface of the scatterer and the Extended integral equations have the observation points inside the scatterer.

Waterman (14) described in his 1969 paper a then new matrix formulation of acoustic scattering. He had previously developed the same method for electromagnetic scattering. (15) The equations generated most nearly resembled those obtained using the variational method. The advantage was that for both surface and volume type scattering, elements of the matrix to be inverted are described by a single surface integral with no singularities in the integrand. Waterman used the interior boundary equation as a constraint in solving the exterior boundary equation. As he stated in the paper this approach was not necessarily new as it appears that Smythe applied it in electrostatics in 1956. (16) The next section presents the derivation of the scattering matrix using this method derived by Waterman. The method of obtaining the scattering matrix has been known by various names, T-Matrix

method, Extended Boundary Condition method and the Null Field Method. We believe that the Extended Boundary Condition method best describes this method. The method has since evolved and is used in many areas of classical scattering determinations. (15,17-22)

### The Extended Boundary Condition (EBC) Method to Determine the Scattered Field

The theoretical basis for the Extended Boundary Condition method is contained in the mathematical formulation of Huygens' principle. (23) This description follows not only Watermans' but also Werby and Chin-Bing. (24) We start with the Helmholtz-Poincare' integral representation of the total field  $U_t$  exterior to the bounded object, which has the following form, (23)

$$(2-1) \quad U_t(r) = U_i(r) + \int_{\sigma} \left[ U_+(r') \frac{\partial G(r, r')}{\partial n} - G(r, r') \frac{\partial U_+(r')}{\partial n} \right] ds$$

where  $U_+(r')$  is the scalar wavefield on the object surface,  $G(r, r')$  is the outgoing Green's function,  $r'$  is taken on the surface of the object, and  $n$  is a unit vector normal to the surface of the object. The surface  $\sigma$  is taken to be the surface of the bounded object. In order to obtain a unique solution, we will need an additional expression. We will use the field interior to the object. This Helmholtz-Poincare' expression is as follows, (23)

$$(2-2) \quad 0 = U_i(r'') + \int_{\sigma} \left[ U_+(r') \frac{\partial G(r'', r')}{\partial n} - G(r'', r') \frac{\partial U_+(r')}{\partial n} \right] ds$$

where  $r''$  is a point taken in the interior of the object. This equation was recognized by Waterman as providing a constraint to eliminate the unknown surface quantities  $U_+$ . These two equations yield the extended boundary condition equations. (25) These equations will now be put into a form amenable to numerical computation. For this example we allow the object to be impenetrable, which requires that

$$(2-3) \quad U_+ = 0.$$

Equation (2-1) becomes

$$(2-4) \quad U_i(r) = U_i(r) - \int_{\sigma} \left[ G(r, r') \frac{\partial U_+(r')}{\partial n} \right] ds$$

and Eq.(2-2) becomes

$$(2-5) \quad 0 = U_i(r'') - \int_{\sigma} \left[ G(r'', r') \frac{\partial U_+(r')}{\partial n} \right] ds$$

In order to solve these expressions, it is convenient to express  $U_i(r)$ ,  $U_+(r')$  and  $G(r, r')$  as some suitable series expansion, which upon truncation leads to matrix equations that can be solved using digital computers. The Green's functions,  $G(r, r')$  is a normal operator and can be expressed by the following biorthogonal series (26)

$$(2-6) \quad G(r, r') = i k \sum_i R e \phi_i(r) \phi_i(r')$$

where  $r_<$  and  $r_>$  is the lesser or greater of the two points  $r$  and  $r'$  relative to the origin of the object. The incident wavefield  $U_i$  is known and can be expressed as, (27)

$$(2-7) \quad U_i(r) = \sum_n a_n \text{Re} \varphi_n(r)$$

where  $\text{Re}$  is the regular part of  $\varphi_n(r)$ . The fact that this expansion Eq. (2-7) can be obtained follows from the Hilbert-Schmidt theorem.(27) Using this and Eq.(2-6), we see that Eq.(2-5) becomes,

$$(2-8) \quad \sum_n a_n \text{Re} \varphi_n(r) = i k \sum_n \int_{\sigma} \text{Re} \varphi_n(r) \varphi_n(r') \frac{\partial U_+(r')}{\partial n} ds$$

$$(2-9) \quad a_n = i k \int_{\sigma} \varphi_n(r') \frac{\partial U_+(r')}{\partial n} ds$$

$U_+(r')$  is now written in some complete set of suitably chosen basis function satisfying completeness on the object surface. The basis functions used were the same as those chosen by Waterman, namely  $\text{Re} \varphi_n(r)$ , where  $\text{Re}$  is the regular part of  $\varphi_n(r)$ . We have not found any problem arising from irregular values, nor have we had problems due to poorly-convergent solutions. Waterman has shown that Eq. (2-10) satisfies closure on the surface of a rigid object:

$$(2-10) \quad U_+(r) = \sum_n b_n \text{Re} \varphi_n(r)$$



Using Eq. (2-10) in Eq. (2-9) results in the following for the incident field expansion coefficients  $a_n$

$$(2-11) \quad a_n = ik \sum_m b_m \int_{\sigma} \varphi_n(r') \frac{\partial \text{Re} \varphi_m(r')}{\partial n} ds$$

$$(2-12) \quad = ik \sum_m b_m Q_{mn} \dots$$

where  $Q_{mn} = \int_{\sigma} \varphi_n(r') \frac{\partial \text{Re} \varphi_m(r')}{\partial n} ds$ . In matrix notation, Eq. (2-11) can be written

$$(2-13) \quad \mathbf{a} = ik \mathbf{Q} \mathbf{b}$$

and the expression for  $U_s(r')$  becomes,

$$(2-14) \quad U_s(r') = \sum_n f_n \varphi_n(r')$$

Recognizing that  $U_s = U_t - U_i$ , the expression for the scattered field expansion coefficients  $f_n$ , becomes,

$$(2-15) \quad \sum_n f_n \varphi_n(r') = -ik \sum_m b_m \int_{\sigma} \text{Re} \varphi_n(r) \varphi_m(r') \frac{\partial \text{Re} \varphi_m(r')}{\partial n} ds$$

$$(2-16) \quad f_n = -ik b_m \int_{\sigma} \text{Re} \varphi_n(r) \frac{\partial \text{Re} \varphi_m(r')}{\partial n} ds$$

$$(2-17) \quad = -ik b_m \text{Re} Q_{mn}$$

where  $\text{Re}Q_{mn} = \int_{\sigma} \text{Re}\varphi_n(r) \frac{\partial \text{Re}\varphi_m(r')}{\partial n} ds$ . In matrix notation,  $f_n$  becomes,

$$(2-18) \quad f = -ik b \text{Re} Q$$

Equation (2-13) can be solved for  $b$ ,

$$(2-19) \quad b = \frac{-i a Q^{-1}}{k}$$

Inserting Eq.(2-19) in Eq.(2-18) one obtains,

$$(2-20) \quad f = -(\text{Re}Q) Q^{-1} a$$

or

$$(2-21) \quad f = T a$$

where  $T = -(\text{Re}Q) Q^{-1}$ . Notice that the matrix  $T$  is only a function of the boundary conditions and the shape of the object. Once the matrix  $T$  is known, the scattered field can be determined from any chosen incident field  $a$ . The Extended Boundary Condition method yields a unique solution to the exterior acoustic problem, and is efficient and numerically stable for a large variety of bounded object shapes. The Extended Boundary Condition method has evolved since its inception in 1965. In the area of acoustic scattering, Werby, (28) Werby, Tango and Green, (29) and Werby and Chin-Bing (24) have made significant improvements to the general method. Not only is this method applicable to solid surface of revolutions but also to shells (30-36) and other

elastic objects. (37-41) Resonance effects are observed and can be predicted using this method. (33,36,39,42,43)

### Far Field Scattering Examples Using the Extended Boundary Condition Method

In this section we will show some examples of the scattered field in the form of scattering amplitude vs. angle, normally called the bistatic angular distribution. (39) Bistatic angular distributions are defined by the case of non-coincident source and receiver, where the receivers are omni directional. Bistatic angular distributions are dependent on object geometry and can be useful in determining such features of object shape as symmetry or elongation. The far field bistatic angular distribution is defined as the following, (38)

$$(2-22) \quad f(\theta) = \frac{2}{ka} \left( \left( \gamma_l^m \right)^{\frac{1}{2}} (-i)^{l+1} e^{ik\rho} P_l^m(\cos\theta) f_{ll'}^m A_{l'}^m(\theta_i) \right)$$

where  $A_{l'}^m(\theta_i)$  is the incident field expansion coefficient, which is dependent upon the angle at which the source insonifies the object,  $a$  is the semi major axis of the object and  $f_{ll'}^m$  is the free space scattering field as determined by the EBC method (see Eq. (2-21)). Therefore the far field bistatic angular distribution is dependent upon two angles (incident and observed), and not just one.

An example of the characteristics of a typical scattering object are shown in Table 1. The incident field was a monochromatic point source. It is assumed that the object is sufficiently far from the point source so that the

incident wave front has infinite radius of curvature that is, it is a plane wave. The three frequencies chosen are given in Table 2, along with other information.

TABLE 1  
...  
OBJECT CHARACTERISTICS

Object Type	Aspect Ratio (L/W)	Boundary Condition	Length(L) (m)	Width(W) (m)
Solid Spheroid	5	Dirichlet	50.	10.

TABLE 2  
EXTENDED BOUNDARY CONDITION INFORMATION

Frequency (Hz)	KL/2	Sound Speed (m/s)	$\lambda$ (m)	Highest Matrix Order	# Matrix
95.5	10.	1500.0	15.7	17	4
191.0	20.	1500.0	7.9	32	7
382.0	40.	1500.0	3.9	64	13

Figure 1 compares the angular distribution with the incident direction along the major axis of symmetry. The object is oriented along the 0-180 degree axis in the figure and the incident field is coming from the direction of the arrow. Angular distribution plot (a) is for a frequency of 95.5 (Hz) or a KL/2 of 10. Where K is the wavenumber and L/2 is half the object's length. The corresponding wavelength is 15.7 (m). The object is approximately 3 wavelengths long. This would represent a low frequency case. Note the

broadness of the field. Even at this low frequency the field is predominantly in the forward direction. As we increase in frequency (and  $KL/2$ ) we note that backscattering (toward the source) is reduced, while it is being focused in the forward direction. The amplitude is also increasing with increasing frequency.

Figure 2 illustrates the case when the object is insonified at an angle of 45 degrees relative to the major axis of symmetry. The top plot is for a frequency of 95.5 (Hz) and the bottom is for 382. (Hz). Note that for the low frequency case, the field is oscillatory in appearance. We also see two peaks, one in the forward direction (225 degrees) and the other in the specular direction (135 degrees). The peaks become more focused in the forward direction as we increase the frequency. The forward diffracted wave becomes more highly focused with increased frequency. Also note that the wave-like appearance of the field at low frequency virtually disappears in the high frequency case. Again we see that the field tends to increase in amplitude as frequency increases.

Figure 3 illustrates the case when the object is being insonified at an angle of 90 degrees or broadside incidence. Note for the low frequency case, the forward and backscattered amplitude are about equal. As we increase in frequency we see that the forward diffracted wave becomes more focused and its amplitude is larger than the backscattered (90 degrees) wave. In fact we see that the backscattered amplitude remains approximately constant. This is because the backscattered amplitude (at 90 degrees incident and 90 degrees observed) is dependent upon geometrical effects and is independent of frequency. Now we turn our attention to some near field examples.

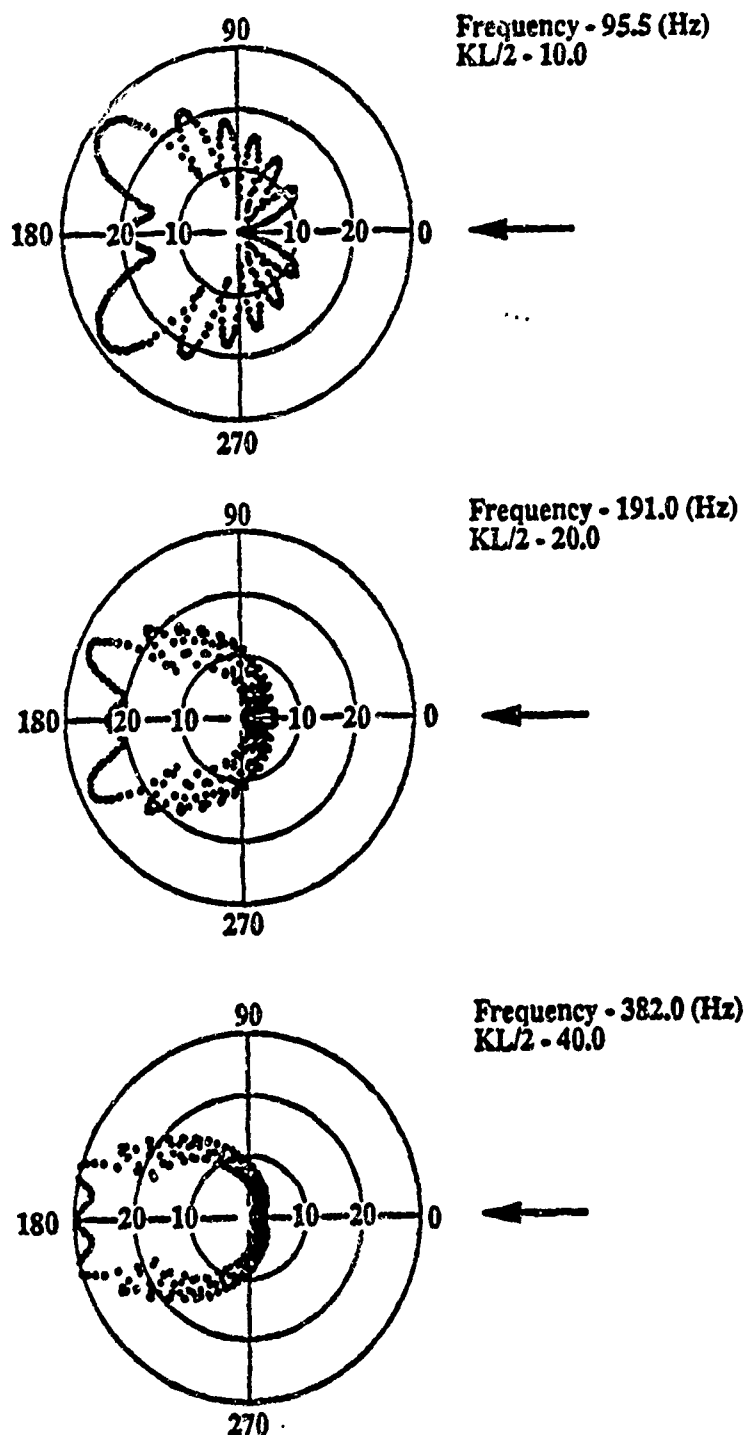


Fig. 1. Angular Distribution of Free Field Form Function for an Object Being Insonified Along the Principle Axis of Symmetry for  $KL/2$  Values of 10, 20, and 40.

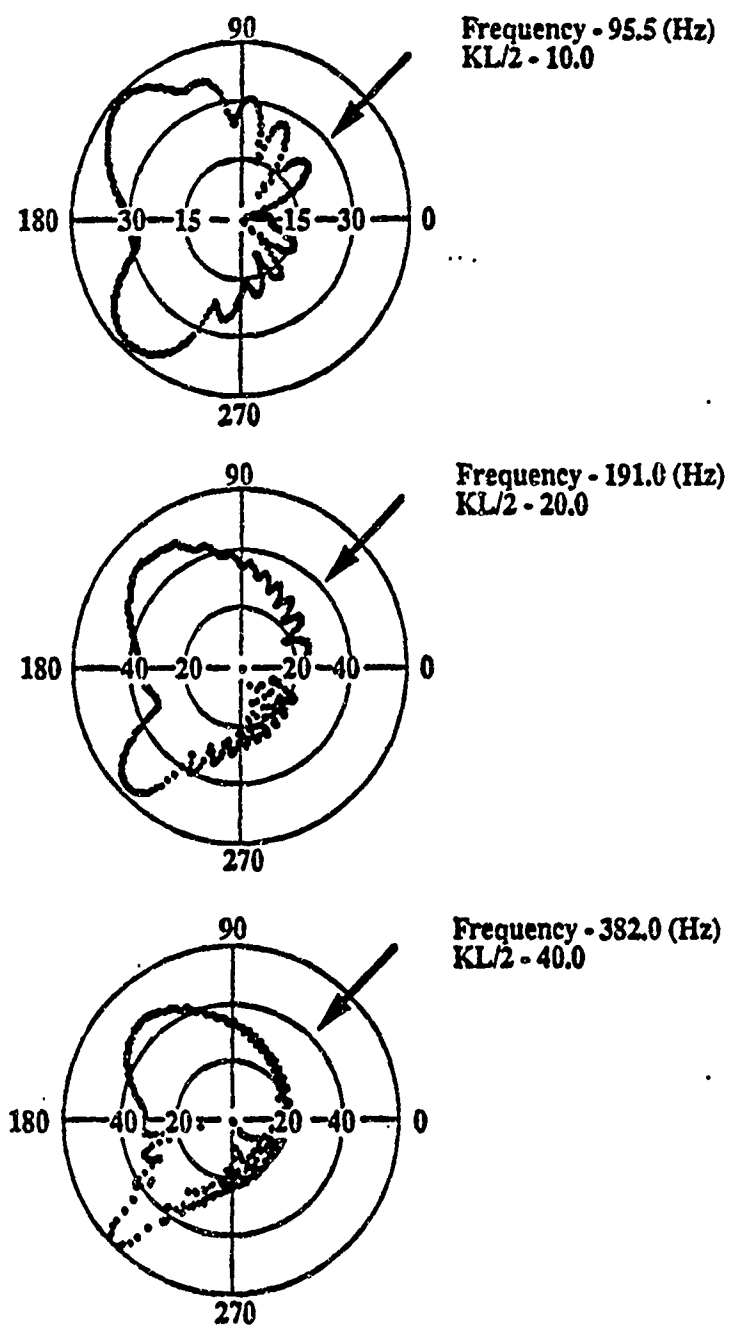


Fig. 2. Angular Distribution of Free Field Form Function for an Object Being Insonified 45 Degrees Relative to the Principle Axis of Symmetry for  $KL/2$  Values of 10, 20, and 40.

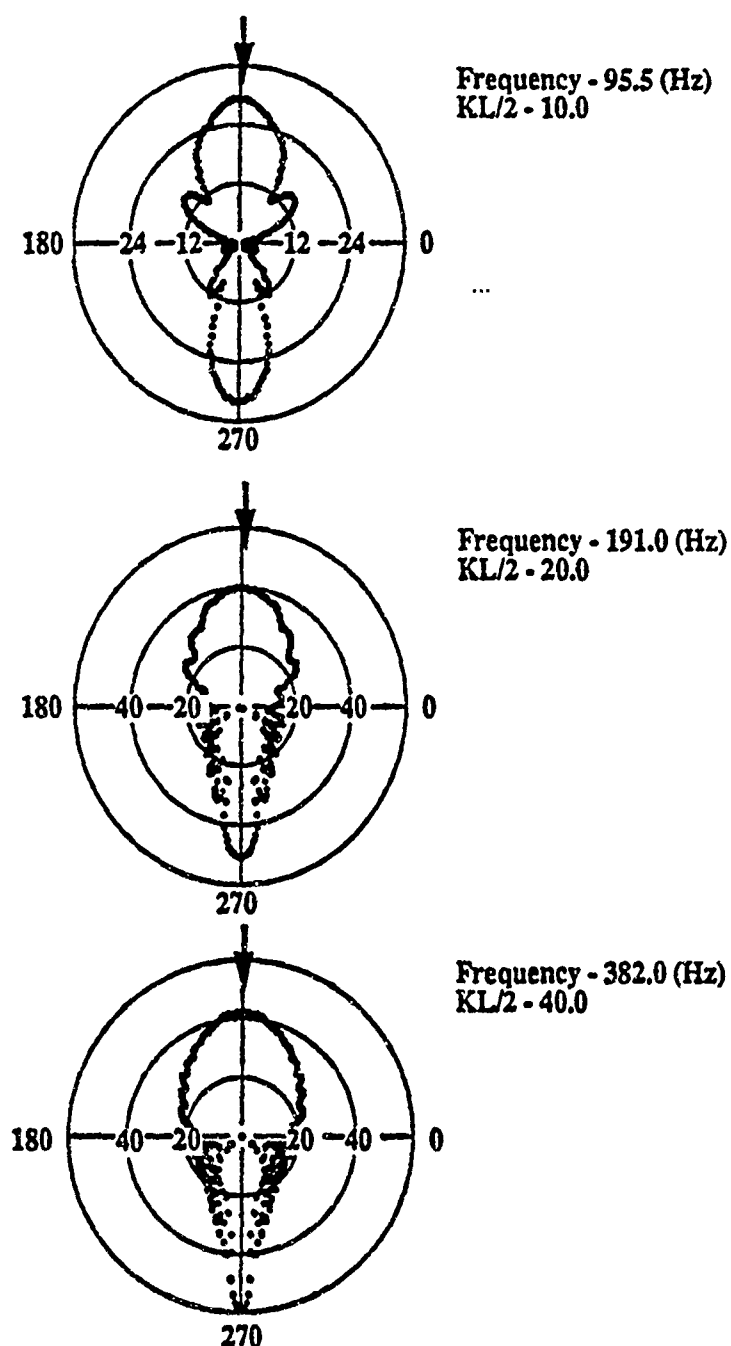


Fig. 3. Angular Distribution of Free Field Form Function for an Object Being Insonified 90 Degrees Relative to the Principle Axis of Symmetry for KL/2 Values of 10, 20, and 40.



# Near Field Scattering Examples Using the Extended Boundary Condition Method

In this section we will show representable examples of the near field form function. The parameters of Tables 1 and 2 from the last section will be used in this section. The near field form function takes the following form,

$$(2-23) \quad f(\theta) = \frac{2\rho}{a} \left( \left( \gamma_1^m \right)^{\frac{1}{2}} h_1^{(1)}(k\rho) P_1^m(\cos\theta) f_{11}^m A_{11}^m(\theta_i) \right).$$

The mathematical surface on which the form function will be evaluated is a spheroid with an aspect ratio of 5:1 a semi-major axis of 125(m) and a semi-minor axis of 25(m). This surface is not the surface of the object but a mathematical surface enclosing the object.

Figure 4 illustrates the field for 3 different frequencies as it is being insonified along the axis of symmetry. Note for the low frequency case (top figure) the field is oscillatory in appearance while in the intermediate (middle figure) and high (bottom figure) frequency cases the field is more strongly focused in the forward direction. The amplitude of the field increases with increasing frequency.

Figure 5 illustrates the case when the object is being insonified at an angle of 45 degrees relative to the principle axis of symmetry. We see the same traits as in the previous figures, with the low frequency case appearing wave-like while the intermediate and high frequency cases are void of this feature. In addition we see the reflected field is in the specular direction. Finally, we see that the amplitude of the forward diffracted field increases with increasing frequency.

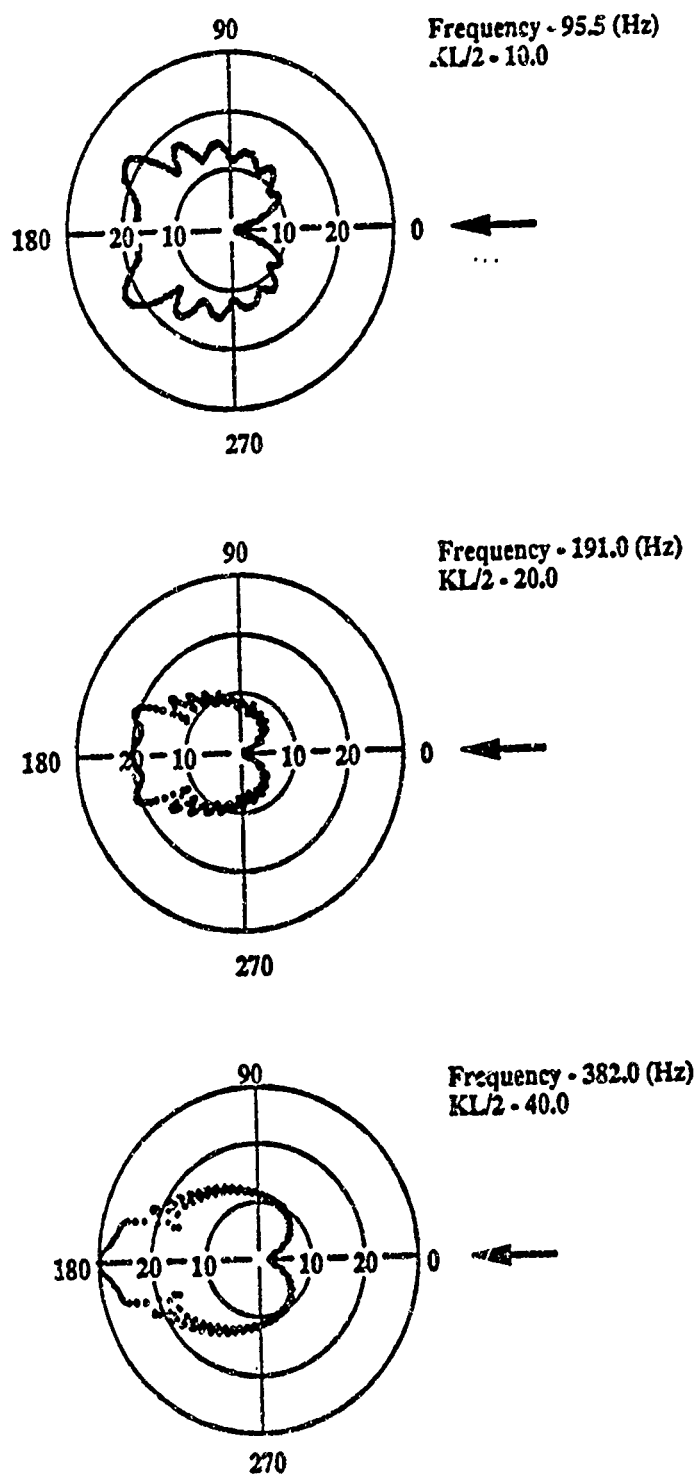


Fig. 4. Angular Distribution of Near Free Field Form Function for an Object Being Insonified Along the Principle Axis of Symmetry for  $KL/2$  Values of 10, 20, and 40.

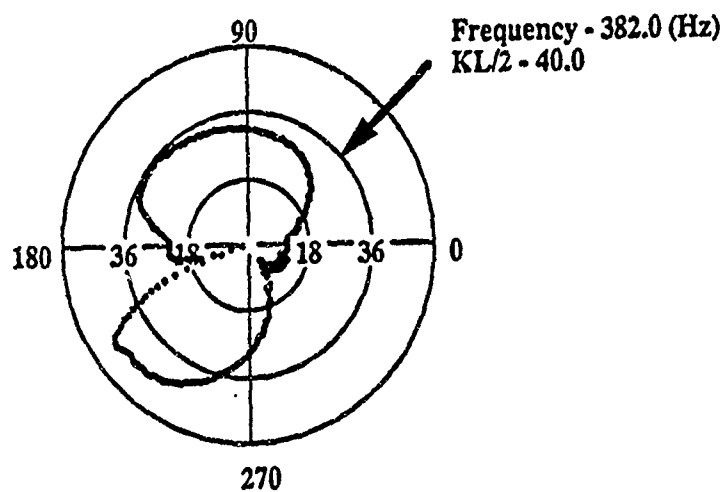
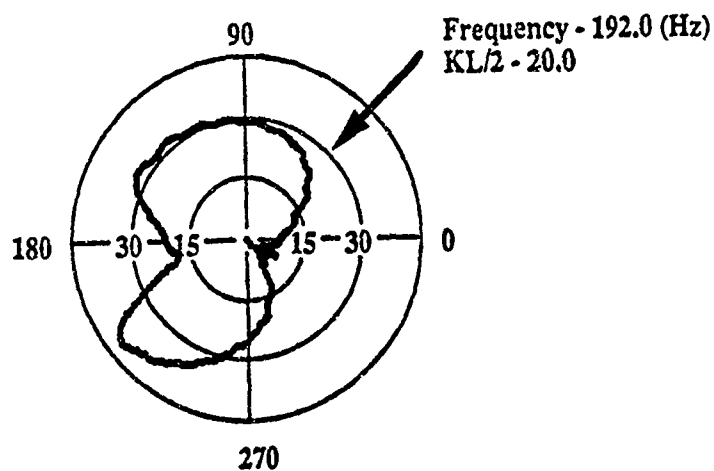
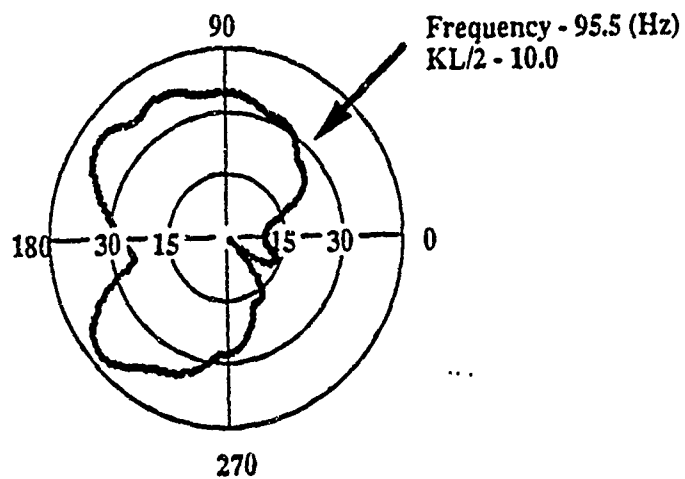


Fig. 5. Angular Distribution of Near Free Field Form Function for an Object Being Insonified 45 Degrees Relative to the Principle Axis of Symmetry for KL/2 Values of 10, 20, and 40.

Figure 6 illustrates the case when the object is being insonified at an angle of 90 degrees from the principal axis of symmetry. We note immediately that the field is not being focused as we increase in frequency but the amplitude is increasing in the forward direction. We also note that the backscattered field remains approximately constant for the three cases shown.

To observe the effect that range has on the field, the surface on which the field was solved was enlarged from a semi-major axis length of 125(m) to 250(m) and a semi-minor axis length of 25(m) to 50(m). The intermediate frequency of 191 (Hz) was selected for this evaluation. Figure 7 illustrates the results for the near field. Three incident angles were investigated 0, 45, and 90 degrees relative to the principle axis of symmetry. By the time the surface is at a range of 10 times the object's dimensions (which is for this case 25x5) the field is approximating the far field result rather well for the 0 and 45 degree incident case. Although this is not the case at 90 degrees, the trend is correct; that is the near field at the outer surface is approaching the far field result, but not as rapidly as for the cases when the object is insonified at an angle of 0 and 45 degrees.

We have shown the angular distribution plots because they will be used in later chapters. There are other ways of showing free space scattering results such as showing the forward or backscattered form function vs  $KL/2$ . In this way one can see resonance locations (in the case of elastic spheroids) or Franz waves (38) which occur when the specular and circumferential waves interact with one another at the field point. To include these would be outside the scope of this dissertation since they have no bearing on the problem. We will now turn our attention to acoustic propagation in a waveguide.

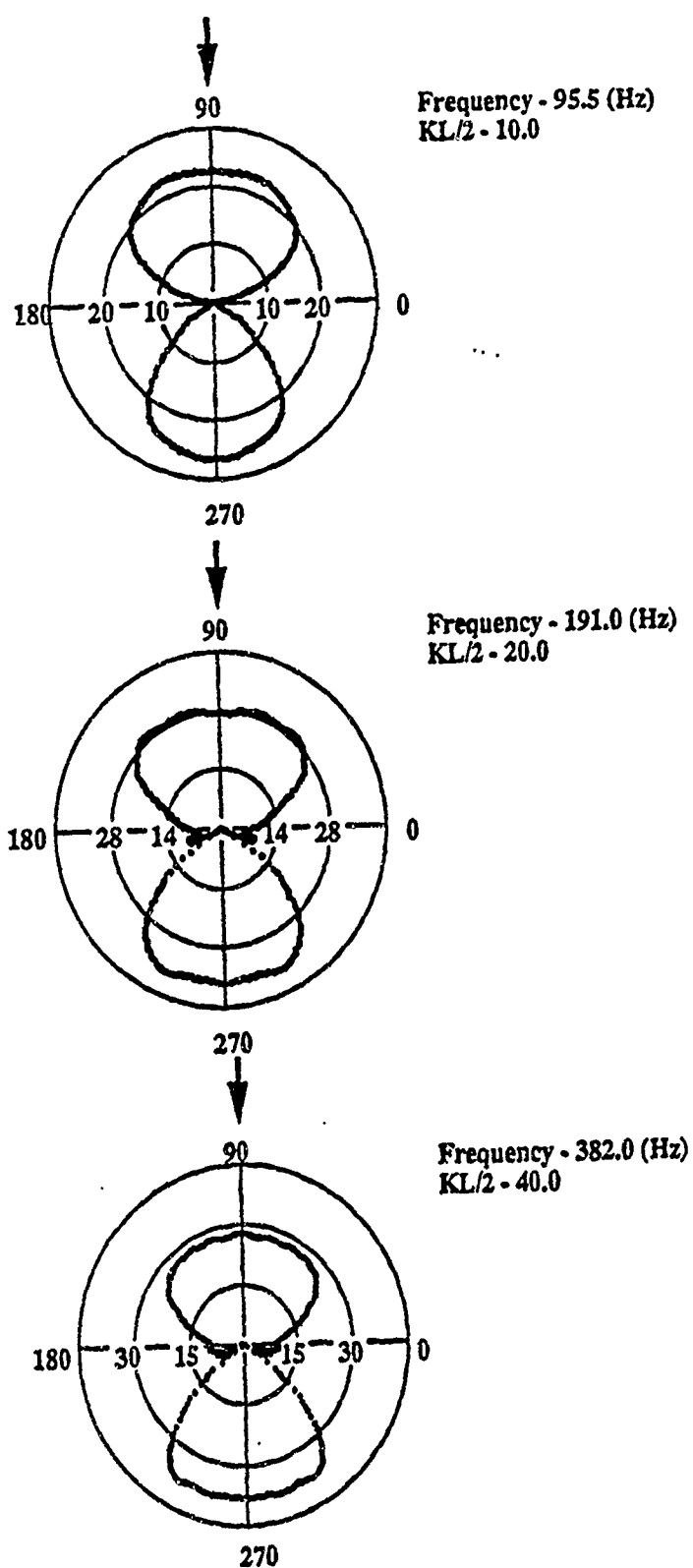


Fig. 6. Angular Distribution of Near Free Field Form Function for an Object Being Insonified 90 Degrees Relative to the Principle Axis of Symmetry for KL/2 Values of 10, 20, and 40.

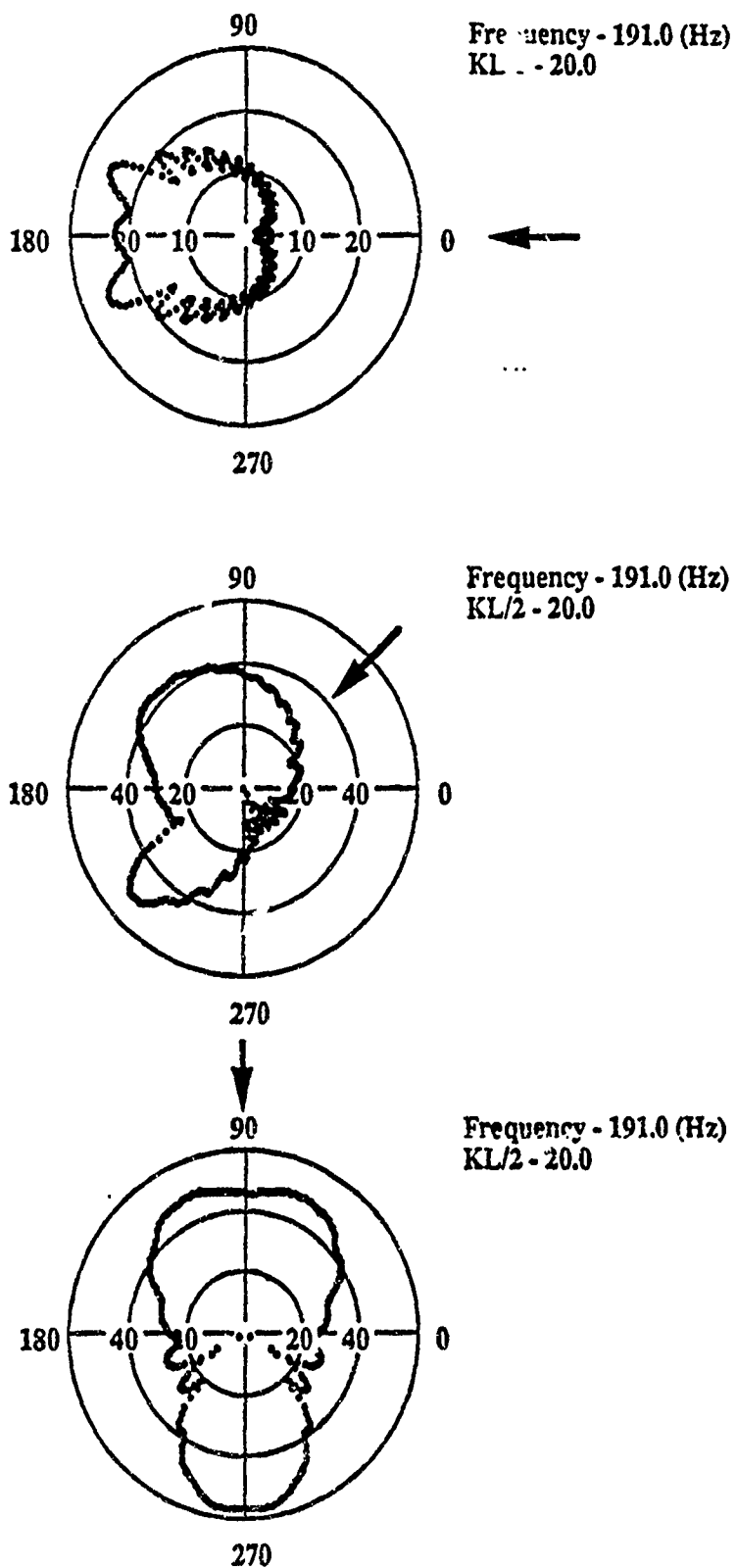


Fig. 7. Angular Distribution of Near Free Field Form Function for an Object Being Insonified 0, 45, and 90 Degrees Relative to the Principle Axis of Symmetry for a  $KL/2$  Value of 20.

## Chapter 3

### ACOUSTIC PROPAGATION IN A WAVEGUIDE

In this chapter we will describe how sound propagates through a shallow water waveguide. We assume that the sound is a small amplitude wavelike disturbance on the hydrodynamic background. We first describe the properties of the fluid equations. We will derive these equations from first principles, and then obtain the equations governing the sound field which we discuss in more detail from two points of view, using Normal Mode theory and Ray theory. We will finish by showing the connection between the two. This section follows the procedure outlined by Ahlowalia and Keller. (1)

#### Properties of a Fluid

Lets begin by considering a large fluid mass, with mass density of  $\rho$ . Within the fluid mass lets define an infinitesimal cube whose sides are of length  $dx$ ,  $dy$ ,  $dz$ . The center of the cube is labeled  $c$ . The pressure at  $c$  is denoted by  $P$ . Figure 8 illustrates the cube.

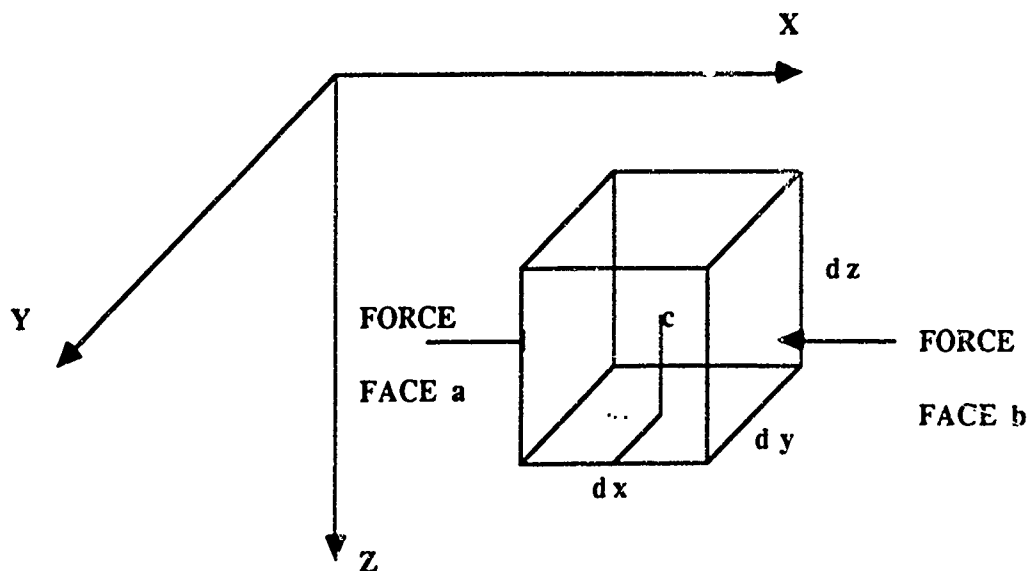


Fig. 8. Geometry for the fluid cube.

The force at c due to hydrostatic pressure on face a of the cube is,

$$(3-1) \quad \text{face}_a = \left( P - \frac{\partial P}{\partial x} \frac{dx}{2} \right) dy \, dz$$

and for face b

$$(3-2) \quad \text{face}_b = \left( P + \frac{\partial P}{\partial x} \frac{dx}{2} \right) dy \, dz$$

the net force in the x direction due to the pressure on these two faces is,

$$(3-3) \quad \left( P - \frac{\partial P}{\partial x} \frac{dx}{2} \right) dy \, dz - \left( P + \frac{\partial P}{\partial x} \frac{dx}{2} \right) dy \, dz = - \frac{\partial P}{\partial x} dx \, dy \, dz$$

By analogy the same procedure can be done for the net force in the y and z direction.

$$(3-4) \quad \text{net force in y direction} = - \frac{\partial P}{\partial y} dx \, dy \, dz$$



$$(3-5) \quad \text{net force in } z \text{ direction} = -\frac{\partial P}{\partial z} dx dy dz$$

The resulting net force is then,

$$(3-6) \quad \begin{aligned} dF_n &= -\left(\frac{\partial P}{\partial x} \hat{i} + \frac{\partial P}{\partial y} \hat{j} + \frac{\partial P}{\partial z} \hat{k}\right) dx dy dz \\ &= -\nabla P dx dy dz \end{aligned}$$

now taking the limit as  $dx$ ,  $dy$  and  $dz$  approach zero, gives for the net force

$$(3-7) \quad \frac{dF_n}{dt} = -\nabla P$$

Equation (3-7) represents the net force per unit volume at the point  $c$ . This is just the internal stress at point  $c$  due to hydrostatic pressure.

The above description was for a fluid without an acoustic source. At this time we introduce an acoustic source in the fluid medium. This is equivalent to having an external force present. We denote the external force by  $\epsilon f_a$  where  $\epsilon$  is a measure of the source strength. We also introduce the force per unit volume due to gravity,  $\rho g$ . Now the total force per unit volume at point  $c$  is equal to,

$$(3-8) \quad F_n = -\nabla P + \rho g + \epsilon f_a$$

We define  $u$  to be the velocity at point  $c$ . Then the acceleration is,

$$(3-9) \quad \begin{aligned} \frac{du}{dt} &= \frac{\partial u}{\partial t} + \frac{\partial u}{\partial x} \frac{dx}{dt} + \frac{\partial u}{\partial y} \frac{dy}{dt} + \frac{\partial u}{\partial z} \frac{dz}{dt} \\ &= \frac{\partial u}{\partial t} + (u \cdot \nabla)u \end{aligned}$$

Using Newton's 2nd law,  $m \mathbf{a} = m \frac{d\mathbf{u}}{dt} = \sum_i \mathbf{F}_i$ , we can write down an expression

that equates the sum of the forces to the mass density times  $d\mathbf{u}/dt$ .

$$\rho \left[ \frac{\partial \mathbf{u}}{\partial t} + (\mathbf{u} \cdot \nabla) \mathbf{u} \right] = -\nabla P + \rho \mathbf{g} + \epsilon f_a$$

$$(3-10) \quad \left[ \frac{\partial \mathbf{u}}{\partial t} + (\mathbf{u} \cdot \nabla) \mathbf{u} \right] = -\frac{\nabla P}{\rho} + \mathbf{g} + \frac{\epsilon f_a}{\rho}$$

This equation is called the equation of momentum.

### Derivation of the Continuity Equation

To derive the continuity equation, we need to define a volume of liquid ( $V$ ), surrounded by a surface  $\sigma$ . Gauss's Theorem (2) states that the rate of flow of the fluid out of the volume equals the flow of the volume through the surface  $\sigma$ .

$$(3-11) \quad \int_V (\nabla \cdot \mathbf{A}) dv = \int_\sigma \mathbf{A} \cdot d\mathbf{\sigma}$$

where  $\mathbf{A}$  is a vector field representing the flow of the fluid. Now the net flow of the fluid out of the volume through the surface results in a reduction of the density inside the volume.

$$(3-12) \quad \int_\sigma \rho \mathbf{u} \cdot d\mathbf{\sigma} = - \int_V \frac{\partial \rho}{\partial t} dv$$

Now substituting Eq. (3-11) in Eq. (3-12),

$$\int_v \nabla \cdot (\rho u) dv = - \int_v \frac{\partial \rho}{\partial t} dv$$

$$(3-13) \quad \nabla \cdot (\rho u) + \frac{\partial \rho}{\partial t} = 0$$

Eq. (3-13) is the continuity of mass equation.

#### Derivation of the Continuity Equation for Entropy

The procedure is the same as the last derivation. We define  $S$  to be the entropy density.

$$\int_v \frac{\partial (S\rho)}{\partial t} dv = - \int_{\sigma} (S\rho u) \cdot d\sigma$$

$$(3-14) \quad = - \int_v \nabla \cdot (S\rho u) dv$$

which through the limiting process becomes,

$$\rho \left[ \frac{\partial S}{\partial t} + (\nabla S) \cdot u \right] + S \left[ \frac{\partial \rho}{\partial t} + \nabla \cdot \rho u \right] = 0$$

the second term is zero and one is left with,

$$(3-15) \quad \frac{\partial S}{\partial t} + (\nabla S) \cdot u = 0$$

which is the continuity of entropy equation.

## Equation of State

Pressure can be considered a function of the fundamental quantities density and entropy. (1)

$$(3-16) \quad P = P(\rho, S)$$

which is just the equation of state.

...

## Bounded Fluid

Now the fluid will be bounded above by a free surface defined by  $z = \eta(x, y, t)$  and below by a rigid surface by  $z = -h(x, y)$ . The pressure above the free surface is constant and is equal to  $P_0$ . There are two boundary conditions on the top surface, the continuity of the pressure across the surface and the continuity of the normal component of velocity across the surface.

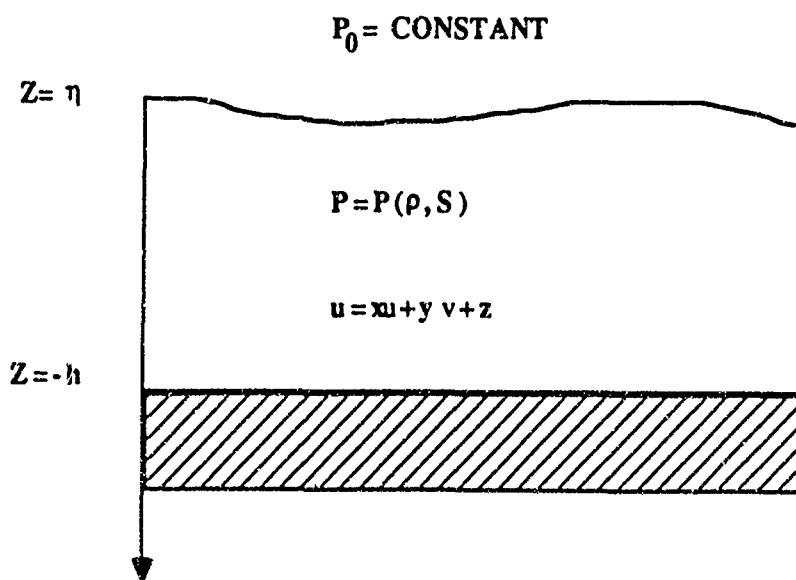


Fig. 9. Waveguide Geometry.

Using the first boundary condition we can equate the pressure on the opposite side of the boundary  $z=\eta$ .

$$(3-17) \quad P[x,y,\eta(x,y,t),t] = P_0 \quad \text{when } z=\eta(x,y,t)$$

To find the normal component of velocity, we need to construct the unit normal vector. Let  $\Phi$  be a scalar function defining the surface,

$$(3-18) \quad \Phi(x,y,z,t) = z - \eta(x,y,t)$$

The unit vector normal to  $\Phi$  is defined as

$$\frac{\nabla\Phi}{|\nabla\Phi|} = -\frac{x}{D} \frac{\partial\eta}{\partial x} - \frac{y}{D} \frac{\partial\eta}{\partial y} + \frac{z}{D}$$

$$(3-19) \quad \text{where} \quad \nabla\Phi = -x \frac{\partial\eta}{\partial x} - y \frac{\partial\eta}{\partial y} + z \quad \text{and} \quad |\nabla\Phi| = \sqrt{\left(\frac{\partial\eta}{\partial x}\right)^2 + \left(\frac{\partial\eta}{\partial y}\right)^2 + 1} = D$$

Evaluating the unit vectors  $x$ ,  $y$ , and  $z$ , we obtain

$$\begin{aligned}
 \frac{\nabla\Phi}{|\nabla\Phi|} \cdot x &\equiv \cos(\alpha) = -\frac{x}{D} \frac{\partial\eta}{\partial x} \cdot x - \frac{y}{D} \frac{\partial\eta}{\partial x} \cdot x + \frac{z}{D} \cdot x \\
 &= -\frac{1}{D} \frac{\partial\eta}{\partial x} \\
 \frac{\nabla\Phi}{|\nabla\Phi|} \cdot y &\equiv \cos(\beta) = -\frac{x}{D} \frac{\partial\eta}{\partial x} \cdot y - \frac{y}{D} \frac{\partial\eta}{\partial x} \cdot y + \frac{z}{D} \cdot y \\
 &= -\frac{1}{D} \frac{\partial\eta}{\partial y} \\
 (3-20) \quad \frac{\nabla\Phi}{|\nabla\Phi|} \cdot z &\equiv \cos(\gamma) = -\frac{x}{D} \frac{\partial\eta}{\partial x} \cdot z - \frac{y}{D} \frac{\partial\eta}{\partial x} \cdot z + \frac{z}{D} \cdot z \\
 &= \frac{1}{D}
 \end{aligned}$$

Now equating the normal component of velocity across the upper surface,

$$(3-21) \quad \frac{u}{D} \left( \frac{\partial\eta}{\partial x} \right) + \frac{v}{D} \left( -\frac{\partial\eta}{\partial y} \right) + \frac{w}{D} = \frac{1}{D} \frac{dx}{dt} \left( -\frac{\partial\eta}{\partial x} \right) + \frac{1}{D} \frac{dy}{dt} \left( -\frac{\partial\eta}{\partial y} \right) + \frac{1}{D} \frac{dz}{dt}$$

Since the derivatives of  $x$  and  $y$  with respect to  $t$  are zero, Eq. (3-20) can be rearranged into the following,

$$(3-22) \quad u \frac{\partial\eta}{\partial x} + v \frac{\partial\eta}{\partial y} + \frac{dz}{dt} = w \quad \text{when } z = \eta(x, y, t)$$

This is the requirement on the velocity components at the top surface. For the bottom surface let

$$(3-23) \quad \Phi(x, y, z, t) = z + h(x, y)$$

For a rigid bottom, the normal component of the velocity vanishes. If we apply the same procedures as were used for the top surface, the results for the bottom surface are,

$$(3-24) \quad \cos(\alpha) = \frac{1}{D} \frac{\partial h}{\partial x}, \quad \cos(\beta) = \frac{1}{D} \frac{\partial h}{\partial y}, \quad \cos(\gamma) = \frac{1}{D}$$

where

$$D \equiv \sqrt{\left(\frac{\partial h}{\partial x}\right)^2 + \left(\frac{\partial h}{\partial y}\right)^2 + 1}$$

$$(3-25) \quad u \frac{\partial h}{\partial x} + v \frac{\partial h}{\partial y} + w = 0 \quad \text{when } z = -h(x,y)$$

The last expression is the requirement on the velocity components at the bottom surface. When  $\epsilon$ , the measure of the source strength, is zero, the Eqs. (3-10), (3-13), (3-15), (3-16), (3-17), (3-22), (3-25) constitute what can be called the basic state equations. When  $\epsilon = 0$  this corresponds to a fluid containing no source. Because of this, the velocity  $u = 0$ . The equation of momentum Eq. (3-10) becomes

$$(3-26) \quad \nabla P = -\rho g.$$

Then the continuity equation for density becomes,

$$(3-27) \quad \frac{\partial \rho}{\partial t} = 0,$$

i.e.  $\rho$  is a function of coordinate only,  $\rho = \rho(z)$ .

The continuity equation for entropy becomes,

$$(3-28) \quad \frac{\partial S}{\partial t} = 0,$$

and the entropy is a function of the  $z$  coordinate only,  $S = S(z)$ . The pressure is still a function of density and entropy, i.e.  $P = P(r, S)$ . The pressure at  $z = 0$  is equal to the pressure on the other side of the top surface,  $P_0$ .

### Acoustic Quantities and Equations

We will now derive what Ahlowalia and Keller (1) call the acoustic quantities. The approach will be to consider the equations which depend on the source term  $\epsilon$ . By differentiating these equations with respect to  $\epsilon$  and evaluating the results at  $\epsilon = 0$ , we obtain the acoustic equations. The acoustic quantities are the individual functions, i.e.  $u$ ,  $P$  etc. differentiated with respect to  $\epsilon$  and evaluated at  $\epsilon = 0$ . Once the acoustic equations are obtained, the wave equation for the acoustic quantity  $P$  will be obtained along with the boundary conditions.



Thus

$$(3-29) \quad \dot{\mathbf{u}} = \left. \frac{\partial \mathbf{u}}{\partial \epsilon} \right|_{\epsilon=0}$$

$$(3-30) \quad \dot{P} = \left. \frac{\partial P}{\partial \epsilon} \right|_{\epsilon=0}$$

$$(3-31) \quad \dot{\rho} = \left. \frac{\partial \rho}{\partial \epsilon} \right|_{\epsilon=0}$$

$$(3-32) \quad \dot{S} = \left. \frac{\partial S}{\partial \epsilon} \right|_{\epsilon=0}$$

$$(3-33) \quad \dot{\eta} = \left. \frac{\partial \eta}{\partial \epsilon} \right|_{\epsilon=0}.$$

Starting with Eq. (3-10), the continuity of momentum equation, and evaluating it at  $\epsilon = 0$  yields

$$(3-34) \quad \frac{\partial \dot{\mathbf{u}}}{\partial t} + \left[ \left( \frac{\partial \mathbf{u}}{\partial \epsilon} \cdot \nabla \right) \mathbf{u} \right]_{\epsilon=0} + \left[ (\mathbf{u} \cdot \nabla) \frac{\partial \mathbf{u}}{\partial \epsilon} \right]_{\epsilon=0} = -\frac{1}{\rho} \nabla P + \frac{\dot{\rho}}{\rho^2} \nabla P + \frac{\mathbf{f}_a}{\rho}$$

We stated earlier that the velocity  $u = 0$  when  $\epsilon = 0$ . However that is not necessarily the case for  $\dot{u}$  :

$$(3-35) \quad \dot{u} = \left. \frac{\partial u}{\partial \epsilon} \right|_{\epsilon=0} \neq 0$$

nor is it for  $\frac{\partial \dot{u}}{\partial t}$  :

$$(3-36) \quad \frac{\partial \dot{u}}{\partial t} = \left. \frac{\partial^2 u}{\partial \epsilon \partial t} \right|_{\epsilon=0} \neq 0$$

Therefore Eq. (3-34) becomes,

$$(3-37) \quad \frac{\partial \dot{u}}{\partial t} = \frac{1}{\rho} \nabla P + \frac{\dot{\rho}}{\rho^2} \nabla P + \frac{f_a}{\rho}.$$

Now consider the continuity of mass equation, Eq. (3-13).

$$(3-38) \quad \left[ \nabla \cdot \left( \frac{\partial \rho}{\partial \epsilon} u \right) \right]_{\epsilon=0} + \left[ \nabla \cdot \rho \left( \frac{\partial u}{\partial \epsilon} \right) \right]_{\epsilon=0} + \frac{\partial \dot{\rho}}{\partial t} = 0$$

the first term is zero because  $\frac{\partial \rho}{\partial \epsilon}$  is equal to zero when evaluated at  $\epsilon = 0$ .

Therefore Eq. (3-38) becomes,

$$(3-39) \quad \left[ \nabla \cdot \rho \left( \frac{\partial u}{\partial \epsilon} \right) \right] + \frac{\partial \dot{\rho}}{\partial t} = 0.$$

Now consider the continuity equation for entropy,

$$(3-40) \quad \frac{\partial \dot{S}}{\partial t} + \left[ \nabla \frac{\partial S}{\partial \varepsilon} \cdot \mathbf{u} \right] \bigg|_{\varepsilon=0} + \left[ \nabla S \cdot \frac{\partial \mathbf{u}}{\partial \varepsilon} \right] \bigg|_{\varepsilon=0} = 0$$

the second term is zero because  $\frac{\partial S}{\partial \varepsilon}$  is equal to zero when evaluated at  $\varepsilon =$

0. Therefore Eq. (3-40) becomes,

$$(3-41) \quad \frac{\partial \dot{S}}{\partial t} + \left[ \nabla S \cdot \frac{\partial \mathbf{u}}{\partial \varepsilon} \right] = 0.$$

Now consider Eq. (3-16), the equation of state,

$$(3-42) \quad \begin{aligned} \dot{P}(\rho, S) &= \frac{\partial P(\rho, S)}{\partial \varepsilon} \bigg|_{\varepsilon=0} = \frac{\partial P}{\partial \rho} \frac{\partial \rho}{\partial \varepsilon} \bigg|_{\varepsilon=0} + \frac{\partial P}{\partial S} \frac{\partial S}{\partial \varepsilon} \bigg|_{\varepsilon=0} \\ &= \frac{\partial P}{\partial \rho} \dot{\rho} + \frac{\partial P}{\partial S} \dot{S} \end{aligned}$$

Now consider Eq. (3-17),

$$(3-43) \quad P(x, y, \eta, t) \Rightarrow \frac{\partial P}{\partial x} \frac{\partial x}{\partial \varepsilon} \bigg|_{\varepsilon=0} + \frac{\partial P}{\partial y} \frac{\partial y}{\partial \varepsilon} \bigg|_{\varepsilon=0} + \frac{\partial P}{\partial \eta} \frac{\partial \eta}{\partial \varepsilon} \bigg|_{\varepsilon=0} + \frac{\partial P}{\partial t} \frac{\partial t}{\partial \varepsilon} \bigg|_{\varepsilon=0} = 0$$

when  $z = \eta = 0$ , we can define  $\dot{P}$  at  $z=0$  as,

$$(3-44) \quad \dot{P} \equiv \left. \frac{\partial P(x, y, \eta, t)}{\partial \epsilon} \right|_{\epsilon=0} = \left. \frac{\partial P}{\partial x} \frac{\partial x}{\partial \epsilon} \right|_{\epsilon=0} + \left. \frac{\partial P}{\partial y} \frac{\partial y}{\partial \epsilon} \right|_{\epsilon=0} + \left. \frac{\partial P}{\partial t} \frac{\partial t}{\partial \epsilon} \right|_{\epsilon=0}$$

now Eq. (3-43) becomes,

$$(3-45) \quad \dot{P} + \frac{\partial P}{\partial \eta} \dot{\eta} = 0 \quad \text{when } z = \eta = 0.$$

Now consider Eq. (3-21)

$$(3-46) \quad \left. \frac{\partial \dot{\eta}}{\partial t} + \frac{\partial u}{\partial \epsilon} \frac{\partial \eta}{\partial x} \right|_{\epsilon=0} + u \left. \frac{\partial \dot{\eta}}{\partial x} \right|_{\epsilon=0} + \left. \frac{\partial v}{\partial \epsilon} \frac{\partial \eta}{\partial y} \right|_{\epsilon=0} + v \left. \frac{\partial \dot{\eta}}{\partial y} \right|_{\epsilon=0} = \left. \frac{\partial w}{\partial \epsilon} \right|_{\epsilon=0}$$

note that  $u = v = w = 0$  when  $\epsilon = 0$  since  $u = 0$ . And since  $\eta = \epsilon f_a(x, y, t)$ ,

$$(3-47) \quad \left. \frac{\partial \eta}{\partial \epsilon} \right|_{\epsilon=0} = 0 \quad \text{and} \quad \left. \frac{\partial \dot{\eta}}{\partial x} \right|_{\epsilon=0} = \left. \frac{\partial \dot{\eta}}{\partial y} \right|_{\epsilon=0} = 0 \quad \text{therefore Eq. (3-46)}$$

becomes,

$$(3-48) \quad \frac{\partial \dot{\eta}}{\partial t} = \dot{w} \quad \text{when } z = 0.$$

Now for the bottom condition, Eq. (3-25)

$$(3-49) \quad \dot{w} + \left( \frac{\partial u}{\partial \varepsilon} \frac{\partial h}{\partial x} \right) \Big|_{\varepsilon=0} + \left( u \frac{\partial h}{\partial x} \right) \Big|_{\varepsilon=0} + \left( \frac{\partial v}{\partial \varepsilon} \frac{\partial h}{\partial y} \right) \Big|_{\varepsilon=0} + \left( v \frac{\partial h}{\partial y} \right) \Big|_{\varepsilon=0} = 0$$

when  $z = -h(x,y)$ . The second and fourth terms are zero, and Eq.

(3-49) becomes,

$$(3-50) \quad \dot{w} + u \frac{\partial h}{\partial x} + v \frac{\partial h}{\partial y} = 0, \quad \text{when } z = -h(x,y).$$

Equations (3-37), (3-39), (3-41), (3-42), (3-45), (3-48), and (3-50) are called the acoustic equations. For instance,  $\dot{p}$  acts like a change in pressure due to source emissions. These equation must now be combined in order to obtain a single equation for the pressure and two boundary condition equations. We start by taking the partial derivative of Eq. (3-39) with respect to time; this leads to

$$(3-51) \quad \frac{\partial^2 \dot{p}}{\partial t^2} + \nabla \cdot \left( \frac{\partial \dot{p}}{\partial t} \mathbf{u} \right) + \nabla \cdot \left( \rho \frac{\partial \mathbf{u}}{\partial t} \right) = 0$$

The second term is zero since the density is not a function of time.

Equation (3-51) becomes,

$$(3-52) \quad \frac{\partial^2 \dot{p}}{\partial t^2} + \nabla \cdot \left( \rho \frac{\partial \mathbf{u}}{\partial t} \right) = 0.$$

From Eq. (3-37) we have an expression for  $\frac{\partial \mathbf{u}}{\partial t}$ . Using this expression in Eq. (3-52) gives after some simplifying,

$$(3-53) \quad \frac{\partial^2 \dot{\rho}}{\partial t^2} - \nabla^2 P + \nabla \cdot \left( \frac{\dot{\rho}}{\rho} \nabla P \right) = - \nabla \cdot \mathbf{f}_a.$$

It is important to remember that these quantities are a function of  $z$  only. Therefore the third term in Eq. (3-53) becomes,

$$(3-54) \quad \nabla \cdot \left( \frac{\dot{\rho}}{\rho} \nabla P \right) = \nabla \cdot \left( \frac{\dot{\rho}(z)}{\rho(z)} z \frac{\partial P}{\partial z} \right) = \nabla \cdot \left( \frac{\dot{\rho}(z)}{\rho(z)} z (-\rho g) \right) = -g \frac{\partial \dot{\rho}}{\partial z}$$

which, when substituted into Eq. (3-53) gives,

$$(3-55) \quad \frac{\partial^2 \dot{\rho}}{\partial t^2} - \nabla^2 P - g \frac{\partial \dot{\rho}}{\partial z} = - \nabla \cdot \mathbf{f}_a.$$

Now taking the partial derivative with respect to time of Eq. (3-41) gives,

$$(3-56) \quad \frac{\partial^2 S}{\partial t^2} + \frac{\partial \mathbf{u}}{\partial t} \cdot \nabla S + \mathbf{u} \cdot \nabla \frac{\partial S}{\partial t} = 0.$$

Since the entropy depends only on  $z$  in the basic state, the partial derivative with respect to time of the entropy is zero. Equation (3-56) becomes,

$$(3-57) \quad \frac{\partial^2 \dot{S}}{\partial t^2} + \frac{\partial \dot{u}}{\partial t} \cdot \nabla S = 0.$$

Now substituting Eq. (3-37) for  $\frac{\partial \dot{u}}{\partial t}$  in Eq. (3-57) gives,

$$(3-58) \quad \frac{\partial^2 \dot{S}}{\partial t^2} + \left[ -\frac{1}{\rho} \nabla P + \frac{\dot{\rho}}{\rho^2} \nabla P + \frac{f_a}{\rho} \right] \cdot \nabla S = 0.$$

Remembering that  $S = S(z)$  and  $P = P(z)$ , we obtain for  $\nabla S$  and for  $\nabla P$ ,

$$(3-59) \quad \nabla S = z \frac{\partial S}{\partial z} \quad \text{and} \quad \nabla P = z \frac{\partial P}{\partial z}.$$

Equation (3-58) becomes after some simplifying,

$$(3-60) \quad \frac{\partial^2 \dot{S}}{\partial t^2} - \frac{1}{\rho} \left( \frac{\partial \dot{P}}{\partial z} + \dot{\rho} g \right) \frac{\partial S}{\partial z} = - \frac{f_a}{\rho} \frac{\partial S}{\partial z}.$$

Now taking the partial derivative of Eq. (3-42) with respect to time twice gives,

$$(3-61) \quad \frac{\partial^2 \dot{P}}{\partial t^2} = \frac{\partial P}{\partial \rho} \frac{\partial^2 \dot{\rho}}{\partial t^2} + \frac{\partial P}{\partial S} \frac{\partial^2 \dot{S}}{\partial t^2}$$

Substituting Eq. (3-55) for  $\frac{\partial^2 \dot{p}}{\partial t^2}$  and Eq. (3-60) for  $\frac{\partial^2 S}{\partial t^2}$  in Eq. (3-61) yields,

$$(3-62) \quad \frac{\partial^2 \dot{P}}{\partial t^2} = \frac{\partial P}{\partial \rho} \left( \nabla^2 \dot{P} + g \frac{\partial \dot{p}}{\partial z} - \nabla \cdot \mathbf{f}_a \right) + \frac{1}{\rho} \frac{\partial P}{\partial S} \frac{\partial S}{\partial z} \left( \frac{\partial \dot{P}}{\partial z} + \dot{\rho} g - \mathbf{f}_{a3} \right).$$

...

Rearranging Eq. (3-62) gives,

$$(3-63) \quad \frac{\partial^2 \dot{P}}{\partial t^2} - \frac{\partial P}{\partial \rho} \nabla^2 \dot{P} = - \frac{\partial P}{\partial \rho} (\nabla \cdot \mathbf{f}_a) + \frac{1}{\rho} \frac{\partial P}{\partial S} \frac{\partial S}{\partial z} \left( \frac{\partial \dot{P}}{\partial z} + \dot{\rho} g - \mathbf{f}_{a3} \right) + g \frac{\partial P}{\partial \rho} \frac{\partial \dot{p}}{\partial z}.$$

We can neglect the last two terms of Eq. (3-63) since  $\dot{p} \approx 0$ ,  $\frac{\partial S}{\partial z} \approx 0$  and  $\frac{\partial \dot{p}}{\partial z} \approx 0$ .

This results in the wave equation,

$$(3-64) \quad \nabla^2 \dot{P} - \frac{1}{c^2} \frac{\partial^2 \dot{P}}{\partial t^2} = (\nabla \cdot \mathbf{f}_a) \quad \text{where} \quad \left( \frac{\partial P}{\partial \rho} \right)^{-1} = \frac{1}{c^2}.$$

The quantity  $c$  is just the speed of sound in the fluid. We will now obtain the equation governing the condition for the top boundary condition. Starting with Eq. (3-45)

$$(3-65) \quad \dot{P} + \eta \frac{\partial P}{\partial z} = 0$$



Equation (3-65) can be rewritten as

$$(3-66) \quad \dot{P} + \eta(-\rho g) = 0$$

but  $\eta < \dot{P}$  when  $z = 0$ . We can therefore neglect this term and Eq. (3-66) becomes,

$$(3-67) \quad \dot{P} = 0 \quad \text{when } z = 0.$$

Consider now the bottom condition. We start by taking the partial derivative of Eq. (3-50) with respect to time. This yields,

$$(3-68) \quad \frac{\partial \dot{w}}{\partial t} + \frac{\partial \dot{u}}{\partial t} \frac{\partial h}{\partial x} + \dot{u} \frac{\partial^2 h}{\partial t \partial x} + \frac{\partial \dot{v}}{\partial t} \frac{\partial h}{\partial x} + \dot{v} \frac{\partial^2 h}{\partial t \partial y} = 0,$$

since  $h$  is a function of  $x$  and  $y$  only, the partial derivative of  $h$  with respect to time is zero. Equation (3-68) becomes,

$$(3-69) \quad \frac{\partial \dot{w}}{\partial t} + \frac{\partial \dot{u}}{\partial t} \frac{\partial h}{\partial x} + \frac{\partial \dot{v}}{\partial t} \frac{\partial h}{\partial x} = 0.$$

We will use expressions for  $\frac{\partial \dot{w}}{\partial t}$ ,  $\frac{\partial \dot{u}}{\partial t}$  and  $\frac{\partial \dot{v}}{\partial t}$  from Eqs. (3-37). Equation (3-69)

becomes after the substitution,

$$(3-70) \quad \left[ -\frac{1}{\rho} \frac{\partial \dot{P}}{\partial z} + \frac{1}{\rho^2} \dot{\rho} \frac{\partial \dot{P}}{\partial z} + \frac{1}{\rho} f_3 \right] + \left[ -\frac{1}{\rho} \frac{\partial \dot{P}}{\partial x} + \frac{1}{\rho^2} \dot{\rho} \frac{\partial \dot{P}}{\partial x} + \frac{1}{\rho} f_1 \right] \frac{\partial h}{\partial x} + \left[ -\frac{1}{\rho} \frac{\partial \dot{P}}{\partial y} + \frac{1}{\rho^2} \dot{\rho} \frac{\partial \dot{P}}{\partial y} + \frac{1}{\rho} f_2 \right] \frac{\partial h}{\partial y} = 0$$

Since the bottom is defined as being rigid, no force is transmitted through the bottom, which says that  $f_1 = f_2 = f_3 = 0$  when  $z = -h(x,y)$ . Finally since  $\dot{p} \approx 0$  we can write Eq. (3-70) as,

$$(3-71) \quad \frac{\partial P}{\partial z} + \frac{\partial P}{\partial x} \frac{\partial h}{\partial x} + \frac{\partial P}{\partial y} \frac{\partial h}{\partial y} = 0 \quad \text{when } z = -h(x,y).$$

This is the bottom boundary condition. We have now defined a boundary value problem for the determination of the acoustic pressure using the wave equation, Eq. (3-64) which governs the problem, subject to the boundary condition at the surface, Eq. (3-67) and at the bottom, Eq. (3-71). In order to solve the problem, we need to know how the sound speed varies with depth, the depth of the waveguide and the source distribution. In underwater acoustics it is common to consider the source to be a point source producing a monochromatic time dependent wave. In this case, we now write the pressure as a function of distance ( $r$ ) and time ( $t$ ),

$$(3-72) \quad P(r, t) = e^{-i\omega t} P(r).$$

Substituting Eq. (3-72) into the wave equation, Eq. (3-64) yields,

$$(3-73) \quad e^{-i\omega t} \left( \nabla^2 P(r) + \frac{\omega^2}{c^2} P(r) \right) = \nabla \cdot \mathbf{f}_a.$$

Defining  $k \equiv \frac{\omega}{c_0}$  and  $n(z) \equiv \frac{c_0}{c(z)}$  where  $c_0$  is a reference sound speed and  $n(z)$  is the index of refraction we have,

$$(3-74) \quad \frac{\omega}{c(z)} = k n(z)$$

and Eq. (3-73) becomes,

$$(3-75) \quad e^{-i\omega t} \left( \nabla^2 P(r) + k^2 n^2(z) P(r) \right) = \nabla \cdot f_a.$$

Suppressing the time dependence of Eq. (3-75) and defining  $q(r)$  as that quantity in parenthesis, we obtain

$$(3-76) \quad q(r) \equiv \nabla^2 P(r) + k^2 n^2(z) P(r)$$

Equation (3-75) can be expressed as,

$$(3-77) \quad q(r) = \nabla \cdot f_a.$$

Equation (3-77) is sometimes referred to as the reduced wave equation or as the Helmholtz equation. (2) The boundary conditions are as follows,

$$(3-78) \quad \dot{P}(r, t) = 0 \Rightarrow P = 0 \text{ when } z = 0 \text{ and}$$

$$(3-79) \quad \frac{\partial P}{\partial z} + \frac{\partial P}{\partial x} \frac{\partial h}{\partial x} + \frac{\partial P}{\partial y} \frac{\partial h}{\partial y} = 0 \Rightarrow \frac{\partial P}{\partial z} + \frac{\partial P}{\partial x} + \frac{\partial P}{\partial y} = 0 \text{ when } z = -h(x, y).$$

The pressure due to Eq. (3-77) subject to the boundary conditions Eq. (3-78) and Eq. (3-79) do not determine  $P$  uniquely, since the homogeneous case ( $q(r)=0$ ) allows solutions which represent waves coming in from infinity. We will need to impose an additional condition in order to uniquely determine  $P$ . The additional condition is that the wave number,  $k$  will become complex,

$$(3-80) \quad k \rightarrow \frac{\omega}{c} + i\alpha.$$

This condition makes the outgoing wave decay to zero at infinity while the incoming wave will be infinite at infinity. The solution will be bounded at infinity and thus eliminate the incoming wave. The pressure  $P(r)$  now takes the following form,

$$(3-81) \quad P(r) \equiv \lim_{\alpha \rightarrow 0} P(r, \alpha).$$

We stated earlier that the source was assumed to be a point source. A point source can be represented by a delta function. The source distribution term,  $\nabla \cdot \mathbf{f}_a$  can be represented by,

$$(3-82) \quad \nabla \cdot \mathbf{f}_a = -\delta(\mathbf{r} - \mathbf{r}_0)$$

where  $\mathbf{r}_0$  is the source position. The point source will be normalized to produce unit strength. Assuming cylindrical coordinates,

$$(3-83) \quad \int_V \delta(\mathbf{r} - \mathbf{r}_0) d\mathbf{r} = 1.$$

Evaluating the integral in Eq. (3-83),

$$\begin{aligned} \int_V \delta(\mathbf{r} - \mathbf{r}_0) d\mathbf{r} &= \int_V f(r) \delta(r) \delta(z - z_0) r d\theta dr dz \\ (3-84) \qquad \qquad \qquad &= 2\pi r \end{aligned}$$

therefore 
$$\delta(\mathbf{r} - \mathbf{r}_0) = \frac{\delta(r) \delta(z - z_0)}{2\pi r} \text{ and } f(r) = \frac{1}{2\pi r}.$$

The Helmholtz equation becomes,

$$(3-85) \qquad \nabla^2 P(r) + k^2 n^2(z) P(r) = \frac{\delta(r) \delta(z - z_0)}{2\pi r}.$$

Recall that  $P(r, t) = P(r) e^{-i\omega t}$ .

We will now consider a simple waveguide, namely the homogeneous waveguide of constant depth. We will solve for the pressure using normal mode theory and ray theory. We will show the connection between the two methods. The normal mode solution is most useful at distances where only a finite number of propagating modes are present and the ray representation is most useful near the source where only the incident field and a few reflected waves need to be considered since spherical spreading diminishes the rest. Since both representations should give the same answer for the pressure (at least mathematically) at any range, we will convert the ray representation into the normal mode representation in order to show the connection.

### Normal Mode Theory

Normal Mode theory has been used to solve a variety of classical phenomena. Problems involving mechanical vibration reduce to that of the harmonic oscillator at small amplitudes of vibration as long as they remain within the elastic limits of the material. The concept is used in the context of finite, discrete systems of masses and springs, stretched strings and membranes, etc. The motion of these systems results in a number of so-called normal modes of vibration, each mode behaving in many ways like an independent harmonic oscillator. (3,4) Normal modes have also been used in bounded continua, such as the acoustic modes of a room. (5) The above examples have infinitely many but discrete eigenfrequencies. The concept of normal modes can also be applied to unbounded continua. An example is the treatment of electromagnetic modes of infinite space used in the quantum theory of fields. (6) Biot and Tolstoy (7) have generalized the procedure to conservative, unbounded, mechanical medium of any type. In principle, normal mode theory can be used to provide a unified point of view of all types of mechanical, electromagnetic, and electromechanical waves.

A water waveguide can be visualized by starting with a rectangular box of dimension  $a$ ,  $b$  and  $h$  corresponding to  $x$ ,  $y$  and  $z$  coordinates. Now allow  $a$  and  $b$  to approach infinity. If we chose appropriate boundary conditions at  $z=0$  and at  $z=h$ , one can generate what is commonly called the ideal or perfect waveguide. (8) The water that occupies the space between the horizontal interfaces at  $z=0$  and  $z=h$  has homogeneous properties. The ideal waveguide, sometimes called the slab waveguide, does not represent a 'real' world environment. A waveguide that better represents a real ocean waveguide would allow the speed of sound in the water to vary in depth and range, i.e.

$c(z,r)$ , where  $c$  is the local speed of sound at the depth position  $z$  and the range position  $r$ . In addition, the bathymetry would vary with range and there would be multiple layers of sediment beneath the water layer, each with its own sound speed, density, sound attenuation, shear speed and shear attenuation. We will consider two variations of the ideal waveguide in Chapters 5 and 6. We will, however, at this point proceed with a discussion of the ideal waveguide.

For a waveguide of constant depth and sound speed, we have  $c(z) \equiv c_0 =$  constant, and  $n(z) = c_0/c(z) = 1$ . The governing equation is the wave equation, Eq. (3-85), here written in its homogeneous form,

$$(3-86) \quad \nabla^2 P(r) + k^2 P(r) = 0$$

The boundary condition at the surface is that the pressure at the surface is zero, i.e. it is a pressure release surface.

$$(3-87) \quad P=0 \text{ at } z=0.$$

The bottom boundary condition is that the normal derivative of the pressure is zero, or that the bottom is rigid.

$$(3-88) \quad \frac{\partial P}{\partial z} = 0$$

The Laplacian in cylindrical coordinates is,(9)

$$(3-89) \quad \nabla^2(\ ) = \frac{1}{r} \frac{\partial}{\partial r} \left( r \frac{\partial(\ )}{\partial r} \right) + \frac{1}{r^2} \frac{\partial^2(\ )}{\partial \theta^2} + \frac{\partial^2(\ )}{\partial z^2}.$$

For this waveguide we assume cylindrical symmetry so the theta term vanishes

$$\frac{\partial^2(\ )}{\partial \theta^2} = 0. \quad \text{The Laplacian then becomes,}$$

$$(3-90) \quad \nabla^2(\ ) = \frac{1}{r} \frac{\partial}{\partial r} \left( r \frac{\partial(\ )}{\partial r} \right) + \frac{\partial^2(\ )}{\partial z^2}.$$

Since the pressure is a function of both  $z$  and  $r$  we can write,

$$(3-91) \quad P \sim \phi(z)\psi(r)$$

and Eq. (3-86) becomes,

$$(3-92) \quad \phi \frac{1}{r} \frac{d}{dr} \left( r \frac{d\psi}{dr} \right) + \psi \frac{d^2 \phi}{dz^2} + k^2 \phi \psi = 0$$

Equation (3-92) can be separated into two parts (possible only

when  $c=\text{constant}$  or  $c=c(z)$ ), one part containing terms dependent in  $r$  and the second part containing terms dependent in  $z$ .

$$(3-93) \quad \frac{1}{\psi} \frac{1}{r} \left[ \frac{d\psi}{dr} + r \frac{d^2 \psi}{dr^2} \right] + \frac{1}{\phi} \frac{d^2 \phi}{dz^2} + k^2 = 0.$$



Denoting  $\frac{d\psi}{dr}$  by  $\psi_r$ , etc Eq. (3-93) now becomes,

$$(3-94) \quad \frac{1}{\psi} \left[ \frac{1}{r} \psi_r + \psi_{rr} \right] = -\frac{1}{\phi} \phi_{zz} - k^2 = -k^2 a^2$$

where  $a^2$  on the RHS is the separation constant. The resulting Ordinary Differential Equations are

$$(3-95) \quad \phi_{zz} + \phi k^2 = k^2 a^2 \phi$$

$$(3-96) \quad \psi_{rr} + \frac{1}{r} \psi_r = -k^2 a^2 \psi.$$

Solving the depth dependent equation Eq. (3-95) first, we know that the general solution will be of the form,

$$(3-97) \quad \phi(z) = A \sin(kz\sqrt{1-a^2}) + B \cos(kz\sqrt{1-a^2}).$$

Due to the surface boundary condition, Eq. (3-87), the constant B in Eq. (3-97) must be equal to zero if Eq. (3-97) is to be a solution. Applying the bottom boundary condition to Eq. (3-97) we have,

$$(3-98) \quad \frac{\partial \phi(z)}{\partial z} = k\sqrt{1-a^2} [A \cos(kz\sqrt{1-a^2})] = 0 \quad |_{z=-h}$$

$$= \cos(k\sqrt{1-a^2}(-h)) = 0$$

$$= \cos(kh\sqrt{1-a^2}) = 0$$

In order for this to be true the following condition must be satisfied,

$$(3-99) \quad k h \sqrt{1 - a^2} = \left( \frac{(2n + 1)}{2} \right) \pi.$$

Solving for  $a$ , we obtain

$$(3-100) \quad a^2 = 1 - \frac{\left( n + \frac{1}{2} \right)^2 \pi^2}{k^2 h^2}$$

we see that there is a distinct, discrete solution  $a_n$ , for each  $n$ . Equation (3-100) can be written as,

$$(3-101) \quad a_n = \sqrt{1 - \frac{\left( n + \frac{1}{2} \right)^2 \pi^2}{k^2 h^2}} \quad n = 0, 1, 2, 3, \dots$$

The final solution for the depth equation is of the form,

$$(3-102) \quad \phi_n(z) = A_n \sin \left( k z \sqrt{1 - a_n^2} \right) \quad n = 0, 1, 2, 3, \dots$$

Now consider the solution to Eq. (3-96), which is Bessels' Equation of the first kind; solutions are,

$$(3-103) \quad \psi(r) = C_1 J_0(kar) + C_2 Y_0(kar).$$

We have the requirement that for any arbitrary  $z$  value,  $P$  is finite at  $r=0$ . This requires that  $C_2$  be equal to zero. Rewriting  $J_0(kar)$  in terms of a sum of Bessel Functions (10) of the first and second kind we obtain,

$$(3-104) \quad H_0^{(1)} = J_0 + iY_0$$

$$(3-105) \quad H_0^{(2)} = J_0 - iY_0 \quad \dots$$

$$(3-106) \quad \psi(r) = CH_0^{(1)}(kar) + DH_0^{(2)}(kar)$$

To solve for the constants in Eq. (3-106), we note that for the radiation condition, (as  $r \rightarrow \infty$ ),  $P$  behaves as an outgoing wave. Therefore, in the limit as  $r \rightarrow \infty$ ,  $\psi(r)$  needs to behave as an outgoing wave. Therefore, choose the Hankel function which represents an outgoing wave. We will use the large argument approximation to the Hankel function in order to determine which Hankel function to keep. The asymptotic form of the Hankel functions are (11)

$$(3-107) \quad H_0^{(1)}(kar) \rightarrow \sqrt{\frac{2}{\pi kar}} e^{i(kar - \frac{\pi}{4})}$$

$$(3-108) \quad H_0^{(2)}(kar) \rightarrow \sqrt{\frac{2}{\pi kar}} e^{-i(kar - \frac{\pi}{4})}$$

Equation (3-107) is an outgoing wave while Eq. (3-108) is an ingoing wave. Since we want an outgoing wave, we therefore choose  $D=0$ . And we are left with

$$(3-109) \quad \psi(r) = C H_0^{(1)}(k a_n r)$$

...

Our expression for the pressure now takes the following form,

$$(3-110) \quad P(r) = \varphi(z)\psi(r) = A_n \sin\left(kz\sqrt{1-a_n^2}\right) H_0^{(1)}(k a_n r)$$

Now the  $a_n$  are positive and either real or imaginary. If it is real then we have propagating modes (trapped modes). If  $a_n$  is imaginary we have non-propagating modes (evanescent modes). (12,13) That is to say that if,

$$(3-111) \quad H_0^{(1)}(k a_n r) \approx \sqrt{\frac{2}{\pi k a_n r}} e^{i(k a_n r - \frac{\pi}{4})},$$

and if  $a_n = i(l)$

$$H_0^{(1)}(k a_n r) \approx \sqrt{\frac{-2i}{\pi k l r}} e^{-l k r} e^{-i\frac{\pi}{4}}.$$

Thus, if  $a_n$  is imaginary,  $P(r)$  decays exponentially as  $r$  increases. We can also determine the number of propagating modes. Since  $a_n$  is positive we have by Eq. (3-100) the condition that

$$(3-112) \quad 1 \geq \left(n + \frac{1}{2}\right)^2 \left(\frac{\pi}{k h}\right)^2$$

we know from Eq. (3-101) that  $a_n$  is,

$$(3-113) \quad a_n = \sqrt{1 - \frac{\left(n + \frac{1}{2}\right)^2 \pi^2}{k^2 h^2}} \quad n = 0, 1, 2, 3, \dots, M$$

We can now set the limit on the number of propagating modes, by the following condition.

$$(3-114) \quad 1 \geq \left(M + \frac{1}{2}\right)^2 \left(\frac{\pi}{k h}\right)^2 \Rightarrow 1 \geq \left(M + \frac{1}{2}\right) \left(\frac{\pi}{k h}\right)$$

$$(3-115) \quad \frac{k h}{\pi} - \frac{1}{2} \geq M .$$

Our expression for the pressure now has the following form

$$(3-116) \quad P(r, z) = \sum_n A_n \sin\left(kz \sqrt{1 - a_n^2}\right) H_0^{(1)}(k a_n r)$$

In order to solve for  $A_n$  we evaluate  $\nabla^2 P$  using Eq. (3-90),

Eq. (3-117)

$$\nabla^2 P = \sum_n A_n \sin\left(kz \sqrt{1 - a_n^2}\right) \left\{ \left[ \frac{\partial^2}{\partial r^2} + \frac{1}{r} \frac{\partial}{\partial r} \right] H_0^{(1)}(k a_n r) - k^2 (1 - a_n^2) H_0^{(1)}(k a_n r) \right\}$$

We have from Eq. (3-85) the inhomogeneous wave equation that

$$(3-118) \quad \frac{-\delta(z-z_0)\delta(r)}{2\pi r} = \nabla^2 P + k^2 P$$

$$= \sum_n A_n \sin\left(kz\sqrt{1-a_n^2}\right) \left\{ \left[ \frac{\partial^2}{\partial r^2} + \frac{1}{r} \frac{\partial}{\partial r} \right] H_0^{(1)}(ka_n r) \right\}$$

...

With help from Appendix B we have,

$$(3-119) \quad \left[ \frac{\partial^2}{\partial r^2} + \frac{1}{r} \frac{\partial}{\partial r} \right] H_0^{(1)}(ka_n r) = \frac{4i\delta(r)}{2\pi r},$$

So that Eq. (3-118) becomes

$$(3-120) \quad \sum_n A_n \sin\left(kz\sqrt{1-a_n^2}\right) = \frac{i\delta(z-z_0)}{4}.$$

Utilizing the orthogonality condition for the depth eigenfunctions (see Eq. (3-102)), (14) we find that  $A_n$  equals

$$(3-121) \quad A_n = \frac{i}{2h} \sin\left(kz_0\sqrt{1-a_n^2}\right)$$

The expression for the pressure now becomes,

$$(3-122) \quad P(r, z) = \frac{i}{2h} \sum_n \sin\left(kz_0\sqrt{1-a_n^2}\right) \sin\left(kz\sqrt{1-a_n^2}\right) H_0^{(1)}(ka_n r).$$

# Ray Theory

We begin again with the time independent wave equation (Helmholtz) Eq. (3-85).

$$(3-123) \quad \nabla^2 P(r) + k^2 n^2(z) P(r) = -\frac{\delta(r) \delta(z - z_0)}{2\pi r}$$

the boundary conditions are the same as for the normal mode case namely that the pressure is zero at the surface and the normal derivative of the pressure is equal to zero when evaluated at the bottom. While we assumed cylindrical symmetry for the normal mode case, we will assume spherical symmetry for the ray representation. The range variable  $R$  is defined as,

$$(3-124) \quad R = \sqrt{r^2 + (z - z_0)^2}.$$

The Laplacian for spherical coordinates is, (15)

$$(3-125) \quad \nabla^2 = \frac{1}{R^2} \frac{\partial}{\partial R} \left( R^2 \frac{\partial}{\partial R} \right) + \frac{1}{R^2 \sin(\theta)} \frac{\partial}{\partial \theta} \left( \sin(\theta) \frac{\partial}{\partial \theta} \right) + \frac{1}{R^2 \sin^2(\theta)} \frac{\partial^2}{\partial \phi^2}.$$

Due to the spherical symmetry, the partial derivatives with respect to  $\theta$  and  $\varphi$  are zero. Therefore Eq. (3-125) becomes,

$$(3-126) \quad \nabla^2 = \frac{1}{R^2} \frac{\partial}{\partial R} \left( R^2 \frac{\partial}{\partial R} \right) \text{ and}$$

$$(3-127) \quad \nabla^2 P = \frac{\partial^2 P}{\partial R^2} + \left( \frac{2}{R} \frac{\partial P}{\partial R} \right).$$

We will use the homogeneous wave equation in order to obtain a general solution and then use the inhomogeneous wave equation to obtain the particular solution. Starting with the homogeneous Helmholtz equation, which is Eq. (3-85) with  $n(z) = 1$  and the source distribution term equal to zero

$$(3-128) \quad \nabla^2 P + k^2 P = 0.$$

Substituting in Eq. (3-127) for  $\nabla^2 P$  we obtain,

$$(3-129) \quad \frac{\partial^2 (RP)}{\partial R^2} + k^2 (RP) = 0.$$



The general solution to Eq. (3-129) is, (16)

$$\begin{aligned}
 RP &= e^{\pm ikR} \\
 P &= \frac{e^{\pm ikR}}{R} \\
 (3-130) \quad &= A \frac{e^{+ikR}}{R} + B \frac{e^{-ikR}}{R} \equiv P_0(R).
 \end{aligned}$$

We will use the radiation condition for spherical waves in order to decide which term in Eq. (3-130) to keep. The radiation condition is, (17)

$$(3-131) \quad \lim_{R \rightarrow \infty} R [P'_0(R) - ikP_0(R)] = 0.$$

When  $P_0(R) = A \frac{e^{+ikR}}{R}$ ,  $P'_0(R) = ikA \frac{e^{+ikR}}{R} - A \frac{e^{+ikR}}{R^2}$  and Eq. (3-130) becomes,

$$(3-132) \quad \lim_{R \rightarrow \infty} \left[ -\frac{Ae^{+ikR}}{R} \right] \Rightarrow 0.$$

When  $P_0(R) = B \frac{e^{-ikR}}{R}$ ,  $P'_0(R) = -ikB \frac{e^{-ikR}}{R} - B \frac{e^{-ikR}}{R^2}$  and Eq. (3-130) becomes,

$$(3-133) \quad \lim_{R \rightarrow \infty} [-2iBe^{-ikR}] \neq 0$$

therefore  $B = 0$  and Eq. (3-130) becomes,

$$(3-134) \quad P_0(R) = A \frac{e^{ikR}}{R}.$$

In order to determine the constant  $A$ , we will use the inhomogeneous wave Equation, Eq. (3-85). We integrate Eq. (3-85) over a volume  $v$  and then take the limit as  $R$  approaches zero:

$$(3-135) \quad \lim_{R \rightarrow 0} \left\{ \int_v \nabla \cdot (\nabla P) dv + k^2 \int_v P dv = - \int_v \delta(z - z_0) \frac{\delta(r)}{2\pi r} dv \right\}.$$

Evaluating the first term with help from Gauss's theorem, (18)

$$(3-136) \quad \int_v \nabla \cdot (\nabla P) dv = \oint_v \nabla P \cdot d\sigma$$

where  $\nabla P = R \left[ \frac{A i k e^{ikR}}{R} - \frac{A e^{ikR}}{R^2} \right]$  and  $d\sigma = R^2 \sin(\theta) d\theta d\phi$ . Equation (3-136)

becomes,

$$(3-137) \quad \int_v \nabla \cdot (\nabla P) dv = \int_{\theta=0}^{\pi} \int_{\phi=0}^{2\pi} A [ikR e^{ikR} - e^{ikR}] \sin(\theta) d\theta d\phi$$

$$= 4\pi A e^{ikR} [ikR - 1].$$

Now evaluating the second term in Eq. (3-135),

$$\begin{aligned}
 k^2 \int_V P dv &= k^2 A \int_0^R R e^{ikR} dR \int_0^\pi \sin\theta d\theta \int_0^{2\pi} d\phi \\
 (3-138) \qquad &= -4\pi A [e^{ikR}(ikR - 1) + 1]
 \end{aligned}$$

and finally evaluating the last term,

$$\begin{aligned}
 (3-139) \qquad - \int_V \delta(z - z_0) \frac{\delta(r)}{2\pi r} dv &= - \frac{1}{2\pi} \int_0^R \delta(r) dr \int_0^{-h} \delta(z - z_0) dz \int_0^{2\pi} d\phi \\
 &= -1
 \end{aligned}$$

Equation (3-135) becomes,

$$\begin{aligned}
 \lim_{R \rightarrow 0} \{ 4\pi A e^{ikR}(ikR - 1) - 4\pi A [e^{ikR}(ikR - 1) + 1] \} &= -1, \\
 (3-140) \qquad \lim_{R \rightarrow 0} \{ 4\pi A \} &= 1,
 \end{aligned}$$

therefore  $A = \frac{1}{4\pi}$  and Eq. (3-130) becomes,

$$(3-141) \qquad P_0(R) = \frac{e^{ikR}}{4\pi R}.$$

So far we have evaluated only the direct ray. We will now evaluate the ray which suffers a single interaction with the surface and the bottom. Any ray which reflects from the surface or bottom obeys the Law of Reflection, (19) which says that the angle of incidence is equal to the reflected angle.

Following the same procedure as for the direct ray, the phase and amplitude can be found for each ray. The ray that reflects once from the surface appears to come from a source located at  $r=0$ ,  $z=-z_0$  (see Fig. (10)). The pressure due to this reflected ray is equal to

$$(3-142) \quad P_{Sref}(r, z) = \frac{e^{ikR'}}{4\pi R'} \quad \text{where} \quad R' = \sqrt{r^2 + (z - (-z_0))^2}$$

and the pressure due to the direct ray is given by Eq. (3-141). The total pressure then at the point  $(r, z)$  due to the direct and surface reflected ray is just the sum of the individual pressures,

$$(3-143) \quad P(r, z) = \frac{e^{ikR}}{4\pi R} + R_s \frac{e^{ikR'}}{4\pi R'}$$

where  $R_s$  is the surface reflection coefficient. The boundary condition for the top surface states that the pressure is zero at  $z=0$ . Using this condition we can

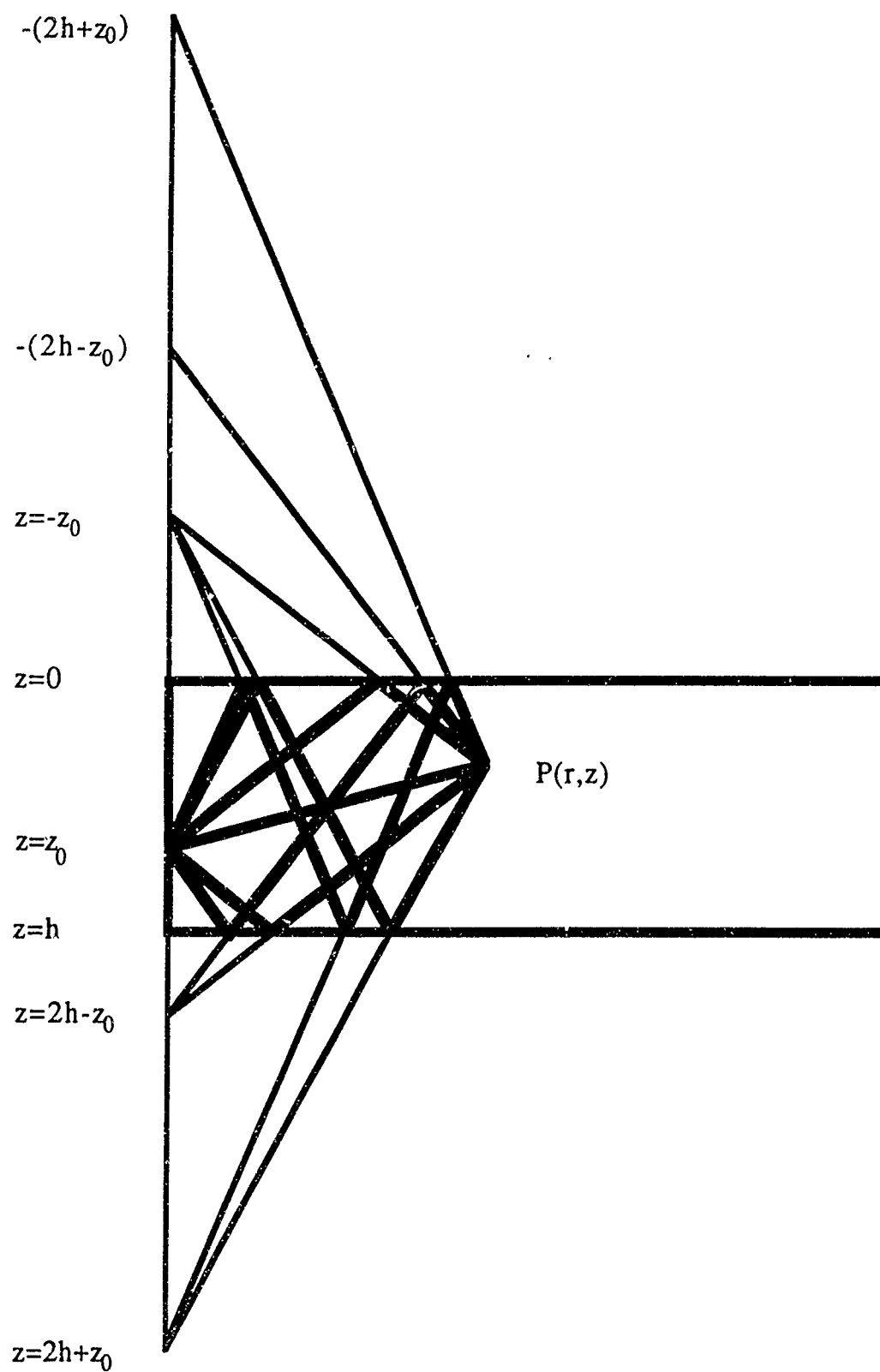


Fig. 10. Rays and their Image Point Source Location.

determine the surface reflection coefficient  $R_s$ .

$$(3-144) \quad P(r, z) \Big|_{z=0} = 0 = \frac{e^{ik\sqrt{r^2 + z_0^2}}}{4\pi\sqrt{r^2 + z_0^2}} [1 + R_s]$$

$$(3-145) \quad \text{whence } R_s = -1$$

Equation (3-143) now becomes,

$$(3-146) \quad P(r, z) = \frac{1}{4\pi} \left[ \frac{e^{ikR}}{R} - \frac{e^{ikR'}}{R'} \right]$$

To determine the pressure at a point  $P(r, z)$  due to the direct ray and a ray which interacts with the bottom once, we proceed as before. The ray which interacts once with the bottom appears to come from the point  $r=0, z=(2h+z_0)$  (see Fig. (10)). The pressure due to this bottom reflected ray is,

$$(3-147) \quad P_{\text{Bref}}(r, z) = \frac{e^{ikR''}}{4\pi R''} \quad \text{where } R'' = \sqrt{r^2 + (z - 2h + z_0)^2}$$

The total pressure at the point  $(r, z)$  due to the direct and the bottom reflected ray is,

$$(3-148) \quad P(r, z) = \frac{e^{ikR}}{4\pi R} + R_B \frac{e^{ikR''}}{4\pi R''}$$

where  $R_B$  is the bottom surface reflection coefficient. Utilizing the bottom boundary condition we can determine the bottom surface reflection coefficient ( $R_B$ ).

$$(3-149) \quad \left. \frac{\partial P(r, z)}{\partial z} \right|_{z=h} = \frac{e^{ik} \left[ \frac{ik(h-z_0)}{r^2 + (h-z_0)^2} - \frac{(h-z_0)}{\sqrt{r^2 + (h-z_0)^2}} \right]}{4\pi} (1 - R_B) = 0$$

it follows that  $R_B = 1$ . Equation (3-148) becomes

$$(3-150) \quad P(r, z) = \frac{1}{4\pi} \left[ \frac{e^{ikR}}{R} - \frac{e^{ikR''}}{R''} \right].$$

This procedure can be generalized for rays that incur multiple reflections. Each of these multiply reflected rays appears to come from an image point. These image points are located at,  $z = \pm z_0 + 2nh$ ,  $n = 0, \pm 1, \pm 2, \dots$

The pressure then is a summation of all these interactions,

$$(3-151) \quad P(r, z) = \frac{1}{4\pi} \sum_{n=-\infty}^{+\infty} (-1)^n \left\{ \frac{e^{ik\sqrt{r^2 + (z - (z_0 + 2nh))^2}}}{\sqrt{r^2 + (z - (z_0 + 2nh))^2}} - \frac{e^{ik\sqrt{r^2 + (z + (z_0 - 2nh))^2}}}{\sqrt{r^2 + (z + (z_0 - 2nh))^2}} \right\}$$

### Connection Between Normal Mode and Ray Theory

There is not a one to one correspondence between modes and rays. In the homogeneous waveguide, all images are required to form one mode and vice versa. However, since both theories give the same answer in the waveguide, they must be equal. We should therefore be able to convert from one representation to the other. With this in mind we will show that the Normal Mode solution and the Ray or Multiple Reflection method from the last section are mathematically connected. We begin with Eq. (3-151), the final form for the pressure in the Ray representation,

$$(3-152) \quad P(r, z) = \frac{1}{4\pi} \sum_{n=-\infty}^{+\infty} (-1)^n \left\{ \frac{e^{ik\sqrt{r^2 + (z - (z_0 + 2nh))^2}}}{\sqrt{r^2 + (z - (z_0 + 2nh))^2}} - \frac{e^{ik\sqrt{r^2 + (z + (z_0 - 2nh))^2}}}{\sqrt{r^2 + (z + (z_0 - 2nh))^2}} \right\}$$

which can be written as,

$$(3-153) \quad P(r, z) = \frac{1}{4\pi} \sum_{n=-\infty}^{+\infty} (-1)^n \{ P(r, z - z_0) - P(r, z + z_0) \}$$



writing  $(-1)^n = e^{in\pi}$  we write,

$$(3-154) \quad P(r, z) = P(r, \gamma_-) - P(r, \gamma_+)$$

where

$$P(r, \gamma_-) = \frac{1}{4\pi} \sum_{-\infty}^{+\infty} \frac{e^{ik\sqrt{r^2 + (\gamma_- - 2nh)^2} - in\pi}}{\sqrt{r^2 + (\gamma_- - 2nh)^2}}$$

and

$$P(r, \gamma_+) = \frac{1}{4\pi} \sum_{-\infty}^{+\infty} \frac{e^{ik\sqrt{r^2 + (\gamma_+ - 2nh)^2} - in\pi}}{\sqrt{r^2 + (\gamma_+ - 2nh)^2}}$$

using the Poisson Sum Formula (20)

$$(3-155) \quad \sum_{n=-\infty}^{+\infty} f(\alpha n) = \frac{\sqrt{2\pi}}{\alpha} \sum_{m=-\infty}^{+\infty} F\left(\frac{2m\pi}{\alpha}\right)$$

where

$$F(q) = \frac{1}{\sqrt{2\pi}} \int_{-\infty}^{+\infty} e^{-iq\omega} f(\omega) d\omega$$

setting  $\alpha = 2\pi$ , we obtain

$$(3-156) \quad \sum_{n=-\infty}^{+\infty} f(2\pi n) = \frac{1}{\sqrt{2\pi}} \sum_{m=-\infty}^{+\infty} F(m),$$

where

$$F(m) = \frac{1}{\sqrt{2\pi}} \int_{-\infty}^{+\infty} e^{-im\omega} f(\omega) d\omega.$$

We can now write  $f(2\pi n)$  as,

$$(3-157) \quad f(\omega) = \frac{e^{ik\sqrt{r^2 + \left(\gamma_- - \frac{\omega h}{\pi}\right)^2} - in\pi}}{\sqrt{r^2 + \left(\gamma_- - \frac{\omega h}{\pi}\right)^2}}$$

Now for  $P(r, \gamma_-)$  we have,

$$(3-158) \quad P(r, \gamma_-) = \frac{1}{8\pi^2} \sum \int_{-\infty}^{+\infty} \frac{e^{ik\sqrt{r^2 + \left(\gamma_- - \frac{\omega h}{\pi}\right)^2} - in\pi - i\frac{\omega}{2}}}{\sqrt{r^2 + \left(\gamma_- - \frac{\omega h}{\pi}\right)^2}};$$

likewise for  $P(r, \gamma_+)$ :

$$(3-159) \quad P(r, \gamma_+) = \frac{1}{8\pi^2} \sum \int_{-\infty}^{+\infty} \frac{e^{ik\sqrt{r^2 + \left(\gamma_+ - \frac{\omega h}{\pi}\right)^2} - in\pi - i\frac{\omega}{2}}}{\sqrt{r^2 + \left(\gamma_+ - \frac{\omega h}{\pi}\right)^2}}$$

If we set  $t = \gamma - \omega h/\pi$ , and  $d\omega = -\pi/h dt$  and restrict ourselves to  $P(r, \gamma_-)$  we find,

$$(3-160) \quad P(r, \gamma_-) = \frac{1}{8\pi h} \sum e^{-i\left(n + \frac{1}{2}\right)\frac{\pi}{h}} \int_{-\infty}^{+\infty} \frac{e^{ik\sqrt{r^2 + t^2} + i\left(n + \frac{1}{2}\right)\frac{t\pi}{h}}}{\sqrt{r^2 + t^2}} dt$$

If we introduce  $\Theta$  by  $t=r \sinh(\Theta)$ , and let  $q=(n+.5)\pi/kh$  then the integral of Eq. (3-160) becomes,

$$\begin{aligned}
 (3-161) \quad \int_{-\infty}^{+\infty} \frac{e^{ik\sqrt{r^2+t^2} + i(n+\frac{1}{2})\frac{t\pi}{h}}}{\sqrt{r^2+t^2}} dt &= \int_{-\infty}^{+\infty} \frac{e^{ikr\sqrt{1+\sinh^2(\Theta)} + ikqt}}{r\sqrt{1+\sinh^2(\Theta)}} r \cosh(\Theta) d\Theta \\
 &= \int_{-\infty}^{+\infty} e^{ikr\sqrt{1-q^2} \cosh(\Theta')} d\Theta'
 \end{aligned}$$

where  $\Theta' = \Theta + \tanh^{-1}(n)$

Now set  $\sinh(\Theta') = s/r$ , so that  $\cosh(\Theta') d\Theta' = ds/r$ ; then

$$(3-162) \quad \cosh(\Theta') = \frac{\sqrt{r^2+s^2}}{r} \quad d\Theta' = \frac{ds}{\sqrt{r^2+s^2}},$$

and Eq.(3-161) becomes,

$$(3-163) \quad \int_{-\infty}^{+\infty} e^{ikr\sqrt{1-q^2} \cosh(\Theta')} d\Theta' = \int_{-\infty}^{+\infty} \frac{e^{ik\sqrt{1-q^2} \sqrt{r^2+s^2}}}{(r^2+s^2)} ds$$

from Magnus et al., (21)

$$(3-164) \quad H_0^{(1)}(kx) = \frac{-i}{\pi} \int_{-\infty}^{+\infty} \frac{e^{ik\sqrt{x^2+t^2}}}{\sqrt{x^2+t^2}} dt$$

Eq.(3-163) then becomes,

$$(3-165) \quad \int_{-\infty}^{+\infty} \frac{e^{ik\sqrt{1-q^2}\sqrt{r^2+s^2}}}{(r^2+s^2)} ds =$$

$$i\pi H_0^{(1)}(kr\sqrt{1-q^2}) = i\pi H_0^{(1)}\left(kr\sqrt{1-\left(n+\frac{1}{2}\right)^2\frac{\pi^2}{k^2h^2}}\right)$$

Finally, Eq.(3-160) becomes,

$$(3-166) \quad P(r, \gamma_-) = \frac{i}{8h} \sum_n e^{-i\left(n+\frac{1}{2}\right)\frac{\pi}{h}} H_0^{(1)}\left(kr\sqrt{1-\left(n+\frac{1}{2}\right)^2\frac{\pi^2}{k^2h^2}}\right).$$

From Eq.(3-101),  $\frac{\gamma_n}{k} = \left(n + \frac{1}{2}\right)\frac{\pi}{kh}$ , where we have defined  $\gamma_n$  by

$$(3-167) \quad \gamma_n^2 = k^2(1 - a_n^2),$$

and now Eq.(3-166) becomes,

$$\begin{aligned}
 (3-168) \quad P(r, \gamma_-) &= \frac{i}{8h} \sum_n e^{-i\left(n + \frac{1}{2}\right)\frac{\pi}{h}} H_0^{(1)}\left(r \sqrt{k^2 - \gamma_n^2}\right) \\
 &= \frac{i}{8h} \sum_n e^{-i\gamma_n \gamma_-} H_0^{(1)}(K_n r).
 \end{aligned}$$

with  $K_n = \sqrt{k^2 - \gamma_n^2}$  and  $\gamma_- = z - z_0$

Finally Eq.(3-168) and the equivalent equation for  $z+z_0$  can be written as,

$$(3-169) \quad P(r, z - z_0) = \frac{i}{8h} \sum_n e^{-i\gamma_n(z - z_0)} H_0^{(1)}(K_n r)$$

$$(3-170) \quad P(r, z + z_0) = \frac{i}{8h} \sum_n e^{-i\gamma_n(z + z_0)} H_0^{(1)}(K_n r)$$

Subtracting Eq. (3-169) from Eq. (3-170) (see Eq. 3-153), one obtains an expression for  $P(r,z)$ ,

$$\begin{aligned}
 (3-171) \quad P(r, z) &= \frac{i}{8h} \sum_n \left( e^{-i\gamma_n(z-z_o)} - e^{-i\gamma_n(z+z_o)} \right) H_0^{(1)}(K_n r) \\
 &= \frac{i}{8h} \sum_n e^{-i\gamma_n z} \left( e^{i\gamma_n z_o} - e^{-i\gamma_n z_o} \right) H_0^{(1)}(K_n r) \\
 &= \frac{i}{8h} \sum_n e^{-i\gamma_n z} (2i \sin(\gamma_n z_o)) H_0^{(1)}(K_n r) \\
 &= \frac{i}{8h} \sum_n \cos(\gamma_n z) - i \sin(\gamma_n z) (2i \sin(\gamma_n z_o)) H_0^{(1)}(K_n r) \\
 &= \frac{i}{8h} \sum_n [2i \cos(\gamma_n z) \sin(\gamma_n z_o) + 2 \sin(\gamma_n z) \sin(\gamma_n z_o)] H_0^{(1)}(K_n r)
 \end{aligned}$$

Since the sum is from  $n=-\infty$  to  $n=+\infty$ , the first term in the RHS vanishes, and the second term equals  $4 \sin(\gamma_n z) \sin(\gamma_n z_o)$ . The result is

$$(3-172) \quad P(r, z) = \frac{i}{2h} \sum_n \sin(\gamma_n z) \sin(\gamma_n z_o) H_0^{(1)}(K_n r)$$

which is Eq. (3-122), the normal mode representation for the acoustic pressure.

## CHAPTER 4

### METHODS DESCRIBING SCATTERING FROM OBJECTS IN A WAVEGUIDE

In this chapter we begin by reviewing a few of the previous methods used to describe acoustical scattering from objects in a waveguide. While the methods given are not exhaustive, they represent the major work in this area. We then formulate the present method based on Huygens' principle. We conclude this chapter by obtaining a general expression for the scattered field far from the object.

#### Previously Used Methods

The problem of describing the scattering of acoustic, electromagnetic, etc. wave energy from an object in free space is difficult. One has to contend with numerical instabilities, ill posed problems etc. When one allows the object to be in a waveguide, the problem greatly increases in difficulty. One of the earliest methods which allowed for numerical answers was the sonar equation approach to scattering from an object in a waveguide. This method simply takes the transmission loss  $(-20\log(P/P_0))$  from the source to the object, adds the target strength due to a single plane wave incident on the object and then adds the transmission loss from the object to the field point (receiver). Mathematically it takes the following form,

$$(4-1) \quad U_s = TL_{so} + TS_{obj} + TL_{or}$$

The problem is that there is only a single number that one obtains from this process. There are no insights as to what physical processes are going on with the scattered field. This method however gave surprisingly good results when the field point (receiver) was in the forward direction, and when the frequency was high enough so that the scattered field was highly focused in the forward direction.

Another approach taken to solve this problem was to use ray theory and follow individual rays as they interacted with the boundaries and the object. In theory this method seems very plausible; however it becomes intractable in practice. This method has been developed by Evans (1) and Werby and Evans (2) for an object in a half space and the theory has been worked out for an object in a waveguide. A similar method has been presented by Hackman et al (3-5) for elastic objects including shells.

A more straightforward method was developed by Evans (6) which decomposed the incident field (composed of a sum of normal modes) into an equivalent plane wave representation. Each of these plane waves are allowed to insonify the object in order to generate the resulting scattered field. This field is then projected onto a cylinder which encloses the object and spans the depth of the waveguide. This method is known as the projection method and its results are compared with the present method in Appendix E.

A method based on matched asymptotics was devised by Collins (7,8) to derive an approximate expression for the field scattered from a spheroid. The matched asymptotic solution consists of an inner solution valid near the scatterer and an outer solution valid away from the scatterer. The two parts of the solution are matched in the region in which they are both valid. The resulting field is then propagated in the waveguide. Sen (9) has reported the use of matched asymptotics to describe scattering of acoustic waves in a



waveguide. He has reported that the method can be used to determine globally valid pressure field junction conditions near a boundary discontinuity.

In addition, Kleshchev has written several papers dealing with scattering from objects in waveguides and/or sound channels. (10-12)

### Proposed Method Based on Huygens' Principle

In 1690, C. Huygens published *Traite' de la Lumière*. In it he discussed a new principle pertaining to the propagation of light. Huygens proposed that at any instant  $t=t_0$ , a point source of light generates a disturbance which is propagated into the surrounding medium as an isolated spherical wave, expanding at the velocity of light. The disturbance at time  $t=t_1$  is due to a succession of disturbances at intermediate times between  $t=t_0$  and  $t=t_1$ . The actual effect then at time  $t=t_1$  is the result of all the secondary disturbances. In order to determine the effect at time  $t=t_1$  caused by an initial disturbance at  $t=t_0$  we then calculate the state at some intermediate time  $t=t'$ , then at  $t=t''$ , etc., until we are at time  $t=t_1$ .

There are some limitations imposed by this theory namely that the rectilinear propagation of light can be accounted for only by assuming that a secondary wave has no effect except at the point where it touches its envelope, and in addition it is assumed that since a disturbance on the envelope of the secondary waves propagates in both the forward and backward direction, only the forward propagated wave was to be considered.

The present method uses the basic concept of Huygens' principle namely that the field propagating away from the object and is not contributing to the field at the receiver can be neglected. Huygens reasoning for making this basic premise was based on empirical observations. We make this assumption

based on the type of propagation model used. Propagation models either allow for one way or two way propagation. If the model performs one way propagation then the field always propagates away from the source and no energy via backscattering from rough surfaces, rough bottoms or objects are considered. If on the other hand the propagation model allows energy to be received from the above mentioned mechanism then the field at the receiver can be dependent on what environmental or physical changes happens in the waveguide beyond the receiver. For example, if beyond the receiver there happens to be a sea-mount (an underwater mountain) then acoustical energy could be scattered back toward the receiver affecting the field at the receiver. In other words, for a one way model, the field at the receiver is dependent on what happens to the field as it approaches the object. For a two-way model, the field at the receiver is dependent on what happens before and after the field reaches the receiver.

We will now formulate the scattering problem. The geometry used to describe the scattering is shown in Fig. 11. There are two regions, region 1 which contains the scatterer, and region 2 where the field will be determined, region 2 is free of sources. The surface  $S_2$  encloses region 2. The surface  $S_2$  is taken to be at a large distance from the region of interest. The surface  $S_1$  is an arbitrary mathematical surface enclosing the scatterer. For free space or unbounded problems the surface  $S_2$  could be extended an infinite distance away from the area of interest.

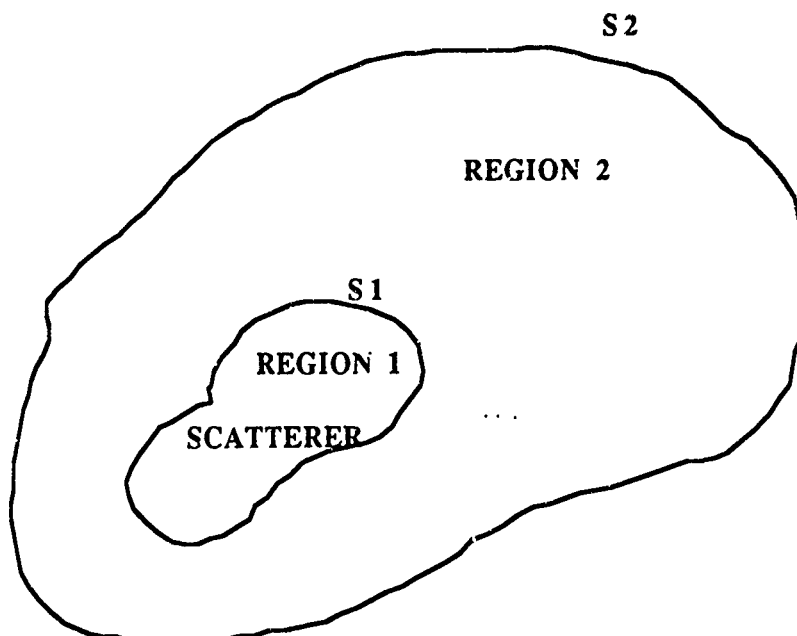


Fig. 11. General Scattering Geometry

For a problem dealing with scattering from an object in a waveguide, the surface S2 can still extend to infinity but this necessitates that we use the Green's function which satisfies the waveguide boundary condition. See Fig. 12.

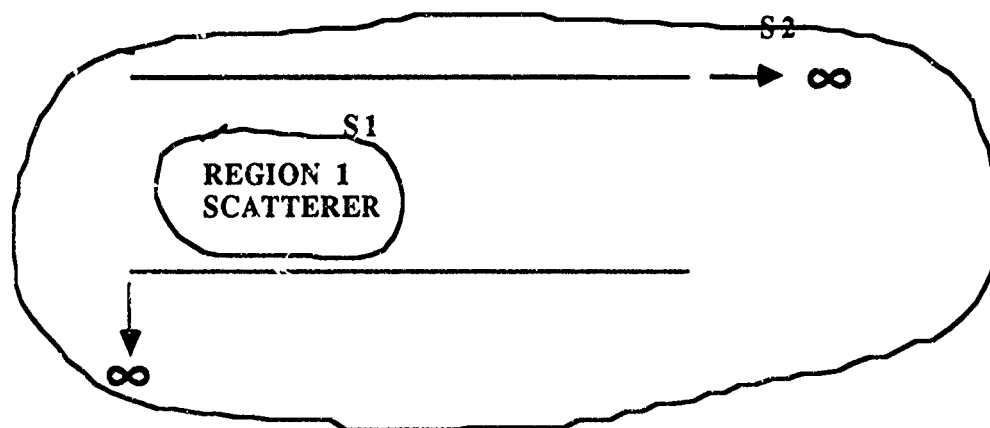


Fig. 12. Specific Scattering Geometry for a Waveguide.

To establish Huygens' principle for the scattering problem we need to develop a relation between the known value of the field on the surface  $S_1$  and the unknown value at the field point (receiver). Assume that the field is a solution to the scalar Helmholtz wave equation,

$$(4-2) \quad (\nabla^2 + k^2)\psi(\mathbf{x}) = 0$$

and the Greens function for the Helmholtz wave equation is given by,

$$(4-3) \quad (\nabla^2 + k^2)G(\mathbf{x} - \mathbf{x}') = \delta(\mathbf{x} - \mathbf{x}')$$

We obtain this relationship by invoking Green's theorem (13) which equates an integral of a vector function over a closed surface to an integral of a related function over the volume enclosed by the surface,

$$(4-4) \quad \int_V (\psi \nabla^2 G - G \nabla^2 \psi) d\mathbf{v}' = \int_S (\psi \nabla G - G \nabla \psi) \cdot \mathbf{n}' ds'$$

where in this case the surface  $S$  is  $S_1 + S_2$ . The surface integral is equal to zero when the observation point (receiver) and the singularities of  $\psi$  lie outside the surface  $S$ . (14) If the field point is inside the surface (in the bounded volume) then the scattered field becomes,

$$(4-5) \quad U_s = \psi(\mathbf{x}) = \int_S (\psi(\mathbf{x}') \nabla G(\mathbf{x} - \mathbf{x}') - G(\mathbf{x} - \mathbf{x}') \nabla \psi(\mathbf{x}')) \cdot \mathbf{n}' ds'$$

This integral over  $S$  is divided into two parts, over the surface  $S_1$  bounding the scatterer, and over the surface at infinity  $S_2$ . Since the field is propagated

from the surface S1 to S2, it is composed of outgoing waves. We are then left with the integral over S1. The scattered field then in region 2 becomes,

$$(4-6) \quad U_s = \int_{S1} (\psi(x') \nabla' G(x - x') - G(x - x') \nabla' \psi(x')) \cdot n' ds'$$

We replace  $\psi$  with the free field scattered field  $f$  which is valid at the surface S1. We then have,

$$(4-7) \quad U_s = \int_{S1} (f(x') \nabla' G(x - x') - G(x - x') \nabla' f(x')) \cdot n' ds'$$

This is the expression for the scattered field far from the object. We apply this expression to two different waveguides in the remaining two chapters.

## CHAPTER 5

### APPLICATION OF HUYGENS' METHOD TO AN ISOVELOCITY WAVEGUIDE

In this chapter we utilize the expression developed in Chapter 4 to describe scattering from an object in an isovelocity waveguide. We begin by solving for the acoustic pressure in the absence of an object. This will be the acoustic field incident upon the object. We then show the development of the near field scattered field (the field that is valid a short distance from the object). We then develop the far field scattered field. We end this chapter with an example which shows that the object acts as a source in the waveguide which implies that the object is now fully integrated into the waveguide. In Appendix E, there is a comparison of this method with the projection method described in Chapter 4.

We utilize Normal Mode theory to determine the incident field. We consider a waveguide consisting of an isovelocity layer of water over an isovelocity half-space. The bathymetry will be flat and the half-space will not support shear. Sound speed in the half-space will be greater than that of the water, as will its density and attenuation likewise will be greater than the water's. Such a waveguide is sometimes called the 'Pekeris' waveguide, (1) since Pekeris was the first to thoroughly investigate it. As mentioned in the introduction, we will solve the acoustic field scattered from the object first using the Pekeris waveguide and then using the more general multilayered waveguide. We begin by deriving the incident field for the Pekeris waveguide. The following development is based on Clay and Medwin. (2)

### Theory

The following assumptions will be made when deriving the incident field.

- 1) The object is in the farfield of the source, this allows the use of the asymptotic form of the Hankel Function.
- 2) There is a pressure release air-water interface, this would correspond to having a boundary condition such that the acoustic pressure evaluated at the surface is equal to zero, i.e.  $P(0)=0$ .
- 3) The pressure is continuous across the water layer (subscript 0) and the semi-infinite half-space (subscript 1). This corresponds to the following boundary condition,

$$P_0 = P_1 \Rightarrow \omega^2 \rho_0 \varphi_0 = \omega^2 \rho_1 \varphi_1 \Rightarrow \rho_0 \varphi_0 = \rho_1 \varphi_1$$

- 4) The vertical component of displacement is equal across the interface of layer 1 and layer 2. This corresponds to the following boundary condition,

$$\left( u_0 \right)_z = \left( u_1 \right)_z \Rightarrow \frac{\partial}{\partial z} \left( \frac{\partial \varphi_0}{\partial t} \right) = \frac{\partial}{\partial z} \left( \frac{\partial \varphi_1}{\partial t} \right)$$

$$\Rightarrow \frac{\partial}{\partial t} \left( \frac{\partial \varphi_0}{\partial z} \right) = \frac{\partial}{\partial t} \left( \frac{\partial \varphi_1}{\partial z} \right)$$

$$\Rightarrow \left( \frac{\partial \varphi_0}{\partial z} \right) = \left( \frac{\partial \varphi_1}{\partial z} \right)$$

- 5) The source produces a symmetric field about the z-axis.

We will write the particle displacement  $d$  and particle velocity  $u$  in terms of the displacement potential  $\Phi$ :

$$(5-1) \quad d = \bar{\nabla} \Phi \quad \text{and} \quad u = \bar{\nabla} \frac{\partial \Phi}{\partial t}.$$

Newton's Second Law becomes

$$(5-2) \quad \begin{aligned} \bar{\nabla} P &= -\rho \frac{\partial u}{\partial t} \\ &= \bar{\nabla} \left( -\rho \frac{\partial^2 \Phi}{\partial t^2} \right) \end{aligned}$$

Solving for the pressure  $P$ , we obtain

$$(5-3) \quad P = -\rho \frac{\partial^2 \Phi}{\partial t^2}$$

where  $\rho$  is the density of the medium. For a harmonic point source, the pressure is

$$(5-4) \quad P = \omega^2 \rho \Phi$$

The governing equation is the wave equation,

$$(5-5) \quad \nabla^2 P = \frac{1}{c^2} \frac{\partial^2 P}{\partial t^2}$$



where  $c$  (water sound speed) is time independent. Substituting Eq. (5-4) into the wave equation, Eq. (5-5) gives the time independent wave equation or Helmholtz equation, (3)

$$\begin{aligned}\nabla^2 \phi &= \frac{1}{c^2} \frac{\partial^2 \phi}{\partial t^2} \\ &= -\left(\frac{\omega^2}{c^2}\right) \phi\end{aligned}$$

or

$$(5-6) \quad \nabla^2 \phi + k^2 \phi = 0$$

where  $k^2 = \omega^2/c^2$ .

We will use the separation of variable technique (4) to solve this equation. The Laplacian in cylindrical coordinate is (5)

$$(5-7) \quad \nabla^2 = \frac{\partial^2}{\partial r^2} + \frac{1}{r} \frac{\partial}{\partial r} + \frac{1}{r^2} \frac{\partial^2}{\partial \Theta^2} + \frac{\partial^2}{\partial z^2}.$$

Because of azimuthal symmetry the Laplacian becomes

$$(5-8) \quad \nabla^2 = \frac{\partial^2}{\partial r^2} + \frac{1}{r} \frac{\partial}{\partial r} + \frac{\partial^2}{\partial z^2}$$

The solution to Eq. (5-6) will take the following form,

$$(5-9) \quad \phi = U(r)Z(z)$$

Using Eq. (5-8) and (5-9) in Eq. (5-6) yields two ordinary differential equations, in range and depth. The range solution is,

$$(5-10) \quad U''(r) + \frac{1}{r}U'(r) + K^2U(r) = 0$$

where  $K^2$  is the separation constant, and the depth solution is,

$$(5-11) \quad Z''(z) + (k^2 - K^2)Z = 0.$$

where  $k^2 = \frac{\omega^2}{c^2}$  is the characteristic wave number and Equation (5-11) can be rewritten as,

$$(5-12) \quad Z''(z) + \gamma^2 Z = 0$$

where  $\gamma^2 = k^2 - K^2$  and is the vertical component of the wave number. The wave number  $k$  is constant in the waveguide, while the horizontal component  $K$  and the vertical component  $\gamma$  will vary with mode number ( $k = \gamma + K$ ).

Consider now Eq. (5-10),

$$(5-10) \quad U''(r) + \frac{1}{r}U'(r) + K^2U(r) = 0$$

this is Bessels' equation of zeroth order, whose solution is the cylindrical Bessel function of the first kind  $J_0(Kr)$  (6) thus

$$(5-13) \quad U(r) = J_0(Kr)$$

The asymptotic form of  $J_0$  is (7)

$$J_0(Kr) \approx \sqrt{\frac{2}{\pi Kr}} \cos\left(Kr - \frac{\pi}{4}\right) \quad \text{when } Kr \gg 1$$

$$(5-14) \quad \approx \frac{1}{\sqrt{2\pi Kr}} \left[ e^{i\left(Kr - \frac{\pi}{4}\right)} + e^{-i\left(Kr - \frac{\pi}{4}\right)} \right]$$

The first exponential represents an incoming wave with infinite amplitude at infinity and the second exponential represents an outgoing wave with zero amplitude at infinity. We are interested only in the outgoing wave, therefore the solution for the radial term takes the following form,

$$(5-15) \quad U(r) \approx \frac{1}{\sqrt{2\pi Kr}} \left[ e^{-i\left(Kr - \frac{\pi}{4}\right)} \right].$$

Now consider the depth solution, Eq. (5-12):

$$(5-12) \quad Z''(z) + \gamma^2 Z = 0$$

the general solution has the following form, (8)

$$(5-16) \quad Z(z) = A \sin(\gamma z) + B \cos(\gamma z)$$

Implementing the surface boundary condition, that is  $P=0$  at  $z=0$ :

$$(5-17) \quad P(r, z, t) = 0$$

$$(5-18) \quad P(r, z, t) = \omega^2 \rho \phi e^{i\omega t} \propto \omega^2 \rho U(r) Z(z) e^{i\omega t}$$

$$(5-19) \quad P(r, 0, t) = \omega^2 \rho U(r) Z(0) e^{i\omega t}$$

which implies that  $Z(0)=0$ , hence  $B=0$  in Eq. (5-16). The depth Eigenfunction then takes the form,

$$(5-20) \quad Z(z) = A \sin(\gamma z)$$

At this time we will derive the characteristic equation for the waveguide. To accomplish this we define the reflection coefficient to be (9)

$$(5-21) \quad R = e^{i2\Phi}$$

The reflection coefficient for the upper layer is given by

$$(5-22) \quad R_u = -1 = e^{i2\Phi_u}$$

which implies  $2\Phi_u = \pi$  or  $\Phi_u = \frac{\pi}{2}$ . When the incident angle  $\Theta_0$  is less than the critical angle,  $\Theta_c$ , the reflection coefficient at the lower interface is given by (10)

$$(5-23) \quad R_l = \frac{\rho_1 c_1 \cos(\Theta_0) - \rho_0 c_0 \cos(\Theta_1)}{\rho_1 c_1 \cos(\Theta_0) + \rho_0 c_0 \cos(\Theta_1)} \quad \text{when} \quad 0 \leq \Theta_0 \leq \Theta_c$$

where by Snell's law  $\Theta_1 = \sin^{-1} \left( \frac{c_1}{c_0} \sin(\Theta_0) \right)$ . When the incident angle is larger than the critical angle and less than  $\frac{\pi}{2}$  the reflection coefficient for the lower interface is given by

$$(5-24) \quad R_1 = e^{i2\Phi_1} \quad \text{when } \Theta_c \leq \Theta_0 \leq \frac{\pi}{2}$$

and it follows that

$$(5-25) \quad \Phi_1 = \tan^{-1} \left( \frac{\rho_0 c_0 b_1}{\rho_1 c_1 \cos(\Theta_0)} \right)$$

where  $b_1 = \sqrt{\left( \frac{c_1}{c_0} \right)^2 \sin^2(\Theta_0) - 1}$ . Utilizing the boundary condition at

$z=h$ , and Eqs. (5-22, 5-24) the characteristic equation becomes,

$$(5-26) \quad R_u R_1 e^{-i2\gamma h} = e^{i2[\Phi_u + \Phi_1 - \gamma h]} = 1$$

rewriting the exponential using trigonometric functions gives,

$$(5-27) \quad \cos(2(\Phi_u + \Phi_1 - \gamma h)) + i \sin(2(\Phi_u + \Phi_1 - \gamma h)) = 1$$

which implies  $2(\Phi_u + \Phi_l - \gamma h) = 2\pi n, n = 0, \pm 1, \pm 2, \dots$

or

$$\gamma_m h - \Phi_u - \Phi_l = (m - 1)\pi \quad m=1, 2, 3, \dots$$

or

$$(5-28) \quad \gamma_m h = \left(m - \frac{1}{2}\right)\pi + \Phi_l.$$

...

We can rewrite the horizontal and vertical components of the wave number as the following,

$$K_m = k \sin(\Theta_m) = \frac{\omega}{c_0} \sin(\Theta_m)$$

and

$$(5-29) \quad \gamma_m = k \cos(\Theta_m) = \frac{\omega}{c_0} \cos(\Theta_m)$$

Equation (5-28) can be solved for  $\omega$  with the help of Eq. (5-29) with the result that

$$(5-30) \quad \omega = \frac{c_0 \left[ \left(m - \frac{1}{2}\right)\pi + \Phi_l \right]}{h \cos(\Theta_m)}$$

which can be rewritten as

$$(5-31) \quad \frac{\omega h \cos(\Theta_m)}{c_0} - \left(m - \frac{1}{2}\right)\pi + \Phi_l = \tan^{-1} \left( \frac{\rho_0 c_0 b_1}{\rho_1 c_1 \cos(\Theta_m)} \right).$$

This can be put in the following form,

$$\begin{aligned}
 h\gamma_m - \left(m - \frac{1}{2}\right)\pi &= \tan^{-1} \left( \frac{\rho_0 \frac{\omega}{c_1} b_1}{\rho_1 \frac{\omega}{c_0} \cos(\Theta_m)} \right) \\
 (5-32) \qquad \qquad \qquad &= \tan^{-1} \left( \frac{\rho_0 \frac{\omega}{c_1} b_1}{\rho_1 k \cos(\Theta_m)} \right)
 \end{aligned}$$

where  $\frac{\omega}{c_1} b_1 = \sqrt{\left(\frac{\omega}{c_0}\right)^2 \sin^2(\Theta_m) - \left(\frac{\omega}{c_1}\right)^2}$ .

Defining

$$(5-33) \qquad b_m \equiv \sqrt{K_m^2 - k_1^2}$$

where  $k_1 = \frac{\omega}{c_1}$ . We now rewrite the right hand side of Eq. (5-32) as the following,

$$(5-34) \qquad \tan^{-1} \left( \frac{\rho_0 \frac{\omega}{c_1} b_1}{\rho_1 k \cos(\Theta_m)} \right) = \tan^{-1} \left( \frac{\rho_0 b_m}{\rho_1 \gamma_m} \right).$$

so that

$$(5-35) \qquad h\gamma_m - \left(m - \frac{1}{2}\right)\pi = \tan^{-1} \left( \frac{\rho_0 b_m}{\rho_1 \gamma_m} \right)$$

or

$$(5-36) \quad \tan\left(h\gamma_m - \left(m - \frac{1}{2}\right)\pi\right) = \left(\frac{\rho_0 b_m}{\rho_1 \gamma_m}\right)$$

The left hand side of Eq. (5-36) can be rewritten as

$$(5-37) \quad \tan\left(h\gamma_m - \left(m - \frac{1}{2}\right)\pi\right) = \frac{\sin\left(h\gamma_m - \left(m - \frac{1}{2}\right)\pi\right)}{\cos\left(h\gamma_m - \left(m - \frac{1}{2}\right)\pi\right)} = \frac{\mp \cos(h\gamma_m)}{\pm \sin(h\gamma_m)} = -\cot(h\gamma_m)$$

After using Eq. (5-37) in Eq. (5-36), the following equality now holds,

$$-\cot(h\gamma_m) = \left(\frac{\rho_0 b_m}{\rho_1 \gamma_m}\right)$$

or

$$(5-38) \quad \tan(h\gamma_m) = -\left(\frac{\rho_1 \gamma_m}{\rho_0 b_m}\right)$$

Equation (5-38) is the characteristic equation for the isovelocity water column overlying an isovelocity half space. It will be used to solve for the eigenvalues  $\gamma_m$ , which are solutions to the depth eigenfunction equation, Eq. (5-12).



Now we will derive the depth eigenfunction for the second layer. The sound pressure is exponentially damped because the incident sound field is totally reflected. Using Snell's law, (11)

$$(5-39) \quad \frac{\sin(\Theta_0)}{c_0} = \frac{\sin(\Theta_1)}{c_1}$$

This implies that

$$\left(\frac{c_1}{c_0}\right)^2 \sin^2(\Theta_0) = 1 - \cos^2(\Theta_1)$$

or

$$(5-40) \quad \cos(\Theta_1) = \sqrt{1 - \left(\frac{c_1}{c_0}\right)^2 \sin^2(\Theta_0)}$$

The argument in the radical is positive if  $\Theta_0 < \Theta_c$  that is, if the incident angle is less than the critical angle. At the critical angle,

$$(5-41) \quad \frac{\sin(\Theta_c)}{c_0} = \frac{\sin(90)}{c_1} \Rightarrow \sin(\Theta_c) = \frac{c_0}{c_1}$$

and

$$(5-42) \quad \cos(\Theta_1) = \sqrt{1 - \left(\frac{c_1}{c_0}\right)^2 \sin^2(\Theta_0)} = 0.$$

When  $\Theta_0 > \Theta_c$ , the argument inside the radical of Eq. (5-42) is negative:

$$\begin{aligned} \cos(\Theta_1) &= \sqrt{-\left[1 - \left(\frac{c_1}{c_0}\right)^2 \sin^2(\Theta_0)\right]} \\ (5-43) \quad &= i \sqrt{\left(\frac{c_1}{c_0}\right)^2 \sin^2(\Theta_0) - 1} \end{aligned}$$

Modes will propagate only in the upper layer only for  $\Theta_0 > \Theta_c$ .

Therefore,

$$\begin{aligned} k_1 \cos(\Theta_1) &= i \sqrt{\left(\frac{\omega}{c_1}\right)^2 \left(\frac{c_1}{c_0}\right)^2 \sin^2(\Theta_0) - k_1^2} \\ (5-44) \quad &= i \sqrt{k^2 \sin^2(\Theta_0) - k_1^2} \end{aligned}$$

Defining  $\beta_m$  by the following:

$$(5-45) \quad \beta_m = k_1 \cos(\Theta_{1m})$$

we find

$$(5-46) \quad \beta_m = i \sqrt{k^2 \sin^2(\Theta_{0m}) - k_1^2}$$

so that

$$(5-47) \quad \beta_m = i \sqrt{K_m^2 - k_1^2} = i b_m$$

$$\text{where } b_m^2 = K_m^2 - k_1^2.$$

The depth eigenfunction for the second layer takes the following form,

$$(5-48) \quad \begin{aligned} Z_m(z) &= C_m e^{i\beta_m(z-h)} + D_m e^{-i\beta_m(z-h)} \\ &= C_m e^{-b_m(z-h)} + D_m e^{b_m(z-h)} \end{aligned}$$

The first term on the right damps the signal as the wave penetrates into the second layer. The second term increases the strength of the signal as it gets farther in the sediment (and farther from the source). We therefore choose  $D_m=0$ . Equation (5-48) now becomes,

$$(5-49) \quad Z_m(z) = C_m e^{-b_m(z-h)} \quad z \geq h$$

We use the boundary condition at the water/fluid bottom interface in order to solve for the modal coefficient  $C_m$ . This requires that the pressure across the interface be continuous:

$$(5-50) \quad \rho_0 Z_{0m}(h) = \rho_1 Z_{1m}(h) \quad (\text{refer to page 77})$$

or

$$\begin{aligned} \rho_0 \sin(\gamma_m h) &= \rho_1 C_m e^{-b_m(h-h)} \\ (5-51) \qquad &= \rho_1 C_m \end{aligned}$$

Therefore

$$(5-52) \qquad C_m = \frac{\rho_0}{\rho_1} \sin(\gamma_m h).$$

Now the depth eigenfunction for the fluid bottom takes the following form:

$$(5-53) \qquad Z_m(z) = \frac{\rho_0}{\rho_1} \sin(\gamma_m h) e^{-b_m(z-h)} \qquad z \geq h$$

Before we can solve for the acoustic pressure in the waveguide, we need to solve the modal coefficient  $A_m$ . The depth eigenfunction equation for the water layer Eq. (5-20) can be rewritten as follows:

$$(5-54) \qquad Z_m(z) = A_m \sin(\gamma_m z).$$

To obtain the modal coefficient  $A_m$  we use the orthogonality of depth eigenfunctions.

$$\begin{aligned}
 & \int_0^\infty \rho_0 Z_m(z) Z_n(z) dz \\
 &= \int_0^\infty \rho_0 \sin(\gamma_m z) \sin(\gamma_n z) dz = 0, \quad m \neq n \\
 (5-55) \quad &= \int_0^\infty \rho_0 \sin^2(\gamma_m z) dz = v_m, \quad m = n
 \end{aligned}$$

Since we expand the source function  $\delta(z-z_0)$  in terms of these orthogonal eigenfunctions  $Z_n$ :

$$(5-56) \quad \delta(z-z_0) = \sum_{n=1} A_n Z_n(z)$$

$$\int_0^\infty \rho_0 Z_m(z) \delta(z-z_0) dz = \sum_n A_n \int_0^\infty \rho_0 Z_m(z) Z_n(z) dz$$

so that

$$(5-57) \quad \rho_0 Z_m(z_0) = A_m v_m$$

or

$$(5-58) \quad A_m = \frac{\rho_0 Z_m(z_0)}{v_m}$$

The sound pressure from Eq. (5-4) is

$$(5-59) \quad P = \omega^2 \rho \phi = \omega^2 \rho_0 \sum_m \phi_m$$

Now

$$(5-60) \quad \begin{aligned} P(r, z, t) &= \omega^2 \rho_0 \sum_m A_m Z_m(z) U_m(r) T(t) \\ &= \omega^2 \rho_0 \sum_m \frac{\rho_0 Z_m(z_0) Z_m(z)}{v_m} \frac{e^{-i(K_m r)}}{\sqrt{2\pi K_m r}} e^{i\frac{\pi}{4}} e^{i\omega t} \end{aligned}$$

Finally,

$$(5-61) \quad P(r, z, t) = C \sum_n Z_n(z_0) Z_n(z) \frac{e^{-i(K_n r)}}{v_n \sqrt{K_n r}} e^{-\alpha_n r}$$

where the constant  $C$  has absorbed all numerical constants, coefficients, and the time dependent term, and we have introduced the attenuation term,  $e^{-\alpha r}$ . A brief discussion of the attenuation term is presented in Appendix D. This is the field in the absence of the object. To obtain the total field with a scattering object present, one would add the scattered field to this incident field. We now proceed to insonify the object using this incident field.

The derivation follows Norton. (12) The geometry is shown in Fig. 13. The object has as body fixed axis,  $X_0, Y_0, Z_0$ , where  $Z_0$  is the axis of symmetry and is parallel to the waveguide boundaries. The angle that the symmetry axis of the object makes with the vertical plane containing the source and the center of the object is labeled  $\alpha$ .

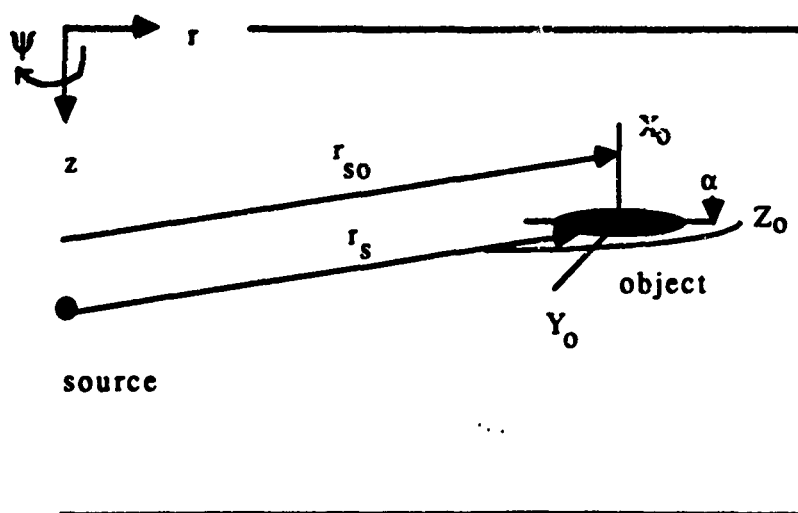


Fig. 13. Waveguide Geometry with Object.

The connection between the cylindrical coordinates of the source and the body-fixed rectangular coordinates of the object is given by

$$(5-62) \quad r_s = r_{s0} - \cos(\alpha)Z_0 - \sin(\alpha)Y_0, \quad z = z_{obj} - X_0$$

Since we required that the object be in the far field of the source,  $r_s \cong r_{s0}$  and the factor  $\sqrt{k_n r_s} \cong \sqrt{k_n r_{s0}}$  is nearly constant in range at the object. Equation (5-61) can be rewritten using the exponential form of the

$\sin(\gamma_n Z)$  term and Eq. (5-62), resulting in the following expression for the incident field in the rectangular system,

$$\begin{aligned}
 (5-63) \quad U_i(r, z) = & C \sum_n \frac{\sin(\gamma_n z_s) e^{i\gamma_n z_{obj} - iK_n r_{so} - \alpha_n r_{so}}}{2iv_n \sqrt{K_n r_{so}}} \\
 & \cdot e^{i(\gamma_n, K_n \sin(\alpha), K_n \cos(\alpha)) \cdot (X_o, Y_o, Z_o)} \\
 & + C \sum_n \frac{-\sin(\gamma_n z_s) e^{-i\gamma_n z_{obj} - iK_n r_{so} - \alpha_n r_{so}}}{2iv_n \sqrt{K_n r_{so}}} \\
 & \cdot e^{i(-\gamma_n, K_n \sin(\alpha), K_n \cos(\alpha)) \cdot (X_o, Y_o, Z_o)}
 \end{aligned}$$

We have specified the depth of the field point to be at the depth of the object,  $z_{obj}$  and  $z_s$  is the source depth. Note that there are two sets of plane waves, a downgoing and upgoing set. They are expanded in a spherical representation so as to be compatible with the T-matrix, since the T-matrix is in a spherical representation.

A spherical coordinate system is established at the center of the object. The angle  $\theta$  is measured from the  $Z_o$  axis, and  $\varphi$  measures the rotation in the  $X_o, Y_o$  plane. The object is invariant under rotation in  $\varphi$ . The angles are defined as follows,

$$(5-64) \quad \theta = \cos^{-1}\left(\frac{Z_o}{\rho}\right), \varphi = \tan^{-1}\left(\frac{X_o}{Y_o}\right), \rho = \sqrt{X_o^2 + Y_o^2 + Z_o^2}$$



The exponential terms of Eq.(5-62) can be rewritten as

$$(5-65) \quad e^{i\mathbf{K} \cdot \mathbf{p}}$$

Where  $\mathbf{K}$  and  $\mathbf{p}$  are given by the following:

$$(5-66) \quad \mathbf{K} = (\pm \gamma_n \mathbf{i} + K_n \sin(\alpha) \mathbf{j} + K_n \cos(\alpha) \mathbf{k}), \quad \mathbf{p} = (X_0 \mathbf{i} + Y_0 \mathbf{j} + Z_0 \mathbf{k})$$

We now expand Eq. (5-65) in spherical waves. The expansion follows Morse and Feshbach. (13)

$$(5-67) \quad e^{i\mathbf{K} \cdot \mathbf{p}} = \sum_{l=0}^{\infty} (2l+1) i^l j_l(kr) \sum_{m=-l}^l \frac{(l-m)!}{(l+m)!} P_l^m(\cos(\theta)) P_l^m(\cos(\theta'))$$

$$\cdot [(\cos(m\phi) \cos(m\phi')) + (\sin(m\phi) \sin(m\phi'))]$$

where  $\theta$  and  $\phi$  are relative to  $\mathbf{K}$  and  $\theta'$  and  $\phi'$  are relative to  $\mathbf{p}$ . If we let

$$\sigma = \begin{pmatrix} 1 = e \\ 0 = o \end{pmatrix}, \text{ and}$$

$$(5-68) \quad \gamma_l^m = \frac{\epsilon_m (2l+1) (l-m)!}{4\pi (l+m)!} \quad \epsilon_0 = 1 \quad \epsilon_m = 2, m \neq 0$$

then Eq. (5-67) becomes,

$$(5-69) \quad e^{i\mathbf{K} \cdot \mathbf{p}} = 4\pi \sum_{l, m, \sigma} i^l \left( \gamma_l^m \right)^{\frac{1}{2}} P_l^m(\cos(\theta)) \begin{cases} \sin(m\phi) \sigma = 0 \\ \cos(m\phi) \sigma = 1 \end{cases}$$

$$\cdot \left( \gamma_l^m \right)^{\frac{1}{2}} j_l(kr) P_l^m(\cos(\theta')) \begin{cases} \sin(m\phi') \sigma = 0 \\ \cos(m\phi') \sigma = 1 \end{cases}$$

Equation (5-69) can be simplified by making the following definition:

$$\begin{aligned}
 a_{l,\sigma}^m &= 4\pi i \left(\gamma_l^m\right)^{\frac{1}{2}} P_l^m(\cos\theta) \begin{cases} \sin(m\varphi)\sigma=0 \\ \cos(m\varphi)\sigma=1 \end{cases} \\
 (5-70) \quad &= 4\pi i Y_{l,\sigma}^m(\theta, \varphi)
 \end{aligned}$$

and,

$$\begin{aligned}
 \text{Re} \Psi_{l,\sigma}^m(\vec{p}) &= \left(\gamma_l^m\right)^{\frac{1}{2}} j_l(kr) P_l^m(\cos(\theta')) \begin{cases} \sin(m\varphi')\sigma=0 \\ \cos(m\varphi')\sigma=1 \end{cases} \\
 (5-71) \quad &= j_l(kr) Y_{l,\sigma}^m(\theta', \varphi')
 \end{aligned}$$

Where  $\text{Re}$  denotes the regular part of  $\Psi$ . Utilizing Eqs. (5-70) and (5-71), Eq. (5-69) takes the following form,

$$(5-72) \quad e^{iK\cdot\vec{p}} = \sum_{l,m,\sigma} a_{l,\sigma}^m \text{Re} \Psi_{l,\sigma}^m(\vec{p})$$

The incident field (Eq. (5-63)) in terms of the spherical coordinates is now given as

$$(5-73) \quad U_i(\vec{p}) = \sum_n \sum_{l,m,\sigma} d_{n,l,\sigma}^m \text{Re} \Psi_{l,\sigma}^m(\vec{p})$$

where  $n$  is the index for the number of modes. The partial waves coefficients

of the incident field are then given by the following,

$$(5-74) \quad \alpha_{n,l,\sigma}^m = \frac{\sin(\gamma_n z_s) e^{-\alpha_n r_{so}}}{2i v_n \sqrt{K_n r_{so}}} \cdot (e^{i(\gamma_n z_{obj} - K_n r_{so})} - e^{-i(\gamma_n z_{obj} + K_n r_{so})}) a_{l,\sigma}^m$$

where  $z_s$  is the depth of the source,  $z_{obj}$  is the depth of the object and  $r_{so}$  is the range from the source to the object. The scattered field about the object is written as (see chapter two)

$$(5-75) \quad f(\vec{p}) = \sum_{n,l,m,\sigma} \beta_{n,l,\sigma}^m \Psi_{l,\sigma}^m(\vec{p})$$

where

$$\beta_{n,l,\sigma}^m = T_{l,l',\sigma}^m \alpha_{n,l',\sigma}^m$$

and

$$\Psi_{l,\sigma}^m(\vec{p}) = h_l(k\rho) Y_{l,\sigma}^m(\theta, \phi)$$

The scattered field given by Eq. (5-75) is valid only near the object before it has a chance to interact with the waveguide boundaries. Notice that the spherical Bessel function used in Eq.(5-71) to describe the regular spherical wave ( $\text{Re} \Psi_{l,\sigma}^m(\vec{p})$ ) is now replaced by the spherical Hankel function to obtain the outgoing spherical wave ( $\Psi_{l,\sigma}^m(\vec{p})$ ). Having the scattered field about the object we can generate the expression for the scattered field far from the object.

The scattered near field does not satisfy the boundary conditions of the waveguide. The solution for the scattered field far from the object (from chapter 4) is:

$$(5-76) \quad U_s(r_s, z) = \int_{\sigma} \left( f(r) \frac{\partial G(r_s, z)}{\partial n} - G(r_s, z) \frac{\partial f(r)}{\partial n} \right) dS$$

where the surface  $\sigma$  is a closed surface enclosing the object. Figure 14 shows the geometry of the waveguide with the object centered at the origin of the  $X_0, Y_0, Z_0$  coordinate system.

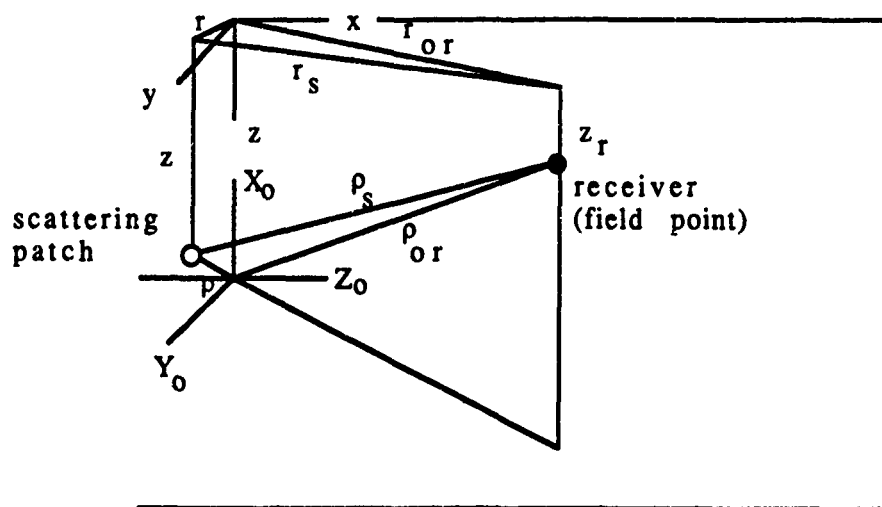


Fig. 14. Geometry of Waveguide from Object to Receiver.

We now need to determine the normal derivative of the scattered field and the Green's function that satisfies the waveguide boundary conditions, and its normal gradient on some arbitrary surface sufficiently near the object.

The appropriate Green's function ( $G(r_s, z)$ ) is given by Eq.(5-61),

$$(5-77) \quad G(r_s, z) = C \sum_n \frac{\sin(\gamma_n z_r) \sin(\gamma_n z) e^{iK_n r_s} e^{-\alpha_n r_s}}{v_n \sqrt{K_n r_s}}$$

where  $z_r$  is the receiver depth and  $r_s$ , to within first order, is given by

$$(5-78) \quad r_s = r_{or} - r \cos(\theta)$$

where  $\theta$  is the angle between  $r$  and  $r_{or}$  and  $r_{or}$  is the distance from the object to the receiver. The Green's function after substituting Eq. (5-78) can be rewritten as

$$(5-79) \quad G(r_s, z) = C \sum_n \frac{\sin(\gamma_n z_r) e^{iK_n r_{or}} e^{-\alpha_n r_{or}}}{v_n \sqrt{K_n r_{or}}} \cdot \frac{\sin(\gamma_n z) e^{-iK_n r \cos(\theta)} e^{\alpha_n r \cos(\theta)}}{\sqrt{1 - \frac{r \cos(\theta)}{r_{or}}}}$$

Substituting Eq. (5-79) into Eq. (5-76) yields for the scattered field

$$(5-80) \quad U_s(r_s, z) = C \sum_n \frac{\sin(\gamma_n z_r) e^{iK_n r_{or}} e^{-\alpha_n r_{or}}}{v_n \sqrt{K_n r_{or}}} B_n$$

where

$$(5-81) \quad B_n = \int_{\sigma} f(\rho) \frac{\partial}{\partial n} \left[ \frac{\sin(\gamma_n z) e^{-iK_n r \cos(\theta)} e^{\alpha_n r \cos(\theta)}}{\sqrt{1 - \frac{r \cos(\theta)}{r_{or}}}} \right] - \frac{\sin(\gamma_n z) e^{-iK_n r \cos(\theta)} e^{\alpha_n r \cos(\theta)}}{\sqrt{1 - \frac{r \cos(\theta)}{r_{or}}}} \frac{\partial}{\partial n} [f(\rho)] \cdot dS$$

Finally combining C and  $B_n$  into a single term  $A_n$ , gives for the scattered field

$$(5-82) \quad U_s(r_s, z) = \sum_n A_n \frac{\sin(\gamma_n z_r) e^{iK_n r_{or}} e^{-\alpha_n r_{or}}}{v_n \sqrt{K_n r_{or}}}$$

This expression satisfies all boundary conditions at the waveguide interfaces and is continuous throughout all space. Note that the solution, Eq. (5-82), is in the form of a guided wave as one would expect for the field far from the source. Now that the scattered far field has been determined, some numerical examples will be presented.

### Examples

In this example we will follow the acoustic field as it propagates from the source to the object, to the receiver. We will determine the total field at the receiver by using the principle of superposition. The characteristics of the sample waveguide are shown in Table 3.

TABLE 3  
WAVEGUIDE CHARACTERISTICS

Water Layer				
Depth (m)	Compression Sound Speed	Wave Speed (m/s)	Density (g/cm**3)	Attenuation (nepers/m)
150	1500		1.0	1.0e-7
Half Space				
Depth (m)	Compression Sound Speed	Wave Speed (m/s)	Density (g/cm**3)	Attenuation (dB/λ)
infinite	1600		1.5	.5

The source will have a frequency of 100 (Hz). Table 4 lists the source, object and receiver locations. For this environment there are 7 propagating modes, as determined by Eq. (5-36).

TABLE 4  
LOCATION PARAMETERS

Source r (m)	Location z (m)	Object r (m)	Location z (m)	Receiver r (m)	Location z (m)
0	50	5000	75	6500	25

Figures 15 and 16 depict the waveguide in a vertical and horizontal view. The horizontal view is looking at the waveguide from the surface down.

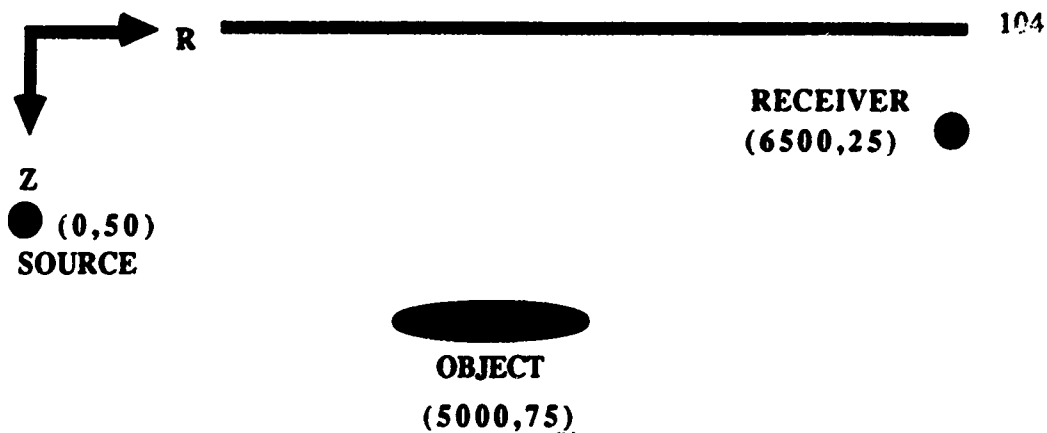


Fig. 15. Vertical (side) View of the Waveguide.

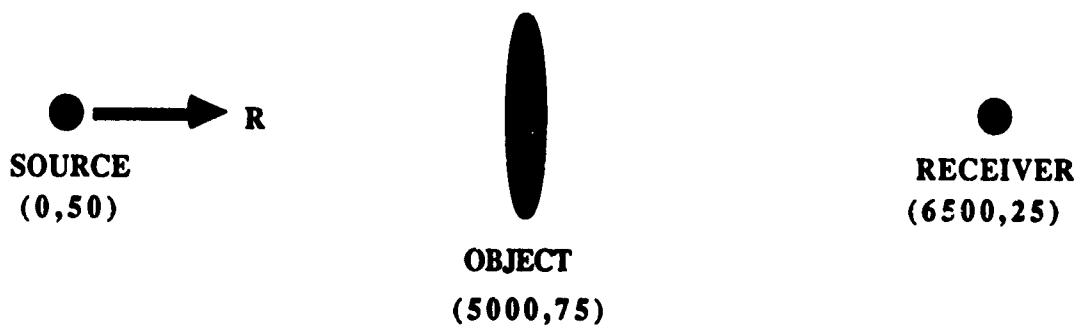


Fig. 16. Horizontal (top) View of the Waveguide.

The source, object and receiver can be at different depths in the waveguide; a requirement on the object is that it must be in the far field of the source. This is because we are assuming that only the discrete propagating



modes contribute to the pressure at the receiver and because we use the asymptotic expression for the Hankel function, (in the solution for the range equation) which is only valid at long ranges. Another requirement is that the object is not so near an interface that the surface on which the near field scattered field is determined comes in contact with the interface. The objects characteristics are shown in Table 5.

TABLE 5  
OBJECT CHARACTERISTICS

Length (m)	Width (m)	Boundary Condition
50	10	Dirichlet

We will now follow the field as it propagates in the waveguide. Figure 17 illustrates the magnitude of the normalized pressure field verses depth at a range of 300 (m). Notice that the pressure at the surface goes to zero as the boundary condition requires. There is an interference pattern due to the summation of the 7 individual modes. Figures 18-24 illustrate the contribution from each mode. Note that mode 3 (Fig. 20) contributes the least to the overall field and that Mode 6 (Fig. 23) and mode 7 (Fig. 24) also contribute very little. Modes 2 (Fig. 19) and 5 (Fig. 22) have the largest contributions to the field.

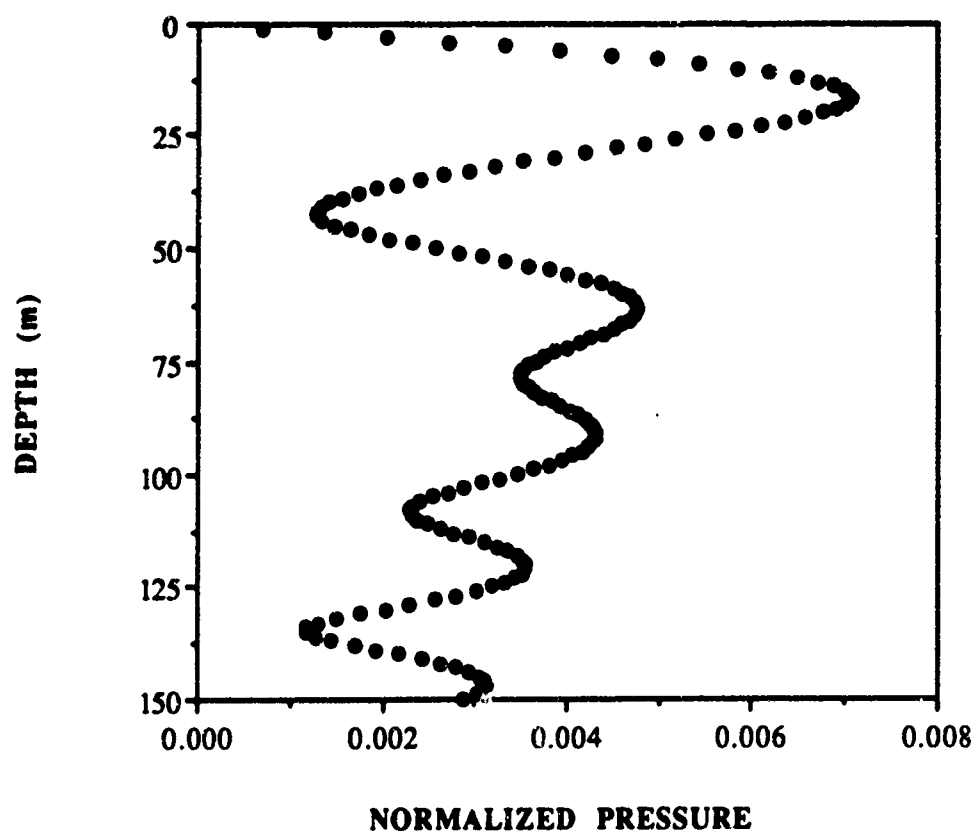


Fig. 17. Point Source Pressure vs. Depth at a Range of 300 (m) from the Source.

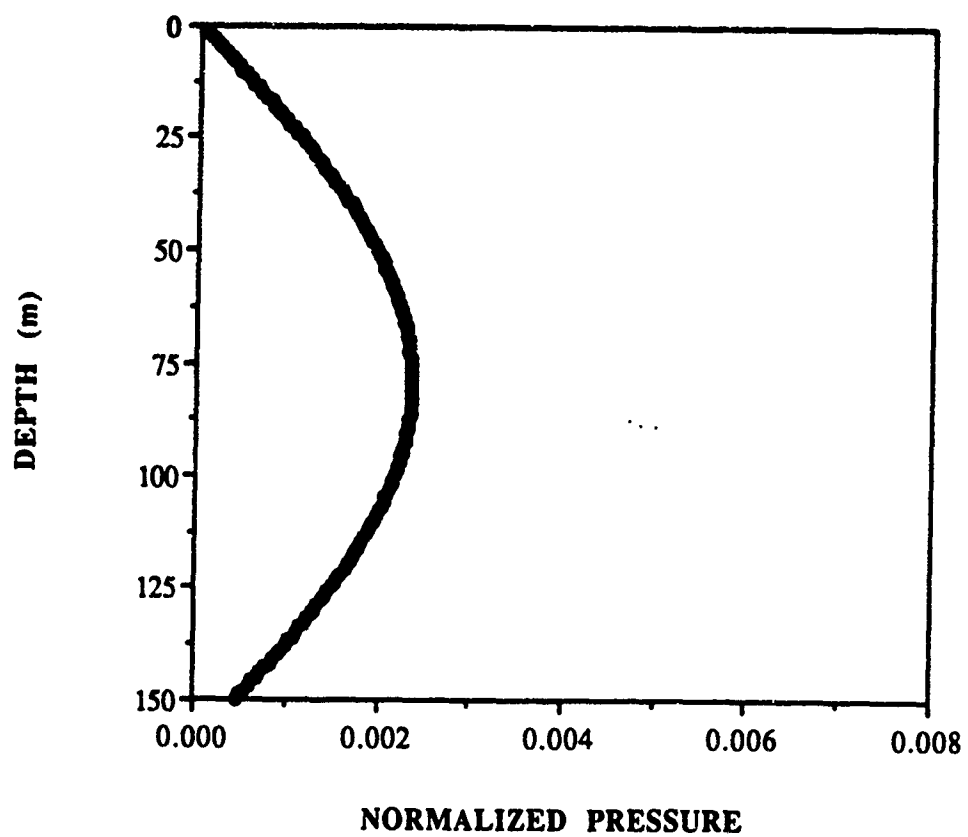


Fig. 18. Point Source Pressure vs. Depth at a Range of 300 (m) from the Source. Mode 1 Only.

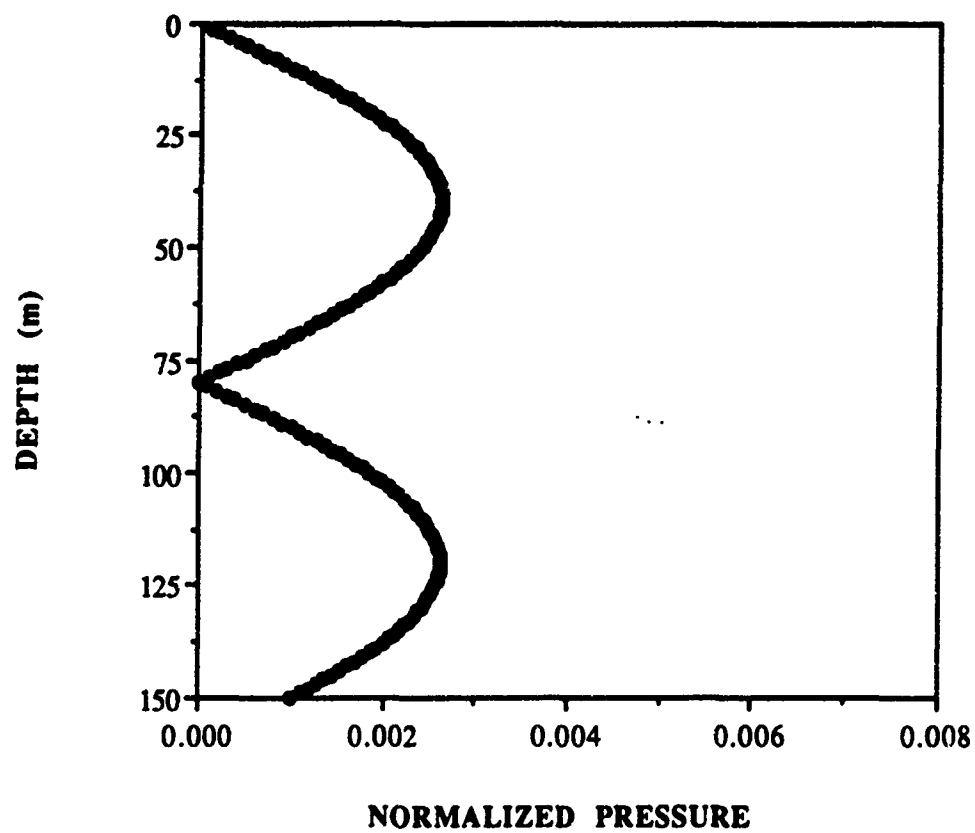


Fig. 19. Point Source Pressure vs. Depth at a Range of 300 (m) from the Source. Mode 2 Only.

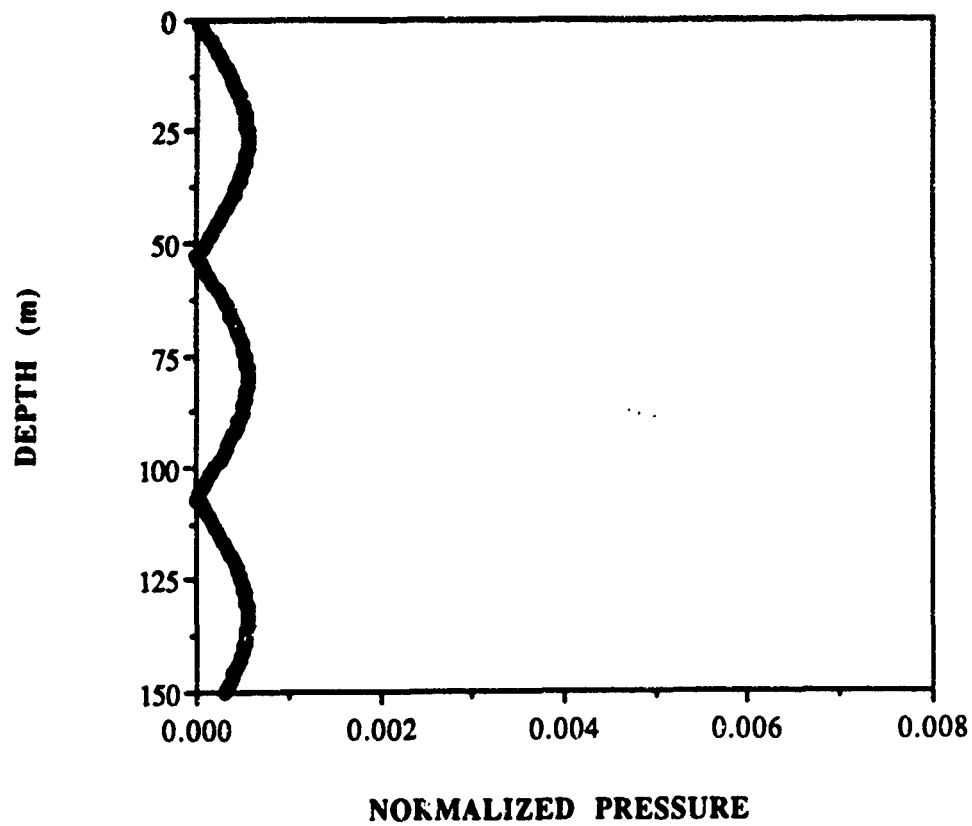


Fig. 20. Point Source Pressure vs. Depth at a Range of 300 (m) from the Source. Mode 3 Only.

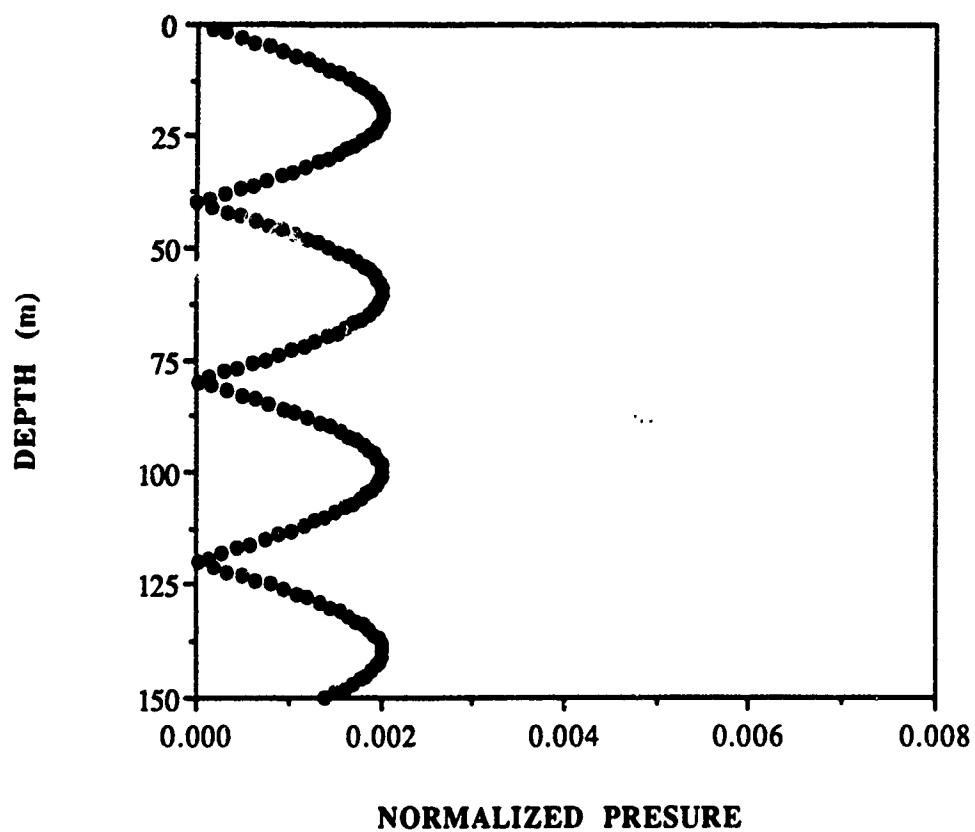


Fig. 21. Point Source Pressure vs. Depth at a Range of 300 (m) from the Source. Mode 4 Only.

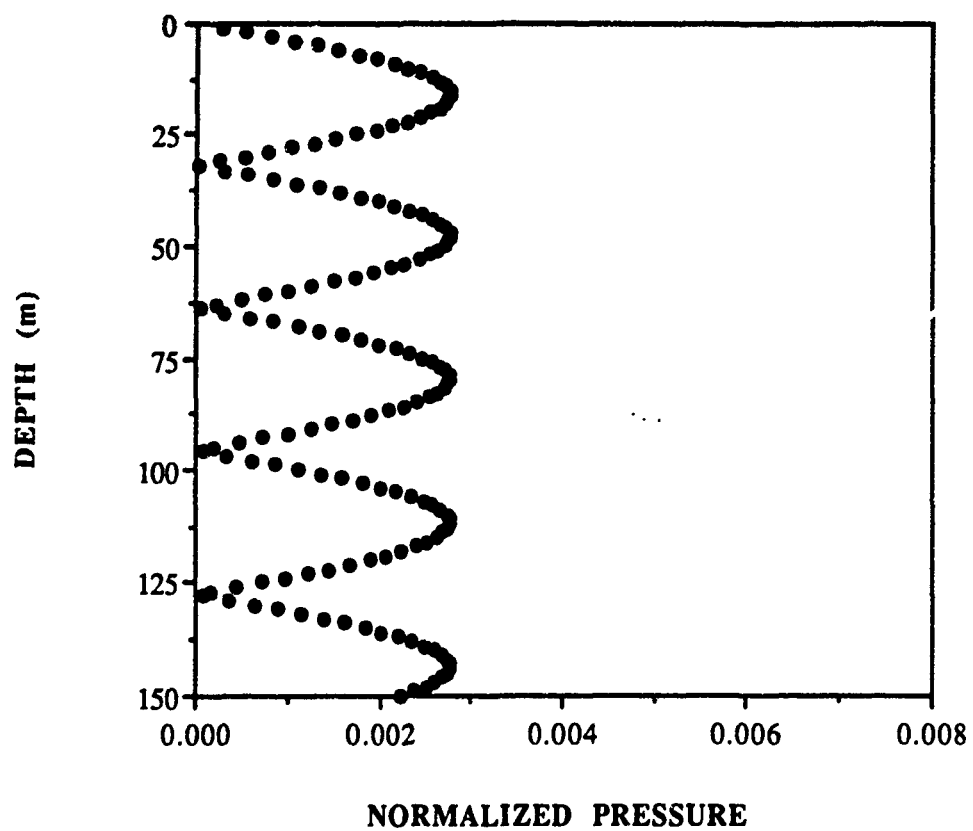


Fig. 22. Point Source Pressure vs. Depth at a Range of 300 (m) from the Source. Mode 5 Only.

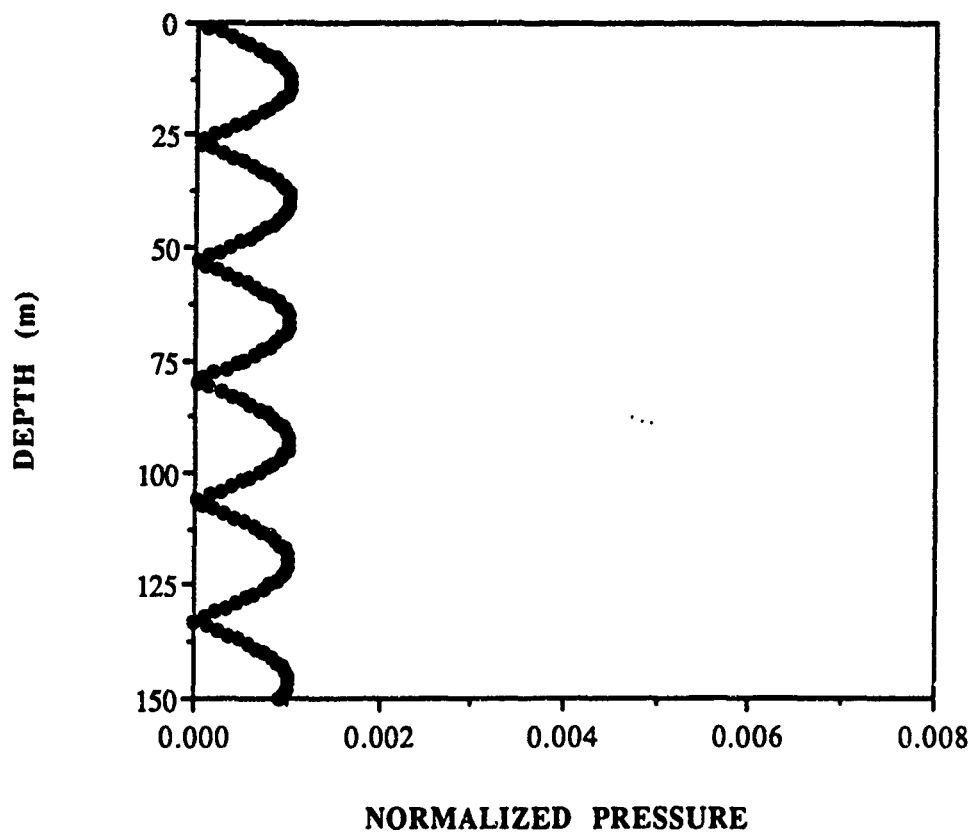


Fig. 23. Point Source Pressure vs. Depth at a Range of 300 (m) from the Source. Mode 6 Only.



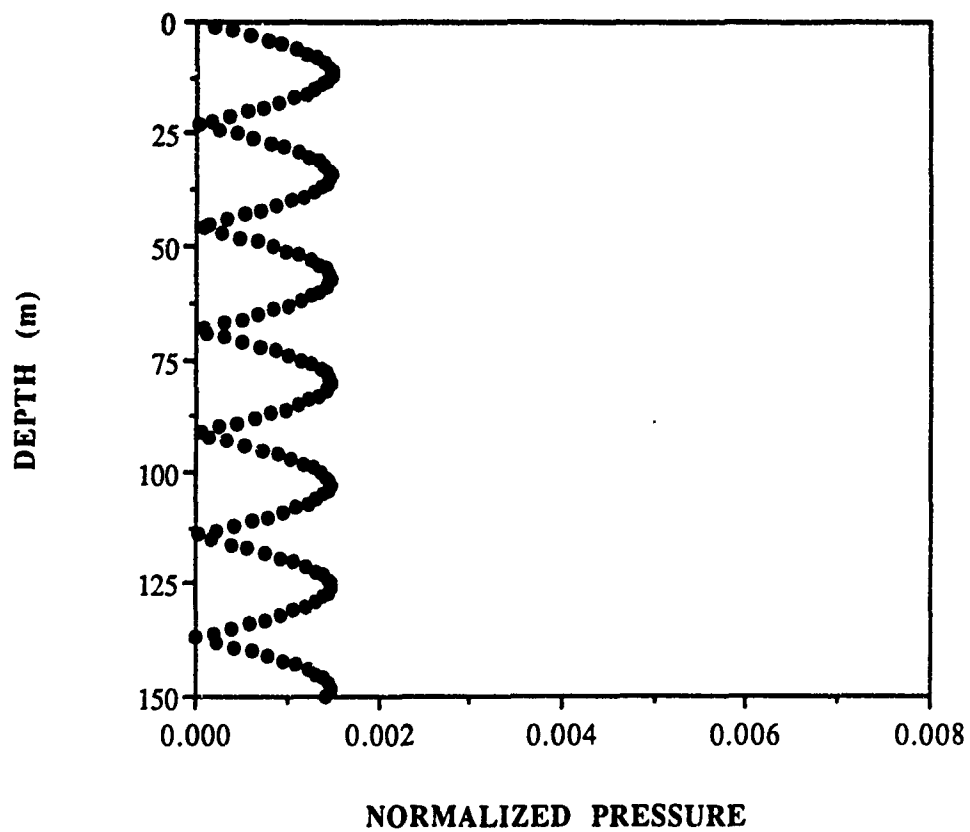


Fig. 24. Point Source Pressure vs. Depth at a Range of 300 (m) from the Source. Mode 7 Only.

We now allow the field to propagate to the object. Figure 25 depicts the magnitude of the normalized pressure field at the object, 5000 (m) from the source. Notice that the interference pattern differs from that shown in Fig. 17, near the source. This is because the higher modes attenuate more quickly than do the lower modes. Notice that the magnitude of the field has decreased to about  $1/5$  its value at the source. Figures 26-32 depicts the contributions from the individual modes. Notice that only the magnitude of each of the modal fields has changed, not the shape. Note also, that the relative strength of mode 6 (Fig. 31) and 7 (Fig. 32) have reversed because of attenuation, due to interaction with the waveguide interfaces. Modes 1 (Fig. 26) and 2 (Fig. 27) now contribute more to the field than any other.

We now look at the scattered pressure field as it propagates from the object. Since the scattered field is not cylindrically symmetric, we will look at the pressure in the vertical plane at 90 degrees relative to the front of the object (backscatter) and 0 degrees (along major axis of symmetry). Figure 33 illustrates the vertical normalized pressure field at a distance of 300 (m) from the object and at an angle of 90 degrees (backscatter). Note that the strength of the field is approximately 2 orders of magnitude less than the incident field. Figures 34-40 illustrate the contributions from the individual modes. Notice also that while the structure of the modes are similar to the incident field modes, their relative contributions are not the same as for the incident field. Modes 1, (Fig. 34) 3, (Fig. 36) 5, (Fig. 38) and 7 (Fig. 40) contribute much more than the corresponding incident field modes. This is because the object, acting

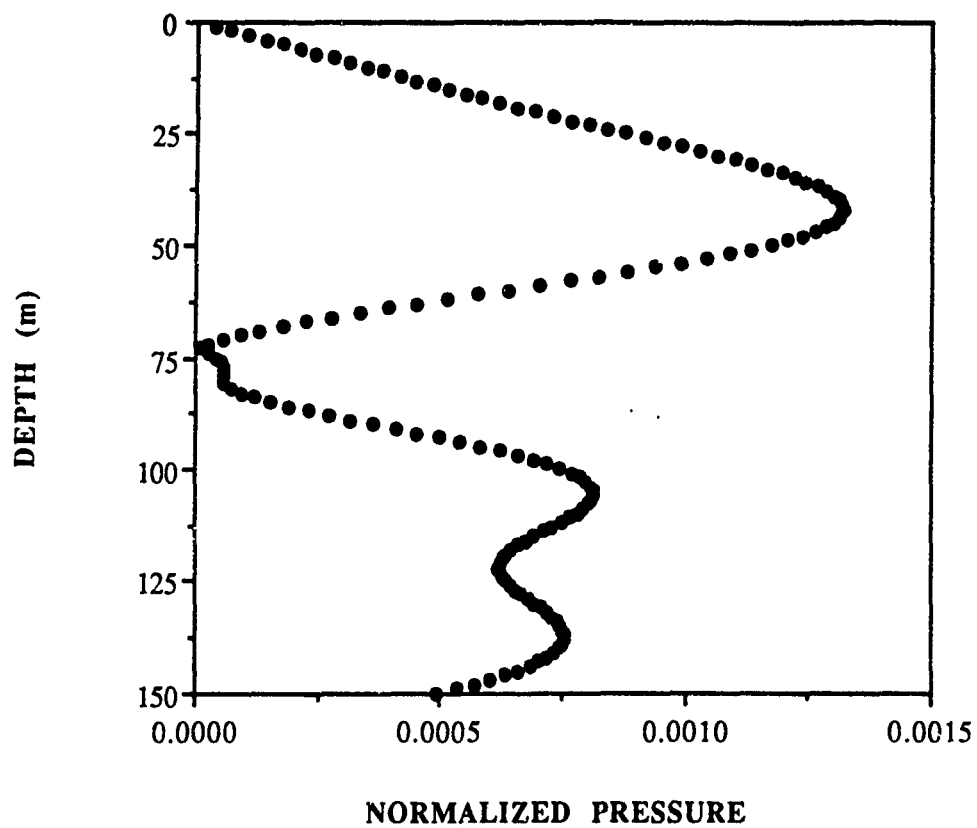


Fig. 25. Point Source Pressure vs. Depth at a Range of 5000 (m) from the Source.

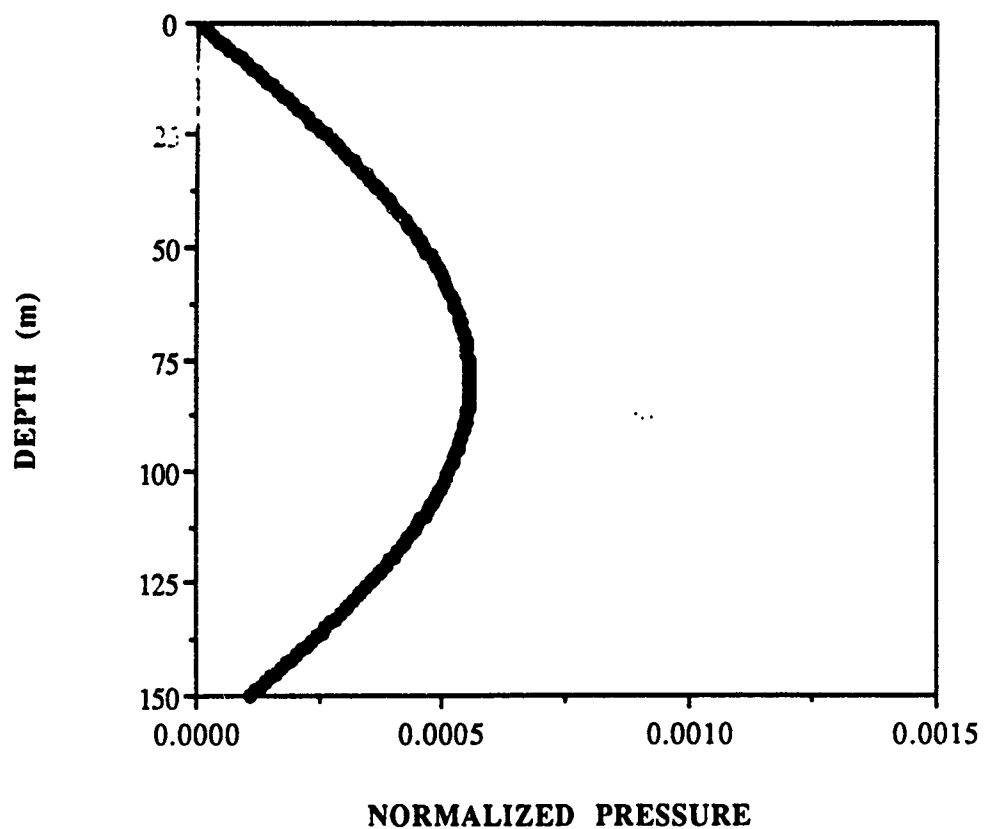


Fig. 26. Point Source Pressure vs. Depth at a Range of 5000 (m) from the Source. Mode 1 Only.

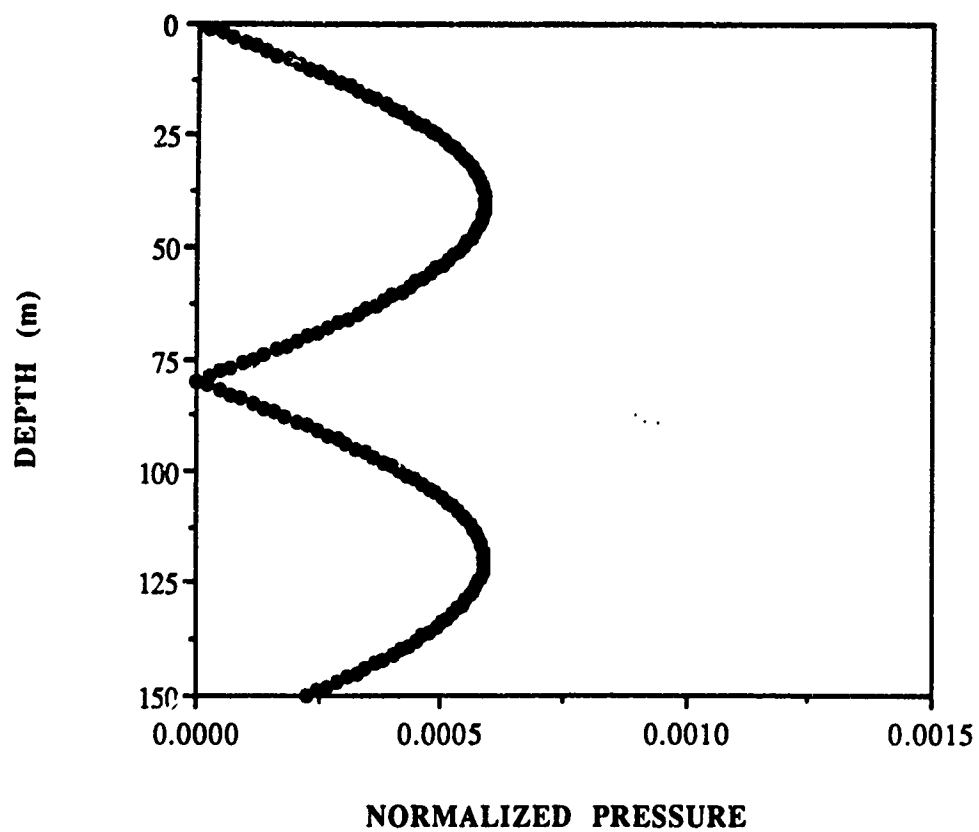


Fig. 27. Point Source Pressure vs. Depth at a Range of 5000 (m) from the Source. Mode 2 Only.

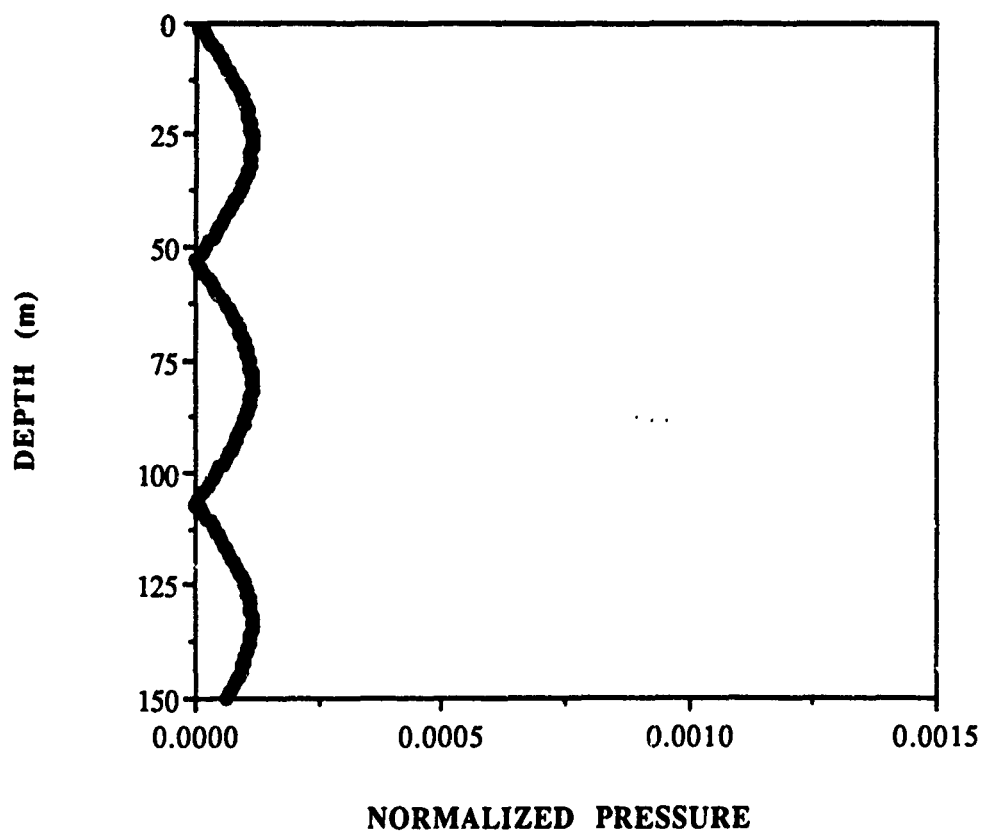


Fig. 28. Point Source Pressure vs. Depth at a Range of 5000 (m) from the Source. Mode 3 Only.

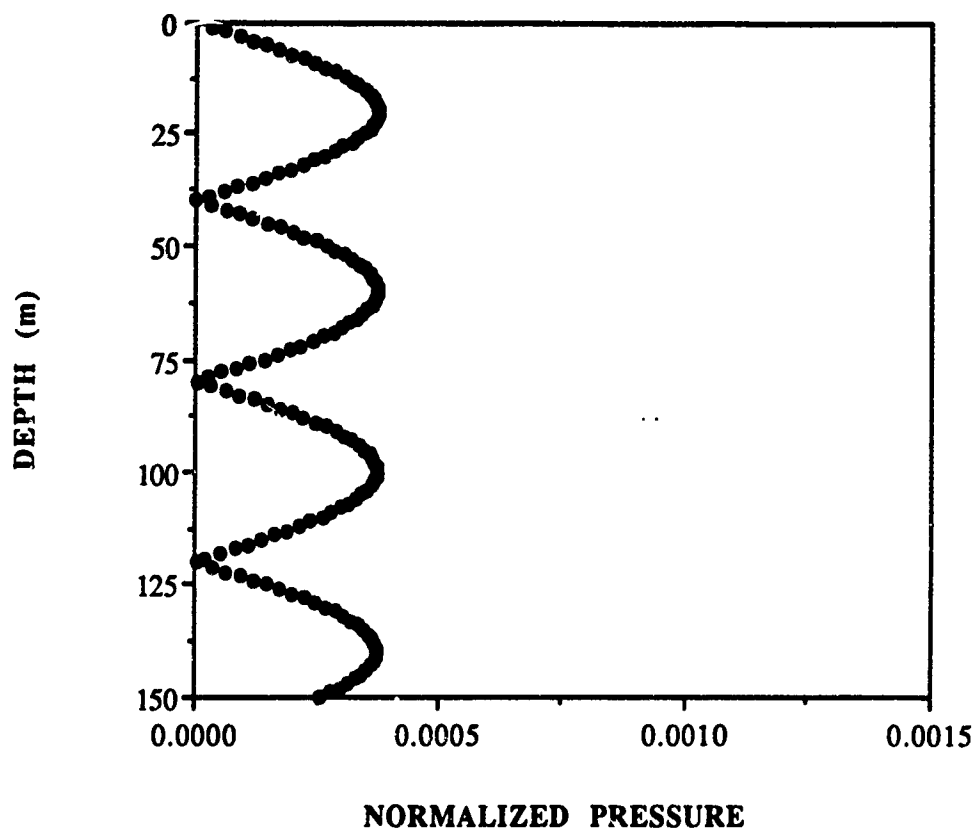


Fig. 29. Point Source Pressure vs. Depth at a Range of 5000 (m) from the Source. Mode 4 Only.

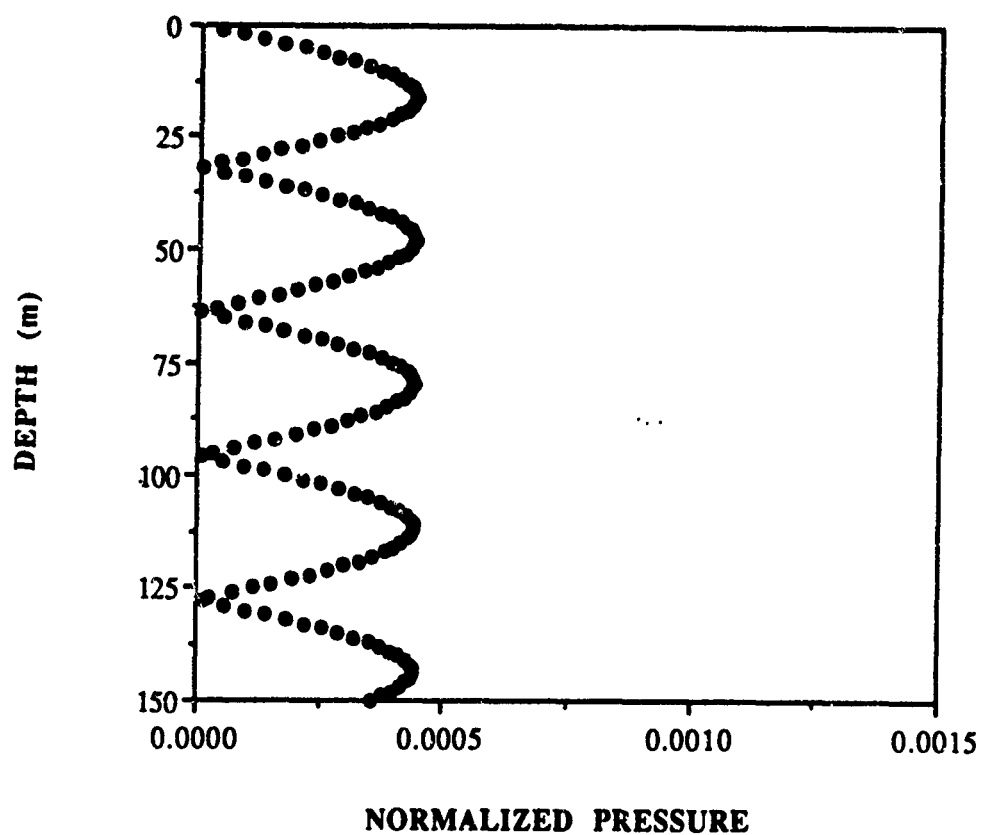


Fig. 30. Point Source Pressure vs. Depth at a Range of 5000 (m) from the Source. Mode 5 Only.



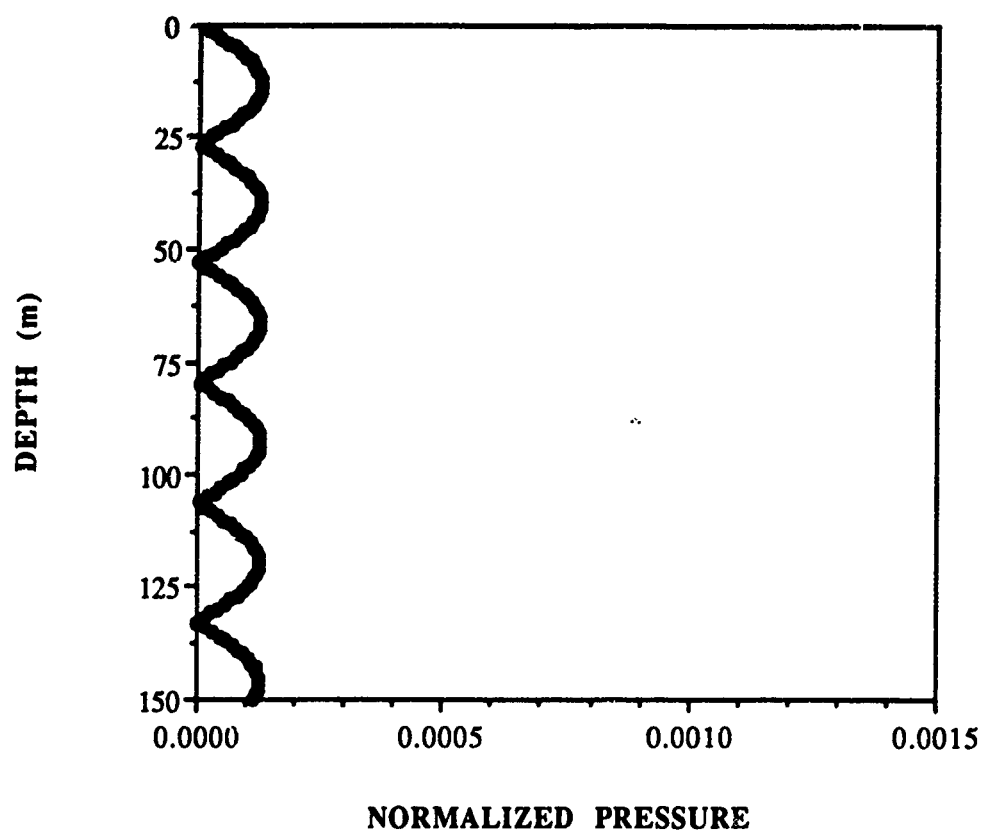


Fig. 31. Point Source Pressure vs. Depth at a Range of 5000 (m) from the Source. Mode 6 Only.

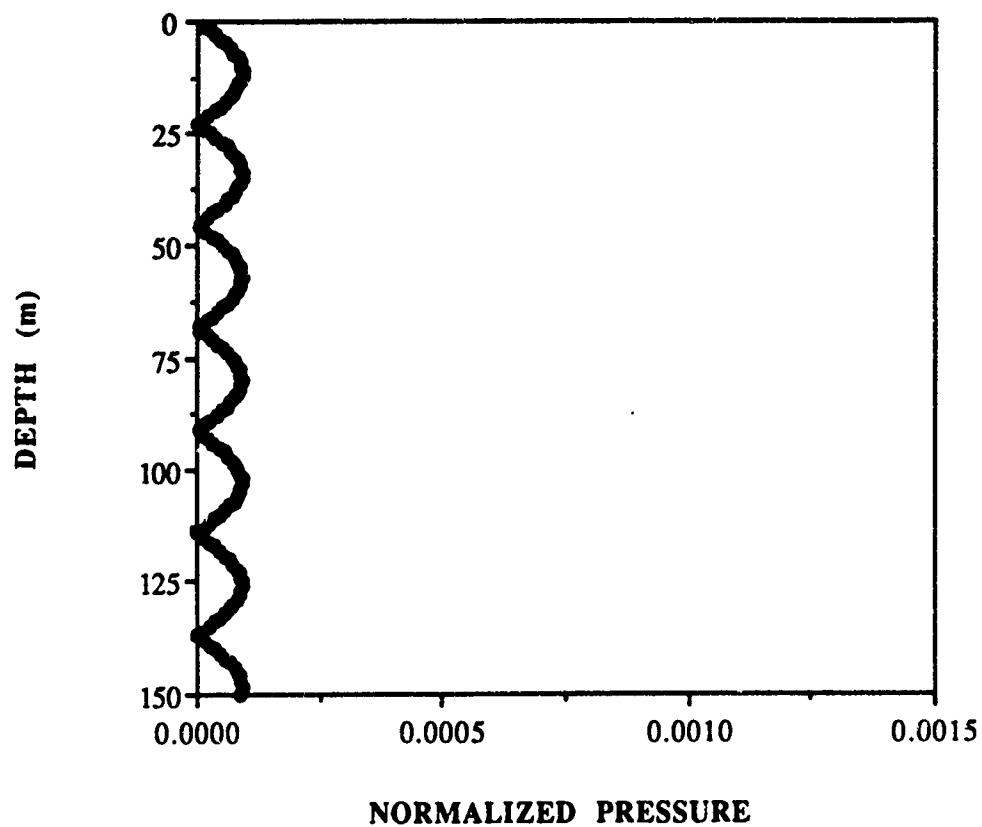


Fig. 32. Point Source Pressure vs. Depth at a Range of 5000 (m) from the Source. Mode 7 Only.

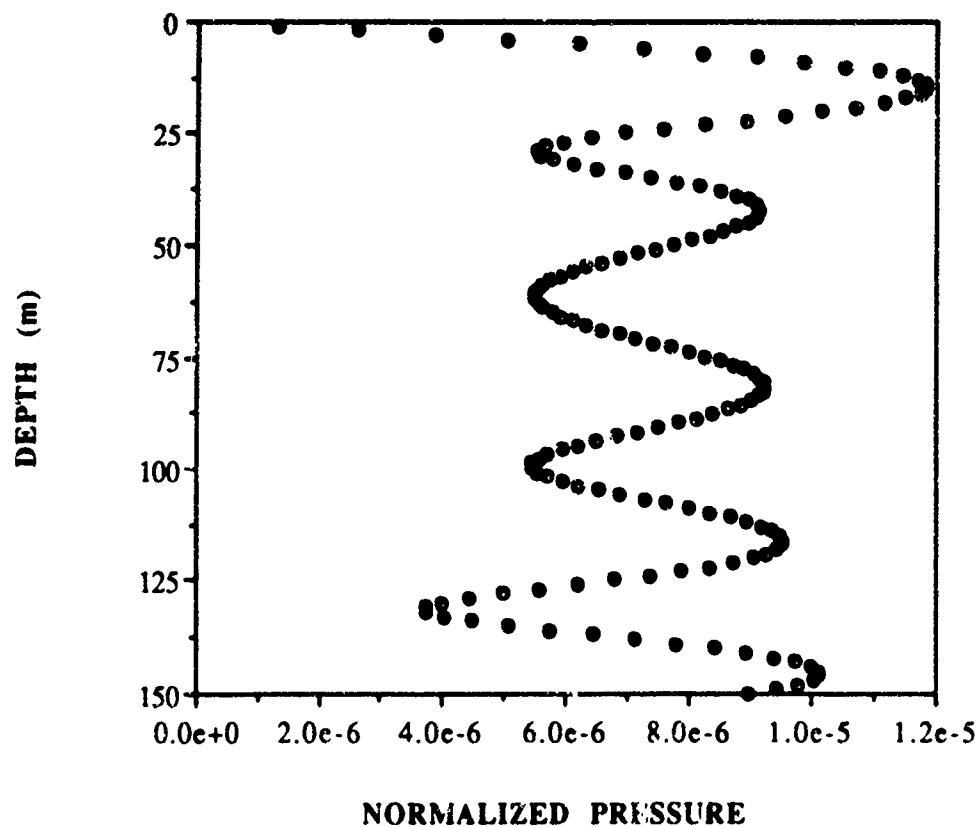


Fig. 33. Objects' Scattered Pressure vs. Depth at a Range of 300 (m) from the Object. Scattered Angle 90 (deg.)

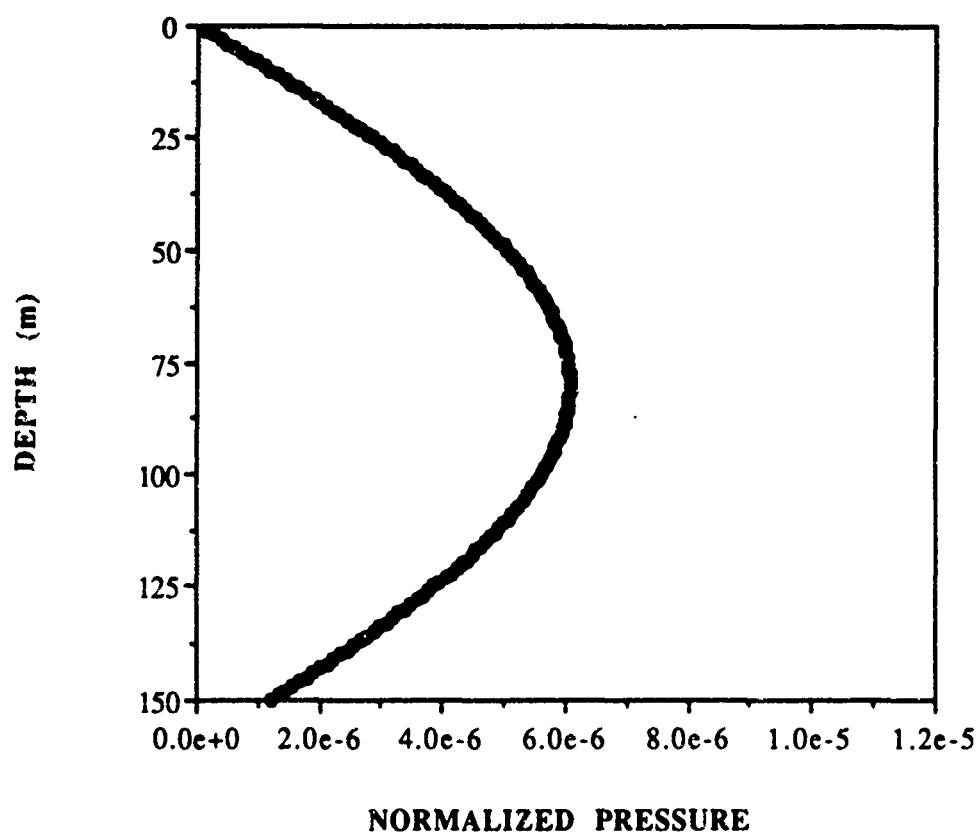


Fig. 34. Objects' Scattered Pressure vs. Depth at a Range of 300 (m) from the Object. Scattered Angle 90 (deg.). Mode 1 Only.

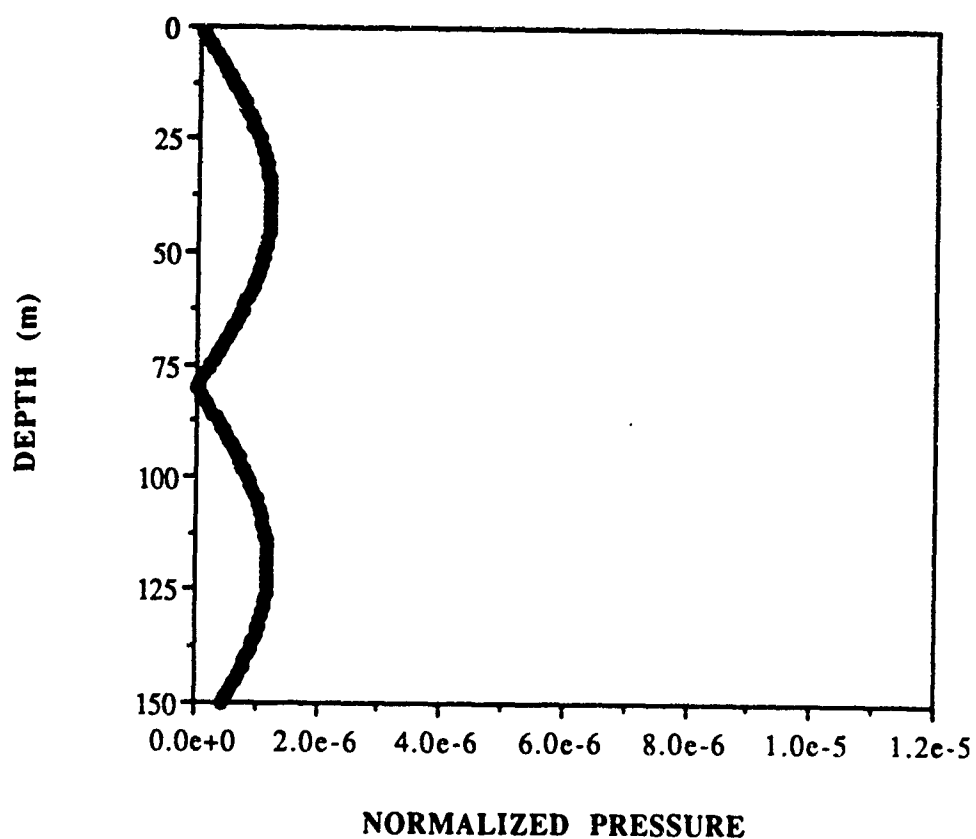


Fig. 35. Objects' Scattered Pressure vs. Depth at a Range of 300 (m) from the Object. Scattered Angle 90 (deg.). Mode 2 Only.

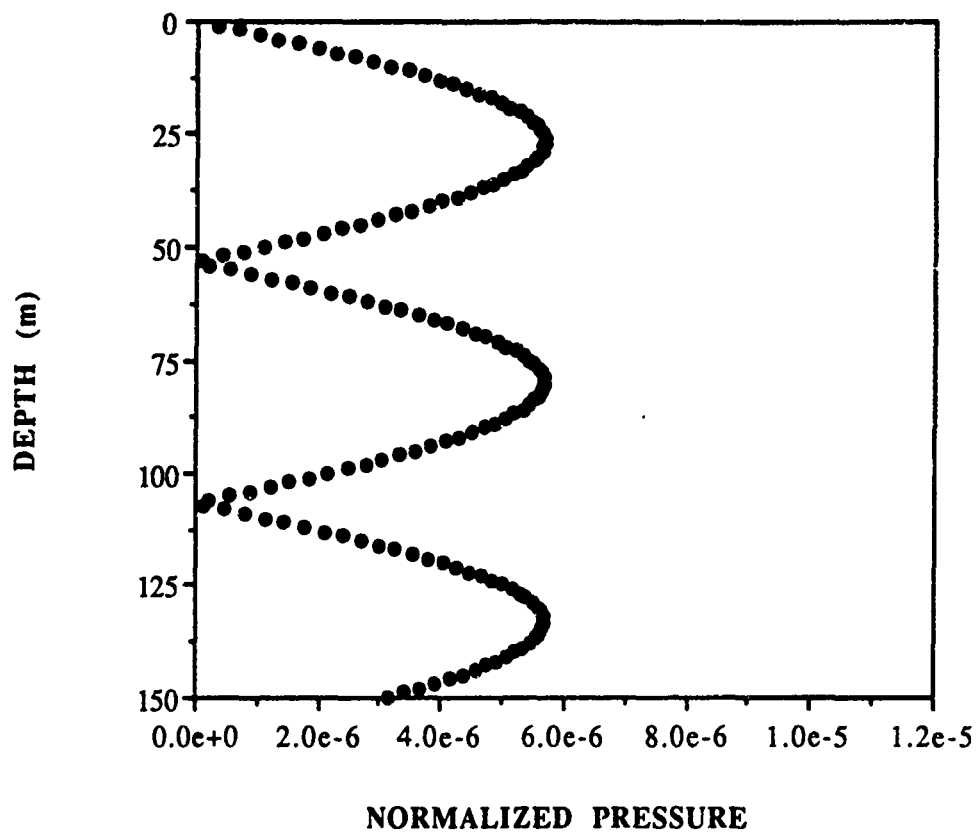


Fig. 36. Objects' Scattered Pressure vs. Depth at a Range of 300 (m) from the Object. Scattered Angle 90 (deg.). Mode 3 Only.

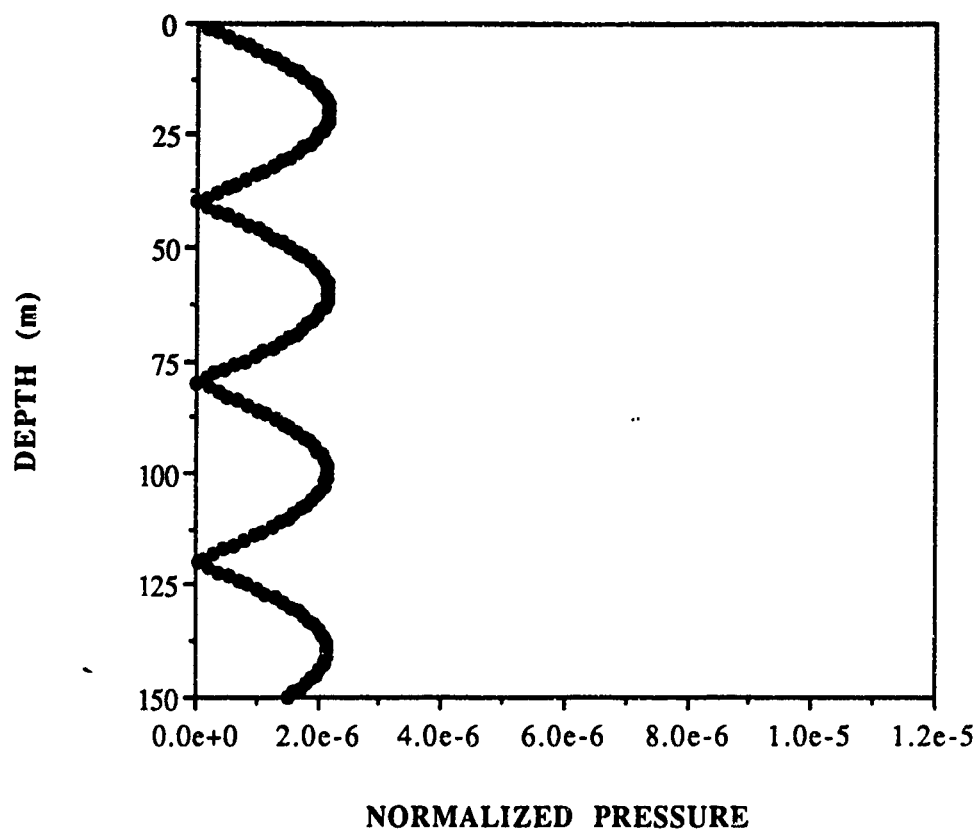


Fig. 37. Objects' Scattered Pressure vs. Depth at a Range of 300 (m) from the Object. Scattered Angle 90 (deg.). Mode 4 Only.

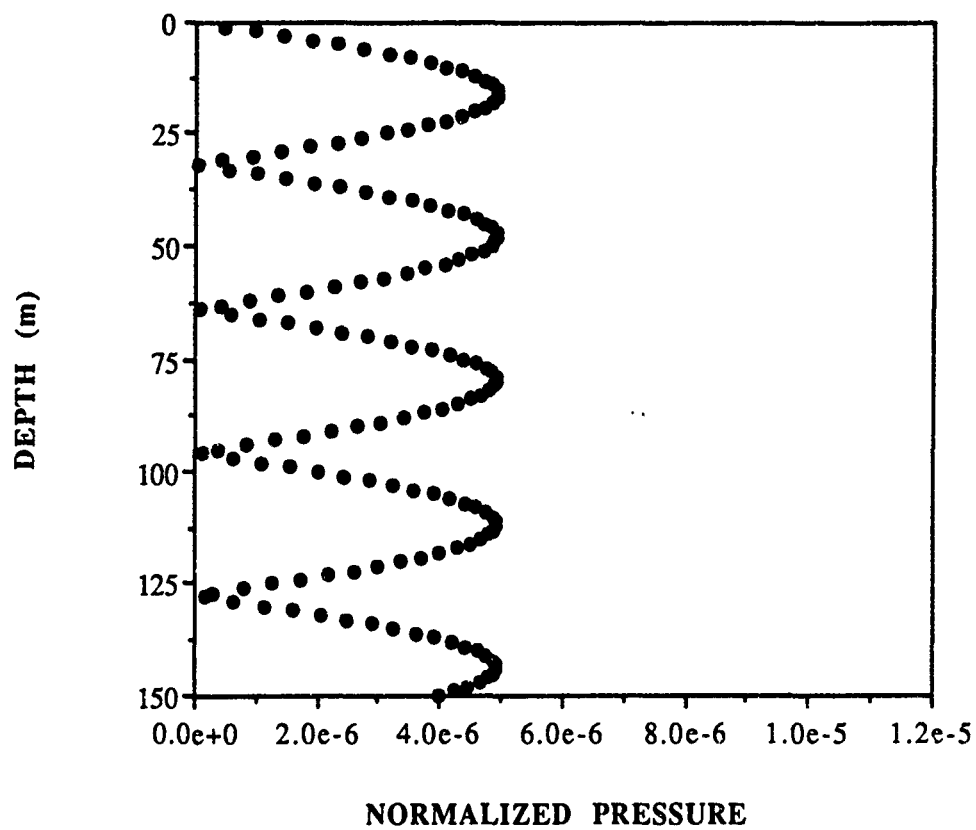


Fig. 38. Objects' Scattered Pressure vs. Depth at a Range of 300 (m) from the Object. Scattered Angle 90 (deg.). Mode 5 Only.



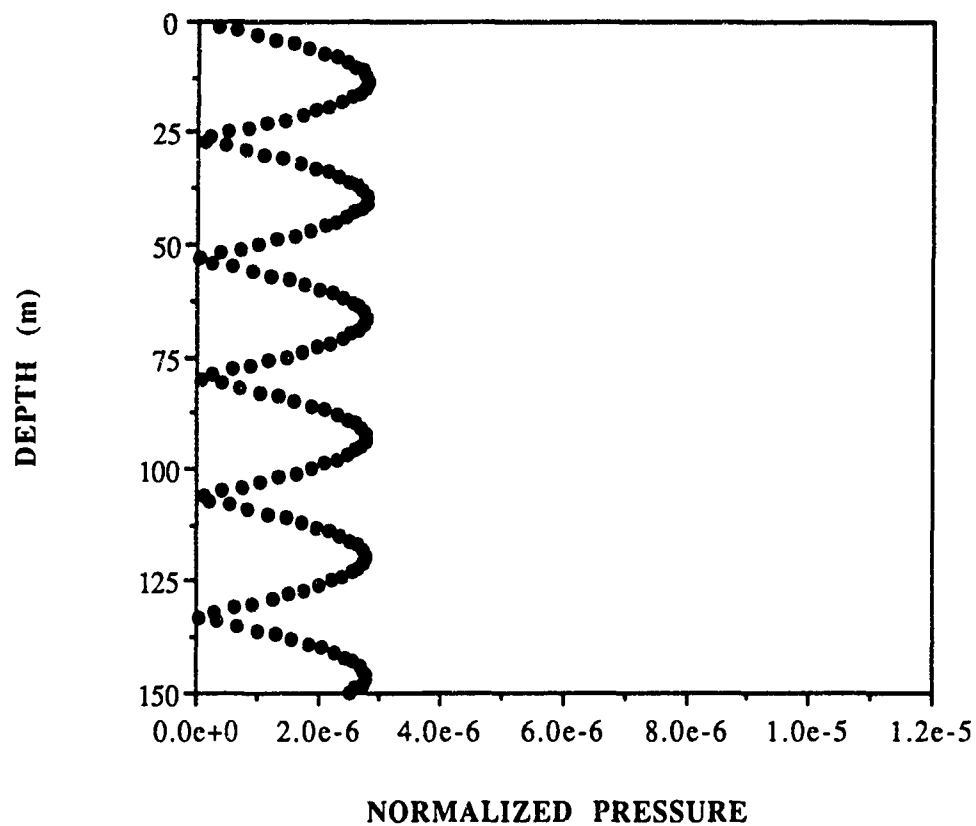


Fig. 39. Objects' Scattered Pressure vs. Depth at a Range of 300 (m) from the Object. Scattered Angle 90 (deg.). Mode 6 Only.

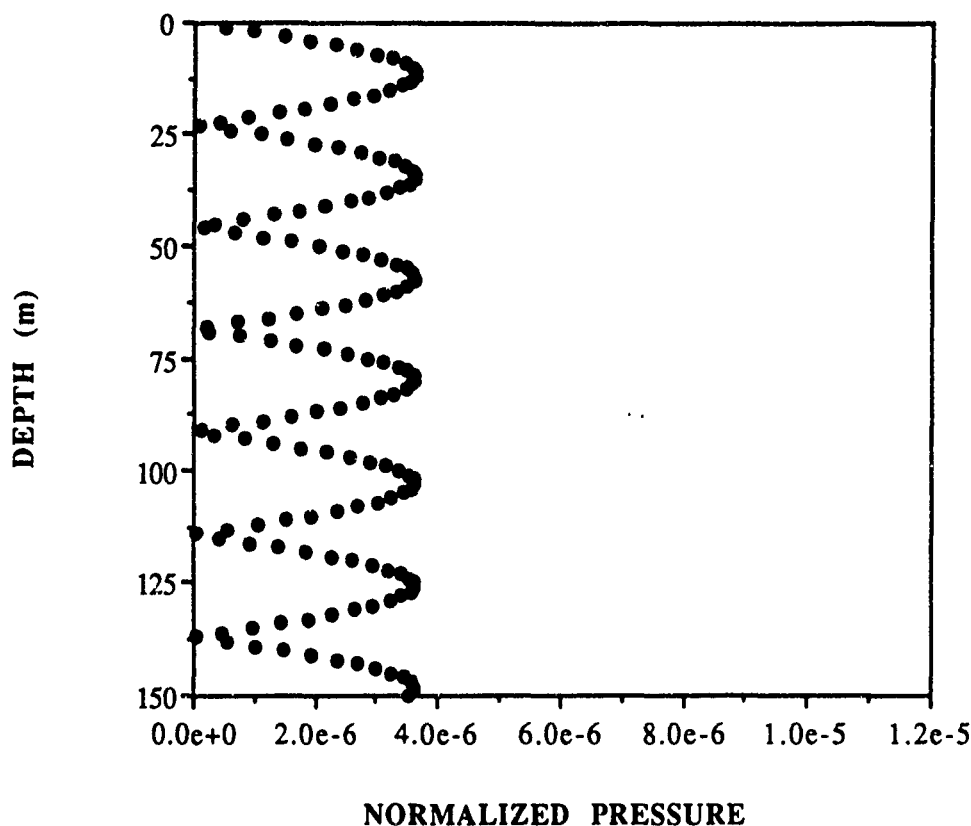


Fig. 40. Objects' Scattered Pressure vs. Depth at a Range of 300 (m) from the Object. Scattered Angle 90 (deg.). Mode 7 Only.

as a source, is introduced into the waveguide and the energy which radiates from it must behave as any other source would behave, propagating according to the restrictions imposed on it by the boundary conditions. These restrictions manifest themselves through the eigenfunctions. If we look at the 7 depth eigenfunctions for this waveguide (Figs. 41-47) we see that modes 2, (Fig. 42) 4, (Fig. 44) and 6 (Fig. 46), each have a null at or very near the mid-point of the waveguide. Modes 1, (Fig. 41) 3, (Fig. 43) 5, (Fig. 45) and 7 (Fig. 47) have a maximum, (or a minimum) at or near the mid-point of the waveguide. When any source is placed at the mid-point of the waveguide the odd numbered modes will be highly excited while the even modes will not.

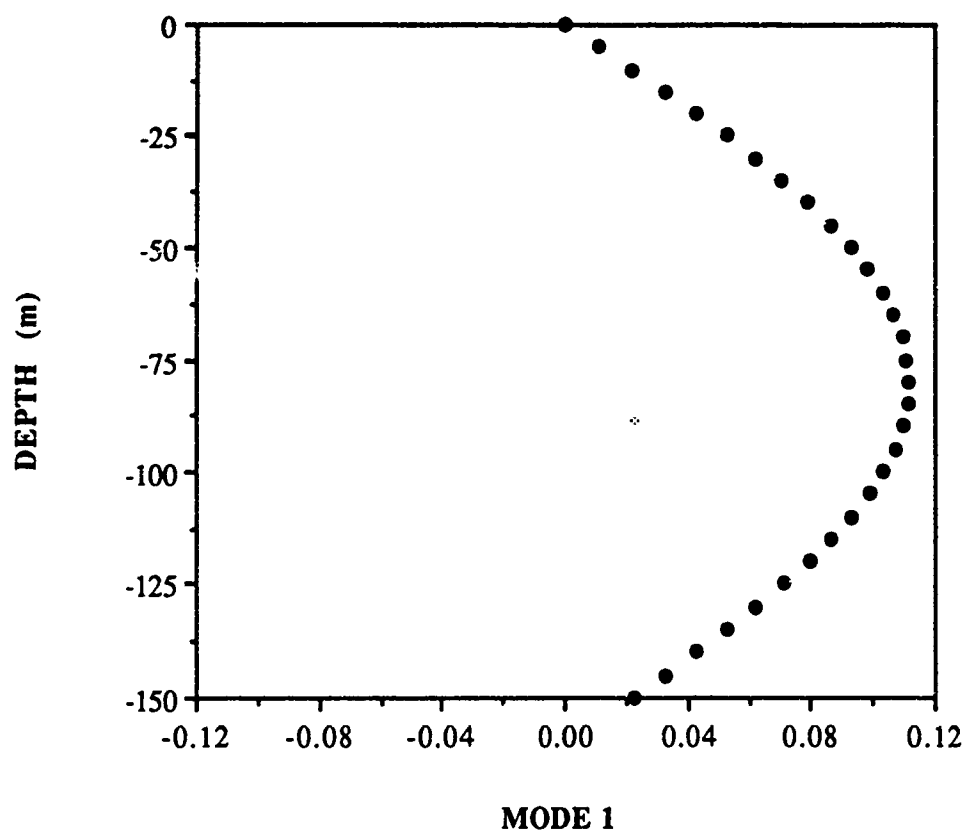


Fig. 41. Mode 1 Depth Eigenfunction.

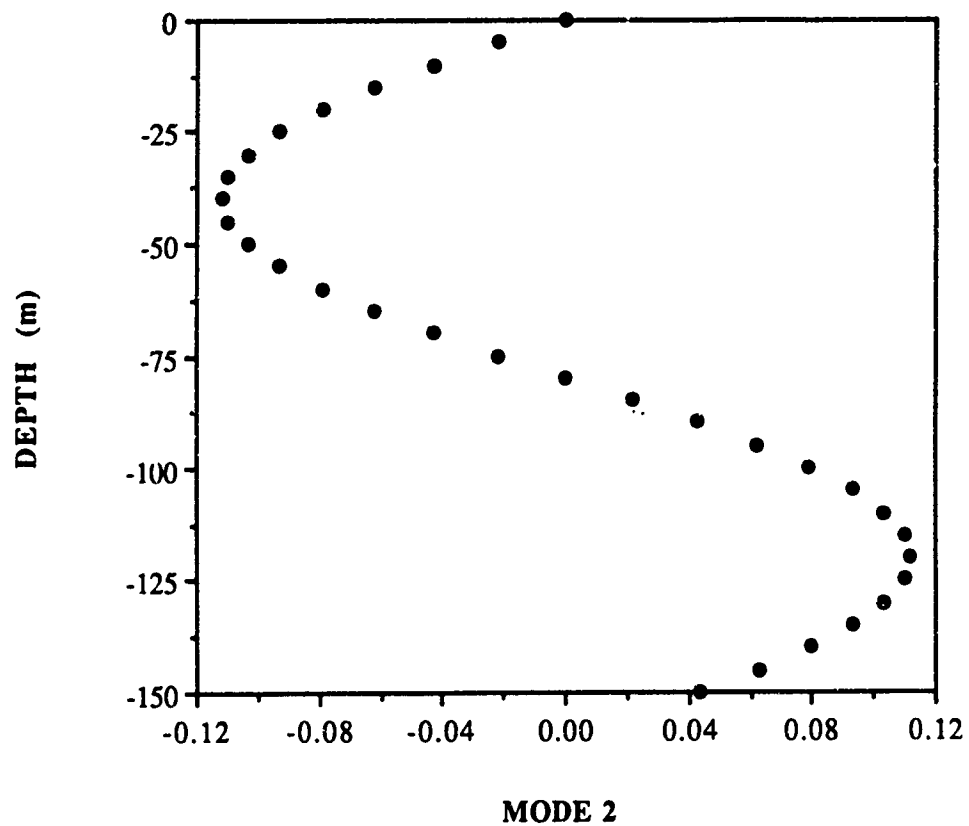


Fig. 42 Mode 2 Depth Eigenfunction.

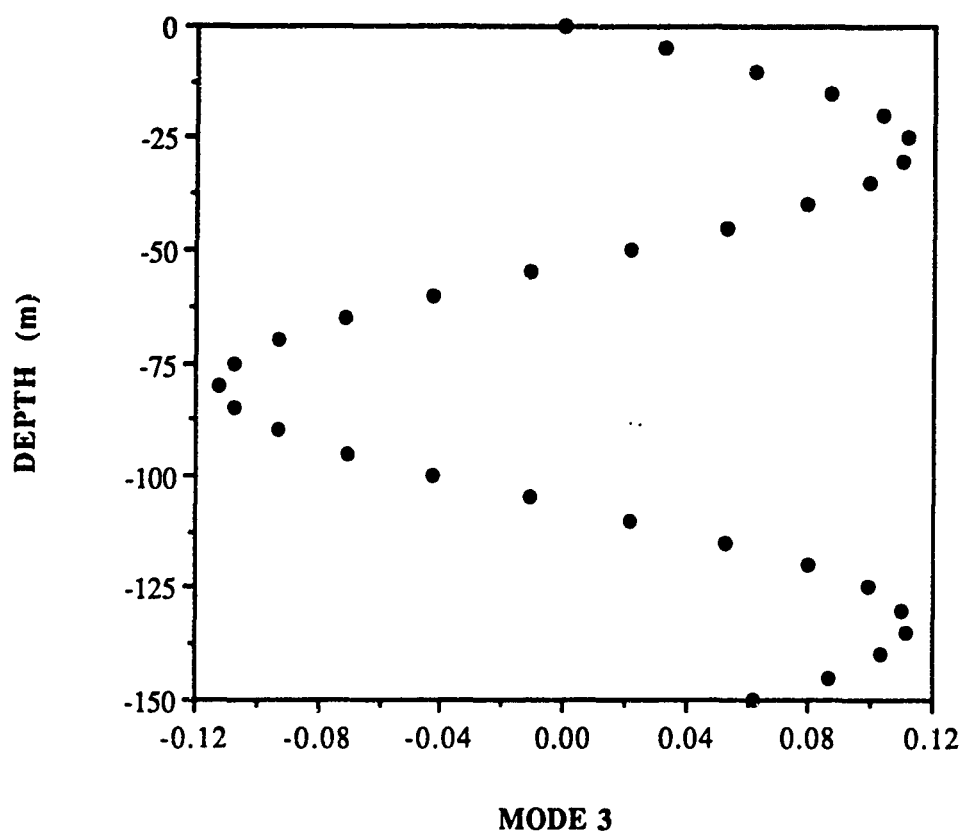


Fig. 43 Mode 3 Depth Eigenfunction.

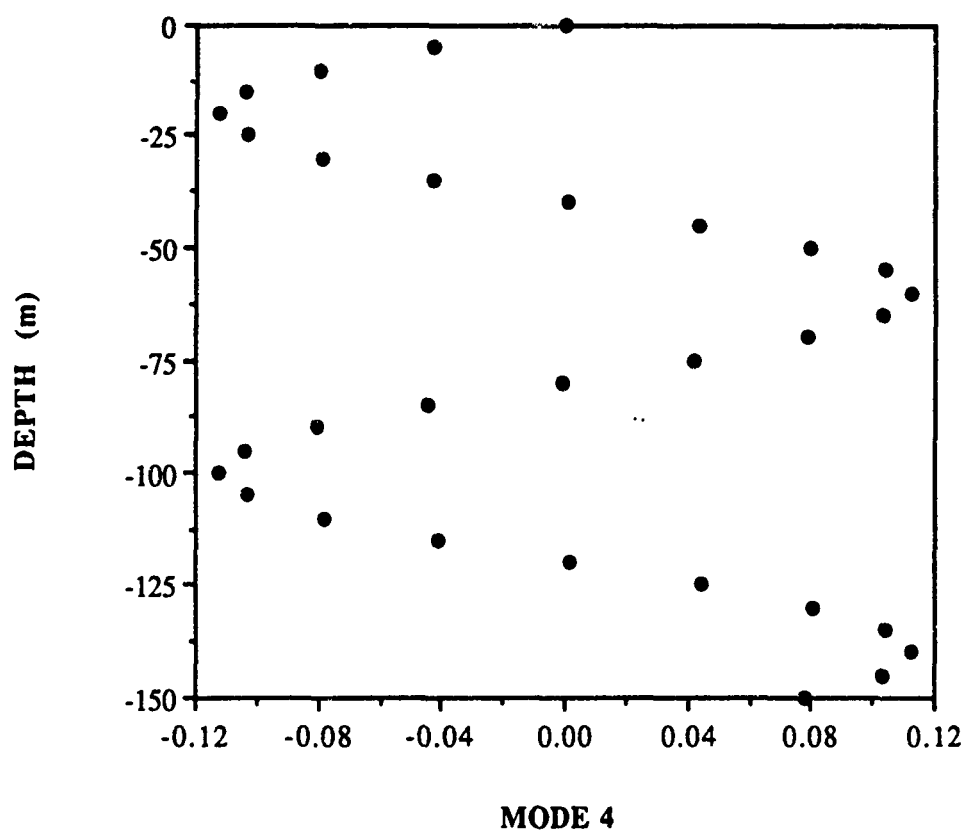
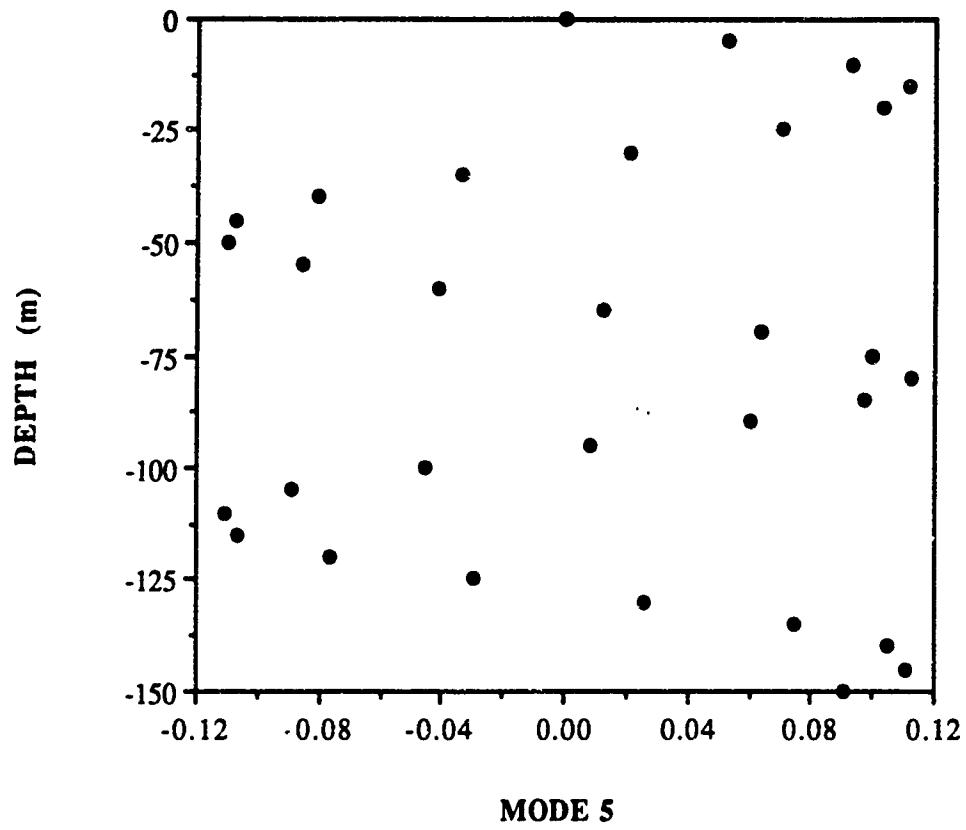


Fig. 44 Mode 4 Depth Eigenfunction.



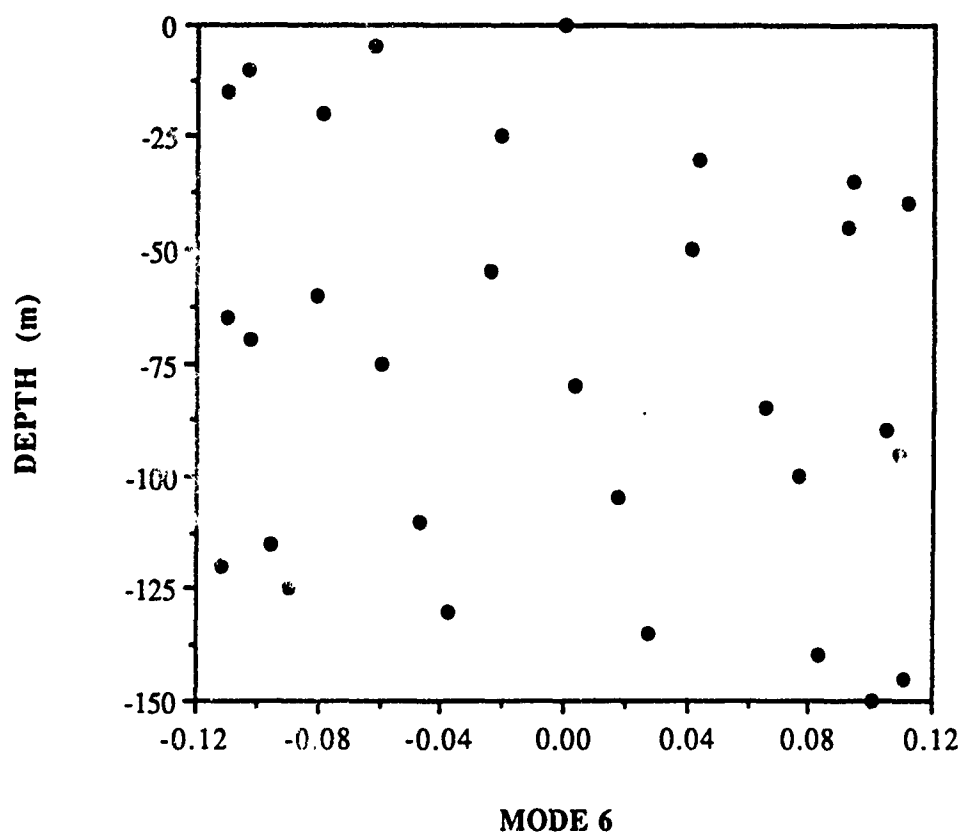


Fig. 46 Mode 6 Depth Eigenfunction.



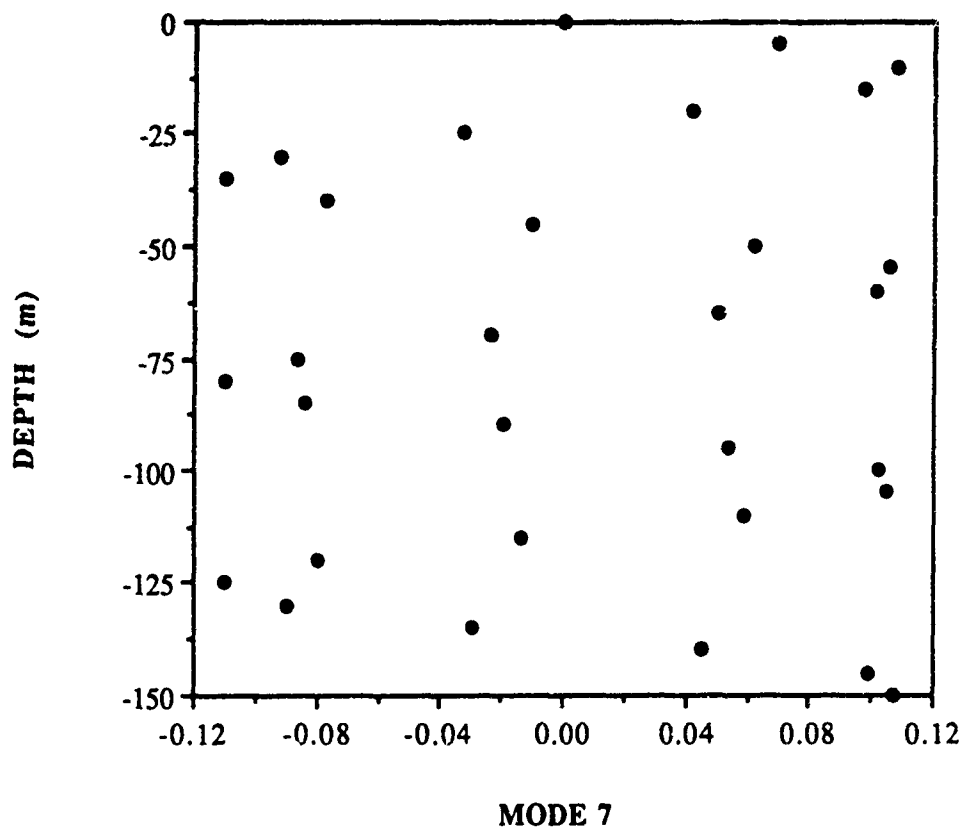


Fig. 47 Mode 7 Depth Eigenfunction.

This is what is happening with the scattered field.

Figure 48 depicts the vertical normalized pressure field at a range of 300 (m) and an angle of 0 degrees from the object. Notice that the field is approximately 1 order of magnitude smaller than the backscattered field and 3 orders of magnitude less than the incident field. It is clear that the scattered field is not symmetric about the object.

It is customary to show acoustic propagation in terms of transmission loss versus range, where transmission loss is  $-20 \log P$  where  $P$  is the normalized pressure. The pressure is normalized relative to the pressure from the point source at a range of 1(m). Figure 49 shows a comparison between the

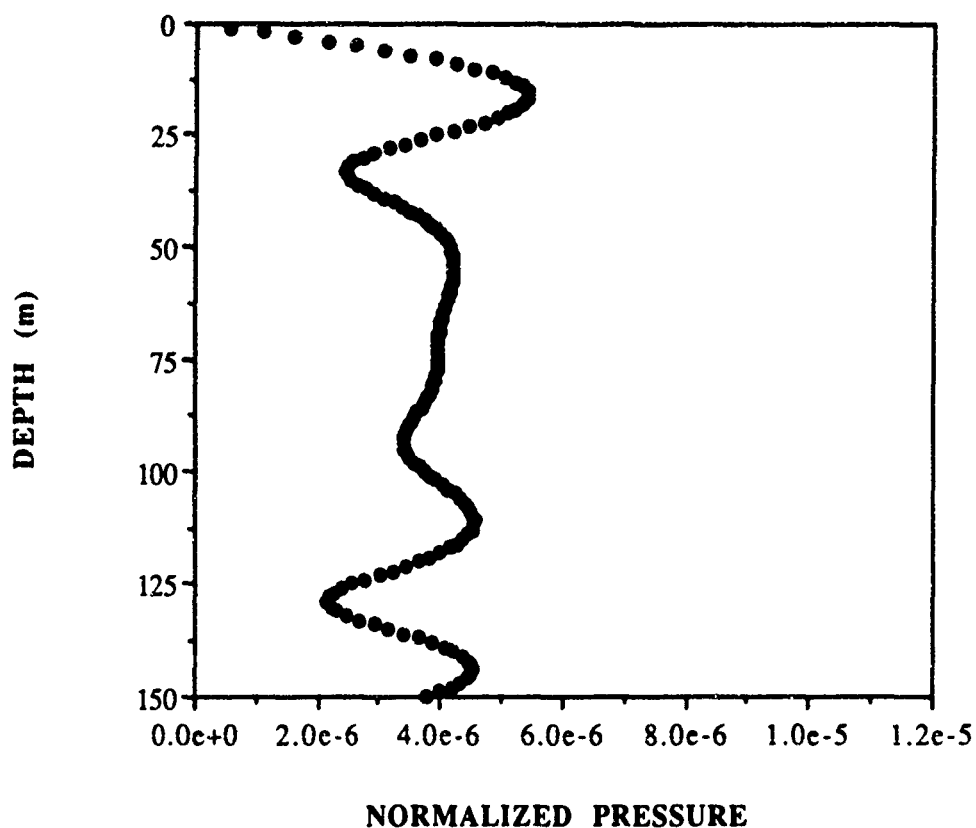


Fig. 48. Objects' Scattered Pressure vs. Depth at a Range of 300 (m) from the Object. Scattered Angle 0 (deg).

point source transmission loss and the forward and backscattered transmission loss of the object. The object is at a range of 5000 (m) from the source. This was obtained by solving for the scattered field 1500 (m) from the object, in both the forward and backward direction. This graphically shows the difference between the two fields. The total field would be a coherent sum of the two. Expressed logarithmically (in dB), there would be little or no change in the incident field, since the scattered field is so small.

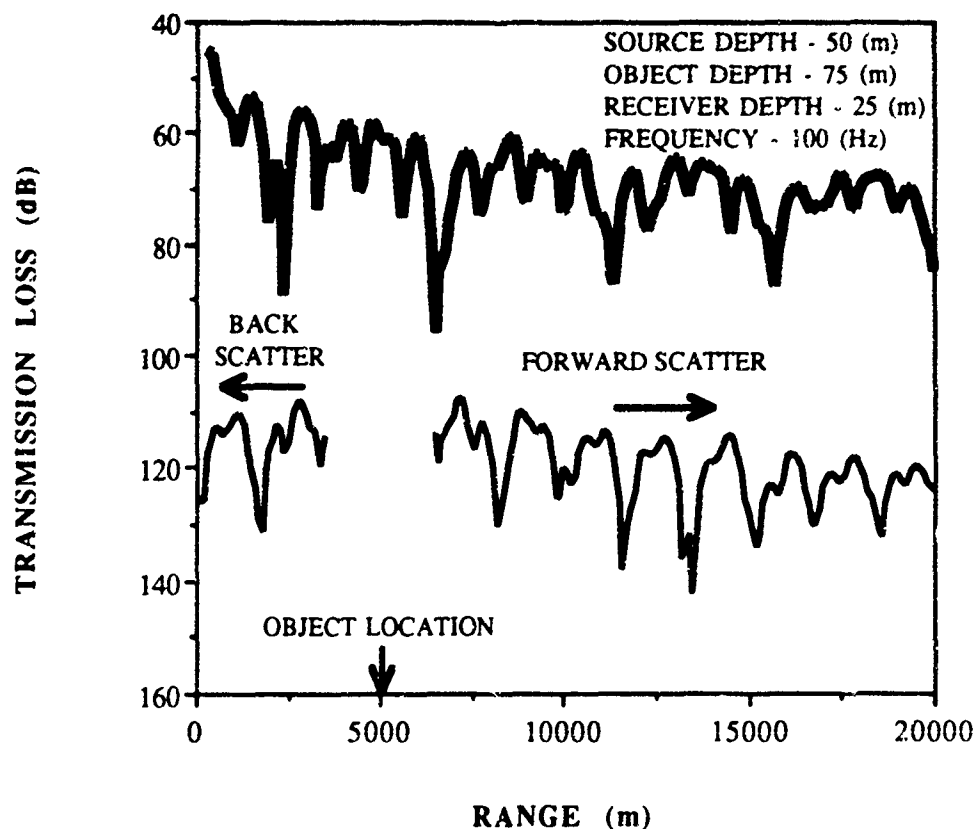


Fig. 49. Comparison of the Transmission Loss vs. Range of the Point Source and the Objects' Scattered Field.

Figure 49 gave a two dimensional view of the incident and scattered field. We now turn our attention to representing the incident, scattered and total field in three dimensions. The idea is illustrated in Fig. 50. A portion of the waveguide is defined by the three dimensional rectangular region; the source is located somewhere in this volume. Next we superimpose a solution grid at some depth in the waveguide. In general the point source and the solution grid will not be at the same depth. At each point of the grid, we determine the pressure and consequently the transmission loss due to the point source. An example is shown in Fig. 51. The source is at a depth of 50 (m) and is at the center of the grid, which is at a depth of 25 (m). Note the cylindrical symmetry produced by the point source, and the modal interference pattern.

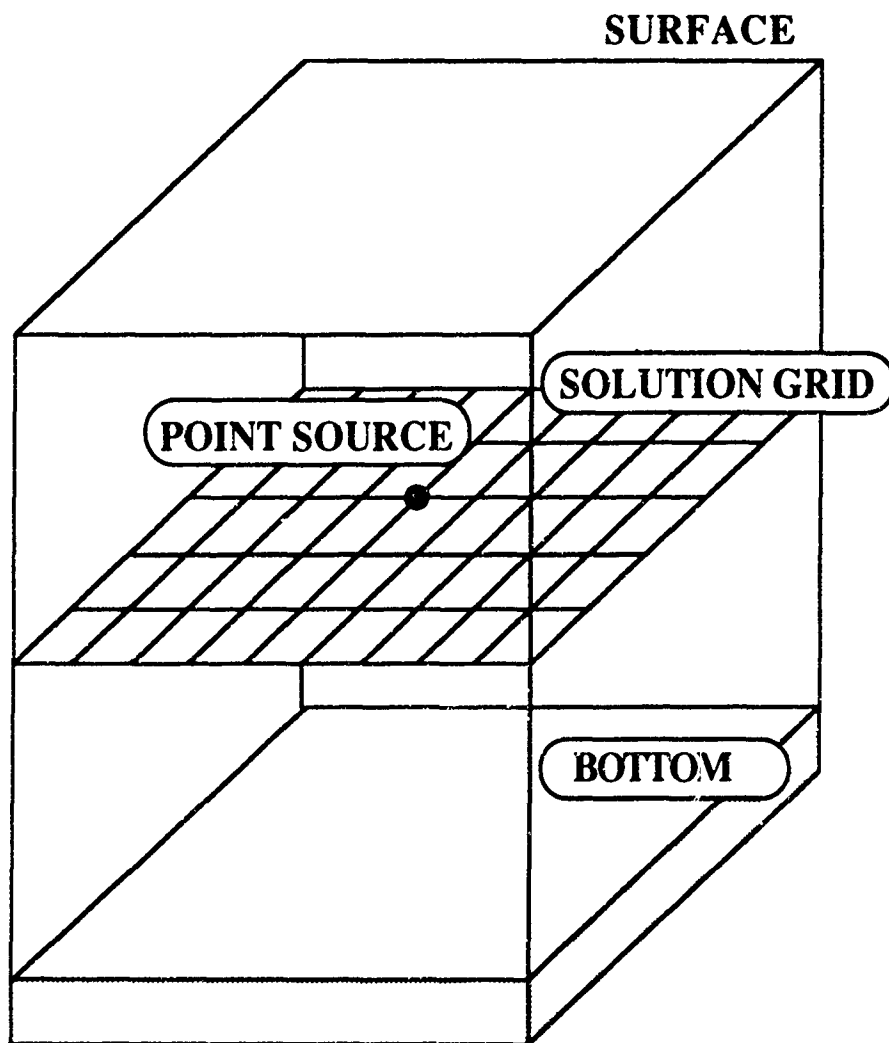


Fig. 50. Schematic Drawing Depicting the Geometry for a Three Dimensional Solution.

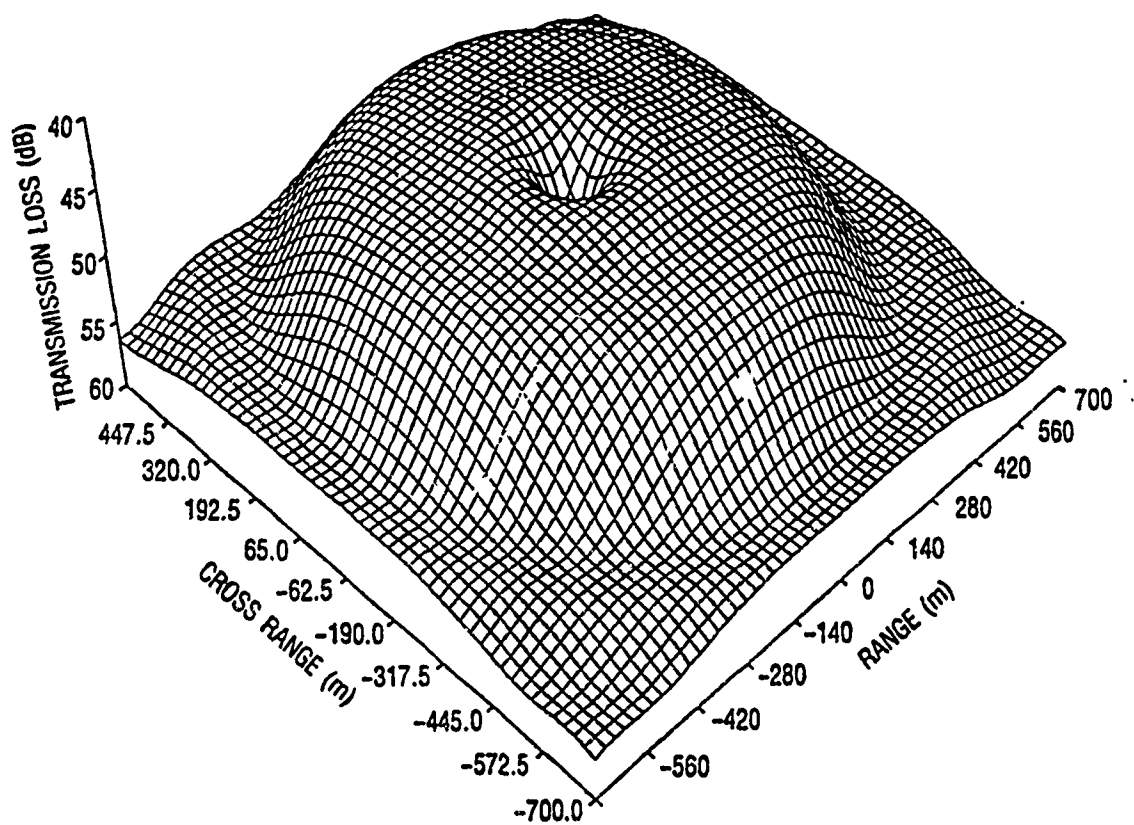


Fig. 51. Three Dimensional Field Produced by a Point Source.

We allow the field shown in Fig. 51 to propagate in the waveguide and allow it to insonify the object. We compute the field in three dimensions between the ranges of 4300 (m) and 5700 (m) with a cross range of 1175 (m); this represents a grid containing 2856 points. Figure 52 depicts the results. Notice how smooth the field is. The lack of structure is due to the small number of modes propagating. There is still a small amount of curvature to the wavefront. Finally we will place the object at a range of 5000 (m) and solve for the scattered field. The results are illustrated in Fig. 53. The most obvious feature is that the scattered field is not azimuthally symmetric. The major axis of symmetry of the object is parallel to the cross range axis. Notice that the forward scattered field is slightly stronger than the backscattered field and that the backscattered field is broader than the forward scattered field. The forward scattered field also appears to have a high pressure lobe on each side of the main field. And finally note that the field emanating from either end of the object, (90 degrees relative to either the forward or backward scattered field) is much lower than any other direction.

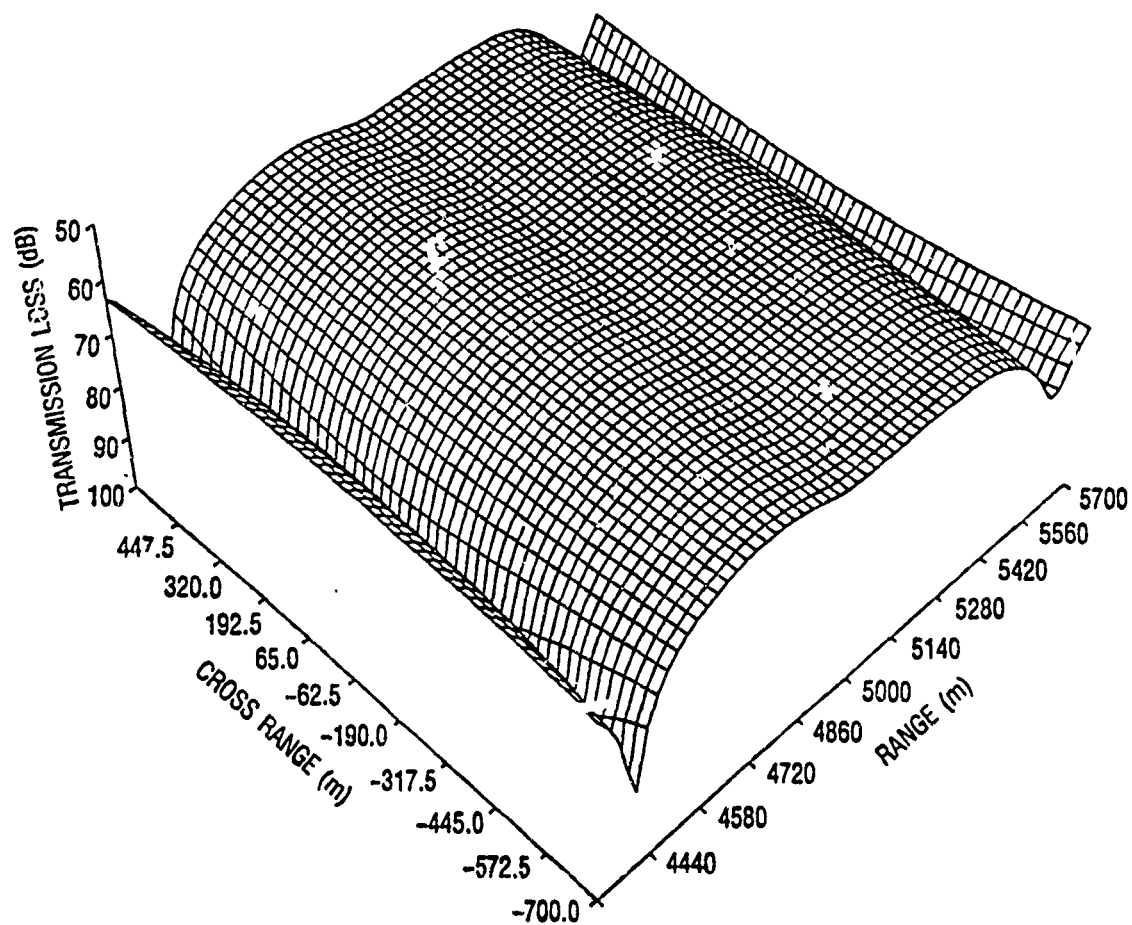


Fig. 52. Three Dimensional Point Source Field Between a Range of 4300 (m) and 5700 (m).

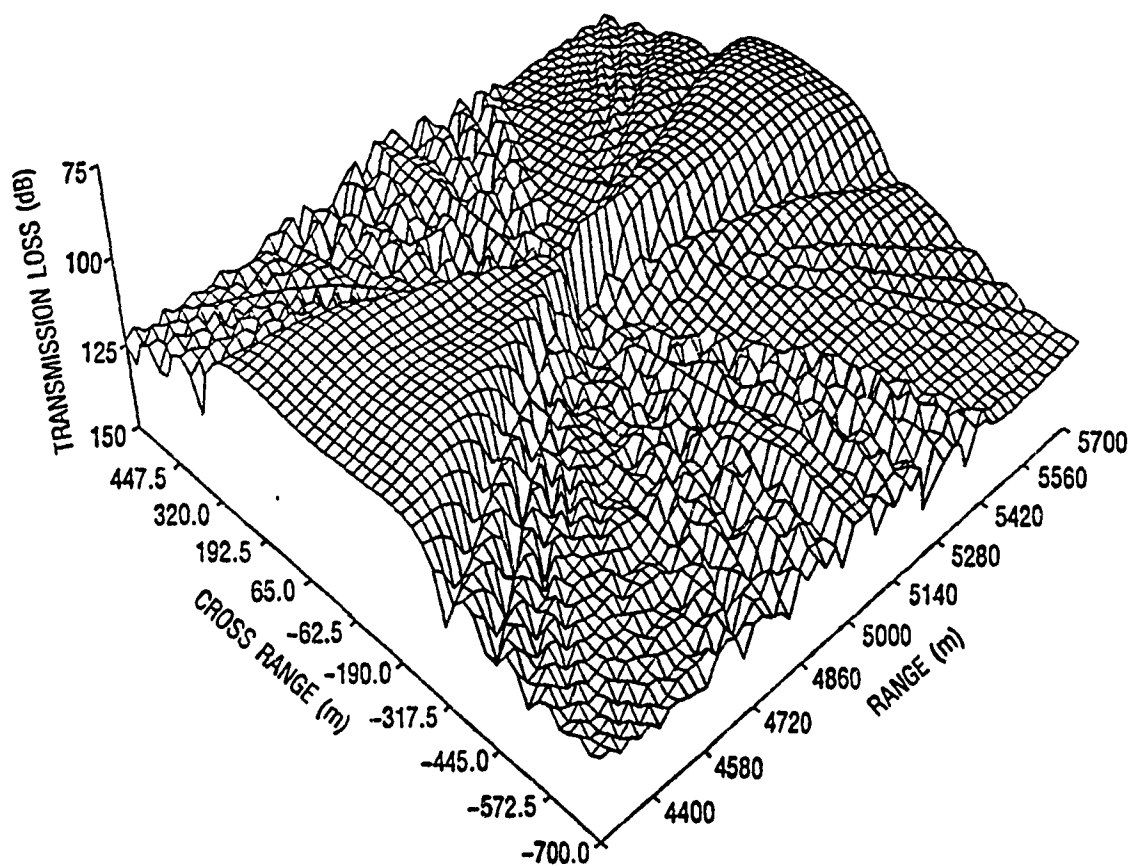


Fig. 53. Three Dimensional Objects' Scattered Field Between a Range of 4300 (m) and 5700 (m) from the Source.



We now investigate in more detail the scattered field of the object. If the object is truly incorporated into the waveguide then we should see both free field and waveguide characteristics in this field. Figure 54 illustrates the free field scattered field (near field) after the object has been insonified by the 7 modes. The field is expressed as transmission loss. The smaller the number, the stronger the signal. The arrow indicates from which direction the incident field is coming.

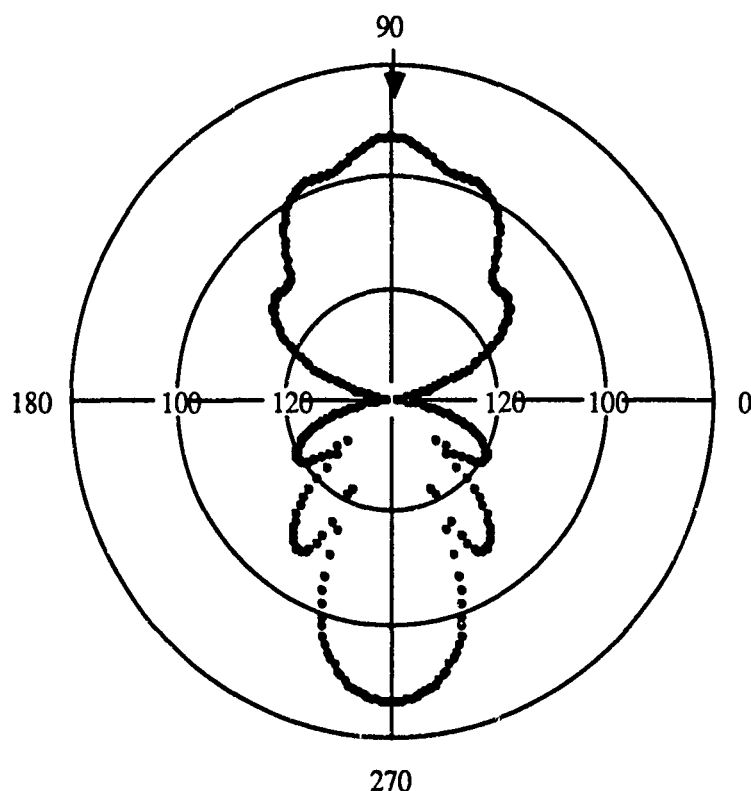


Fig. 54. The Objects' Free Field Scattered Field vs Angle, After 7 Modes Insonified It.

Comparing Fig. 54 with Fig. 53 we can make the following observations. First, in both cases, the forward scattered field is narrower than the backscattered field. Second, from Fig. 54 we see that the forward scattered field

does indeed have well pronounced side lobes. Third, in both cases the field is the weakest along the major axis of symmetry. We now look at the field produced by a point source at the objects' depth of 75 (m). Figure 55 illustrates the field. We notice that this field peaks at two separate ranges. The first is at approximately 100 (m) and the other is at approximately 400 (m). Referring to the field of the object in Fig. 53, we notice a very slight undulation of both the forward and back field. The peak of this undulation is occurring at approximately 400 (m) from the object. This would correspond to the second peak in Fig. 55. The first peak is not observed. It could be that the objects' free field effects are dominant close to the object since the field has not propagated long in the waveguide. This indicates that we have coupled the free field scattered field into the waveguide.

We now coherently add the incident field, Fig. 52, and the scattered field, Fig. 53 to obtain the total field, which is illustrated in Fig. 56. There is no discernable difference between the total field and the incident field of Fig. 52. If, however, we look at the difference (in dB space) between the total field and the incident field, we will be left with just the change in the field due to the object. Figure 57 shows this difference: the effect of the object is limited to the forward and backward direction. The largest effect is observed in the backward direction due to the fact that there is a minimum in the incident field at this location. The difference is less than 2 (dB). In the forward direction we see that the scattered field does indeed have an effect, but it is very slight, only 1 (dB) or less.

Having obtained the total field for a coherent addition of the incident and scattered fields for a single-layer waveguide, we proceed to a multilayered waveguide in which the sound speed will vary with depth.

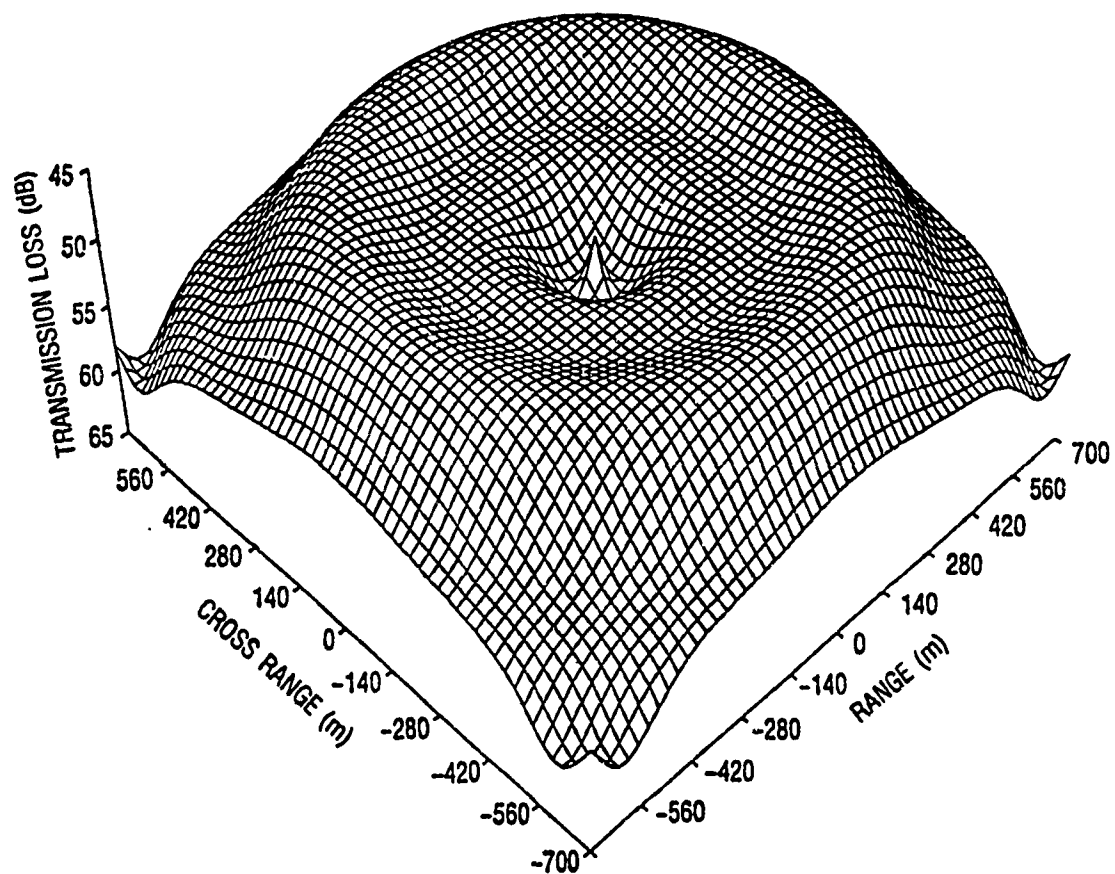


Fig. 55. Three Dimensional Field Produced by a Point Source at the Objects' Depth of 75 (m).

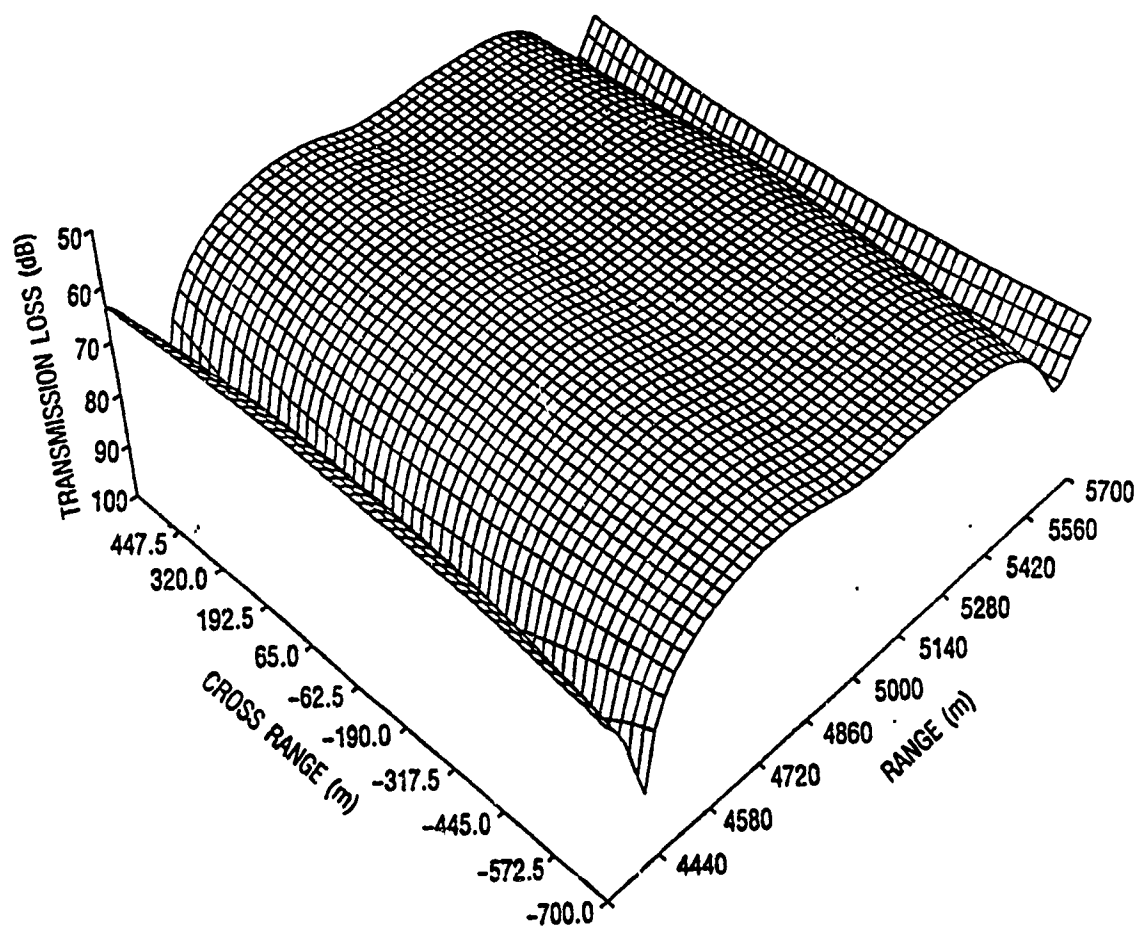


Fig. 56. Three Dimensional Total Field.

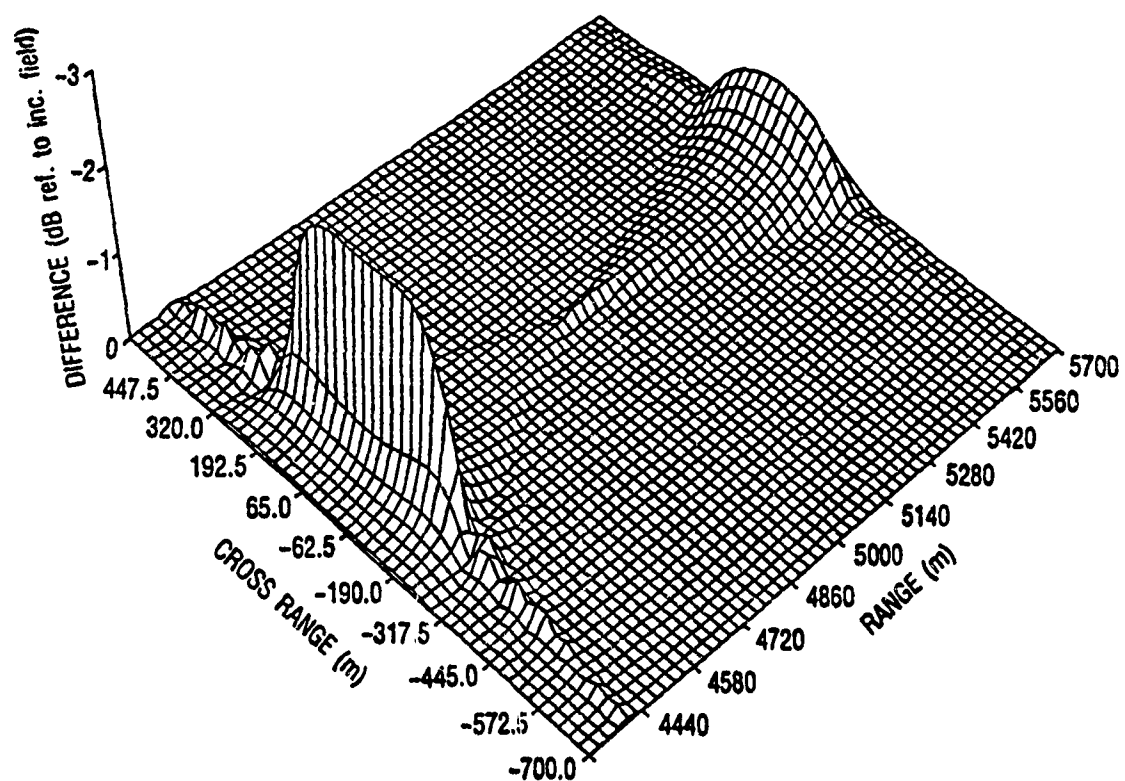


Fig. 57. Three Dimensional Difference Field Between the Total Field and the Incident Field.

## CHAPTER 6

### APPLICATION OF HUYGENS' PRINCIPLE TO A MULTILAYERED WAVEGUIDE

In this chapter we develop the scattered field for an object in a waveguide consisting of multiple isovelocity water and sediment layers. Because the general development is the same as in Chapter 5, we will only point out the difference between the two expressions due to the differences in the waveguides. We conclude this chapter with an example: we will explore what happens to the field when the object is insonified by only a few of the propagating modes. This can happen when the source is in a duct or sound channel and the object is outside of this feature. In Appendix E, we compare this method with the projection method described method in Chapter 4.

#### Theory

The development of the field due to a harmonic point source in a waveguide consisting of many isovelocity layers is given by Tolstoy. (1,2) We start with the expression for the acoustic field, previously developed

$$(6-1) \quad P(r, z) = C \sum_n \frac{Z_n(z_s) Z_n(z)}{\sqrt{K_n r}} e^{-\alpha_n r} e^{-i K_n r}$$

where  $Z_n$  is the depth eigenfunction,  $K_n$  is the horizontal eigenvalue,  $z$  is the depth of the field point and  $z_s$  is the source depth. The horizontal range

between the source and the field point (receiver) is given by  $r$  and  $\alpha_n$  is the modal attenuation coefficient, (See appendix D for further information). The attenuation term takes into account energy losses due to interaction with the boundaries and losses due to propagation of the signal in the water. The geometry of the waveguide with the object is the same as illustrated in Figs. 13 and 14. The derivation of the incident field is the same as for the isovelocity case of Chapter 5 except that the depth eigenfunctions of Equation (6-1) take a different form. They are as follows,

$$(6-2) \quad Z_n(z_s) = A_n \sin(\gamma_n z_s) + B_n \cos(\gamma_n z_s)$$

$$(6-3) \quad Z_n(z) = A_n \sin(\gamma_n z) + B_n \cos(\gamma_n z)$$

Where  $\gamma_n$  is the vertical eigenvalue.

The expression equivalent to Eq.(5-63) is the following:

$$(6-4) \quad P(r, z) = C \sum_{n=1}^N \frac{A_n \sin(\gamma_n z_s) + B_n \cos(\gamma_n z_s)}{\sqrt{K_n r_{so}}} e^{-\alpha_n r_{so}} \\ \cdot \left( \frac{A_n}{2i} + \frac{B_n}{2} \right) e^{i(\gamma_n Z_{obj} - K_n r_{so})} e^{i(\gamma_n, K_n \sin(\alpha_{inc}), K_n \cos(\alpha_{inc})) \cdot (X_o, Y_o, Z_o)} \\ + C \sum_{n=1}^N \frac{A_n \sin(\gamma_n z_s) + B_n \cos(\gamma_n z_s)}{\sqrt{K_n r_{so}}} e^{-\alpha_n r_{so}} \\ \cdot \left( \frac{-A_n}{2i} + \frac{B_n}{2} \right) e^{-i(\gamma_n Z_{obj} + K_n r_{so})} e^{i(-\gamma_n, K_n \sin(\alpha_{inc}), K_n \cos(\alpha_{inc})) \cdot (X_o, Y_o, Z_o)}$$

The incident field in terms of the spherical coordinates is now given as

$$(6-5) \quad U_i(\rho) = \sum_n \sum_{l, m, \sigma} \alpha_{n, l, \sigma}^m \operatorname{Re} \Psi_{l, \sigma}^m(\rho)$$

where  $n$  is the index specifying the number of modes and  $l, m, \sigma$  are the indices for the spherical harmonics. The partial waves coefficients (Equivalent to Eq. (5-74)), of the incident field are given by the following,

$$(6-6) \quad \alpha_{n, l, \sigma}^m = C \frac{A_n \sin(\gamma_n z_s) + B_n \cos(\gamma_n z_s)}{\sqrt{K_n r_{so}}} e^{-\alpha_n r_{so}} \\ \cdot \left( \left( \frac{A_n}{2i} + \frac{B_n}{2} \right) e^{i(\gamma_n Z_{obj} - K_n r_{so})} \right) a_{l, \sigma}^m \\ + C \frac{A_n \sin(\gamma_n z_s) + B_n \cos(\gamma_n z_s)}{\sqrt{K_n r_{so}}} e^{-\alpha_n r_{so}} \\ \cdot \left( \left( \frac{-A_n}{2i} + \frac{B_n}{2} \right) e^{-i(\gamma_n Z_{obj} + K_n r_{so})} \right) a_{l, \sigma}^m$$

where  $z_s$  is the depth of the source,  $z_{obj}$  is the depth of the object and  $r_{so}$  is the range from the source to the object. The scattered field about the object has



the same form as Eq. (5-75) namely,

$$(6-7) \quad f(\rho) = \sum_{n,l,m,\sigma} \beta_{n,l,\sigma}^m \psi_{l,\sigma}^m(\rho)$$

where,

$$\beta_{n,l,\sigma}^m = T_{l,l',\sigma}^m \alpha_{n,l',\sigma}^m$$

and

$$\psi_{l,\sigma}^m(\rho) = h_l(k\rho) Y_{l,\sigma}^m(\theta, \varphi)$$

The development of the scattered field far from the object is equivalent to that developed in chapter 5. The difference is due to the fact that we now have different depth eigenfunctions shown in Eqs. (6-2) and (6-3).

The solution for the scattered field far from the object is the same as Eq. (5-76) namely,

$$(6-8) \quad U_s(r_s, z) = \int_{\sigma} \left( f(r) \frac{\partial G(r_s, z)}{\partial n} - G(r_s, z) \frac{\partial f(r)}{\partial n} \right) ds$$

where the surface  $\sigma$  is chosen at a suitable region circumscribing the object. The scattered field is written as

$$(6-9) \quad U_s(r_s, z) = C \sum_n \frac{Z_n(z_r)}{\sqrt{K_n r_{or}}} e^{-\alpha_n r_{or}} e^{-K_n r_{or}} B_n$$

where

$$B_n = \int_{\sigma} f(\rho) \frac{\partial}{\partial n} \left[ \frac{Z_n(z)}{\sqrt{1 - \frac{r \cos \theta}{r_{or}}}} e^{\alpha_n r \cos \theta} \frac{e^{iK_n r \cos \theta}}{e^{iK_n r \cos \theta}} \right] - \frac{Z_n(z)}{\sqrt{1 - \frac{r \cos \theta}{r_{or}}}} e^{\alpha_n r \cos \theta} \frac{e^{iK_n r \cos \theta}}{e^{iK_n r \cos \theta}} \frac{\partial}{\partial n} [f(\rho)] \cdot ds$$

and  $z_r$  is the depth of the receiver.

This expression satisfies all boundary conditions at the waveguide interfaces and is continuous throughout all space.

### Examples

In this example we have placed the source and receiver in a weak sound channel, and the object has been placed near the bottom, Fig. 58 illustrates the geometry. The waveguide has 35 water layers and 3 sediment layers overlying the semi-infinite half space. The sound speed profile is shown in Fig. 59. The source is again at 100 (Hz). There are 16 propagating modes for this environment.

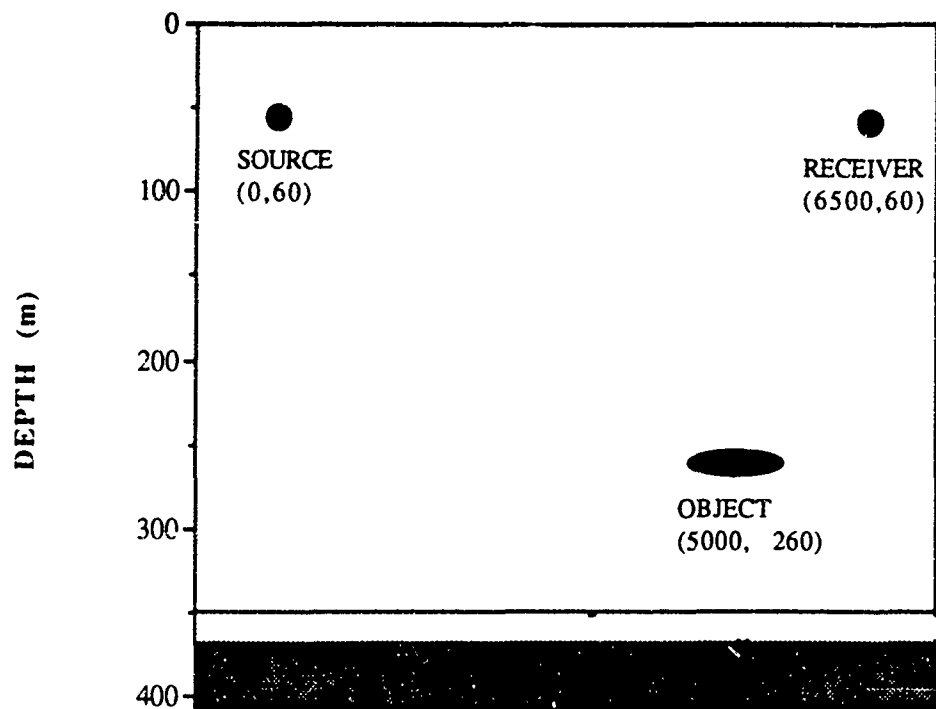


Fig. 58. Waveguide Geometry.

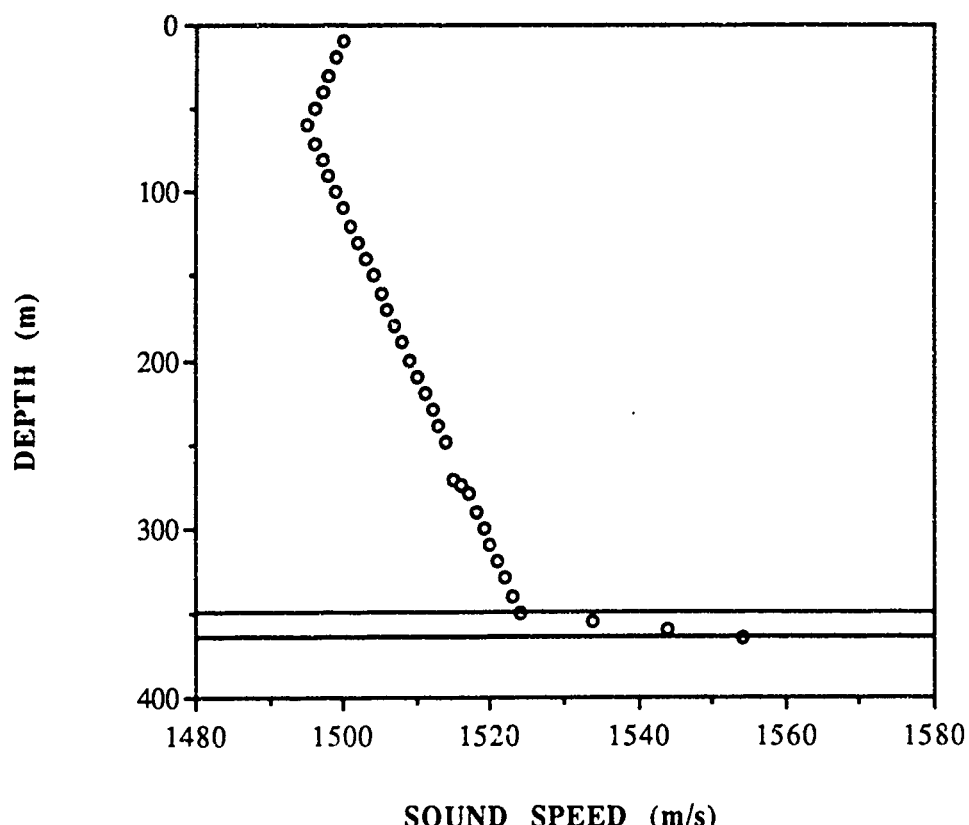


Fig. 59. Sound Speed Profile.

The characteristics of the object are the same as for the example in Chapter 5. We now allow the source to propagate to the object. Since the source is located at the apex of a sound channel the field produced by the lower order modes is concentrated in this channel. This means that with the object located outside the sound channel, those modes that remain in the sound channel will have little or no effect on the object. This can easily be illustrated by again isolating the modes at the object and looking at the vertical distribution of the scattered pressure due to the individual modes. In this example the first three modes have very little effect upon the object (See Figs. 61-64) with mode number 4 being the first mode to insonify the object with any appreciable energy. We therefore look at the vertical pressure at the

object due to the source insonifying it. Figure 60 illustrates the field. Notice that the field peaks at the source depth of 60 (m). The secondary peak results from the modal contributions which are not contained in the sound channel. This would correspond to higher order modes. The field diminishes very quickly after this secondary peak.

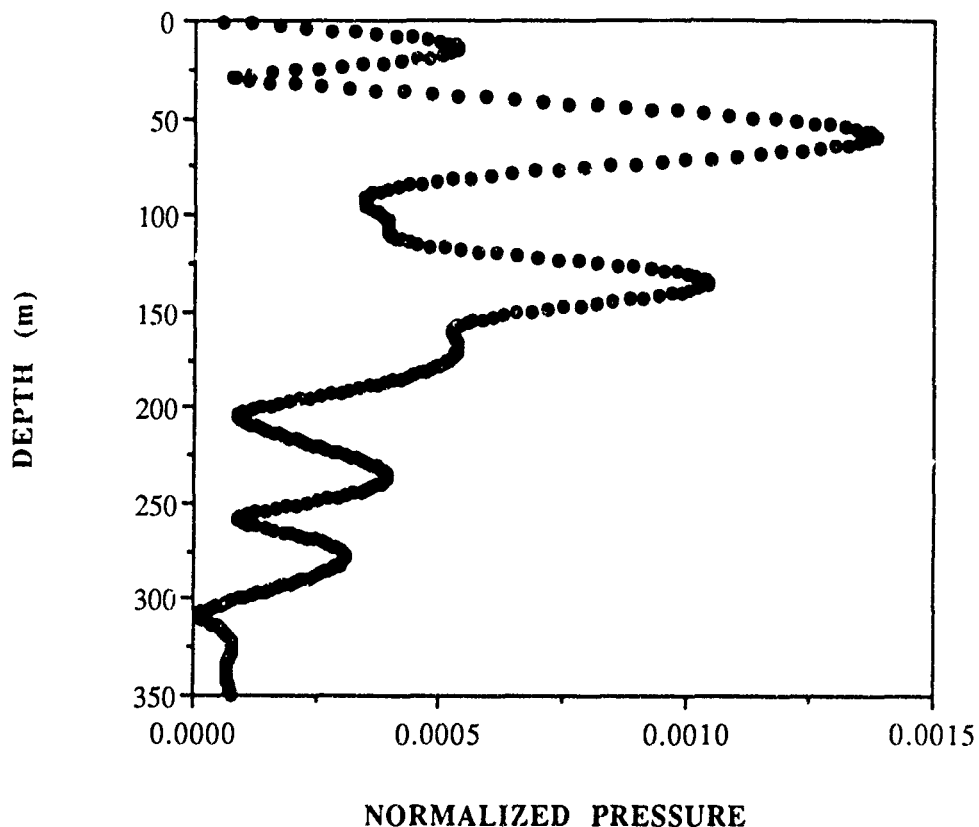


Fig. 60. Point Source Pressure vs. Depth at the Object, 5000 (m) from the Source.

We will now look at the effect that each of the first four modes have at the object. Figures 61-64 shows the pressure vs. depth at the object for the first four modes.

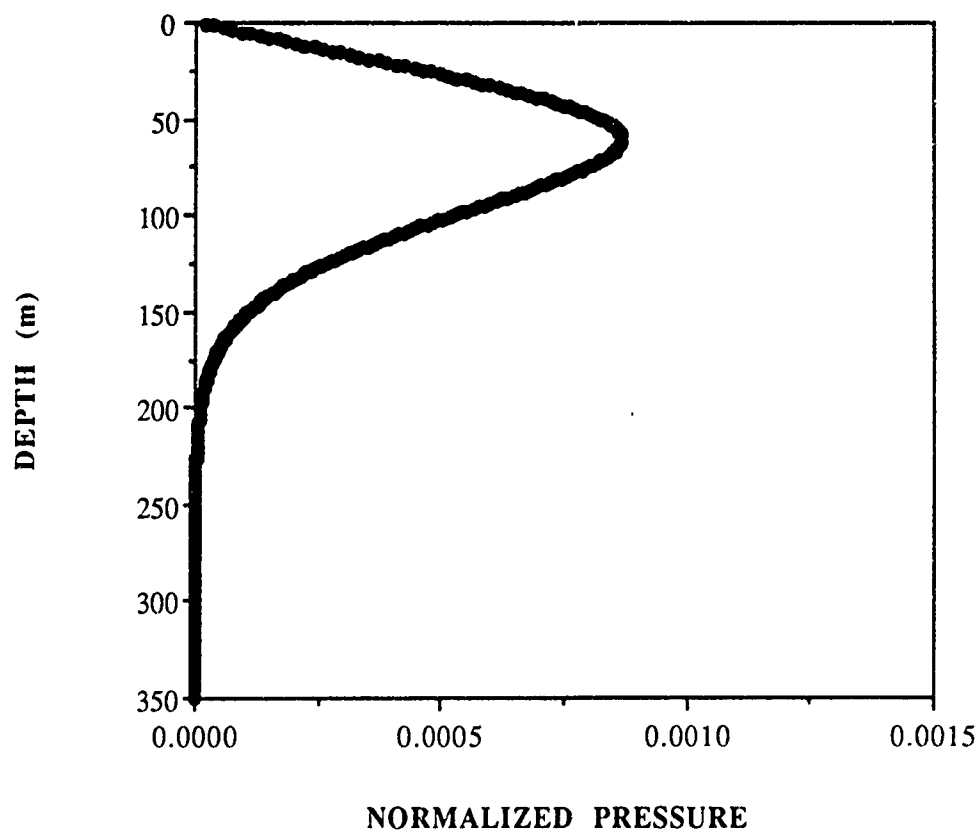


Fig. 61. Point Source Pressure vs. Depth at the Object, 5000 (m) from the Source. Mode 1 Only.

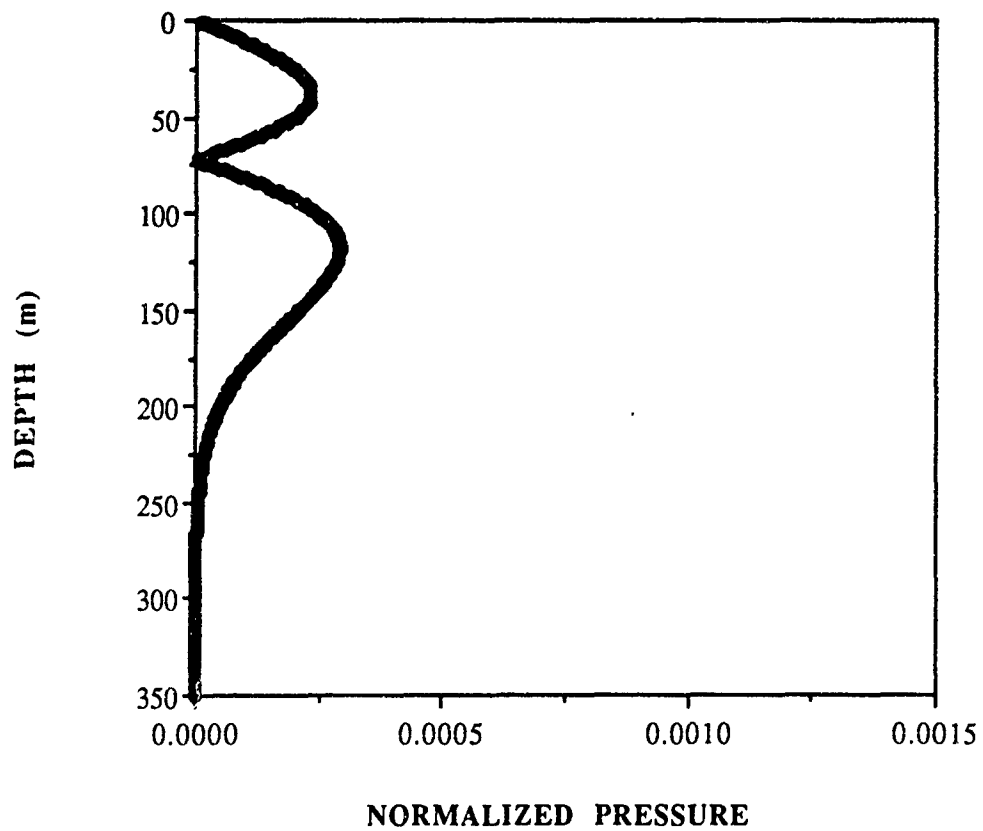


Fig. 62. Point Source Pressure vs. Depth at the Object, 5000 (m) from the Source. Mode 2 Only.

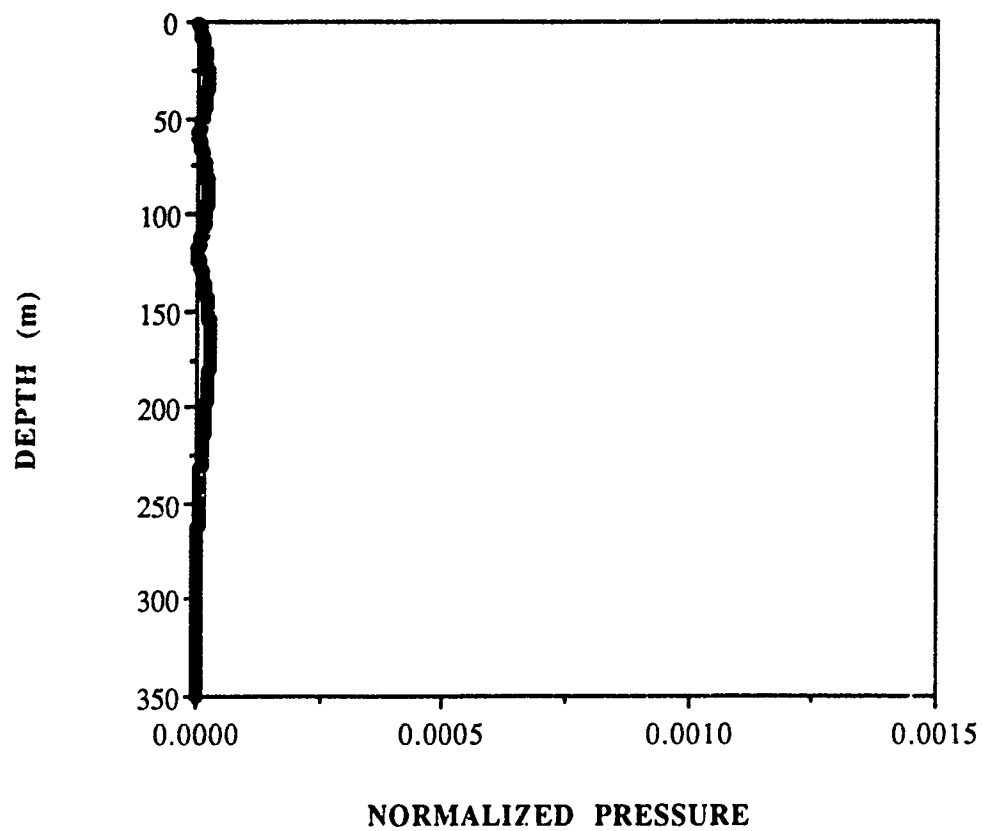


Fig. 63. Point Source Pressure vs. Depth at the Object, 5000 (m) from the Source. Mode 3 Only.



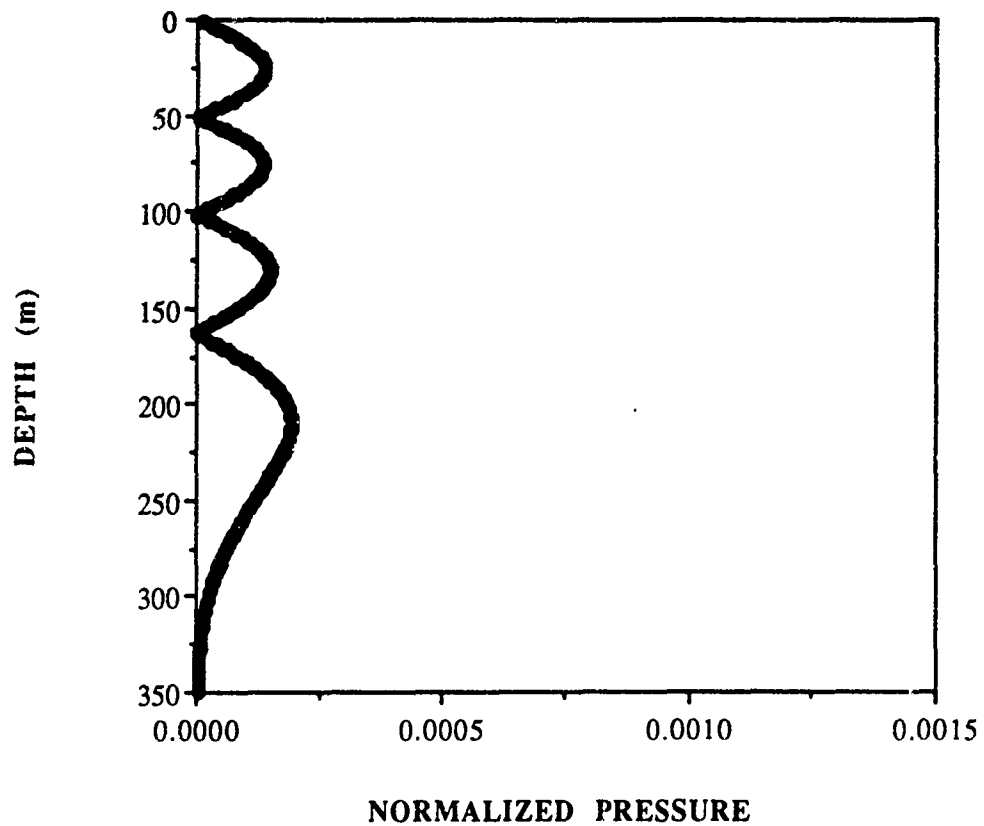


Fig. 64. Point Source Pressure vs. Depth at the Object, 5000 (m) from the Source. Mode 4 Only.

Notice that for mode 1 (Fig. 61) the maximum pressure is contained within the sound channel. The pressure dies off exponentially after a depth of 150 (m). This is to be expected since this mode is evanescent after this depth. This is also true for mode 2, (Fig. 62) we see the exponential decay of the pressure field at a greater depth than for mode one. Again this is consistent with mode theory, which states that the higher order modes will travel at a steeper angle and as such they will penetrate through the sound channel more than the lower order modes. Mode three (Fig. 63) is not excited by the point source and does not contribute much at any depth. Finally we see that for mode 4 (Fig. 64) the pressure is significantly larger at the object's depth of 260 (m). The field still decays exponentially starting approximately at the depth of the object.

Now we allow this field (all 16 modes) to insonify the object. Figure 65 shows the resulting field at a range of 1500 (m) in the forward direction (270 degree scattered angle). The field is approximately 3 orders of magnitude less than the incident field. One can see that the field is very complex, resulting from modal interactions. The field is not contained in the sound channel since the object, which is generating this field, is not within the sound channel. We will now look separately at the first four modes contained in this scattered field. Figures 66-69 depict the pressure vs. depth for the first four modes.

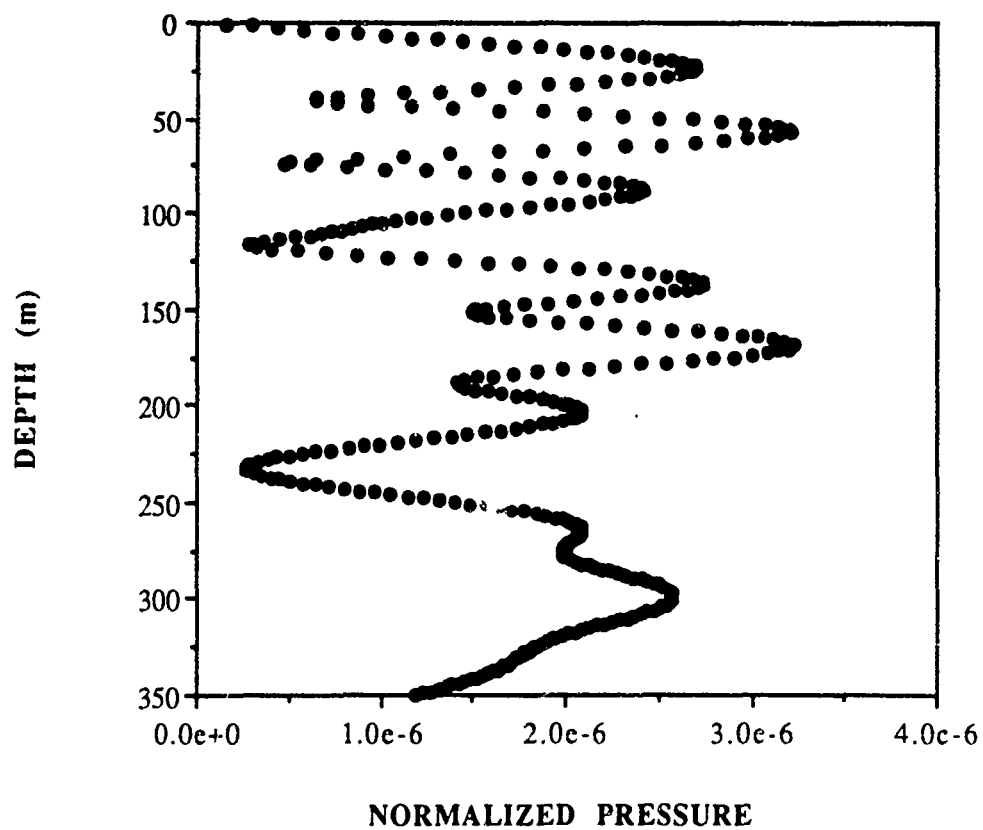


Fig. 65. Objects' Pressure vs. Depth at the Receiver, 1500 (m) from the Object. Scattered Angle 270 (deg).

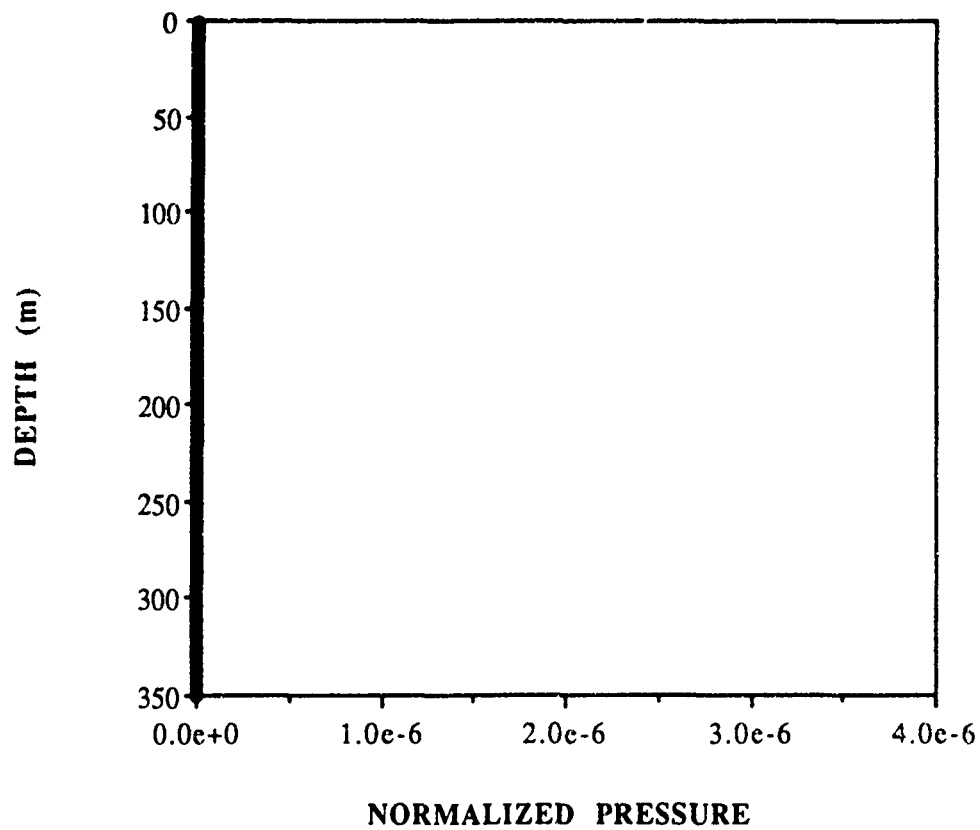


Fig. 66. Objects' Pressure vs. Depth at the Receiver, 1500 (m) from the Object. Scattered Angle 270 (deg). Mode 1 Only.

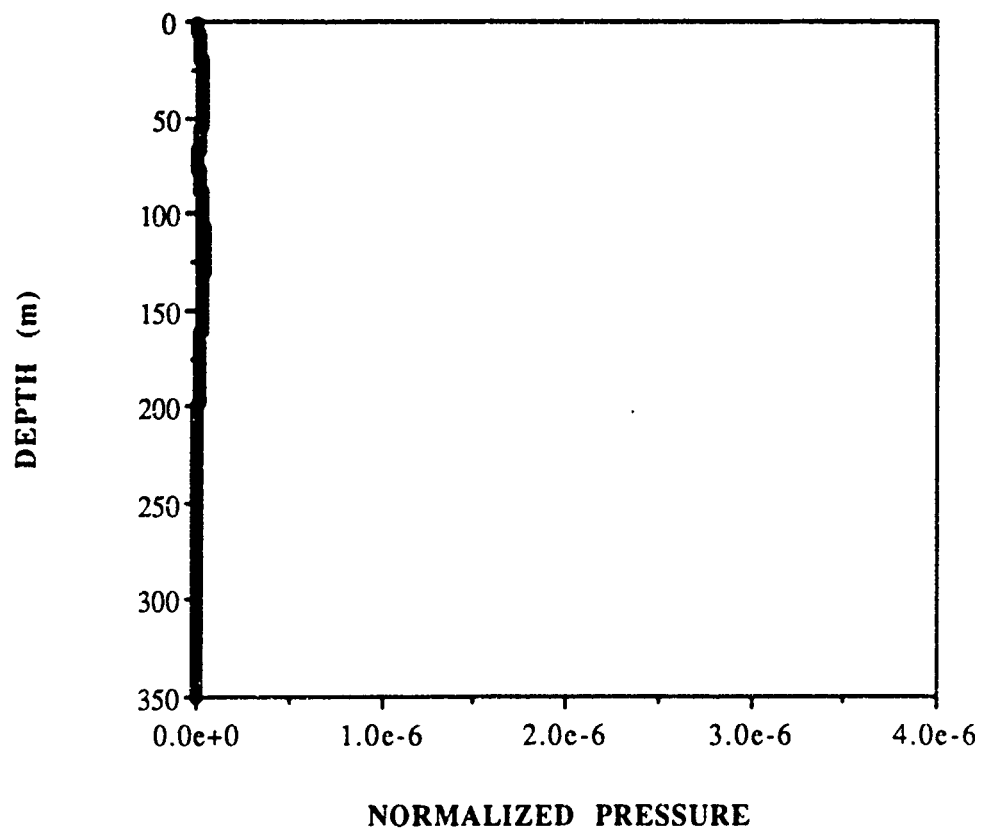


Fig. 67. Objects' Pressure vs. Depth at the Receiver, 1500 (m) from the Object. Scattered Angle 270 (deg). Mode 2 Only.

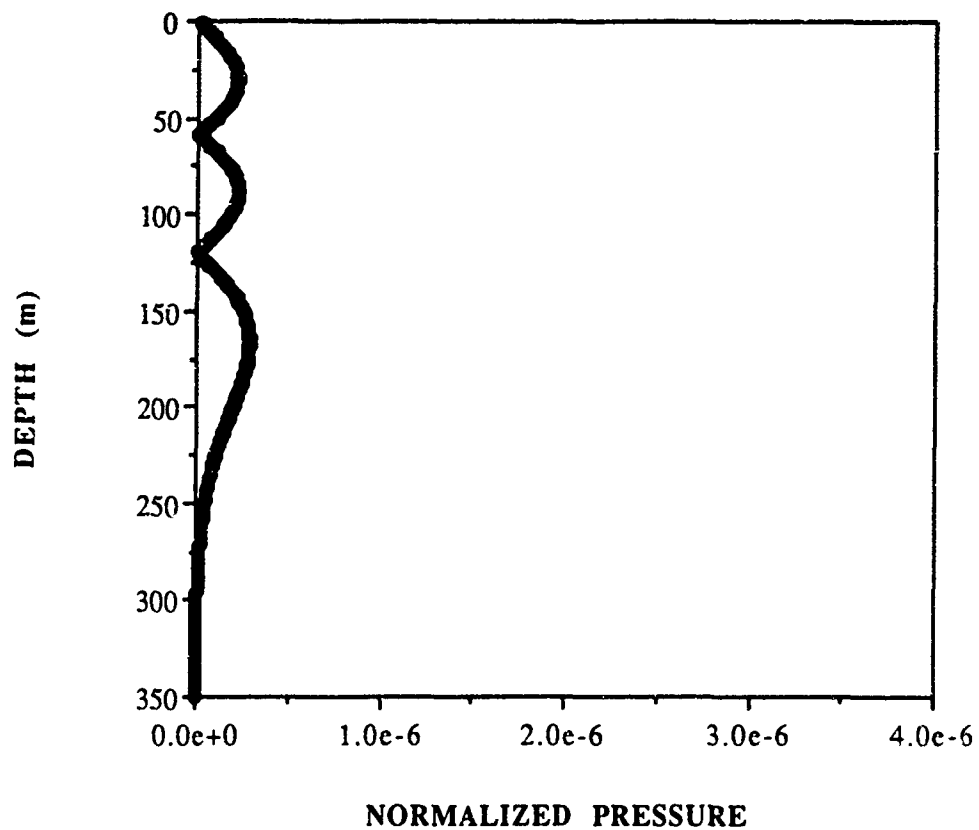


Fig. 68. Objects' Pressure vs. Depth at the Receiver, 1500 (m) from the Object. Scattered Angle 270 (deg). Mode 3 Only.

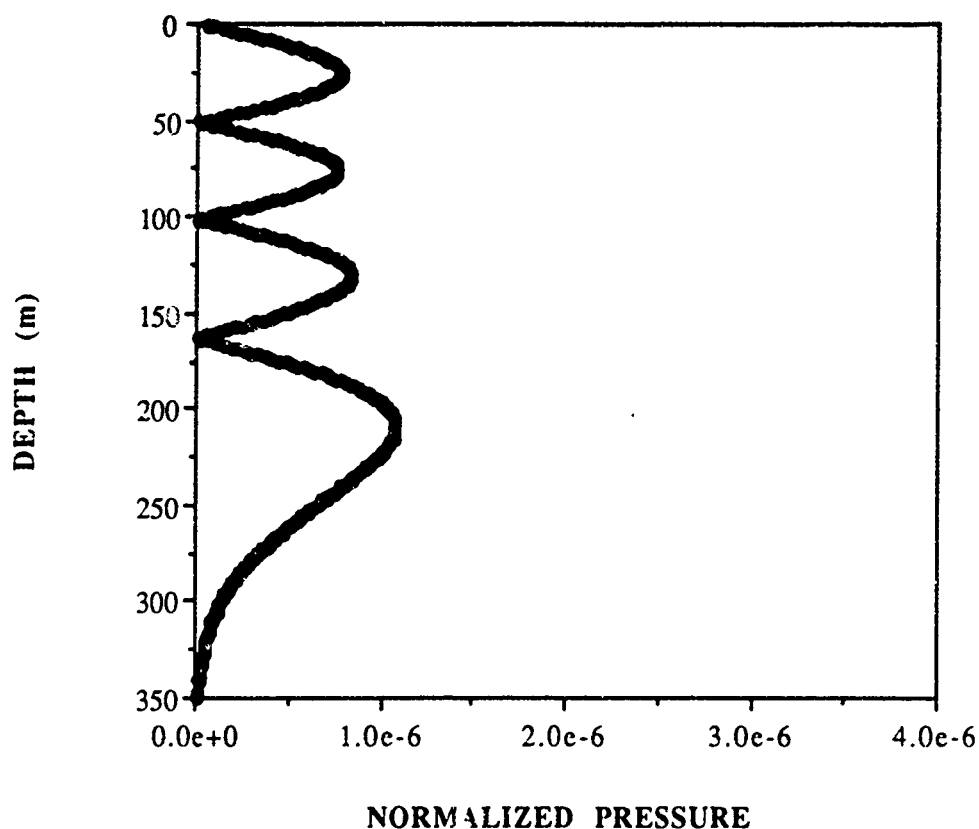


Fig. 69. Objects' Pressure vs. Depth at the Receiver, 1500 (m) from the Object. Scattered Angle 270 (deg). Mode 4 Only.

Notice that the excitation of the first mode (Fig. 66) is very weak through the entire depth of the waveguide. The magnitude of the normalized pressure is on the order of  $10^{-9}$ . Mode 2 (Fig. 67) is also very weak. There is a slight variation with depth of the field. One would not expect that these two modes would be excited since they are both highly evanescent at the depth of the object. We see that mode 3 (Fig. 68) is excited along with mode 4 (Fig. 69). These and the higher order modes are not affected by the sound channel. This kind of modal behavior is typical of a point source. Since the object is producing this signal, this is another indication that the object is coupled to the waveguide.

We now compare the point source's and object's transmission loss with range. Figure 70 illustrates the results.

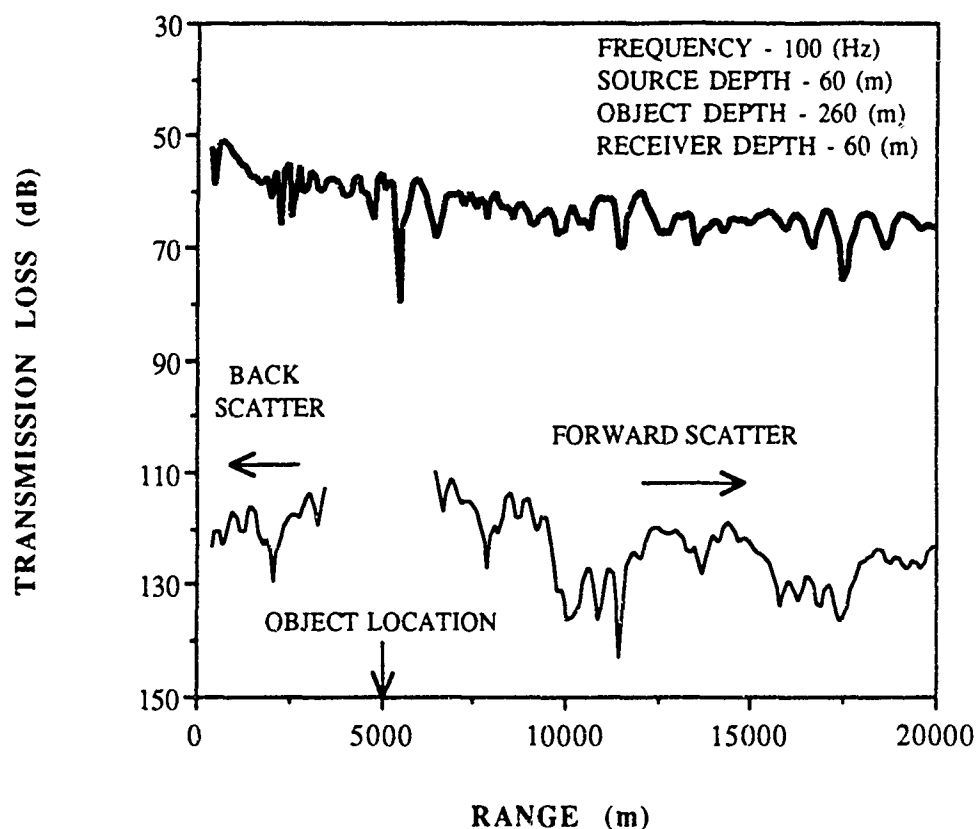


Fig. 70. Comparison of the Transmission Loss vs. Range of the Point Source and the Objects Scattered Field.

The point source field (heavy solid line) decays very little with range. This is consistent with our observation that most of the energy is contained within the sound channel. A sharp contrast to this is the scattered field of the object. It varies greatly in amplitude over a smaller horizontal distance. The scattered field is approximately 70 (dB) smaller than the incident field. Again this is consistent with what we saw when looking at the first four modes.



We now look at the three dimensional field. Figure 71 depicts the incident field at a range from 4300 (m) to 5700 (m), with the cross-range coordinate varying from -700 to 700 (m). There is more variability of the field than for the previous case (Fig. 52) again due to the fact that more modes are propagating. The wave front is slightly curved, as is to be expected with a field that is cylindrically symmetric. Figure 72 depicts the scattered field for the same location in the waveguide, however the object is at the center of the grid. We notice that this field looks very similar to the scattered field produced in the waveguide of the last chapter. This field appears to be increasing in strength as it propagates from the object. We also see some of the same features as in the last chapter, namely that the field is strongest in the forward and backward direction, but still narrower in the forward direction. The side lobes that were present in the last chapter are not as prevalent. We compare this field to the free space scattered field (Fig. 73) that was produced by allowing the object to be insonified by the propagating modes and then compare it to the three dimensional field (Fig. 74) produced by the point source at the objects' depth in the waveguide. We do this for the same reason that we did it in Chapter 5, namely to verify that we have correctly coupled the objects' field into the waveguide.

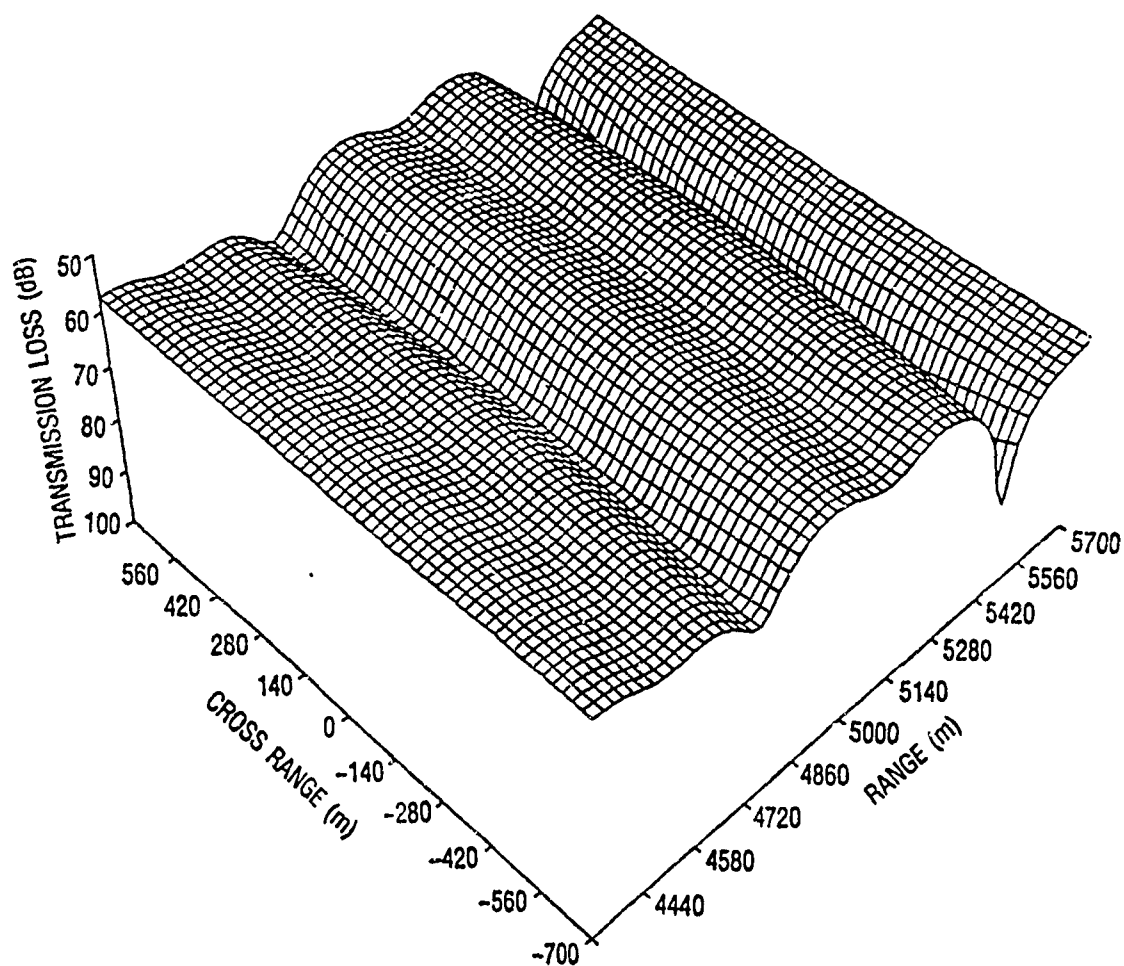


Fig. 71. Three Dimensional Point Source Field Between a Range of 4300 (m) and 5700 (m).

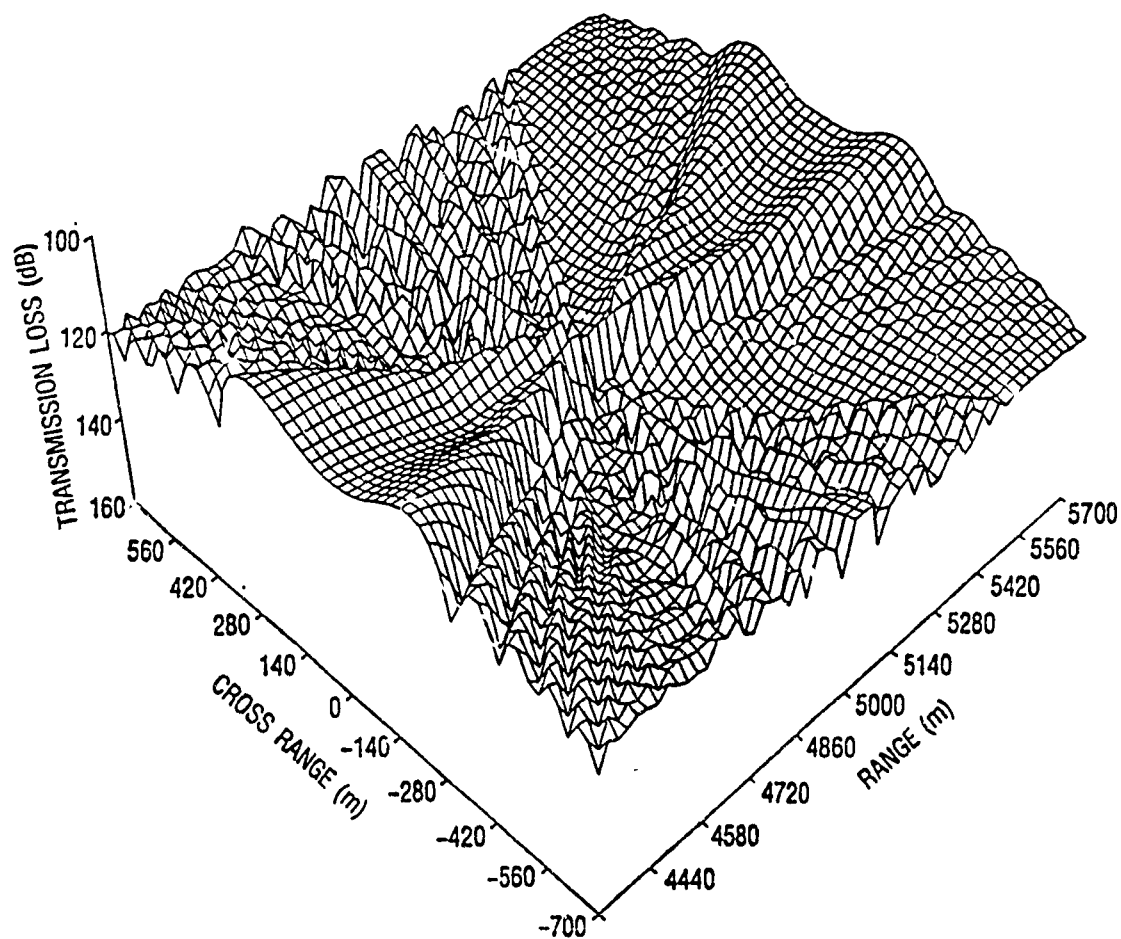


Fig. 72. Three Dimensional Objects' Scattered Field Between  $\rho$  Range of 4300 (m) and 5700 (m) from the Source.

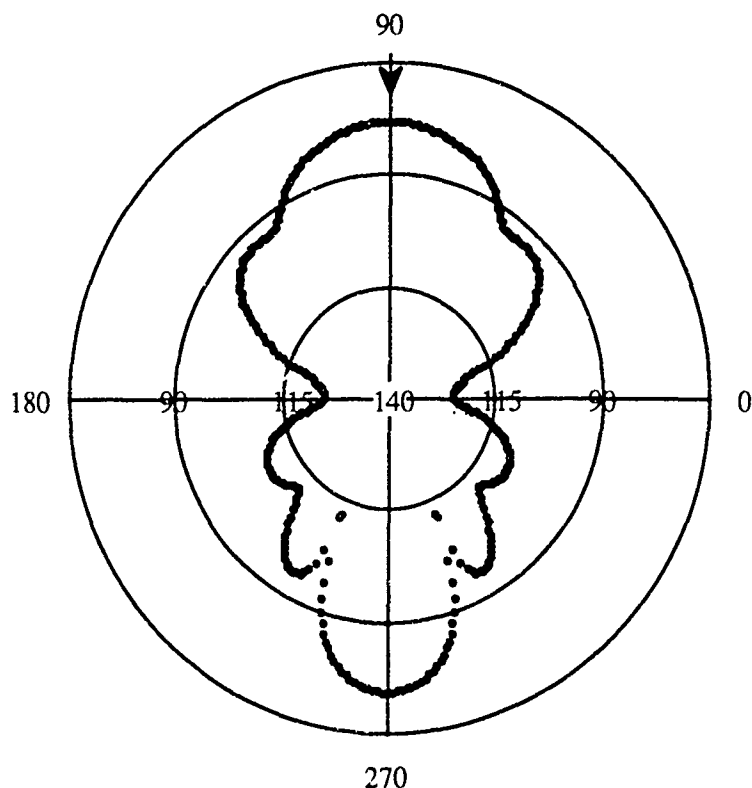


Fig. 73. The Objects' Free Field Scattered Field vs. Angle, After 16 Modes Have Insonified It.

Notice that the free space scattered field is similar to the field obtained in Chapter 5. There are differences, however. The field is stronger than the field in Chapter 5 and there was a peak in the backscattered field produced by the waveguide of Chapter 5 which is absent for this waveguide. The side lobes are present but they are not as pronounced as in the last chapter which is consistent with what we saw in Fig. (72). We also see that the forward scattered field is narrower than the backscattered field. There is a greater difference between the forward and backward fields. This difference is difficult to see in Fig. 72 but it is evident in the two dimensional plot (Fig. 70), where it is seen to be about 3 (dB). Figure (74) gives a three dimensional illustration of the field produced by a point source located at the same depth as the object. The

waveguide effect on the field allows the field to increase over the range increment as was observed in Fig. 71. It appears that the field of the object is being correctly coupled to the waveguide. We now determine the total field, which is shown in Fig. 75.

There is no observable difference between the total field and the incident field of Fig. (70). This was to be expected because the large difference in amplitude between the two fields. On a difference plot however (Fig. 76), the difference between the incident and total fields is evident. Notice that the largest difference occurs in the forward direction where the incident field has a minimum. This difference is on the order of a half of a decibel.

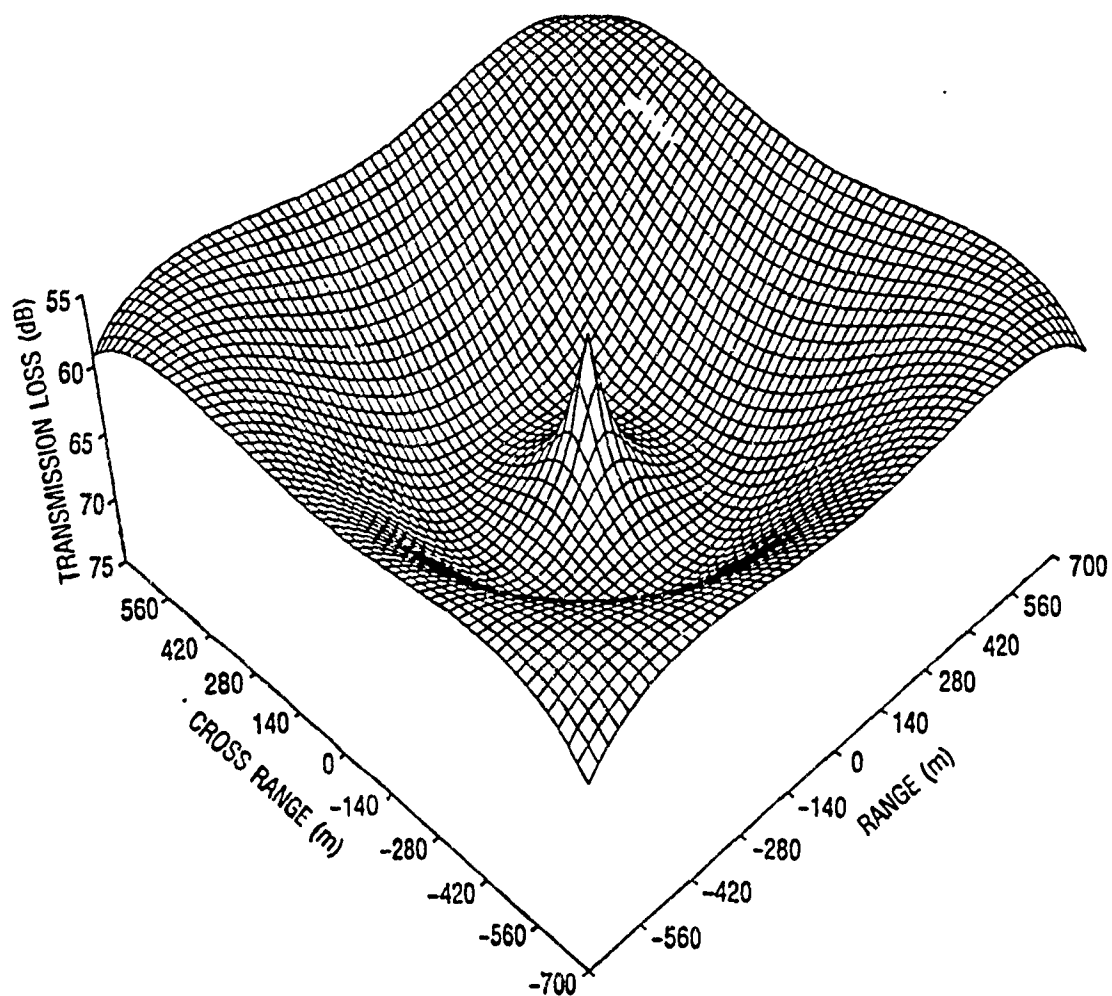


Fig. 74. Three Dimensional Field Produced by a Point Source at the Objects' Depth of 260 (m).

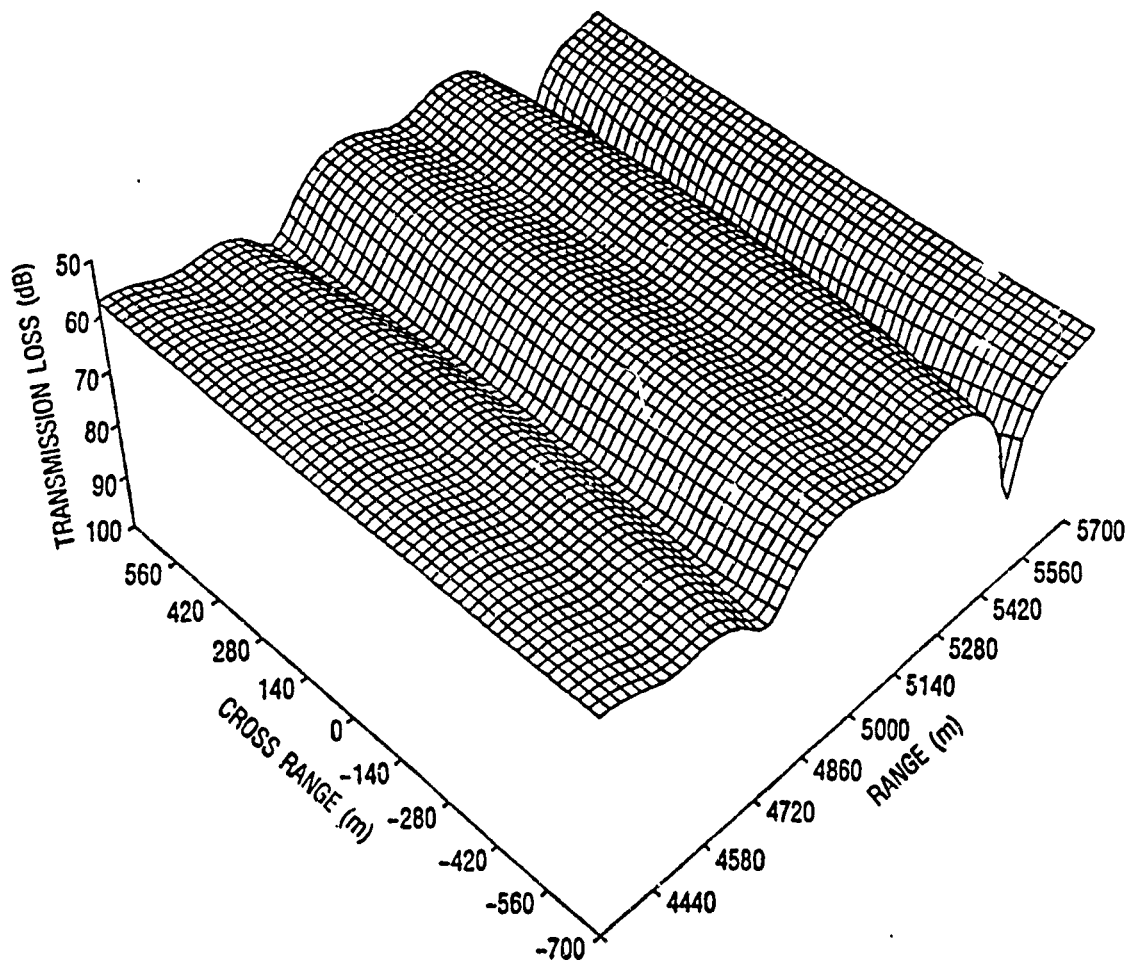


Fig. 75. Three Dimensional Total Field.

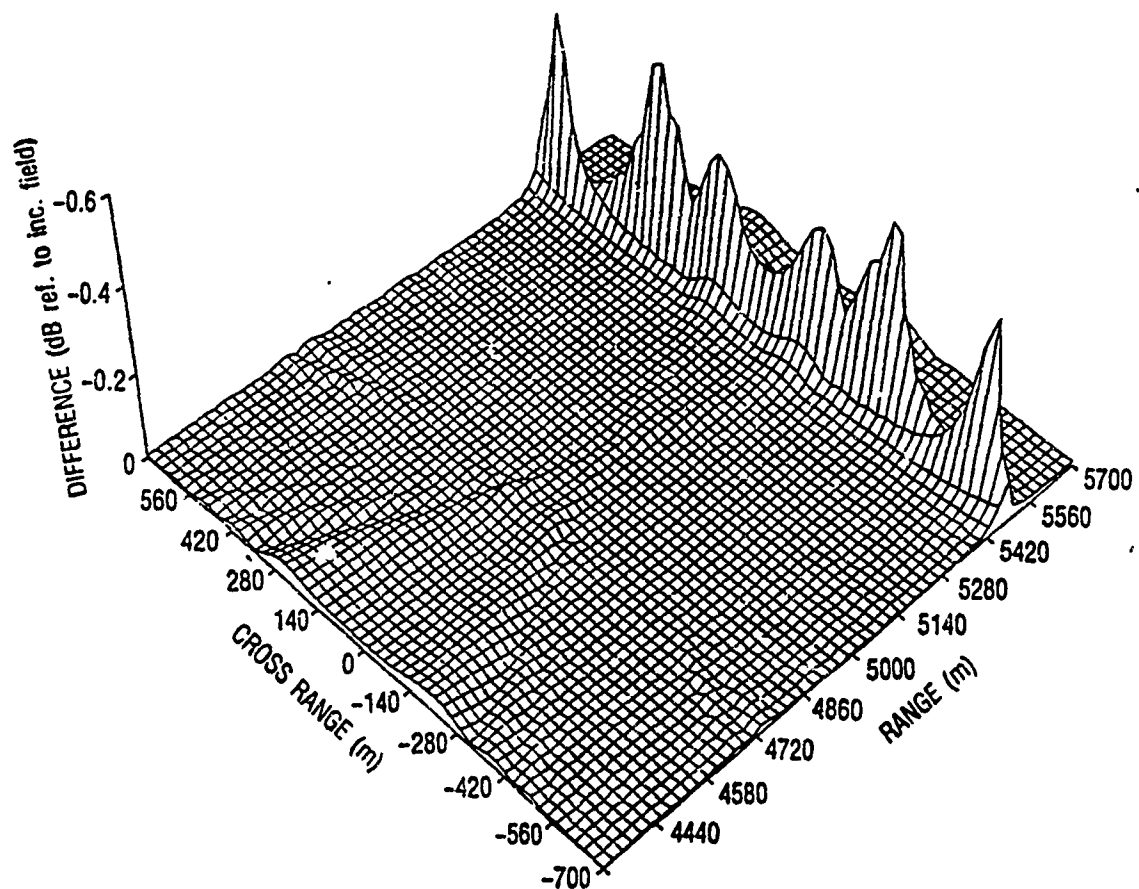


Fig. 76. Three Dimensional Difference Field Between the Total Field and the Incident Field.



## CONCLUSIONS

We have developed a method to describe acoustical scattering from an object in a waveguide. We have done so by using Normal Mode theory to describe the incident field. Each mode (at the object) was decomposed into a pair of up going and down going plane waves. We next used a Transition matrix to determine the near field scattered field from these plane waves incident upon the object. By utilizing Huygens' principle we obtained a far field solution which satisfied all boundary conditions and preserves continuity of the solution throughout all space.

We have shown through examples that the object is correctly coupled to the waveguide. We have shown that the objects scattered field acts as a secondary source by showing that this scattered field obeyed the same boundary conditions as the point source field.

This method of determining the scattered field from a three dimensional object allows one to determine not only the correct target strength (intensity), but also to properly determine the phase. In addition this method allows one to investigate the interaction between the incident field with the waveguide, the incident field with the object, and the object's scattered field with the waveguide. In this manner a better understanding of the ongoing physical processes can be obtained.

APPENDIX A: COMPARISON BETWEEN THE E. B. C METHOD AND AN ANALYTICAL  
SOLUTION FOR THE SCATTERED FIELD PRODUCED BY A PLANE WAVE INCIDENT  
UPON A SPHERE.

In this appendix we will show a comparison between the scattered field as solved for by the Extended Boundary Condition method and the analytic solution for the case when a plane wave is incident upon a sphere. The analytic expression is given in Morse and Feshbach (1) as:

$$(A-1) \quad \Psi_s = -\sum_n (2n+1) i^{(n+1)} e^{-i\delta_n(ka)} \sin[\delta_n(ka)] P_n(\cos\theta) h_n(kr)$$

where  $k$  is the wave number,  $r$  is the distance from the sphere,  $\delta_n$  is the phase angle,  $\theta$  is the observed angle and  $a$  is the radius of the sphere. The important parameters are listed in Table A1.

TABLE A1  
PROBLEM PARAMETERS

Sphere Diameter (m)	Boundary Conditions	Distance from Sphere (m)
2	Dirichlet	100

The "Distance from Sphere" value in Table A1 is the distance from the sphere that the scattered field was obtained. Three frequencies were examined. They were, 59.68 (Hz), 596.8 (Hz), and 5968. (Hz). This resulted in  $K_{1/2}$  values of .25, 2.5 and 25. The three frequencies were selected because they represented a

low, medium and high frequency case. Figures A1, A2, and A3 shows the comparison between the methods for the different frequencies (the forward direction is at 0 deg.). In all cases the open circles are the analytic solution while the black dot is the E. B. C. solution. Notice in all cases the agreement is quite good. The E. B. C. code has been tested thoroughly by Dr. Mike Werby of the Naval Ocean Research and Development Activity. This particular test was performed as a check on the validity of the E.B.C. code used in the present work.

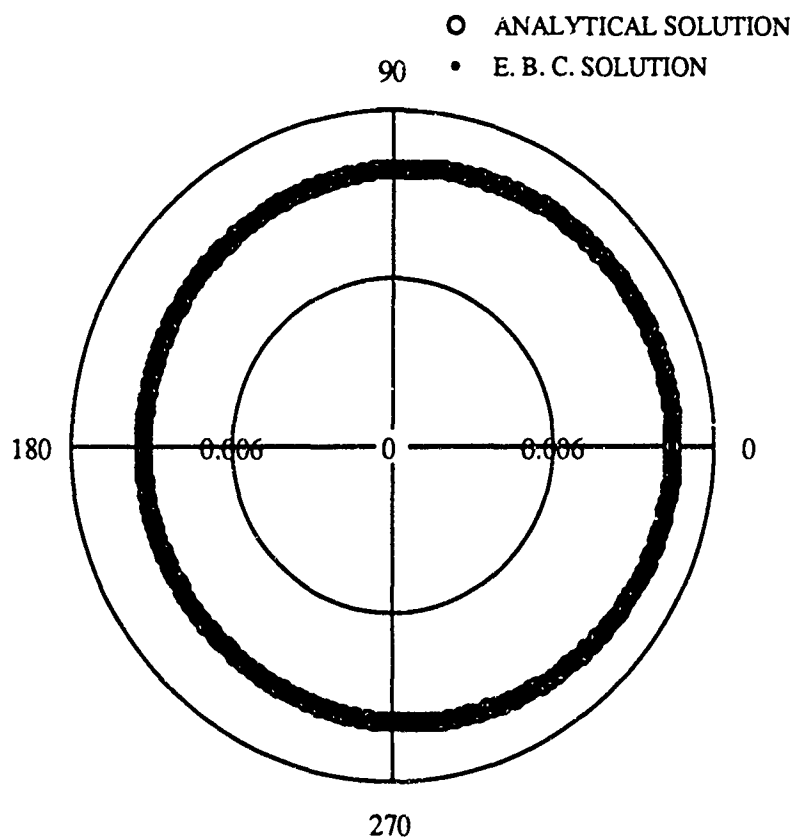


Fig. A1. Comparison Between the Analytic Solution and the E. B. C. Solution for a Plane Wave Incident Upon a Sphere for a Frequency of 59.68 (Hz).

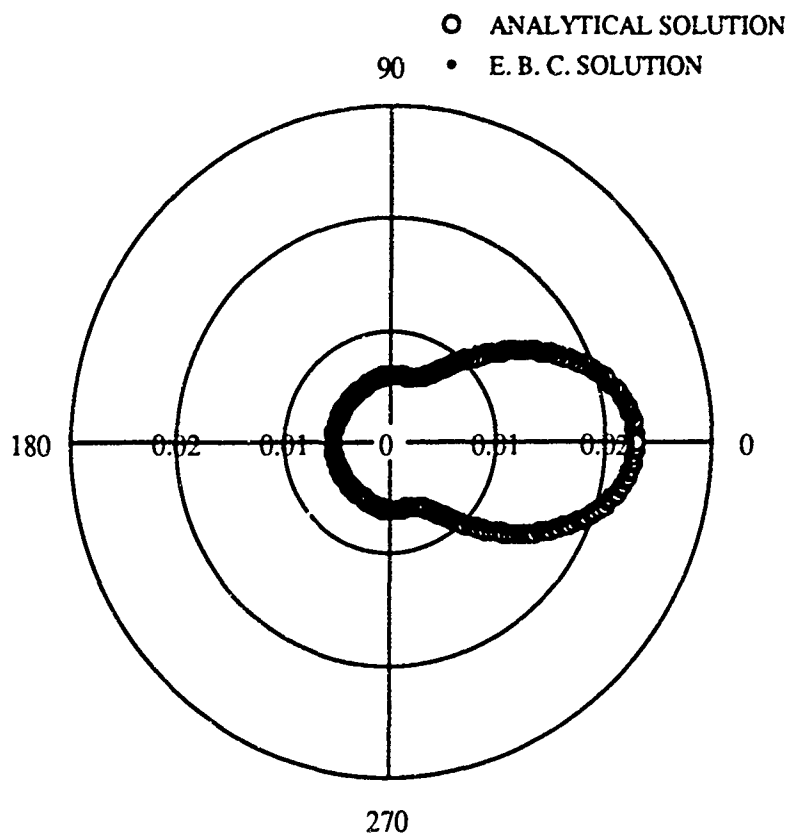


Fig. A2. Comparison Between the Analytic Solution and the E. B. C. Solution for a Plane Wave Incident Upon a Sphere for a Frequency of 596.8 (Hz).

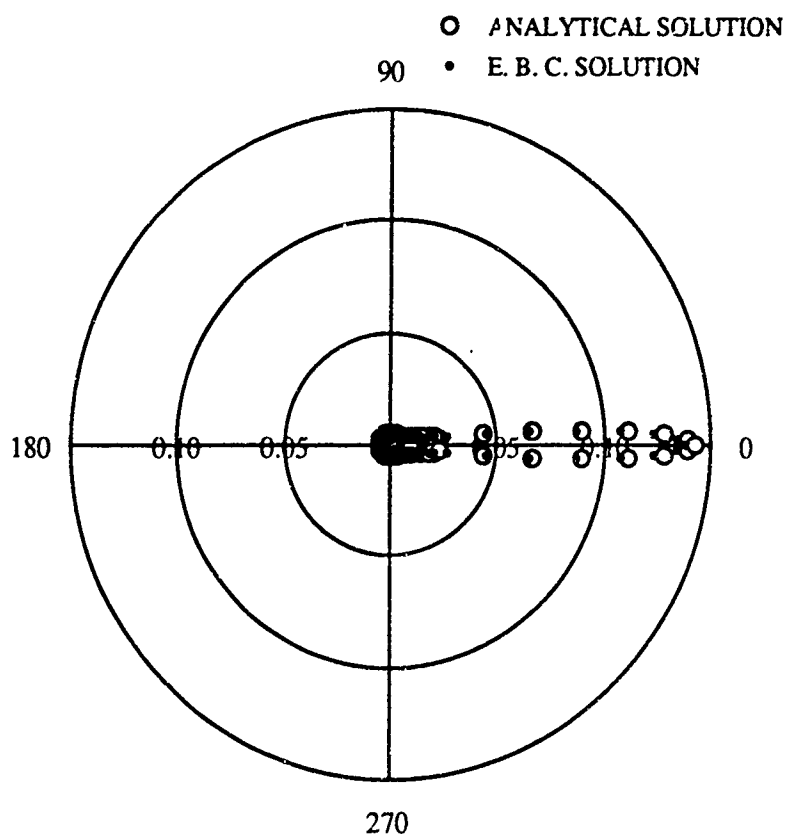


Fig. A3. Comparison Between the Analytic Solution and the E. B. C. Solution for a Plane Wave Incident Upon a Sphere for a Frequency of 5968. (Hz).

## APPENDIX B: DERIVATION OF EQ. (3-122)

We need to evaluate

$$(B-1) \quad \left[ \frac{\partial^2}{\partial r^2} + \frac{1}{r} \frac{\partial}{\partial r} + k^2 a_n^2 \right] H_0^{(1)}(k a_n r) = ?$$

where  $H_0^{(1)}(k a_n r) = J_0(k a_n r) + i Y_0(k a_n r)$ .

Since the Bessel function is analytic for all ranges, we need to show how Eq. (B-1) behaves when  $r \neq 0$  and when  $r = 0$ .

First consider the case when  $r \neq 0$ . The derivative of the Neuman function with respect to  $r$  is

$$(B-2) \quad Y'_0 \equiv \frac{d}{dr}(Y_0(k a_n r)) = \frac{d(k a_n r)}{dr} \frac{d}{d(k a_n r)} Y_0(k a_n r).$$

We have the relationship,  $\frac{d}{dx} Y_0(x) = -Y_1(x)$ . (1)

Equation (B-2) now takes the following form,

$$(B-3) \quad Y'_0 = k a_n [-Y_1(k a_n r)] = -k a_n Y_1(k a_n r)$$

Taking the second derivative of the  $Y_0$  gives,

$$\begin{aligned}
 (B-4) \quad Y_0'' &= \frac{d^2}{dr^2} [Y_0(k a_n r)] = \frac{d}{dr} [Y_0'(k a_n r)] = \\
 &= \frac{d}{dr} [-i k a_n Y_1(k a_n r)] \\
 &= \frac{d(k a_n r)}{dr} \frac{d}{d(k a_n r)} [-k a_n Y_1(k a_n r)] \\
 &= k a_n (-k a_n) \frac{d}{d(k a_n r)} Y_1(k a_n r) \\
 &= -k^2 a_n^2 \left[ \frac{Y_0(k a_n r) - Y_2(k a_n r)}{2} \right]
 \end{aligned}$$

We have used the following relationship concerning the derivative of the Neuman function of the first order, (1)

$$(B-5) \quad \frac{d}{dx} Y_1(x) = \frac{1}{2} (Y_0(x) - Y_2(x)) .$$

Now letting the operator of Eq. (B-1) operate on  $iY_0(k a_n r)$ , we obtain, with help from the above relationships,

$$\begin{aligned}
 \text{(B-6)} \quad & \left[ \frac{\partial^2}{\partial r^2} + \frac{1}{r} \frac{\partial}{\partial r} + k^2 a_n^2 \right] iY_0(k a_n r) \\
 &= i \left[ Y_0'' + \frac{1}{r} Y_0' + k^2 a_n^2 Y_0 \right] \\
 &= i \left[ \frac{-k^2 a_n^2}{2} (Y_0 - Y_2) + \frac{1}{r} (-k a_n Y_1) + k^2 a_n^2 Y_0 \right] \\
 &= i \left[ \left( \frac{k^2 a_n^2}{2} \right) Y_0 - \left( \frac{k a_n}{r} \right) Y_1 + \left( \frac{k^2 a_n^2}{2} \right) Y_2 \right]
 \end{aligned}$$

The recursion formula  $Y_2(x) = \frac{2}{x} Y_1(x) - Y_0(x)$  leads to the following for

$$Y_2(x) \quad (1)$$

$$\begin{aligned}
 \text{(B-7)} \quad & Y_2(k a_n r) = \frac{2}{k a_n r} Y_1(k a_n r) - Y_0(k a_n r) \\
 &= i \left[ \left( \frac{k^2 a_n^2}{2} \right) Y_0 - \left( \frac{k a_n}{r} \right) Y_1 + \left( \frac{k^2 a_n^2}{2} \right) \left( \frac{2}{k a_n r} (Y_1 - Y_0) \right) \right] \\
 &= 0
 \end{aligned}$$



Now when  $r=0$ , we will use the small  $r$  approximation, (2) for the Neuman function,

$$(B-8) \quad Y_0(0) \approx \frac{2}{\pi}(1 \ln(x) + \gamma - 1 \ln(2)), \quad \gamma = .577 \dots$$

$$(B-9) \quad Y_0(k a_n r) \approx \frac{2}{\pi} \left( 1 \ln \left( \frac{k a_n r}{2} \right) \right) \text{ for small } r$$

and taking the derivative with respect to  $r$  of Eq. (B-9) gives

$$(B-10) \quad Y'_0 = \frac{d}{dr}(Y_0(k a_n r)) = \frac{d}{dr} \left[ \frac{2}{\pi} 1 \ln \left( \frac{k a_n r}{2} \right) \right] = \frac{2}{\pi r}$$

now doing the same to Eq. (B-10) gives,

$$(B-11) \quad Y''_0 = \frac{d^2}{dr^2}(Y_0(k a_n r)) = \frac{d}{dr}(Y'_0) = \frac{d}{dr} \left( \frac{2}{\pi r} \right) = - \left( \frac{2}{\pi r^2} \right)$$

Now solving Eq. (B-1) for the Neuman function at small  $r$  gives,

$$(B-12) \quad \left[ \frac{\partial^2}{\partial r^2} + \frac{1}{r} \frac{\partial}{\partial r} + k^2 a_n^2 \right] i Y_0(k a_n r)$$

$$= i \left[ Y''_0 + \frac{1}{r} Y'_0 + k^2 a_n^2 Y_0 \right]$$

$$= i \left[ \frac{-2}{\pi r^2} + \frac{1}{r} \left( \frac{2}{\pi r} \right) + k^2 a_n^2 \left( \frac{2}{\pi} \right) 1 \ln \left( \frac{k a_n r}{2} \right) \right]$$

$$= i \left( \frac{2}{\pi} \right) k^2 a_n^2 1 \ln \left( \frac{k a_n r}{2} \right)$$

Multiplying Eq. (B-12) by  $r$  and integrating gives

$$(B-13) \quad \int_{\frac{2}{ka_n}}^0 \left[ \frac{\partial^2}{\partial r^2} + \frac{1}{r} \frac{\partial}{\partial r} + k^2 a_n^2 \right] i Y_0(k a_n r) r dr$$

$$= i \left( \frac{2}{\pi} \right) k^2 a_n^2 \int_{\frac{2}{ka_n}}^0 \ln \left( \frac{k a_n r}{2} \right) r dr$$

$$= i \left( \frac{2}{\pi} \right) 4 \int_{\frac{2}{ka_n}}^0 (k a_n r) \ln \left( \frac{k a_n r}{2} \right) d \left( \frac{k a_n r}{2} \right)$$

$$= i \left( \frac{2}{\pi} \right) 4 \left[ \frac{(k a_n r)^2}{8} \ln \left( \frac{k a_n r}{2} \right) - \frac{(k a_n r)^2}{16} \right]_{\frac{2}{ka_n}}^0$$

$$= i \left( \frac{2}{\pi} \right) 4 \left\{ [0 \ln(0)] - \left[ \frac{1}{2} \ln(1) - \frac{1}{4} \right] \right\} = i \left( \frac{2}{\pi} \right)$$

Summarizing the results,

$$(B-15) \quad \left[ \frac{\partial^2}{\partial r^2} + \frac{1}{r} \frac{\partial}{\partial r} + k^2 a_n^2 \right] H_0^{(1)}(k a_n r) = 0, r \neq 0$$

$$(B-16) \quad \int \left[ \frac{\partial^2}{\partial r^2} + \frac{1}{r} \frac{\partial}{\partial r} + k^2 a_n^2 \right] H_0^{(1)}(k a_n r) = i \left( \frac{2}{\pi} \right), r \rightarrow 0$$

$$(B-17) \quad \int i \left( \frac{2}{\pi} \right) \delta(r) dr = i \left( \frac{2}{\pi} \right)$$

We therefore have as the solution for Eq. (B-1) the following,

$$(B-18) \quad \left[ \frac{\partial^2}{\partial r^2} + \frac{1}{r} \frac{\partial}{\partial r} + k^2 a_n^2 \right] H_0^{(1)}(k a_n r) = i \left( \frac{2}{\pi} \right) \delta(r)$$

or

$$(B-19) \quad \left[ \frac{\partial^2}{\partial r^2} + \frac{1}{r} \frac{\partial}{\partial r} + k^2 a_n^2 \right] H_0^{(1)}(k a_n r) = \frac{4i \delta(r)}{2\pi r}$$

### APPENDIX C: VALIDATION OF PROPAGATION MODELS

This appendix shows the comparison between the horizontal eigenvalues generated by the SACLANT Center Normal Mode Acoustic Propagation (SNAP) (1) model and both the isovelocity normal mode model which was developed for the Pekeris waveguide (i.e. isovelocity water layer over a high speed isovelocity fluid half space), and for a multilayered waveguide, consisting of numerous isovelocity water and sediment layers. Table (C1) lists the waveguide parameters.

TABLE C1  
PARAMETERS FOR THE ISOVELOCITY WAVEGUIDE

Depth (m)	Sound Speed (m/s)	Density (g/cm**3)
0.0	1500.0	1.0
150.0	1500.0	1.0
150.0+	1600.0	2.0

Table (C2) shows the comparison between the Pekeris waveguide model and the SNAP model determination of the horizontal eigenvalues, with the magnitude of the difference between the two models.

TABLE C2

## COMPARISON OF HORIZONTAL EIGENVALUES GENERATED BY THE SNAP AND PEKERIS WAVEGUIDE MODEL

Pekeris Waveguide Program	SNAP Program	Magnitude of Difference
Horizontal Eigenvalue	Horizontal Eigenvalue	
0.4184382396D+00	0.4184382379D+00	.1D-08
0.4171019040D+00	0.4171019027D+00	.1D-08
0.4148351550D+00	0.4148351369D+00	.1D-07
0.4115958809D+00	0.4115958645D+00	.1D-07
0.4073444101D+00	0.4073443901D+00	.3D-07
0.4020511324D+00	0.4020510729D+00	.5D-07
0.3957339603D+00	0.3957339045D+00	.5D-07

For this example there were 7 modes propagating. The largest difference between the eigenvalues were on the order of  $1 \times 10^{-6} \text{ m}^{-1}$  and the smallest difference was  $1 \times 10^{-7} \text{ m}^{-1}$ . Figure (C1) depicts the transmission loss vs. range for the environment depicted in Table (C1). Notice that the structure between the two models are identical but that the transmission loss generated by the Pekeris Waveguide model is off by a factor of  $\sqrt{\frac{\pi}{4}}$ . It's obvious that the difference is just a constant since the level of variation does not change with range. It is obvious that the Pekeris Waveguide model will give as accurate results as SNAP for these rather simplistic environments.

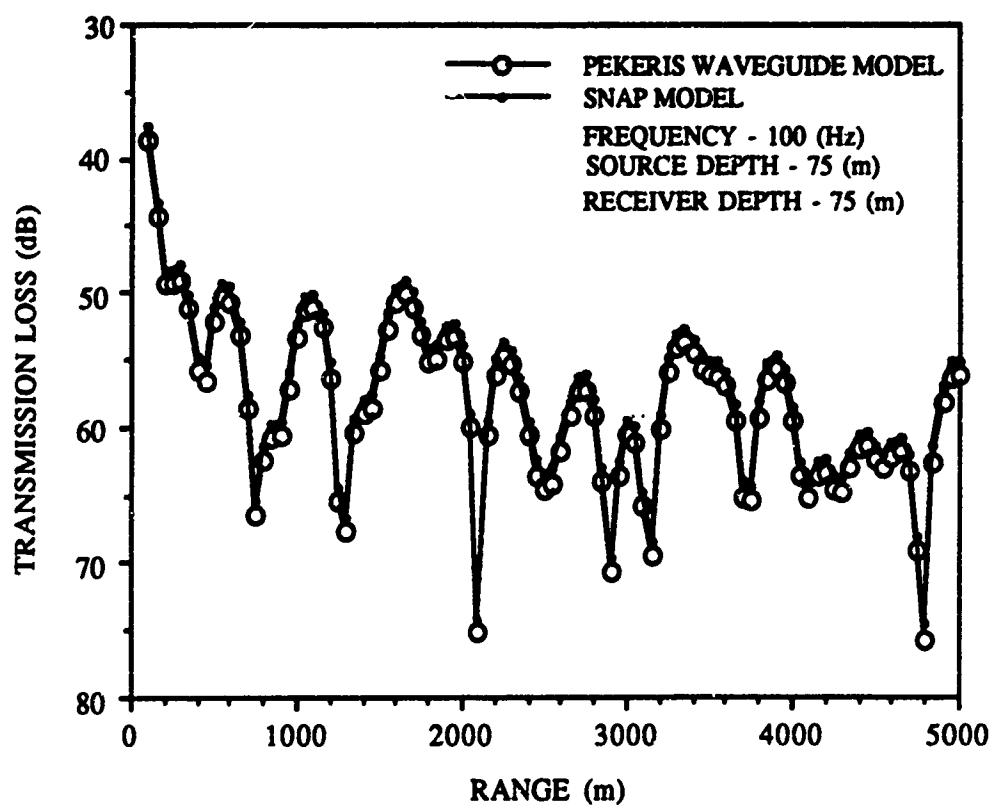


Fig. C1. Comparison of Transmission Loss Between the SNAP and Pekeris Waveguide Model.

We compare the horizontal eigenvalues generated by the Pekeris Waveguide model (see chapter 5) and the MultiLayered Waveguide model, the results are as in Table (C3).

**COMPARISON OF HORIZONTAL EIGENVALUES GENERATED BY THE MULTILAYERED  
AND PEKERIS WAVEGUIDE MODEL**

<b>Multilayered Waveguide Model</b>	<b>Pekeris Waveguide Model</b>	<b>Magnitude of Difference</b>
<b>Horizontal Eigenvalue</b>	<b>Horizontal Eigenvalue</b>	
0.4184382396D+00	0.4184382396D+00	0.
0.4171019040D+00	0.4171019040D+00	0.
0.4148351550D+00	0.4148351550D+00	0.
0.4115958809D+00	0.4115958809D+00	0.
0.4073444101D+00	0.4073444101D+00	0.
0.4020511324D+00	0.4020511324D+00	0.
0.3957339603D+00	0.3957339603D+00	0.

Out to 10 decimal places there is no difference. Figures (C2) and (C3) shows the comparison between the depth eigenfunctions for mode 1 and mode 2, as generated by the Pekeris Waveguide and the MultiLayered Waveguide model.

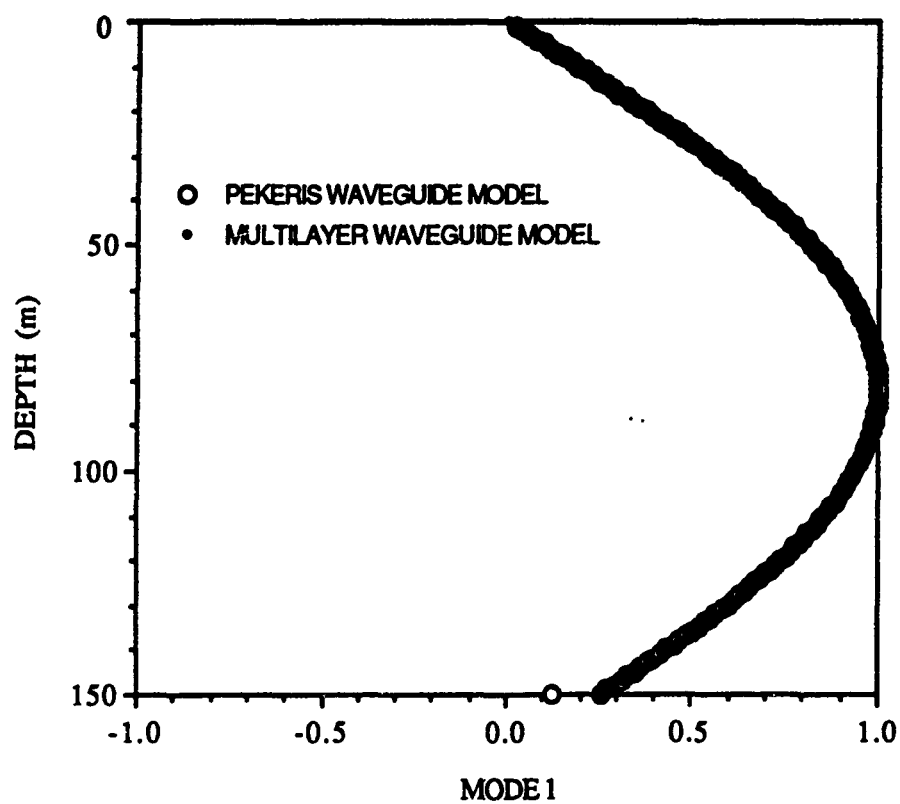


Fig. C2. Comparison of the First Depth Eigenfunction Generated by the Pekeris and MultiLayered Model.



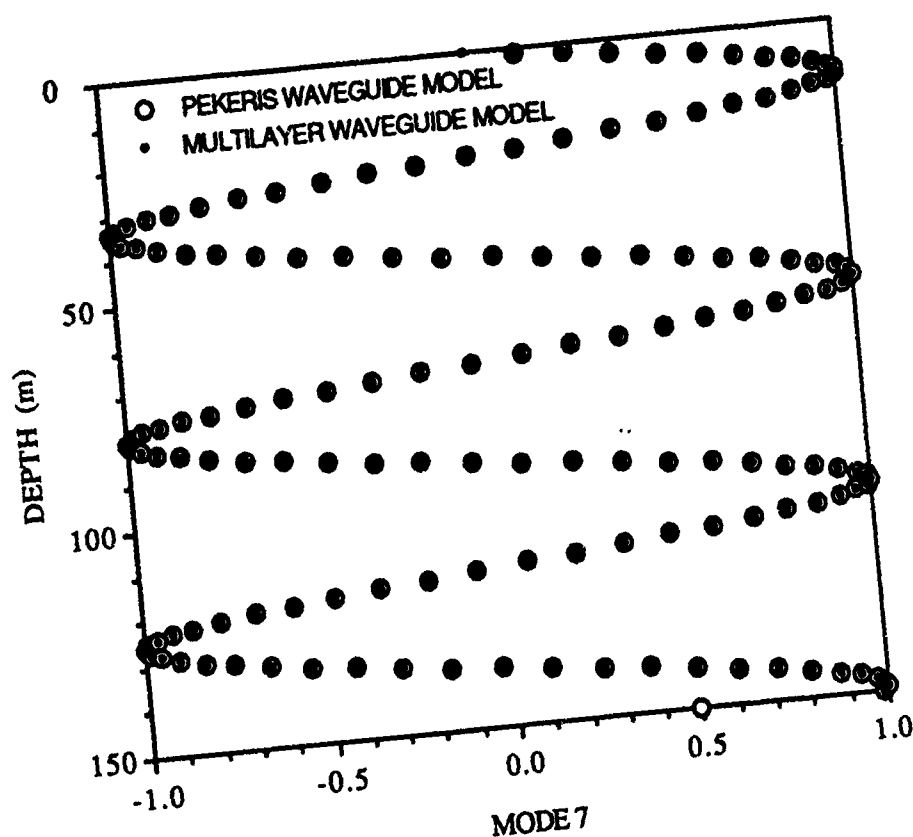


Fig. C3. Comparison of the Second Depth Eigenfunction Generated by the Pekeris and MultiLayered Model.

Figure (C4) shows the Transmission loss comparison between the Pekeris Waveguide and the MultiLayered Waveguide model. Note that the structure between the two are identical and we see that again the transmission loss generated by the Pekeris Waveguide model is off by a constant factor of  $\sqrt{\frac{\pi}{4}}$ . This would suggest that the transmission loss generated by the MultiLayered model and by SNAP would agree perfectly.

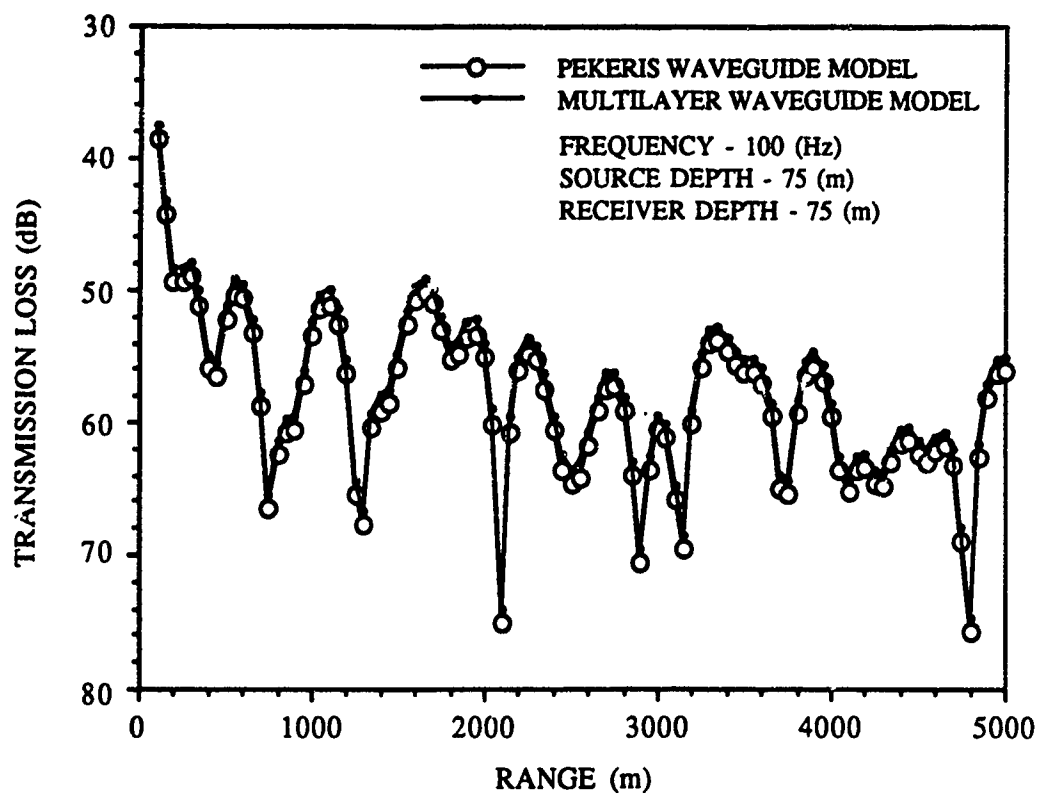


Fig. C4. Comparison of the Transmission Loss Generated by the Pekeris and MultiLayered Waveguide Models.

Figure (C5) shows this comparison. Note the good agreement between the two models.

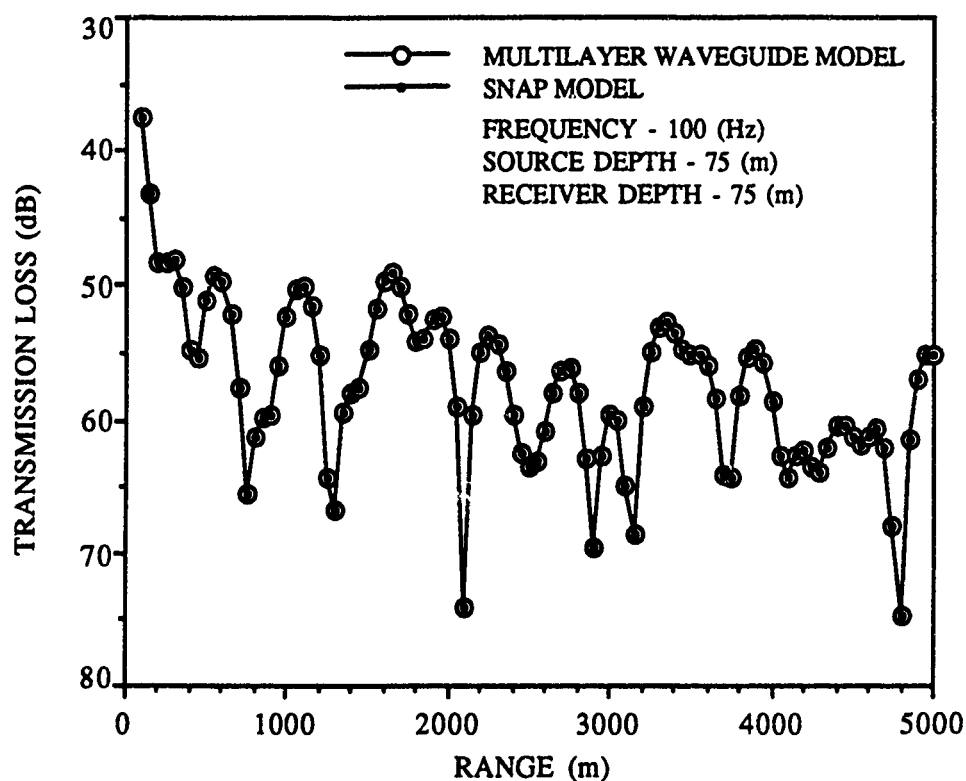


Fig. C5. Comparison of the Transmission Loss Generated by the MultiLayered and SNAP Model.

With confidence in the MultiLayered model, we now compare SNAP and the MultiLayered model for a slightly more complex environment, a three layered environment. The environment is depicted in Fig. (C6), with the water layer having the lowest sound speed, the sediment layer the next and the half space the highest.

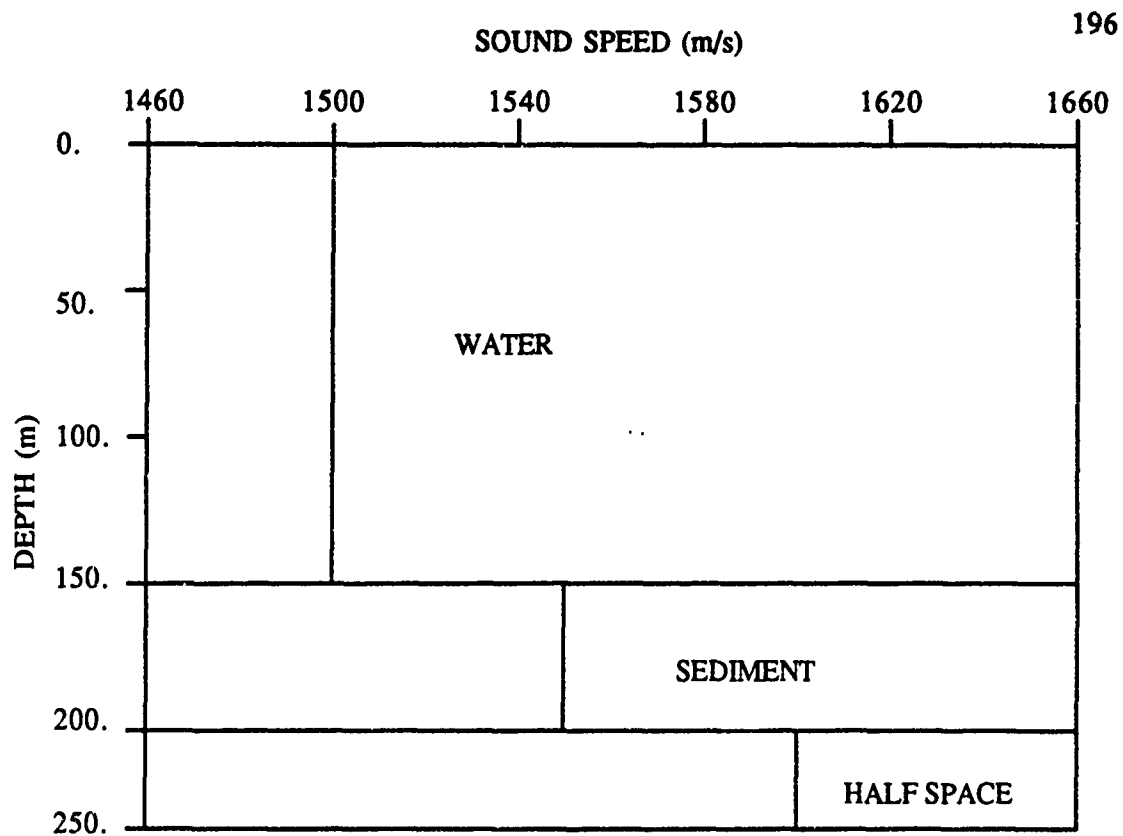


Fig. C6. The Second Waveguide Used to Validate the MultiLayered Waveguide Model.

We compare the transmission loss generated by both models for this environment in Fig. (C7).

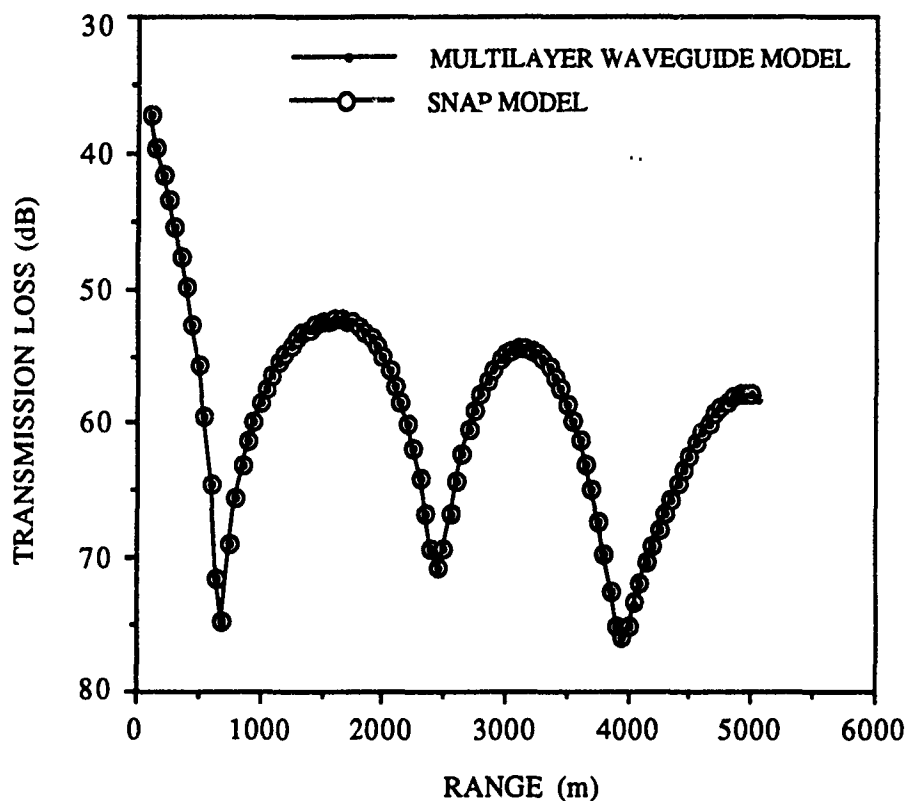


Fig. C7. Comparison of the Transmission Loss Generated by the MultiLayered Waveguide Model and by SNAP.

We now investigate a much more complex environment. This environment is shown in Fig. (C8). It consists of 13 water layers, two sediment layers, and a half space. Figures (C9) and (C10) compares the depth eigenfunction generated by SNAP and by the MultiLayered model for mode 1 and mode 2 for this environment. They show good agreement between the two models. Figure (C11) shows the comparison of the transmission loss between SNAP and the MultiLayered model for this environment.

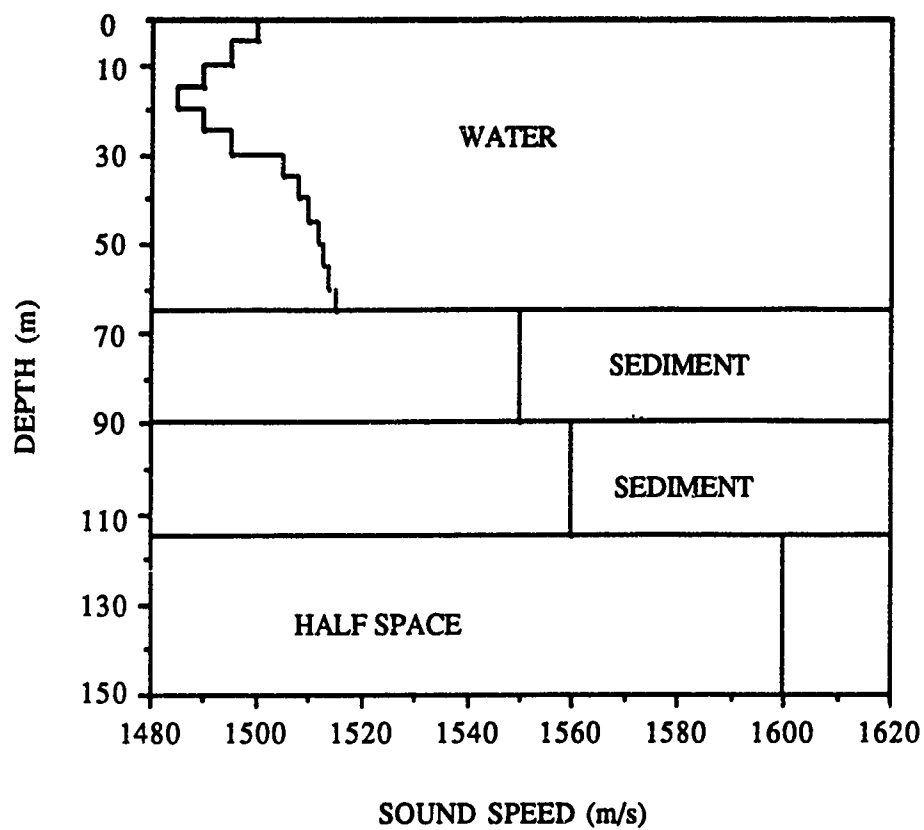


Fig. C8. The Third Test Waveguide Used to Validate the MultiLayered Waveguide Model.

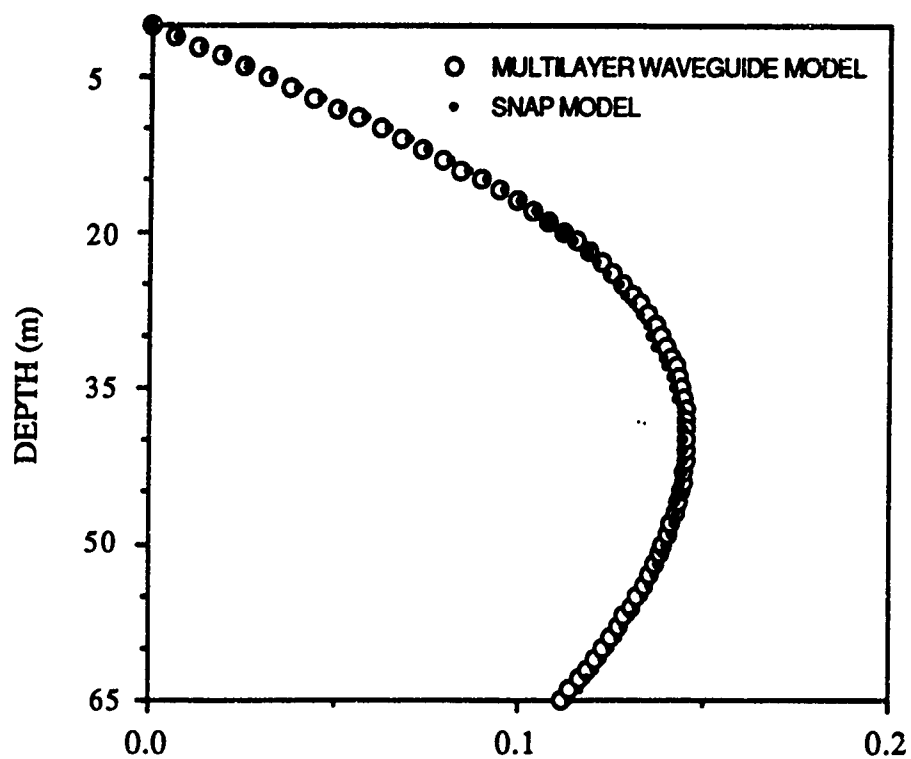


Fig. C9. Comparison of the First Depth Eigenfunction Generated by the MultiLayered and SNAP Model for the Third Test Waveguide.

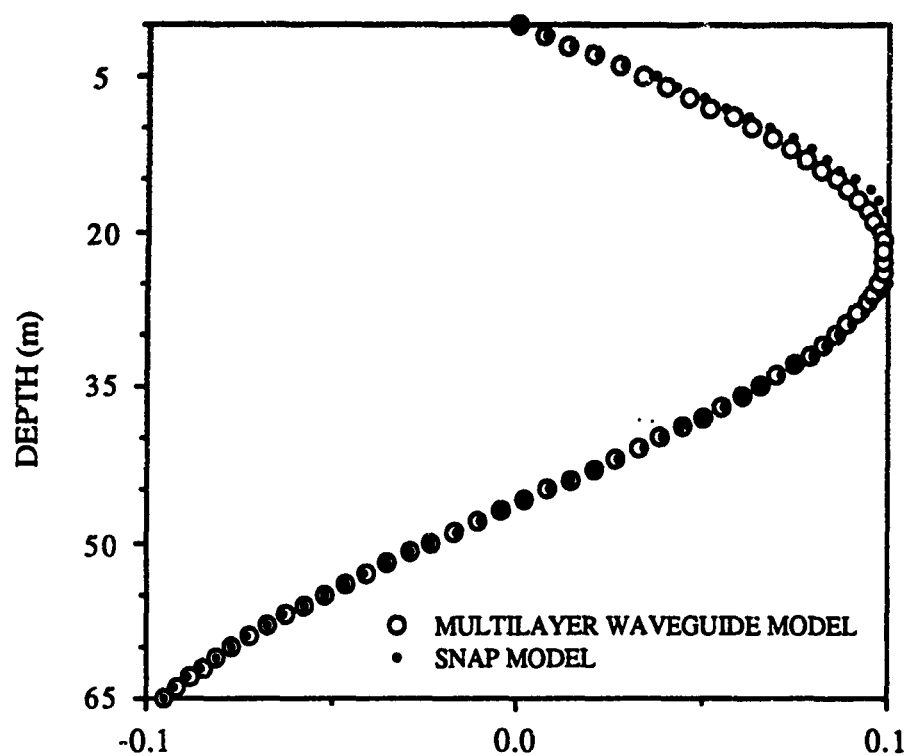


Fig. C10. Comparison of the Second Depth Eigenfunction Generated by the MultiLayered and SNAP Model for the Third Test Waveguide.



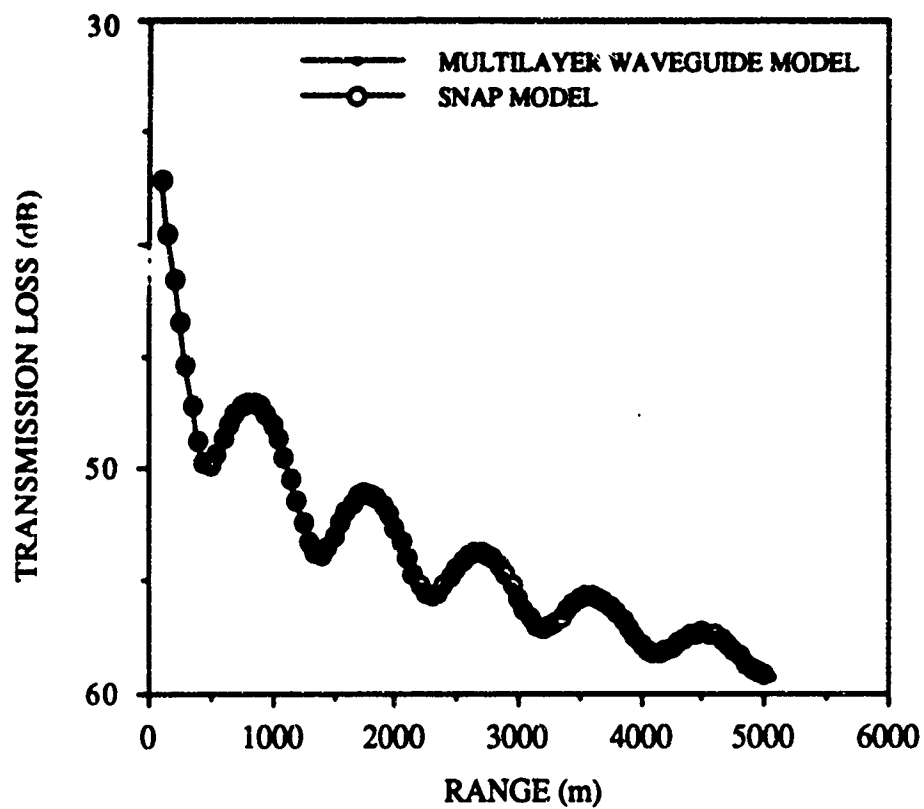


Fig. C11. Comparison of Transmission Loss Generated by the MultiLayered and SNAP Model for the Third Test Waveguide.

The final test of the MultiLayered model is against data, which are taken from Ingenito and Wolf. (2) The sound speed profile is shown in Fig. (C12).

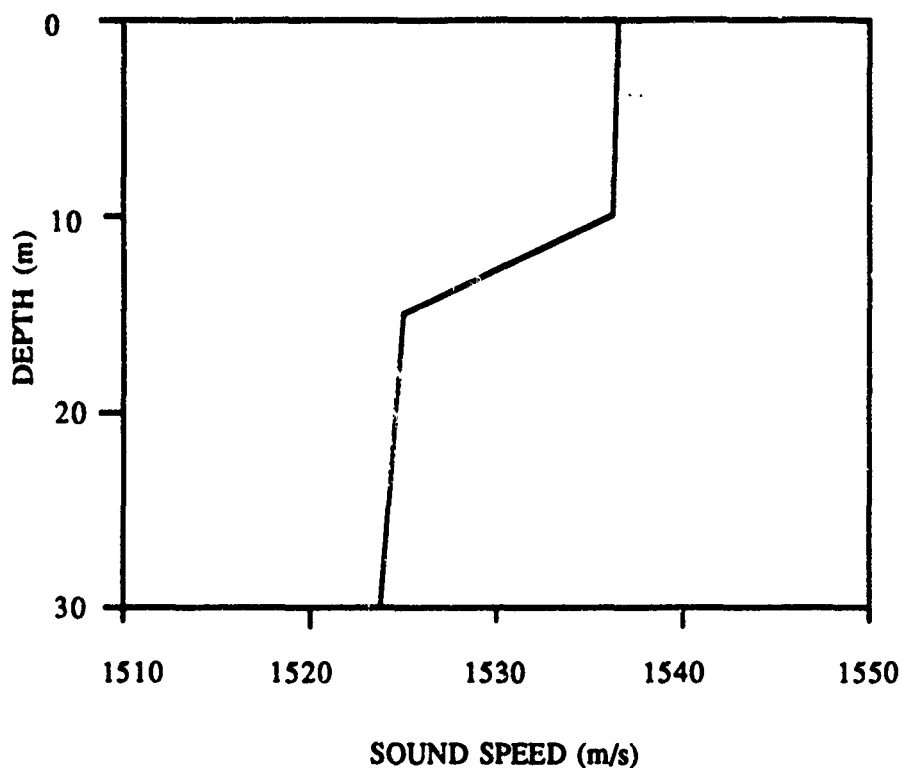


Fig. C12. Sound Speed Profile after Ingenito and Wolf.

The model vs. data comparison for 400 (Hz) is shown in Fig. (C13), along with the model calculation by Ingenito and Wolf. Note that the agreement is quite good. Table (C5) compares the horizontal eigenvalues generated by each model and gives the absolute difference between the two. The largest difference is  $1 \times 10^{-3} \text{ m}^{-1}$ .

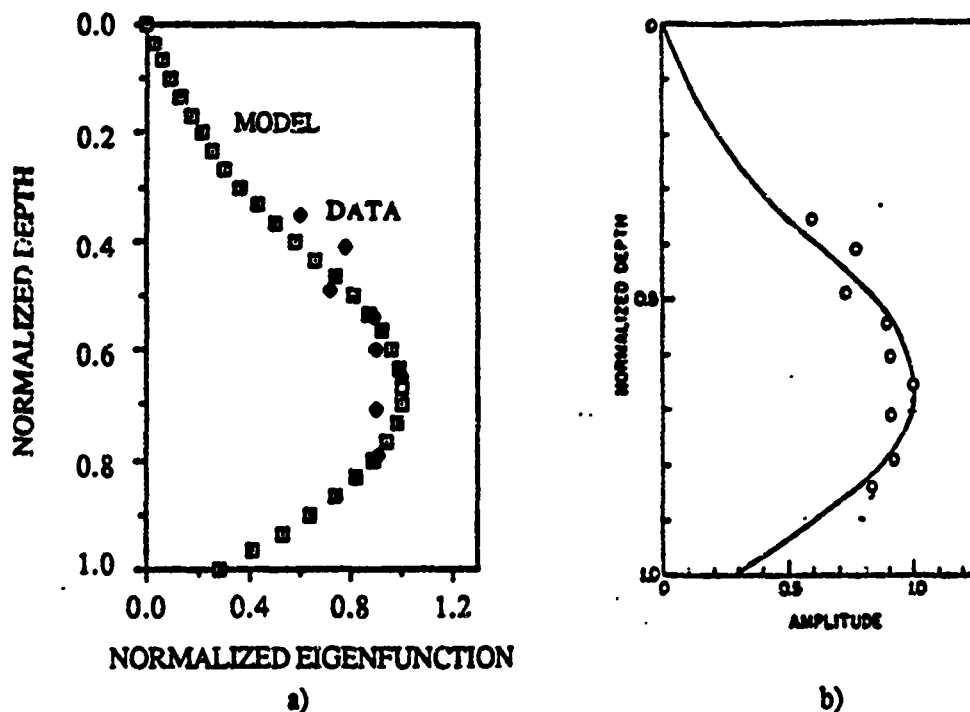


Fig. C13. a) Comparison of the First Depth Eigenfunction for 400 (Hz) Generated by the MultiLayered Waveguide Model and Data. b) Comparison of Model Results With Data as Presented by Ingenito and Wolf.

TABLE C4

COMPARISON OF HORIZONTAL EIGENVALUES GENERATED BY THE MULTILAYERED WAVEGUIDE MODEL AND THE SNAP MODEL FOR A FREQUENCY OF 400 (Hz)

MultiLayered Waveguide Model	SNAP Model	Magnitude of Difference
Horizontal Eigenvalue	Horizontal Eigenvalue	
0.1643477015D+01	0.1643473073D+01	.3D-05
0.1632167076D+01	0.1632159020D+01	.8D-05
0.1617969309D+01	0.1617967663D+01	.1D-05
0.1598583468D+01	0.1598577065D+01	.6D-05
0.1572341994D+01	0.1572336591D+01	.5D-05
0.1549392552D+01	0.1549390991D+01	.1D-05
0.1534040267D+01	0.1534034656D+01	.5D-05
0.1499363280D+01	0.1499358976D+01	.4D-05
0.1470642438D+01	0.1470634678D+01	.7D-05
0.1437511941D+01	0.1437498305D+01	.1D-04
0.1387679442D+01	0.1387678929D+01	.5D-06
0.1345397981D+01	0.1345388765D+01	.9D-05

Figure (C14) show the comparison between the transmission loss generated by the two models. The agreement is quite good.

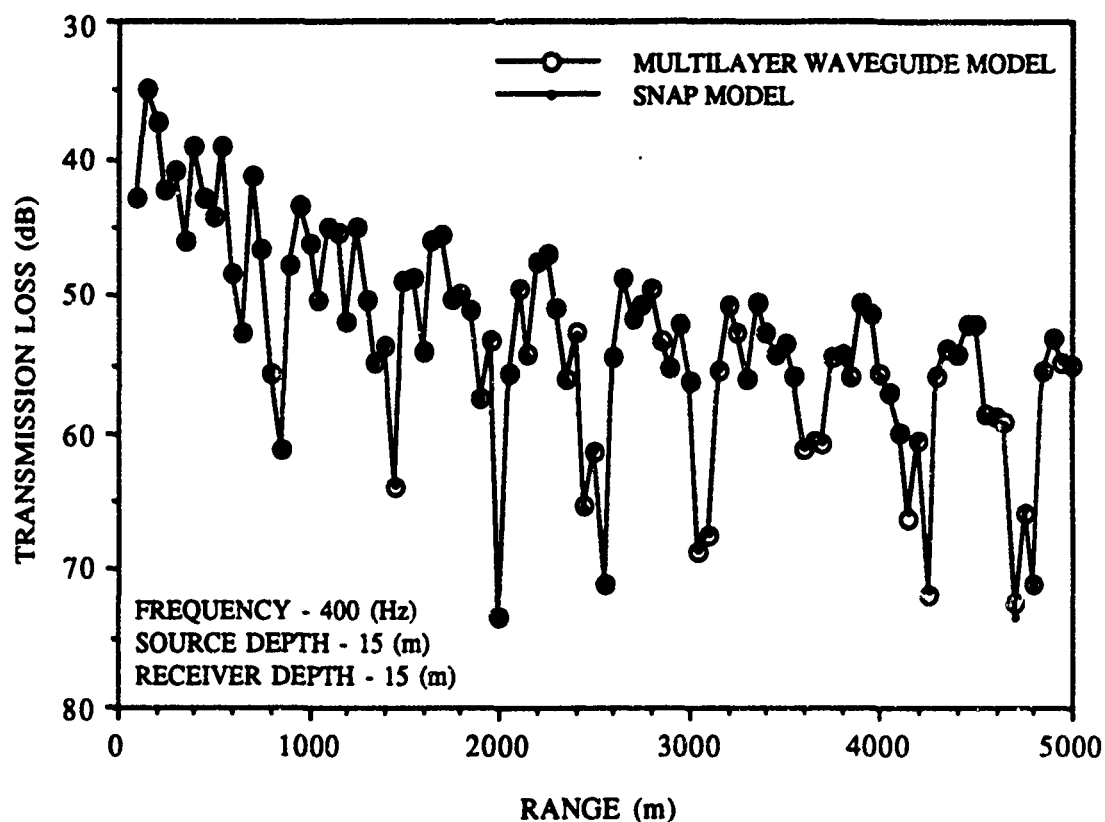


Fig. C14. Comparison of Transmission Loss Generated at a Frequency of 400 (Hz) by the MultiLayered and SNAP Model Using the Sound Speed Profile of Fig. (C12).

Figure (C15) shows the model vs. data comparison at 750 (Hz). Again the agreement is quite good. Table (C5) compares the horizontal eigenvalues as determined by each model. The largest difference is again  $1 \times 10^{-3} \text{ m}^{-1}$ .

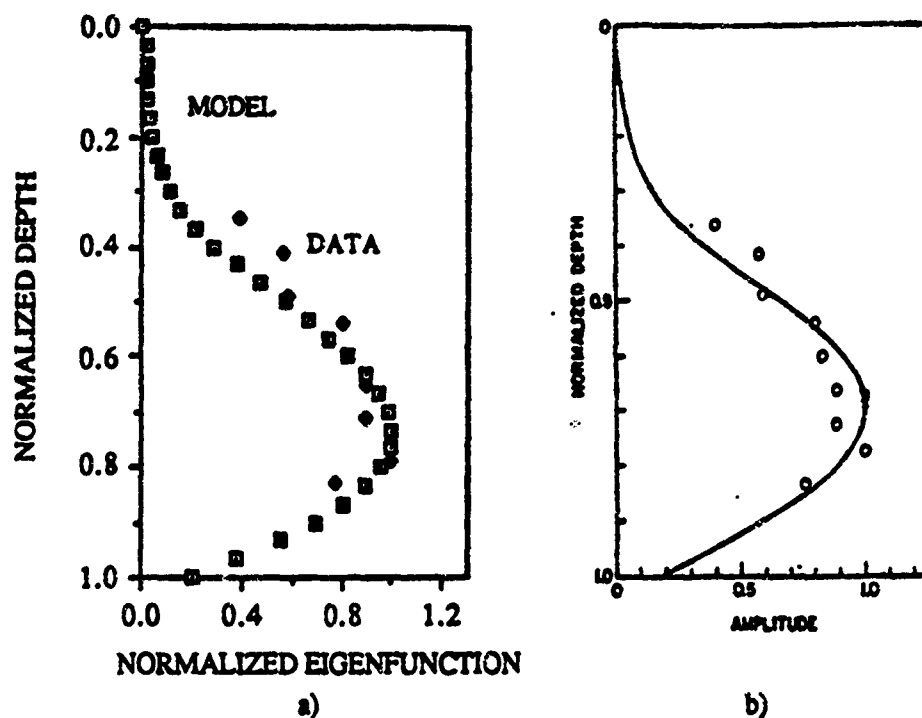


Fig. C15. a) Comparison of the First Depth Eigenfunction for 750 (Hz) Generated by the MultiLayered Waveguide Model and Data. b) Comparison of Model Results With Data as Presented by Ingenito and Wolf.

TABLE C5

COMPARISON OF HORIZONTAL EIGENVALUES GENERATED BY THE MULTILAYERED  
WAVEGUIDE MODEL AND THE SNAP MODEL FOR A FREQUENCY OF 750 (Hz)

MultiLayered Waveguide Model	SNAP Model	Magnitude of Difference
Horizontal Eigenvalue	Horizontal Eigenvalue	
0.3086479467D+01	0.3086475129D+01	.4D-05
0.3077106218D+01	0.3077095247D+01	.1D-04
0.3064396577D+01	0.3064383452D+01	.1D-04
0.3054483253D+01	0.3054480991D+01	.2D-05
0.3039869244D+01	0.3039859840D+01	.9D-05
0.3022117375D+01	0.3022111962D+01	.5D-05
0.3000974575D+01	0.3000965802D+01	.8D-05
0.2976025500D+01	0.2976016499D+01	.9D-05
0.2948016738D+01	0.2948006350D+01	.1D-04
0.2930876943D+01	0.2930875337D+01	.1D-05
0.2914863167D+01	0.2914853243D+01	.9D-05
0.2889885853D+01	0.2889880707D+01	.5D-05
0.2872611077D+01	0.2872596332D+01	.1D-04
0.2838535723D+01	0.2838528599D+01	.7D-05
0.2811841177D+01	0.2811827591D+01	.1D-04

Figure (C16) compares the transmission loss generated by the two models; agreement is quite good.

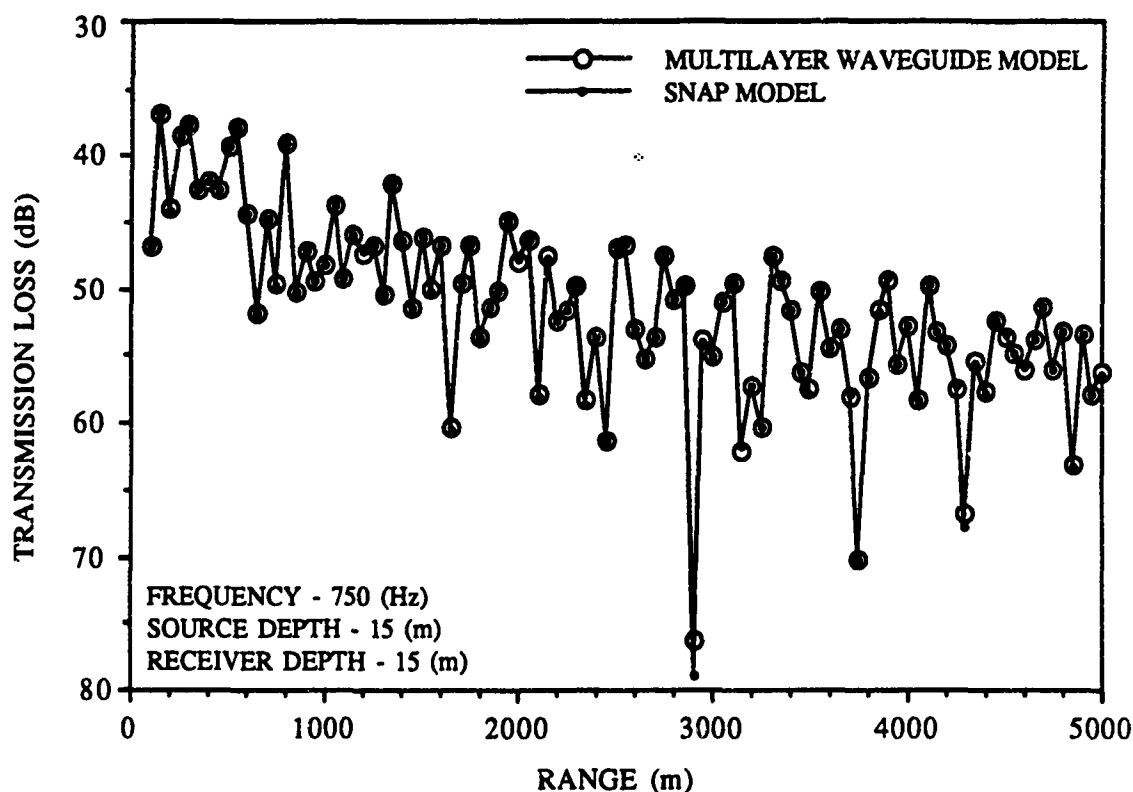


Fig. C16. Comparison of Transmission Loss Generated at a Frequency of 750 (Hz) by the MultiLayered and SNAP Model Using the Sound Speed Profile of Fig. (C12).

Finally we test the model against data at a frequency of 1500 (Hz). The comparison is shown in Fig. (C17). Good agreement is again obtained. Table (C6) shows the comparison between the horizontal eigenvalues generated by the two models. The largest difference is approximately  $1 \times 10^{-3} \text{ m}^{-1}$ .

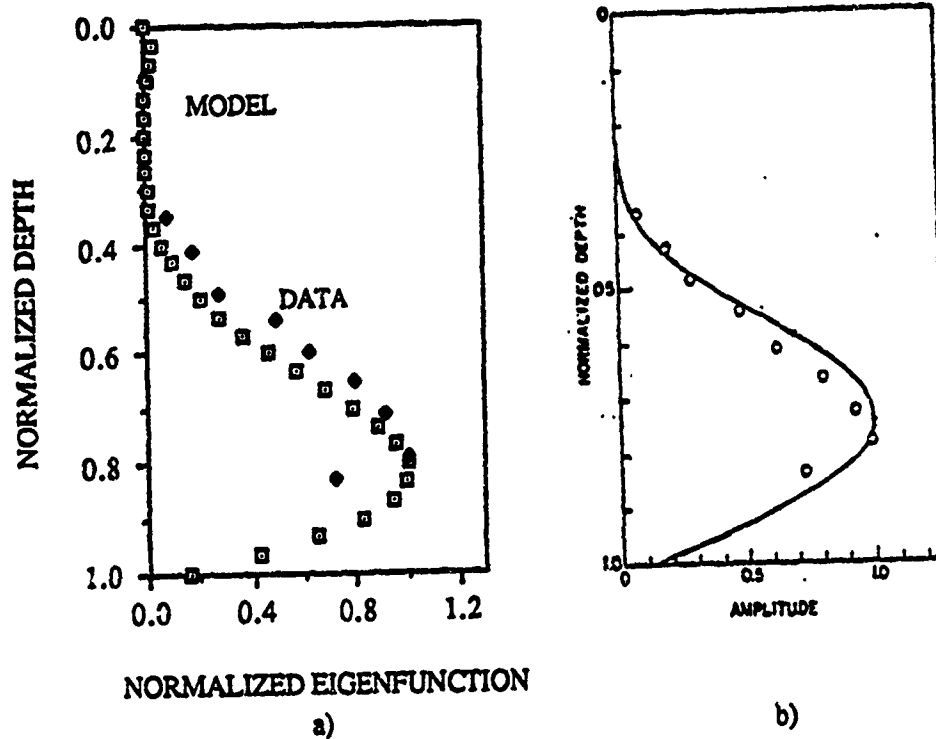


Fig. C17. a) Comparison of the First Depth Eigenfunction for 1500 (Hz) Generated by the MultiLayered Waveguide Model and Data. b) Comparison of Model Results With Data as Presented by Ingenito and Wolf.



TABLE C6

COMPARISON OF HORIZONTAL EIGENVALUES GENERATED BY THE MULTILAYERED  
WAVEGUIDE MODEL AND THE SNAP MODEL FOR A FREQUENCY OF 1500 (Hz)

MultiLayered Waveguide Model	SNAP Model	Magnitude of Difference
Horizontal Eigenvalue	Horizontal Eigenvalue	
0.6178208386D+01	0.6178205701D+01	.2D-05
0.6170829629D+01	0.6170825078D+01	.4D-05
0.6161214393D+01	0.6161204743D+01	.9D-05
0.6147548359D+01	0.6147527882D+01	.2D-04
0.6134282776D+01	0.6134262291D+01	.2D-04
0.6126957355D+01	0.6126951385D+01	.5D-05
0.6116767898D+01	0.6116757846D+01	.1D-04
0.6105159734D+01	0.6105157746D+01	.1D-05
0.6091359606D+01	0.6091353580D+01	.6D-05
0.6075254880D+01	0.6075252494D+01	.2D-05
0.6057488415D+01	0.6057480164D+01	.8D-05
0.6037737287D+01	0.6037726331D+01	.1D-04
0.6016358465D+01	0.6016350572D+01	.7D-05
0.5992942428D+01	0.5992931846D+01	.1D-04
0.5967737123D+01	0.5967721190D+01	.1D-04

Figure (C18) shows the comparison between the two models. And we see again that there is good agreement between the two models.

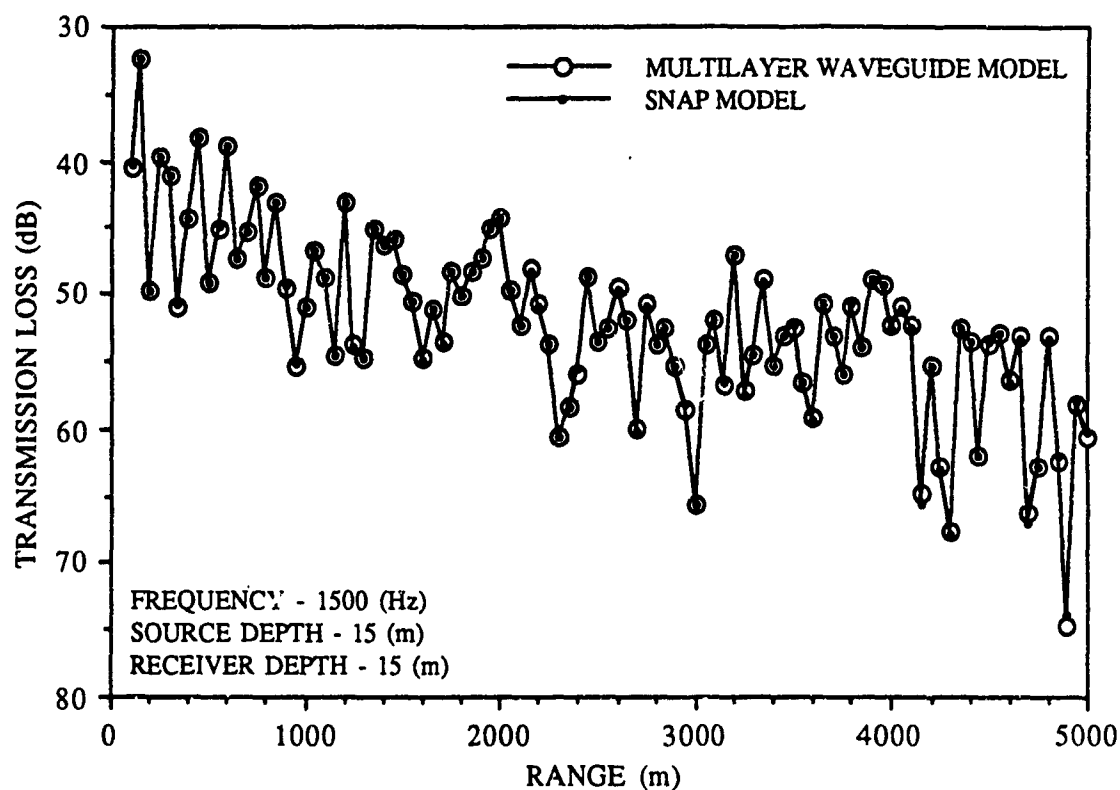


Fig. C18. Comparison of Transmission Loss Generated at a Frequency of 1500 (Hz) by the MultiLayered and SNAP Model Using the Sound Speed Profile of Fig. (C12).

Based on the preceding comparisons of horizontal eigenvalues, transmission loss, and eigenfunctions we conclude that both the Pekeris Waveguide model and the MultiLayered Waveguide model can generate the acoustic pressure at a field point with sufficient accuracy for the purpose of this project.

#### APPENDIX D: MODAL ATTENUATION COEFFICIENTS USED IN THE NORMAL MODE PROGRAMS.

This appendix gives a brief overview of the modal attenuation coefficients used in the normal mode propagation models. When a propagating mode is excited it will decay with range at a steady rate. Each mode however will not decay at the same rate. The higher order modes will decay more quickly than the lower order modes. This can be visualized by remembering that the higher order modes propagate at a higher angle and thus interact with the bottom more than the lower order modes. When mode decay is present, the wave number becomes complex, that is  $k \rightarrow k + i\beta$  where  $k$  is the wave number (propagation constant) and  $\beta$  is the attenuation coefficient of a plane wave.

Tindle (1) has developed an expression for the modal attenuation coefficients for a waveguide consisting of an isovelocity water layer overlaying a semi-infinite isovelocity half space. The expression is

$$(D.1) \quad \alpha_n = \frac{(\omega\beta / C_2 k_2) \gamma_{1n}^2}{\gamma_{1n} \gamma_{2n}^2 H[(\rho_2 \gamma_{1n} / \rho_1 \gamma_{2n}) + (\rho_1 \gamma_{2n} / \rho_2 \gamma_{1n})] + \gamma_{1n}^2 + \gamma_{2n}^2}$$

in dB/m.

Each parameter is explained below,

$f$ =frequency	(Hz)
$\omega = 2\pi f$	(Hz)
$\beta = .056f/1000.$	(dB/m)
$C_2$ = Compressional Sound Speed in Half Space	(m/s)
$k_2$ =Wave Number in Half Space	(m <sup>-1</sup> )
$\gamma_{1n}$ =Vertical Component of Wave Number in Water Layer	(m <sup>-1</sup> )
$\gamma_{2n}$ =Vertical Component of Wave Number in Half Space	(m <sup>-1</sup> )
$H$ =Water Depth	(m)
$\rho_1$ =Density of Water	(kg/m <sup>3</sup> )
$\rho_2$ =Density of Half Space	(kg/m <sup>3</sup> )

This expression is not valid when the waveguide consists of multiple isovelocity water and sediment layers. In that case we have to resort to perturbation theory (2) which produces the following expression,

$$(D-2) \quad \alpha_n = (\omega / k_n) \int_0^\infty \left( \frac{\beta p}{C} \right) Z_n^2(z) dz$$

Ingenito (3) gives a brief but through description of the development of Eq. (D-2), where  $k_n$  is the horizontal eigenvalue,  $\beta$  is the attenuation coefficient  $C$  is the compressional sound speed and  $Z_n(z)$  is the depth eigenfunction. The above equation is valid throughout the depth of the waveguide.

The attenuation coefficient for the water layers ( $\beta_0$ ) is given by the following expression, (4)

$$(D-3) \quad \beta_0 = \frac{\tau_0}{f} \left( 0.007f^2 + 0.155 \frac{1.7f^2}{(1.7)^2 + f^2 \cdot 10^{-6}} \right) 10^{-9}$$

where the attenuation coefficient for the sediment layers and the halfspace is an input into the model. Physically what happens when losses are assumed to occur primarily in the sediment is that the bottom boundary condition requires that for each mode, power must flow from the water into the bottom. Therefore for each unit horizontal distance traveled the the total power loss for a mode must equal the power transmitted into the bottom by that mode.

Equation (D-1) was used in the Pekeris Waveguide Model and Eq. (D-2) was used in the MultiLayer Model to account for losses in the sediment, while Eq. (D-3) was used for each model for the attenuation coefficient in the water.

# **APPENDIX E: COMPARISON OF THE SCATTERED FIELD OBTAINED USING THE PRESENT METHOD AND A PROJECTION METHOD.**

The material in this appendix was presented at the 2nd Joint Meeting of the Acoustical Society of America and the Acoustical Society of Japan which was held at Honolulu, Hi. (1) The projection method was developed by Evans (2) and has been presented by Norton. (3-4) The characteristics of the scattering object are presented in Table E1.

**TABLE E1**  
**OBJECT CHARACTERISTICS**

Length 25	(m)	Width 5	(m)	Boundary Conditions Dirichlet
--------------	-----	------------	-----	----------------------------------

The scattering geometry is shown in Fig. (E1).

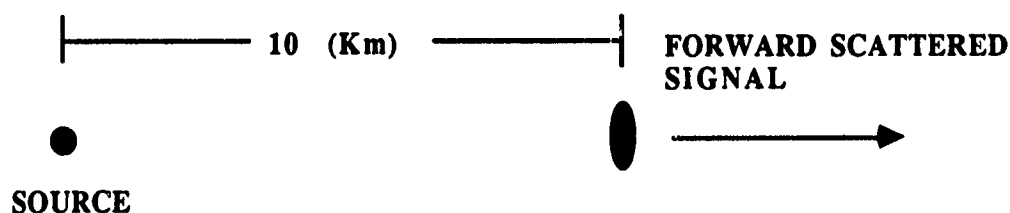


**Fig. E1. Geometry for the Scattering Problem.**

Two waveguides were investigated. The first had a isovelocity water layer overlaying an isovelocity halfspace. The second waveguide consisted of 43

water layers and 4 sediment layers over a halfspace. The first waveguide had the source, object and receiver all at a depth of 75(m). The waveguide characteristics are listed in Table E2.

TABLE E2  
ISOVELOCITY WAVEGUIDE CHARACTERISTICS

Water Layer			
Depth (m)	Compressional Sound Speed (m/s)	Density (g/cm**3)	Attenuation (nepers/m)
150	1500	1.0	1.0 E-6
Half Space			
Depth (m)	Compressional Sound Speed (m/s)	Density (g/cm**3)	Attenuation (dB/λ)
semi-inf	1600	2.0	.15

Figure (E2) shows a comparison of the transmission loss vs range between the two methods for a frequency of 100 (Hz). The current method based on Huygens' principle is the solid line and the projection method is the dotted line. They are not identical but the agreement is very good. Figure (E3) is a comparison between the two for the same waveguide at a frequency of 450 (Hz). Again the agreement is quite good.

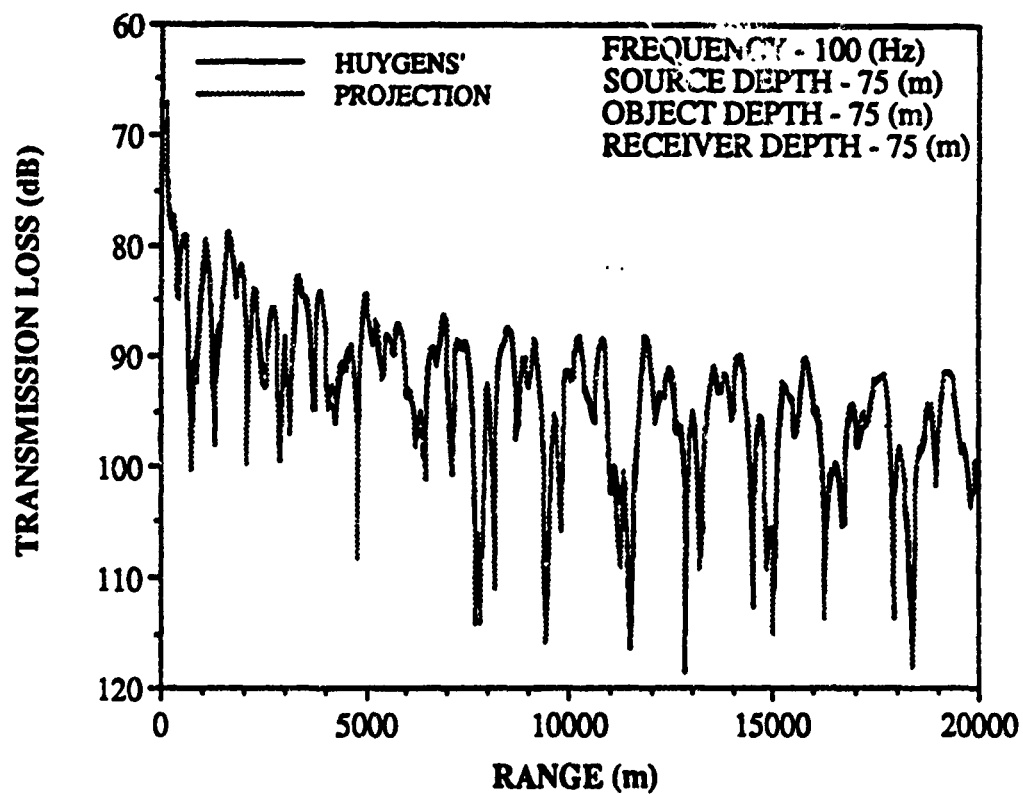


Fig. E2. Comparison Between the Scattered Field Generated From the Model Using Huygens' Principle and the Projection Method for a Frequency of 100 (Hz).



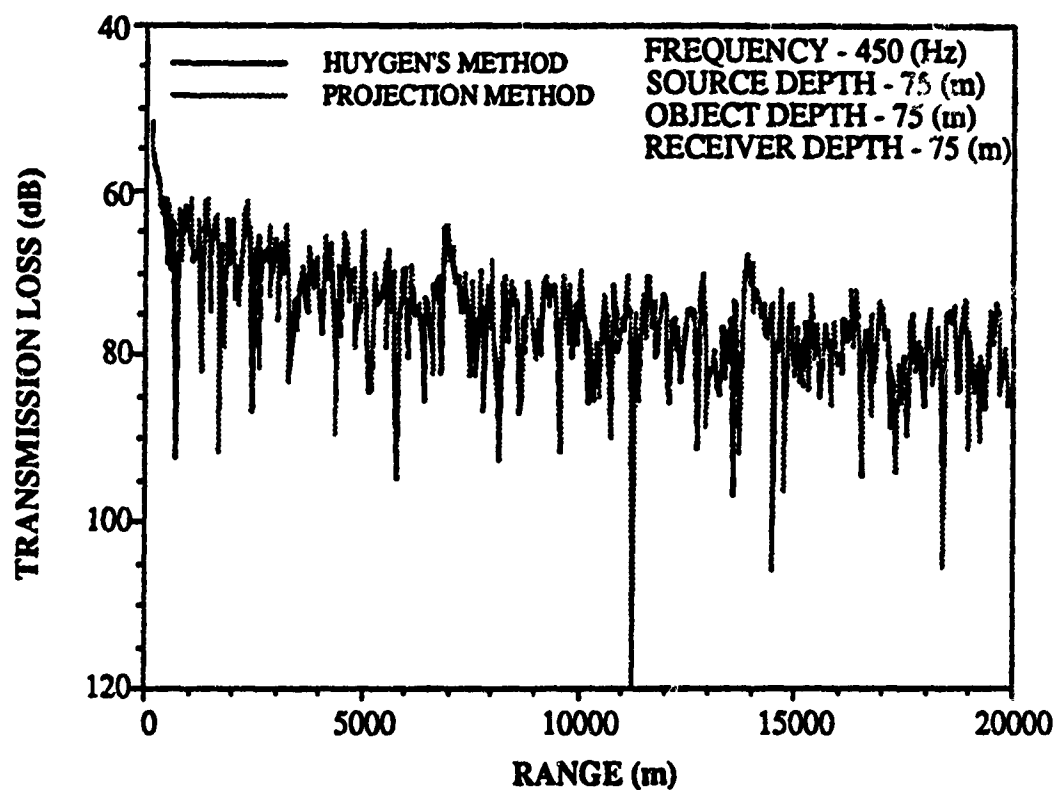


Fig. E3. Comparison Between the Scattered Field Generated From the Model Using Huygens' Principle and the Projection Method for a Frequency of 450 (Hz).

Figure (E4) illustrates the multilayered waveguide used. The source object and receiver are all at 60 (m). Note at the source depth we have a minimum in the sound speed, which results in a weak sound channel. Figure (E5) shows a comparison between the scattered field expressed as transmission loss vs range for the two methods. Also plotted in this case is the field produced by a point source. The range axis is therefore relative either to the point source or to the location of the object depending on which field is under consideration. The fields were plotted this way because the field produced by the object should show the same structure as that produced by a point source, albeit the level should be much lower. It is clearly shown that not only are the two methods agreeing quite well but they both show structure similar to a point source. In Fig. (E6) we show the results for a frequency of 450 (Hz). Again we have excellent agreement between the two methods.

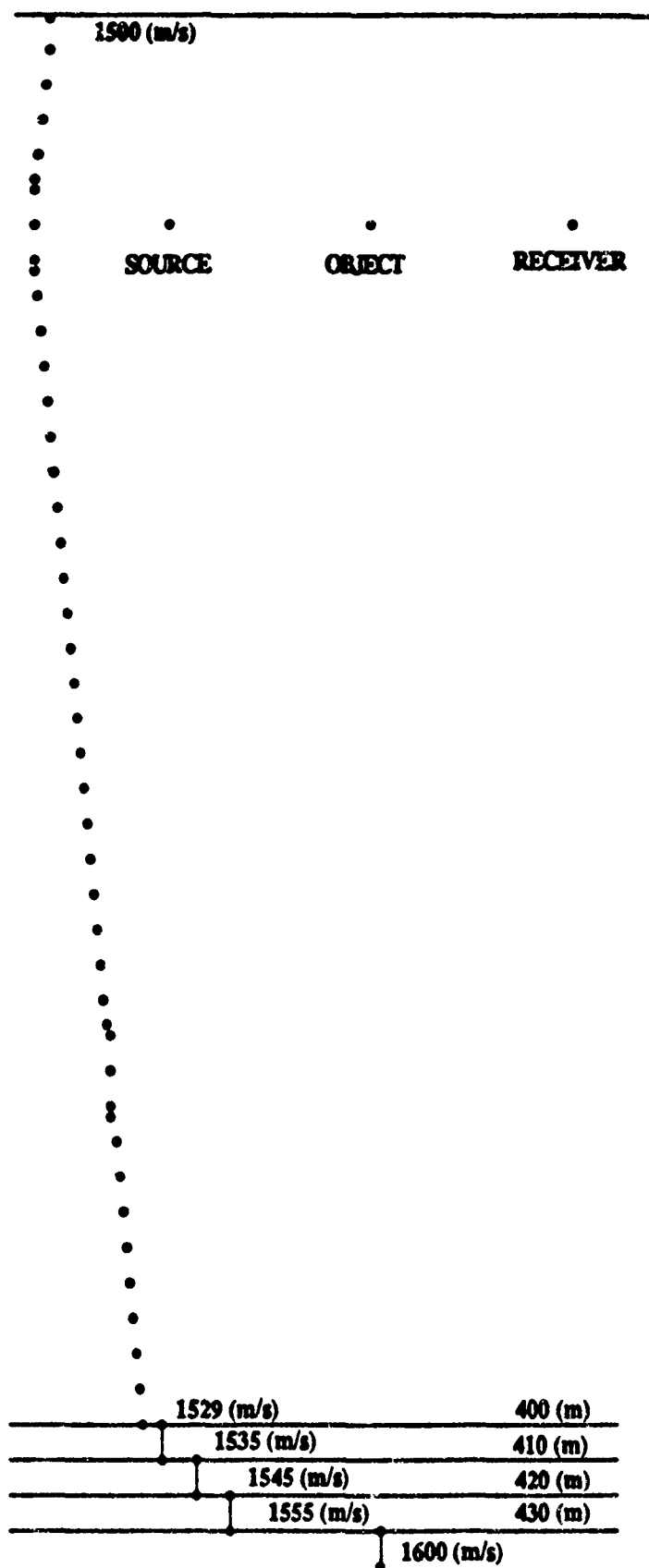


Fig. E4. Sound Speed Profile Used in the Multilayered Waveguide Comparison

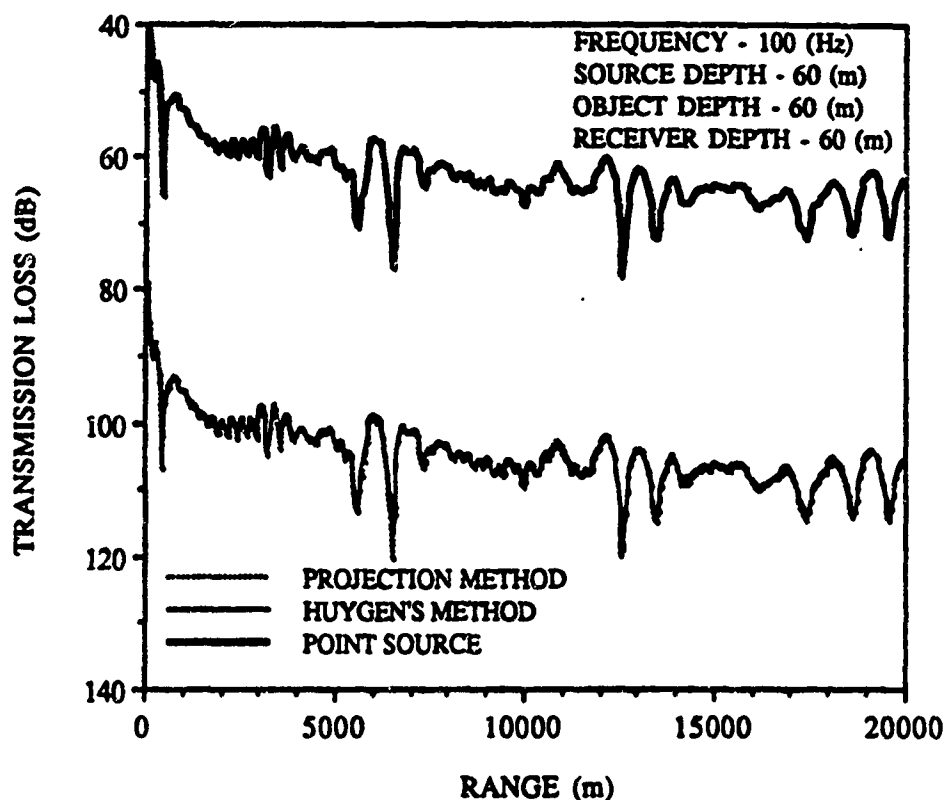


Fig. E5. Comparison between the Field Produced by a Point Source and the Object Using the Method Based on Huygens' Principle and the Projection Method for a Frequency of 100 (Hz). There are a Total of 47 Layers in the Waveguide.

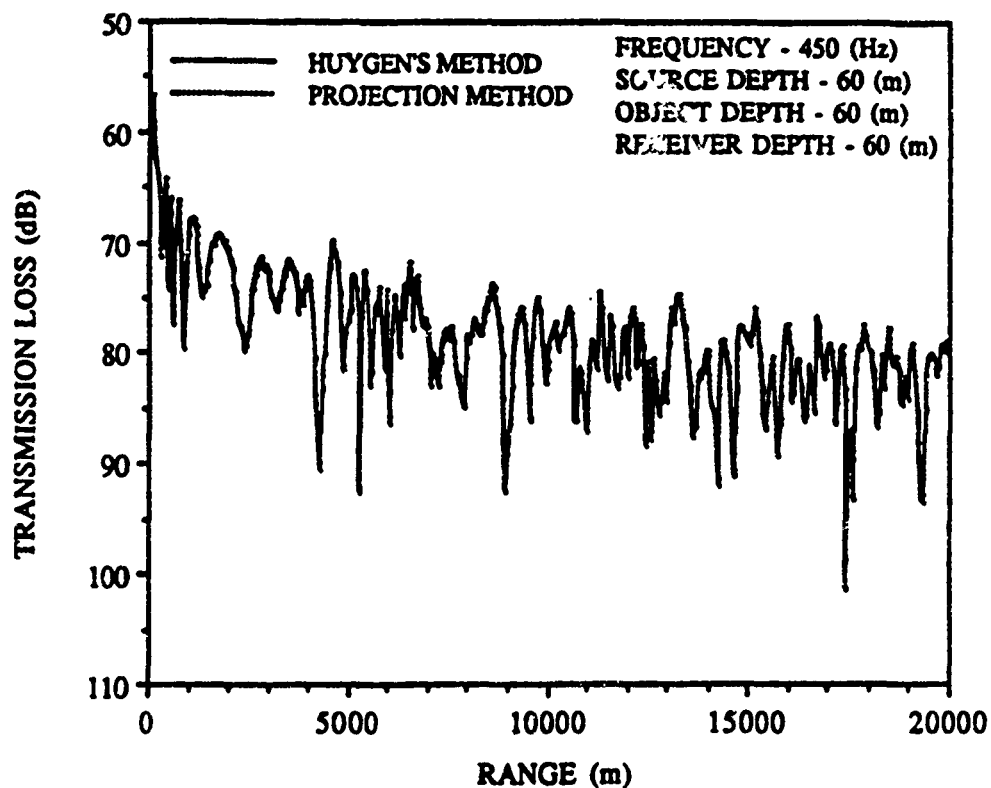


Fig. E6. Comparison Between the Scattered Field Generated Using the Method Based on Huygens' Principle and the Projection Method for a Frequency of 450 (Hz). There are a Total of 47 Layers in the Waveguide.

## ENDNOTES

## Notes to Pages 4-5

## CHAPTER TWO: FREE SPACE SCATTERING

1. James E. Burke, "Low-Frequency Scattering by Soft Spheroids," J. Acoust. Soc. Am., 39 (1960), 826-831.
2. James E. Burke, "Long-Wavelength Scattering by Hard Spheroids," J. Acoust. Soc. Am., 40 (1966), 325-330.
3. James E. Burke, "Scattering by Penetrable Spheroids," J. Acoust. Soc. Am., 43 (1968), 871-875.
4. C. Yeh, "Scattering of Acoustic Waves by a Penetrable Prolate Spheroid. I. Liquid Prolate Spheroid," J. Acoust. Soc. Am., 42 (1967), 518-521.
5. P. Morse and H. Feshbach, Methods of Theoretical Physics, (New York: McGraw-Hill, 1953) 494-523.
6. H. Levine and J. Schwinger, "On the Theory of Diffraction by an Aperture in an Infinite Plane Screen. I," Phys. Rev. 74 (1948), 958-974.
7. K. K. Mei and J. G. Van Bladel, "Scattering by Perfectly-Conducting Rectangular Cylinders," IEEE Trans. on Antenna and Propagation, Vol. 11 (March 1963), 185-192.
8. Mogens G. Andreasen, "Scattering from Parallel Metallic Cylinders With Arbitrary Cross Sections," IEEE Trans. on Antenna and Propagation, Vol. 12 (November 1964), 746-754.
9. Mogens G. Andreasen, "Scattering from Bodies of Revolution," IEEE Trans. on Antenna and Propagation, Vol. 13 (March 1965), 303-310.
10. Robert P. Banaugh and Werner Goldsmith, "Diffraction of Steady Acoustic Waves by Surfaces of Arbitrary Shape," J. Acoust. Soc. Am., 35 (1963), 1590-1601.

## Notes to Pages 5-6

11. J. Cesar Monzon, "Three-Dimensional Scattering by an Infinite Homogeneous Anisotropic Circular Cylinder: A Spectral Approach," IEEE Trans. on Antenna and Propagation, Vol. AP-35 (June 1987), 670-682.
12. L. H. Chen and D. G. Schweikert, " Sound Radiation from an Arbitrary Body," J. Acoust. Soc. Am., 35 (1963), 1620-1632.
13. I. Toyoda, M. Matsuhara, and N. Kumagai, "Extended Integral Equation Formulation for Scattering Problems from a Cylindrical Scatterer," IEEE Trans. on Antenna and Propagation, Vol. 36 (November 1988), 1580-1586.
14. P. C. Waterman, " New Foundation of Acoustic Scattering," J. Acoust. Soc. Am., 45 (1969), 1417-1429.
15. P. C. Waterman, " Matrix Formulation of Electromagnetic Scattering," Proc. IEEE, 53 (1965), 805-812.
16. W. R. Smyth, "Charged Right Circular Cylinder," J. Appl. Phys. 27 (1956), 917-920.
17. P. C. Waterman, " Matrix Theory of Elastic Wave Scattering II. A New Conservative Law," J. Acoust. Soc. Am., 63 (1977), 1320-1325.
18. B. A. Peterson, V. V. Varadan, and V. K. Varadan, " T-Matrix Approach to Study the Vibration Frequencies of Elastic Bodies in Fluids," J. Acoust. Soc. Am., 74 (1983), 1051-1056.
19. A. Bostrum, "Scattering of Stationary Acoustic Waves by an Elastic Obstacle Immersed in a Fluid," J. Acoust. Soc. Am., 67 (1980), 390-398.
20. A. Bostrum, "Scattering by a Smooth Elastic Obstacle," Tech. Report 79-14, Inst. Theoret. Physics, Goteborg University, Goteborg, Sweden (1979).
21. W. M. Visscher, "A New Way to Calculate Scattering of Acoustic and Elastic Waves," J. Appl. Phys., 7 (1980).
22. Y. H. Pao, "The Transition Matrix for the Scattering of Acoustic Waves and Elastic Waves," in Modern Problems in Elastic Wave Propagation. (New York: Wiley and Interscience, 1978).

## Notes to Pages 6-11

23. B. B. Baker and E. T. Copson, The Mathematical Theory of Huygens' Principle, (Oxford: Clarendon Press, 1953).
  
24. M. F. Werby and S. Chin-Bing, "Some Numerical Techniques and Their use in the Extension of T-Matrix and Null-Field Approaches to Scattering," Int. J. Comp. Math. Appls., 11 (1985), 717-731.
  
25. M. F. Werby and G. J. Tango, "Application of the Extended Boundary Condition Equations to Scattering from Fluid-Loaded Bounded Objects," Engr. Analysis, Vol. 5, No. 1 (1988), 12-20.
  
26. P. Morse and H. Feshbach, Methods of Theoretical Physics, (New York: McGraw-Hill, 1953), 884-886.
  
27. F. Tricomi, Integral Equations, (New York: Dover Press, 1967).
  
28. M. F. Werby, "A Coupled Higher-Order T-Matrix," J. Acoust. Soc. Am., (submitted 1987).
  
29. M. F. Werby, G. Tango and L. H. Green, "Eigenvalue and Similarity Transformation Methods in the Solution of Acoustical Scattering Problems," 1st IMACS Symposium on Computational Acoustics, New Haven, CT., to appear J. Comp. Math. Appls. (1987).
  
30. S. Basker, V. V. Varadan and V. K. Varadan, "Thin Shell Theories and Acoustic Wave Scattering by Infinitely Long Cylindrical Shells of Arbitrary Cross Section," J. Acoust. Soc. Am., 75 (1984), 1673-1679.
  
31. M. F. Werby and L. H. Green, "An Extended Unitary Approach for Acoustical Scattering from Elastic Shells Immersed in a Fluids" J. Acoust. Soc. Am., 74 (1983), 625-630.
  
32. M. F. Werby and G. Gaunard, "Transition from Soft to Hard Behavior in Scattering from Submerged Thin Elastic Shells," Acoustics Letts. 9, (1986), 111.
  
33. G. Gaunard and M. F. Werby, "Proper Background Choice in Resonance Scattering from Elastic Shells," Int. J. Solids Structures, 22, (1986), 1149.



## Notes to Pages 11-20

34. M. F. Werby and G. Gaunard, "Sound Scattering from Spheroidal Shells in Water," in Proceedings ASME Pressure Vessels Piping Conference, (New York: ASME Press, 1985).
35. M. F. Werby and L. H. Green, "A Comparison of Acoustical Scattering from Fluid-Loaded Elastic Shells and Sound Soft Objects," J. Acoust. Soc. Am., 76 (1984), 1227-1230.
36. G. Gaunard and M. F. Werby, "Resonance Response of Submerged Acoustically-Excited Thick and Thin Shells," J. Acoust. Soc. Am., 77 (1985), 2081-2093.
37. Y. H. Pao and V. Varatharajulo, "Huygens' Principle, Radiation Condition, and Integral Formula for the Scattering of Elastic Waves," J. Acoust. Soc. Am., 59 (1976), 1361-1370.
38. L. R. Dragonette, "Evaluation of the Relative Importance of Circumferential or Creeping Waves in Acoustic Scattering from Rigid and Elastic Solid Cylinders and Cylindrical Shells," NRL Report 8216 (1978).
39. M. F. Werby and G. J. Tango, "Numerical Study of Material Properties of Submerged Elastic Objects Using Resonance Response," J. Acoust. Soc. Am., 79 (1986), 1260-1268.
40. M. F. Werby, "Reply to 'Comment on 'A Comparison of Acoustical Scattering from Fluid-Loaded Elastic Shells and Sound-Soft Objects,'" J. Acoust. Soc. Am., 81 (1987), 783-787.
41. M. F. Werby and L. H. Green, "Correspondence Between Acoustical Scattering from Spherical and End-On Incident Spheroidal Shells," J. Acoust. Soc. Am., 81 (1983), 783-787.
42. G. C. Gaunard and H. Uberall, "RST Analysis of Monostatic and Bistatic Acoustic Echoes from Spheres," J. Acoust. Soc. Am., 73 (1983), 1-12.
43. L. Flax, G. C. Gaunard and H. Uberall, "Theory of Resonance Scattering," in Physical Acoustics, XV (Edited by W. P. Mason and R. N. Thurston), (New York: Academic Press, 1981) Chapter 3, 191-194.

## Notes to Pages 23-51

## CHAPTER THREE: ACOUSTIC PROPAGATION IN A WAVEGUIDE

1. Daljit S. Ahluwalia and Joseph B. Keller, "Exact and Asymptotic Representations of the Sound Field in a Stratified Ocean," in Wave Propagation and Underwater Acoustics. Lecture Notes in Physics 70, edited by Joseph B. Keller and John S. Papadakis, (Berlin: Springer-Verlag, 1977), 14-85.
2. G. Arfken, Mathematical Methods for Physicists, (Orlando: Academic Press, 3rd. Edition, 1985) 57-58.
3. H. Goldstein, Classical Mechanics, (Reading: Addison-Wesley, 1980) 253-258.
4. Keith R. Symon, Mechanics, (Reading: Addison-Wesley, 3rd Edition, 1971) 191-201.
5. Lord Rayleigh, Theory of Sound II, (New York: Dover Publications, 1945) 69-78
6. W. Heitler, The Quantum Theory of Radiation, (Glasgow: Oxford University Press, 1954) 40-45.
7. M. A. Biot and I. Tolstoy, "Formulation of Wave Propagation in Infinite Media by Normal Coordinates with an Application to Diffraction," J. Acoust. Soc. Am., 29 (1957), 381-391.
8. I. Tolstoy and C. S. Clay, Ocean Acoustics. Theory and Experiment in Underwater Sound, (New York: American Institute of Physics, 1987) 98-105.
9. G. Arfken, Mathematical Methods for Physicists, (Orlando: Academic Press, 3rd. Edition, 1985) 97.
10. G. Arfken, Mathematical Methods for Physicists, (Orlando: Academic Press, 3rd. Edition, 1985) 604-608.
11. G. Arfken, Mathematical Methods for Physicists, (Orlando: Academic Press, 3rd. Edition, 1985) 616-621.

## Notes to Pages 52-72

12. I. Tolstoy and C. S. Clay, Ocean Acoustics, Theory and Experiment in Underwater Sound, (New York: American Institute of Physics, 1987) 36.
13. William Elmore and Mark Heald, Physics of Waves, (New York: Dover Publications, Inc., 1969) 69.
14. C. S. Clay and H. Medwin, Acoustical Oceanography: Principles and Applications, (New York: John Wiley and Sons, 1977) 295-296.
15. G. Arfken, Mathematical Methods for Physicists, (Orlando: Academic Press, 3rd. Edition, 1985) 104.
16. G. Arfken, Mathematical Methods for Physicists, (Orlando: Academic Press, 3rd. Edition, 1985) 454-463.
17. Daljit S. Ahluwalia and Joseph B. Keller, " Exact and Asymptotic Representations of the Sound Field in a Stratified Ocean," in Wave Propagation and Underwater Acoustics. Lecture Notes in Physics 70, edited by Joseph B. Keller and John S. Papadakis, (Berlin: Springer-Verlag, 1977), 21.
18. G. Arfken, Mathematical Methods for Physicists, (Orlando: Academic Press, 3rd. Edition, 1985) 57-58.
19. C. S. Clay and H. Medwin, Acoustical Oceanography: Principles and Applications, (New York: John Wiley and Sons, 1977) 32-35.
20. P. Morse and H. Feshbach, Methods of Theoretical Physics, (New York: McGraw-Hill, 1953) 467.
21. W. Magnus, F. Obelettinger and R. P. Soni, Formulas and Theorems for the Special Functions of Mathematical Physics, (New York: Springer-Verlog, 1966) 82.

## CHAPTER FOUR: METHODS DESCRIBING SCATTERING FROM OBJECTS IN A WAVEGUIDE

1. Richard B. Evans, "Acoustic Scattering from a Rigid Object in a Halfspace and a Slab Waveguide," NORDA Tech Note 304, (Jan. 1985).

## Notes to Pages 72-76

2. M. F. Werby and R. B. Evans, "Scattering from Objects in Unbounded and Bounded Oceans," IEEE Jour. Oceanic Engr. OE-12 (April 1987).
3. R. H. Hackman and G. S. Sammelmann, "Acoustic Scattering in an Inhomogeneous Waveguide: Theory," J. Acoust. Soc. Am. 80, (1986) 1447-1458.
4. G. S. Sammelmann and R. Hackman, "Acoustic Scattering in a Homogeneous Waveguide," J. Acoust. Soc. Am. 82, (1987) 324-336.
5. R. Hackman and G. S. Sammelmann, "Long-Range Scattering in a Deep Oceanic Waveguide," J. Acoust. Soc. Am. 83, (1988) 1776-1793.
6. Richard B. Evans, Guy V. Norton, and M. F. Werby, "A Practical Method for Computing Acoustic Scattering Caused by a Submerged Object in a Waveguide," NORDA Tech Note 349, (Aug. 1987).
7. M. D. Collins and M. F. Werby, "Scattering from an ellipsoid Submerged in the Ocean," J. Acoust. Soc. Am. Suppl. 1,82, (Fall 87), S105.
8. M. D. Collins and M. F. Werby, "A Parabolic Equation Model for Scattering in the Ocean," J. Acoust. Soc. Am. 85, (1989) 1895-1902.
9. Rahul Sen, "Scattering of Acoustic Waves in a Waveguide," J. Acoust. Soc. Am. Suppl. 1,81, (Spring 87), S42.
10. A. A. Kleshchev and L. L. Klyukin, "Spectral Characteristics of Sound Scattering by a Body in a Sound Channel," Sov. Phys. Acoust. 20, (Nov.-Dec. 1974) 143-145.
11. A. A. Kleshchev, "Sound Scattering by Spheroidal Bodies near an Interface," Sov. Phys. Acoust. 23, (Nov.-Dec. 1977) 400-410.
12. A. A. Kleshchev, "Sound Scattering by a Spheroidal Body at an Interface," Sov. Phys. Acoust. 25, (Jan.-Feb. 1979) 143-145.
13. G. Arfken, Mathematical Methods for Physicists, (Orlando: Academic Press, 3rd. Edition, 1985) 57-58.

## Notes to Pages 76-89

14. B. B. Baker and E. T. Copson, The Mathematical Theory of Huygens' Principle, (Oxford: Clarendon Press, 1953).

## CHAPTER FIVE: APPLICATION OF HUYGENS' METHOD TO AN ISOVELOCITY WAVEGUIDE

1. C. L. Pekeris, "Theory of Propagation and Explosive Sound in Shallow Water," Geol. Soc. Am. Mem., 27, (1948).

2. C. S. Clay and H. Medwin, Acoustical Oceanography: Principles and Applications, (New York: John Wiley and Sons, 1977) 288-317.

3. G. Arfken, Mathematical Methods for Physicists, (Orlando: Academic Press, 3rd. Edition, 1985) 57-58.

4. G. Arfken, Mathematical Methods for Physicists, (Orlando: Academic Press, 3rd. Edition, 1985) 448-451.

5. G. Arfken, Mathematical Methods for Physicists, (Orlando: Academic Press, 3rd. Edition, 1985) 97.

6. G. Arfken, Mathematical Methods for Physicists, (Orlando: Academic Press, 3rd. Edition, 1985) 454-463.

7. G. Arfken, Mathematical Methods for Physicists, (Orlando: Academic Press, 3rd. Edition, 1985) 616-622.

8. G. Arfken, Mathematical Methods for Physicists, (Orlando: Academic Press, 3rd. Edition, 1985) 454-463.

9. C. S. Clay and H. Medwin, Acoustical Oceanography: Principles and Applications, (New York: John Wiley and Sons, 1977) 61-64.

10. C. S. Clay and H. Medwin, Acoustical Oceanography: Principles and Applications, (New York: John Wiley and Sons, 1977) 32-35.

11. C. S. Clay and H. Medwin, Acoustical Oceanography: Principles and Applications, (New York: John Wiley and Sons, 1977) 295-296.

## Notes to Pages 94-202

12. Guy V. Norton and M. F. Werby, "Some Numerical Approaches to Describe Acoustical Scattering from Objects in a Waveguide," Mathl. Comput. Modeling, 11, (1988) 81-86.

13. P. M. Morse and H. Feshbach, Methods of Theoretical Physics II, (New York: McGraw-Hill, 1953) 1466.

## CHAPTER SIX: APPLICATION OF HUYGENS' METHOD TO A MULTILAYERED WAVEGUIDE

1. Ivan Tolstoy, "Note on the Propagation of Normal Modes in Inhomogeneous Media," J. Acoust. Soc. Am., 27, (March 1955) 274-277.

2. Ivan Tolstoy, "Resonant Frequencies and High Modes in Layered Wave Guides," J. Acoust. Soc. Am., 28, (November 1956) 1182-1192.

## APPENDIX A: COMPARISON OF THE SCATTERED FIELD USING THE EXTENDED BOUNDARY CONDITION METHOD AND THE ANALYTICAL SOLUTION FOR A PLANE WAVE INCIDENT ON A SPHERE.

1. P. Morse and H. Feshbach, Methods of Theoretical Physics II, (New York: McGraw-Hill, 1953) 1483-1486.

## APPENDIX B: DERIVATION OF EQ. (3-122).

1. G. Arfken, Mathematical Methods for Physicists, (Orlando: Academic Press, 3rd. Edition, 1985) 602.

2. M. Abramowitz and I. Stegun, Handbook of Mathematical Functions, (New York: Dover Publications, Inc., 1970) 360.

## APPENDIX C: VALIDATION OF PROPAGATION MODELS

1. Finn B. Jensen and M. C. Ferla, "SNAP: The SACLANTCEN Normal Mode Acoustic Propagation Model," SACLANTCEN Mem. SM-121, (Jan. 1979).

2. Frank Ingenito and Stephen N. Wolf, "Acoustic Propagation an Shallow Water Overlaying a Consolidated Bottom," J. Acoust. Soc. Am., 60, (September 1976) 611-617.

## Notes to Pages 211-214

## APPENDIX D: MODAL ATTENUATION COEFFICIENTS USED IN THE NORMAL MODE PROGRAMS.

1. C. Tindle, "Attenuation Parameters from Normal Mode Measurements," J. Acoust. Soc. Am., 71, (May 1982) 1145-1148.
2. K. E. Hawker, W. Williams and T. Foreman, "A Study of the Acoustical Effects of Sub-Bottom Absorption," J. Acoust. Soc. Am., 65, ( 1979) 360-367.
3. Finn B. Jensen and M. C. Ferla, "SNAP: The SACLANTCEN Normal Mode Acoustic Propagation Model," SACLANTCEN Mem. SM-121, (Jan. 1979).
4. Frank Ingenito, "Measurements of Mode Attenuation Coefficients in Shallow Water," J. Acoust. Soc. Am., 53, ( 1973) 858-863.

## APPENDIX E: COMPARISON OF SCATTERED FIELD DEVELOPED USING PRESENT METHOD AND A PROJECTION METHOD.

1. Guy Norton, M. F. Werby, and M. D. Collins, "Benchmark Comparison of Underwater Acoustic Scattering Models," J. Acoust. Soc. Am., Suppl. 1 84, ( Fall 1988) S219.
2. Richard B. Evans, Guy. V. Norton, and M. F. Werby, "A Practical Method for Computing Acoustic Scattering Caused by a Submerged Object in a Waveguide," NORDA Tech Note 349, (Aug. 1987).
3. Guy V. Norton and M. F. Werby, " Some Numerical Approaches to Describe Acoustical Scattering from Objects in a Waveguide," Mathl. Comput. Modeling, 11, (1988) 81-86.
4. Guy V. Norton, "A Numerical Approach to Describe Acoustical Scattering from an Object in a Waveguide Using a Projection Technique," Second IMACS Symposium on Computational Acoustics, (March 14-17, 1989).

## LIST OF REFERENCES

- Abramowitz, M., and I. Stegun. 1970. Handbook of Mathematical Functions. New York: Dover Publications, Inc.
- Ahluwalia, Daljit S., and Joseph B. Keller. 1977. Exact and Asymptotic Representations of the Sound Field in a Stratified Ocean. In Wave Propagation and Underwater Acoustics, Lecture Notes in Physics 70, ed. Joseph B. Keller and John S. Papadakis, 14-85. Berlin: Springer-Verlag.
- Andreasen, Mogens G. 1964. Scattering from Parallel Metallic Cylinders With Arbitrary Cross Sections. IEEE Trans. on Antenna and Propagation Vol. 12:746-754.
- \_\_\_\_\_. 1965. Scattering from Bodies of Revolution. IEEE Trans. on Antenna and Propagation Vol. 13:303-310.
- Arfken, G. 1985. Mathematical Methods for Physicists. 3rd ed. Orlando: Academic Press.
- Baker, B. B., and E. T. Copson. 1953. The Mathematical Theory of Huygens' Principle. Oxford: Clarendon Press.
- Banaugh, Robert P., and Werner Goldsmith. 1963. Diffraction of Steady Acoustic Waves by Surfaces of Arbitrary Shape. J. Acoust. Soc. Am. 35:1590-1601.
- Basker, S., V. V. Varadan, and V. K. Varadan. 1984. Thin Shell Theories and Acoustic Wave Scattering by Infinitely Long Cylindrical Shells of Arbitrary Cross Section. J. Acoust. Soc. Am. 75:1673-1679.
- Biot, M. A., and I. Tolstoy. 1957. Formulation of Wave Propagation in Infinite Media by Normal Coordinates with an Application to Diffraction. J. Acoust. Soc. Am. 29:381-391.
- Bostrum, A. 1979. Scattering by a Smooth Elastic Obstacle. Tech. Report 79-14. Inst. Theoret. Physics, Goteborg University, Goteborg, Sweden.
- \_\_\_\_\_. 1980. Scattering of Stationary Acoustic Waves by an Elastic Obstacle Immersed in a Fluid. J. Acoust. Soc. Am. 67:390-398.



- Burke, James E. 1960. Low-Frequency Scattering by Soft Spheroids. J. Acoust. Soc. Am. 39:826-831.
- \_\_\_\_\_. 1966. Long-Wavelength Scattering by Hard Spheroids. J. Acoust. Soc. Am. 40:325-330.
- \_\_\_\_\_. 1968. Scattering by Penetrable Spheroids. J. Acoust. Soc. Am. 43:871-875.
- Chen, L. H., and D. G. Schweikert. 1963. Sound Radiation from an Arbitrary Body. J. Acoust. Soc. Am. 35:1620-1632.
- Clay, C. S., and H. Medwin. 1977. Acoustical Oceanography: Principles and Applications. New York: John Wiley and Sons.
- Collins, M. D., and M. F. Werby. 1987. Scattering from an ellipsoid Submerged in the Ocean. J. Acoust. Soc. Am. Suppl. 1 82:S105.
- \_\_\_\_\_, and M. F. Werby. 1989. A Parabolic Equation Model for Scattering in the Ocean. J. Acoust. Soc. Am. 85:1895-1902.
- Dragonette, L. R. 1978. Evaluation of the Relative Importance of Circumferential or Creeping Waves in Acoustic Scattering from Rigid and Elastic Solid Cylinders and Cylindrical Shells. NRL Rep. 8216.
- Elmore, William, and Mark Heald. 1969. Physics of Waves. New York: Dover Publications, Inc..
- Evans, Richard B. 1985. Acoustic Scattering from a Rigid Object in a Halfspace and a Slab Waveguide. NORDA Tech Note 304.
- \_\_\_\_\_, Guy V. Norton, and M. F. Werby. 1987. A Practical Method for Computing Acoustic Scattering Caused by a Submerged Object in a Waveguide. NORDA Tech Note 349.
- Flax, L., G. C. Gaunard and H. Uberall. 1981. Theory of Resonance Scattering. In Physical Acoustics, ed. W. P. Mason and R. N. Thurston, 191-194, vol. XV. New York: Academic Press.
- Gaunard, G., and H. Uberall. 1983. RST Analysis of Monostatic and Bistatic Acoustic Echoes from Spheres. J. Acoust. Soc. Am. 73:1-12.
- \_\_\_\_\_, and M. F. Werby. 1985. Resonance Response of Submerged Acoustically-Excited Thick and Thin Shells. J. Acoust. Soc. Am. 77:2081-2093.
- \_\_\_\_\_, and M. F. Werby. 1986. Proper Background Choice in Resonance Scattering from Elastic Shells. Int. J. Solids Structures 22:1149.
- Goldstein, H. 1980. Classical Mechanics. Reading: Addison-Wesley.

- Hackman, R. H., and G. S. Sammelmann. 1986. Acoustic Scattering in an Inhomogeneous Waveguide: Theory. J. Acoust. Soc. Am. 80:1447-1458.
- \_\_\_\_\_, and G. S. Sammelmann. 1988. Long-Range Scattering in a Deep Oceanic Waveguide. J. Acoust. Soc. Am. 83:1776-1793.
- Hawker, K. E., W. Williams, and T. Foreman. 1979. A Study of the Acoustical Effects of Sub-Bottom Absorption. J. Acoust. Soc. Am. 65:360-367.
- Heitler, W. 1954. The Quantum Theory of Radiation. Glasgow: Oxford University Press.
- Ingenito, Frank. 1973. Measurements of Mode Attenuation Coefficients in Shallow Water. J. Acoust. Soc. Am. 53:858-863.
- \_\_\_\_\_, and Stephen N. Wolf. 1976. Acoustic Propagation in Shallow Water Overlaying a Consolidated Bottom. J. Acoust. Soc. Am. 60:611-617.
- Jensen, Finn B., and M. C. Ferla. 1979. SNAP: The SACLANTCEN Normal Mode Acoustic Propagation Model SACLANTCEN Mem. SM-121.
- Kleshchev, A. A., and L. L. Klyukin. 1974. Spectral Characteristics of Sound Scattering by a Body in a Sound Channel. Sov. Phys. Acoust. 20:143-145.
- \_\_\_\_\_. 1977. Sound Scattering by Spheroidal Bodies near an Interface. Sov. Phys. Acoust. 23:400-410.
- \_\_\_\_\_. 1979. Sound Scattering by a Spheroidal Body at an Interface. Sov. Phys. Acoust. 25:143-145.
- Levine, H., and J. Schwinger. 1948. On the Theory of Diffraction by an Aperture in an Infinite Plane Screen. I. Phys. Rev. 74:958-974.
- Magnus, W., F. Oberhettinger and R. P. Soni. 1966. Formulas and Theorems for the Special Functions of Mathematical Physics. New York: Springer-Verlag.
- Mei, K. K., and J. G. Van Bladel. 1963. Scattering by Perfectly-Conducting Rectangular Cylinders. IEEE Trans. on Antenna and Propagation 11:185-192.
- Monzon, J. Cesar. 1987. Three-Dimensional Scattering by an Infinite Homogeneous Anisotropic Circular Cylinder: A Spectral Approach. IEEE Trans. on Antenna and Propagation Vol. AP-35:670-682.
- Morse, P., and H. Feshbach. 1953. Methods of Theoretical Physics. New York: McGraw-Hill.

- Norton, Guy V., and M. F. Werby. 1988. Some Numerical Approaches to Describe Acoustical Scattering from Objects in a Waveguide. Mathl. Comput. Modeling 11:81-86.
- \_\_\_\_\_, M. F. Werby, and M. D. Collins. 1988. Benchmark Comparison of Underwater Acoustic Scattering Models. J. Acoust. Soc. Am. Suppl. 1 84:S219.
- \_\_\_\_\_. 1989. A Numerical Approach to Describe Acoustical Scattering from an Object in a Waveguide Using a Projection Technique. Second IMACS Symposium on Computational Acoustics.
- Pao, Y. H., and V. Varatharajulo. 1976. Huygens' Principle, Radiation Condition, and Integral Formula for the Scattering of Elastic Waves. J. Acoust. Soc. Am. 59:1361-1370.
- \_\_\_\_\_. 1978. The Transition Matrix for the Scattering of Acoustic Waves and Elastic Waves. In Modern Problems in Elastic Wave Propagation. New York: Wiley and Interscience.
- Pekeris, C. L. 1948. Theory of Propagation and Explosive Sound in Shallow Water. Geol. Soc. Am. Mem. 27.
- Peterson, B. A., V. V. Varadan, and V. K. Varadan. 1983. T-Matrix Approach to Study the Vibration Frequencies of Elastic Bodies in Fluids. J. Acoust. Soc. Am. 74:1051-1056.
- Rayleigh, Lord. 1945. Theory of Sound II. New York: Dover Publications.
- Sammelmann, G. S., and R. Hackman. 1987. Acoustic Scattering in a Homogeneous Waveguide. J. Acoust. Soc. Am. 82:324-336.
- Sen, Rahul. 1987. Scattering of Acoustic Waves in a Waveguide. J. Acoust. Soc. Am. Suppl. 1 81:S42.
- Smyth, W. R. 1956. Charged Right Circular Cylinder. J. Appl. Phys. 27:917-920.
- Symon, Keith R. 1971. Mechanics. 3d ed. Reading: Addison-Wesley.
- Tindle, C. 1982. Attenuation Parameters from Normal Mode Measurements. J. Acoust. Soc. Am. 71:1145-1148.
- Tolstoy, Ivan. 1955. Note on the Propagation of Normal Modes in Inhomogeneous Media. J. Acoust. Soc. Am. 27:274-277.
- \_\_\_\_\_. 1956. Resonant Frequencies and High Modes in Layered Wave Guides. J. Acoust. Soc. Am. 28:1182-1192.
- \_\_\_\_\_, and C. S. Clay. 1987. Ocean Acoustics. Theory and Experiment in Underwater Sound. New York: American Institute of Physics.

- Toyoda, I., M. Matsuhara, and N. Kumagai. 1988. Extended Integral Equation Formulation for Scattering Problems from a Cylindrical Scatterer. IEEE Trans. on Antenna and Propagation Vol. 36:1580-1586.
- Tricomi, F. 1967. Integral Equations. New York: Dover Press.
- Visscher, W. M. 1980. A New Way to Calculate Scattering of Acoustic and Elastic Waves. J. Appl. Phys. 7.
- Waterman, P. C. 1965. Matrix Formulation of Electromagnetic Scattering. Proc. IEEE 53:805-812.
- \_\_\_\_\_. 1969. New Foundation of Acoustic Scattering. J. Acoust. Soc. Am. 45:1417-1429.
- \_\_\_\_\_. 1977. Matrix Theory of Elastic Wave Scattering II. A New Conservative Law. J. Acoust. Soc. Am. 63:1320-1325.
- Werby, M. F., and L. H. Green. 1983. An Extended Unitary Approach for Acoustical Scattering from Elastic Shells Immersed in a Fluids. J. Acoust. Soc. Am. 74:625-630.
- \_\_\_\_\_, and L. H. Green. 1983. Correspondence Between Acoustical Scattering from Spherical and End-On Incident Spheroidal Shells. J. Acoust. Soc. Am. 81:783-787.
- \_\_\_\_\_, and L. H. Green. 1984. A Comparison of Acoustical Scattering from Fluid-Loaded Elastic Shells and Sound Soft Objects. J. Acoust. Soc. Am. 76:1227-1230.
- \_\_\_\_\_, and S. Chin-Bing. 1985. Some Numerical Techniques and Their use in the Extension of T-Matrix and Null-Field Approaches to Scattering. Int. J. Comp. Math. Appls. 11:717-731.
- \_\_\_\_\_, and G. Gaunard. 1985. Sound Scattering from Spheroidal Shells in Water. In Proceedings ASME Pressure Vessels Piping Conference, New York: ASME Press.
- \_\_\_\_\_, and G. Gaunard. 1986. Transition from Soft to Hard Behavior in Scattering from Submerged Thin Elastic Shells. Acoustics Letts. 9:111.
- \_\_\_\_\_, and G. J. Tango. 1986. Numerical Study of Material Properties of Submerged Elastic Objects Using Resonance Response. J. Acoust. Soc. Am. 79:1260-1268.
- \_\_\_\_\_. 1987. A Coupled Higher-Order T-Matrix. J. Acoust. Soc. Am. submitted.
- \_\_\_\_\_, G. Tango, and L. H. Green. 1987. Eigenvalue and Similarity Transformation Methods in the Solution of Acoustical Scattering Problems. 1st IMACS Symposium on Computational Acoustics, New Haven, CT., to appear J. Comp. Math. Appls.

- \_\_\_\_\_. 1987. Reply to 'Comment on 'A Comparison of Acoustical Scattering from Fluid-Loaded Elastic Shells and Sound-Soft Objects. J. Acoust. Soc. Am. 81:783-787.
- \_\_\_\_\_, and R. B. Evans. 1987. Scattering from Objects in Unbounded and Bounded Oceans. IEEE Jour. Oceanic Engr. OE-12.
- \_\_\_\_\_, and G. J. Tango. 1988. Application of the Extended Boundary Condition Equations to Scattering from Fluid-Loaded Bounded Objects. Engr. Analysis. Vol. 5, No. 1:12-20.
- Yeh, C. 1967. Scattering of Acoustic Waves by a Penetrable Prolate Spheroid. I. Liquid Prolate Spheroid. J. Acoust. Soc. Am. 42:518-521.

# Distribution List

Assistant Secretary of the Navy  
Research, Development & Acquisition  
Navy Department  
Washington DC 20350-1000

Chief of Naval Operations  
Navy Department  
Washington DC 20350-2000  
Attn: OP-71  
OP-987

Chief of Naval Operations  
Oceanographer of the Navy  
U.S. Naval Observatory  
34th & Massachusetts Ave. NW  
Washington DC 20392-1800  
Attn: OP-096  
OP-0961B

David W. Taylor Naval Research Center  
Bethesda MD 20084-5000  
Attn: Commander

Fleet Antisub Warfare Tng Ctr-Atl  
Naval Station  
Norfolk VA 23511-6495  
Attn: Commanding Officer

Naval Oceanographic Office  
Stennis Space Center MS 39522-5001  
Attn: Commanding Officer

Naval Oceanography Command  
Stennis Space Center MS 39529-5000  
Attn: Commander

Naval Oceanographic & Atmospheric  
Research Laboratory  
Stennis Space Center MS 39529-5004  
Attn: Code 100  
Code 105  
Code 115  
Code 125L (10)  
Code 125P  
Code 200  
Code 300

Naval Ocean Systems Center  
San Diego CA 92152-5000  
Attn: Commander

Naval Postgraduate School  
Monterey CA 93943  
Attn: Superintendent

Naval Research Laboratory  
Washington DC 20375  
Attn: Commanding Officer  
Library, M. Bradley (3)  
Code TD, L. Bernard

Naval Underwater Systems Center  
Newport RI 02841-5047  
Attn: Commander

Naval Underwater Systems Center Det  
New London Laboratory  
New London CT 06320  
Attn: Officer in Charge

Office of Naval Research  
800 N. Quincy St.  
Arlington VA 22217-5000  
Attn: Code 10D/10P, Dr. E. Silva  
Code 112, Dr. E. Hartwig  
Code 12  
Code 10

Office of Naval Research  
ONR European Office  
PSC 802 Box 39  
FPO AE 09499-0700  
Attn: Commanding Officer

Office of Naval Technology  
800 N. Quincy St.  
Arlington VA 22217-5000  
Attn: Code 20, Dr. P. Selwyn  
Code 228, Dr. M. Briscoe  
Code 234, Dr. C. Votaw

Scripps Institution of Oceanography  
University of California  
291 Rosecrans St  
San Diego CA 92106-3505

Space & Naval Warfare Sys Com  
Director of Navy Laboratories  
SPAWAR 005  
Washington DC 20363-5100  
Attn: Commander

Woods Hole Oceanographic Institution  
P.O. Box 32  
Woods Hole MA 02543  
Attn: Director

# REPORT DOCUMENTATION PAGE

Form Approved  
OMB No 0704-0188

Public reporting burden for this collection of information is estimated to average 1 hour per response, including the time for reviewing instructions, searching existing data sources, gathering and maintaining the data needed, and completing and reviewing the collection of information. Send comments regarding this burden estimate or any other aspect of this collection of information, including suggestions for reducing this burden, to Washington Headquarters Services, Directorate for Information Operations and Reports, 1215 Jefferson Davis Highway, Suite 1204, Arlington, VA 22202-4302, and to the Office of Management and Budget, Paperwork Reduction Project (0704-0188), Washington, DC 20503.

1. Agency Use Only (Leave blank)		2. Report Date. October 1991		3. Report Type and Dates Covered. Final	
4. Title and Subtitle.  Theory and Application of Scattering from an Object in an Ocean Waveguide				5. Funding Numbers.  Job Order No 12211B Program Element No 0601153N Project No 03202 Task No 350 Accession No DN255011	
6. Author(s).  Guy V. Norton					
7. Performing Organization Name(s) and Address(es).  Naval Oceanographic and Atmospheric Research Laboratory Ocean Science Directorate Stennis Space Center, Mississippi 39529-5004				8. Performing Organization Report Number.  NOARL Report 28	
9. Sponsoring/Monitoring Agency Name(s) and Address(es).				10. Sponsoring/Monitoring Agency Report Number.	
11. Supplementary Notes.					
12a. Distribution/Availability Statement.  Approved for public release; distribution is unlimited. Naval Oceanographic and Atmospheric Research Laboratory, Stennis Space Center, Mississippi 39529-5004.				12b. Distribution Code.	
13. Abstract (Maximum 200 words).  A method was developed to describe acoustical scattering from an object in a waveguide by using normal mode theory to describe the incident field. Each mode is decomposed at the object into a pair of upgoing and downgoing plane waves. A transition matrix was used (developed via the extended boundary condition method of Waterman) to determine the resulting near-field scattered field. The far-field scattered field was determined by invoking Huygens' principle. This far-field solution satisfies all boundary conditions and preserves continuity of the solution throughout all space.  The examples show that the object is correctly coupled to the waveguide. This was done by showing that the object's scattered field acts as a secondary source and that this scattered field obeyed the same boundary conditions as the point source field.  This method of determining the scattered field from a three-dimensional object allows one to determine not only the correct target strength (intensity), but also to properly determine the phase. In addition, this method allows the investigation of the interaction between the incident field and the waveguide, the incident field with the object, and the object's scattered field with the waveguide. In this manner, a better understanding of the ongoing physical processes can be obtained.					
14. Subject Terms.  acoustic scattering, shallow water, waveguide propagation				15. Number of Pages. 252	
				16. Price Code.	
17. Security Classification of Report Unclassified	18. Security Classification of This Page. Unclassified	19. Security Classification of Abstract. Unclassified	20. Limitation of Abstract. None		